ARRIVAL DIRECTIONS OF MEDIUM ENERGY COSMIC RAYS IN THE SOUTHERN HEMISPHERE

A Thesis submitted to the

University of Adelaide

for admission to the Degree of

Doctor of Philosophy

by

David John Bird B.Sc. (Hons)

January 1991

FOR MY WIFE

ELIZABETH ANNE

Contents

Summary

As the study of cosmic rays enters its ninth decade of investigation, several facets of this field, most notably the origin of these high energy particles, remain at least partially unresolved. Investigations into the arrival directions of these particles (and also of Ultra-High-Energy (U.H.E.) γ-rays) provide one line of investigation through which these problems may be resolved, or at least limited to some extent. Unfortunately, the arrival directions of charged cosmic ray particles are effectively randomised by the galactic magnetic field producing an *almost* isotropic flux of primary cosmic rays.

This thesis presents the results of an investigation into the anisotropy of the arrival directions of cosmic rays of energies between 3×10^{14}eV and 10^{17}eV, recorded by the Buckland Park Extensive Air Shower Array at a latitude of 35°S, over the period June 1984 to May 1989. In addition to this work, the Buckland Park Array was also upgraded by the author to improve the array performance for future anisotropy investigations.

The introductory chapters of this thesis briefly review the history of cosmic ray research and the current status of investigations into the various properties of the primary cosmic ray flux, followed by a more detailed discussion of the initiation, development, and detection of Extensive Air Showers, which are the avenue through which these high energy cosmic rays are indirectly detected.

Chapter 3 describes in detail the instrument used in this investigation, the Buckland Park Extensive Air Shower Array. The components of this array, together with the development, data collection and analysis for the period 1984 to 1989 are discussed, with particular emphasis on the analysis carried out by the author on data collected over this period in fitting shower parameters to each event. The design and implementation of modifications to the array carried out during 1989 and 1990 by the author are then described and preliminary results of the modified array behaviour are presented which were found to be in line with both computer simulated results and design specifications.

The history of, and analysis techniques commonly employed in investigations of the anisotropy of the primary cosmic ray flux are reviewed in detail in Chapter 4. Following this, the results of the analysis of the 1984 to 1989 data set for anisotropy in the primary cosmic ray flux are presented in Chapter 5, including a detailed discussion of the techniques employed in attempting to remove external effects from the data. After identifying and removing a portion of data found to be severely contaminated with an apparently artificial effect of unknown origin, which could not be effectively removed from these data, no significant anisotropy amplitudes were found in the remaining data, and appropriate upper limits, consistent with previous determined results were calculated over the energy range 3×10^{14}eV to 10^{17}eV. In addition to these results, remarkable agreement of first harmonic phases with previous results was found, which is surprising in the absence of any significant amplitude measurements.

In recent years, U.H.E. γ-ray astronomy has become a major part of cosmic ray research, and in Chapter 6, the results of recent searches using data collected by the author over the period March 1988 to May 1989 for U.H.E. γ-rays from several sources including SN1987A are presented, as part of the on-going U.H.E. γ-ray program at Buckland Park.

The concluding chapter summarises the results presented in this thesis, and makes suggestions for future work.

Statement

This thesis contains neither material which has been accepted for the award of any other degree or diploma, nor, to the best of the author's knowledge and belief, any material previously published or written by any other person, except where due reference is made.

Signed:

David Bird

Acknowledgements

In such a major project, there are many people who have contributed, each in their own way, and it is a pleasure to acknowledge their contributions.

Firstly, I wish to thank : my supervisor, Dr. Roger Clay, whose assistance and advice has been a source of encouragement and enlightenment throughout my candidature; my predecessors (Phil C., Dave, Peter, Greg, Bruce, Phil E., Claire, Dominic, and Stephen) for their contributions to the Buckland Park E.A.S. Array and their assistance in many and varied ways, in particular Dominic and Phil E. for advice on the array and associated computer programming, Bruce for proof-reading the early drafts, and Stephen for his company; the 'new' CRGGC (Anthony S., Anthony L., Janice, Mike, Rishi, Andrew, and Gary) for their support and help, in particular Andrew for his help with simulations and computing advice in general, and Rishi, for his contribution to the 'new' Buckland Park E.A.S. Array; Neville Wild for his infinite patience and advice on all technical and electronic aspects of the array operation; Dr. Ray Protheroe for interesting conversations and useful help on some of the theoretical aspects of this project; the Electronics Services group for the construction of the 12-channel T.D.C. (and providing service under warranty); Brian Inwood and Mark Ferraretto for their assistance in main-frame computing, and Don Creighton and the Large Computer Users Group for providing copious amounts of computer C.P.U. time and disk space; Alex Didenko for keeping an eye on the array and for his help in the general maintenance of the array.

In addition I would also like to thank the following people: the four generations of honours students who have passed through the Department of Physics and Mathematical Physics during my candidature for their friendships; the many other friends I have made within the Department during my candidature for their help and encouragement; the Astronomical Society of Australia for providing the opportunity through the Harley

Wood Winter Schools and annual conferences to meet fellow students in other states and to the friends I have made, in particular to Anne, Shaun, Andrew and Tim from the University of Sydney; Dr. Dave Jauncey and Dr. Bob Duncan of CSIRO, and Dr. Bob Preston of JPL for providing the unique opportunity of being involved in the Australian VLBI network, and visiting JPL during my candidature; Douglas Adams, Arthur C. Clarke, and Isaac Asimov for their inspirational writing, both science fiction and non-fiction science.

I wish also to thank my friends outside of university who have helped me through for their encouragement and presence, especially those from the Bellevue Heights Baptist Church and associated youth groups.

Finally, I wish to thank my family, to Mum and Dad and Russell, who have provided for me throughout the majority of my candidature and without whom this would not have been possible. And to my wife, Elizabeth Anne, who has persevered with me through the dark times, and helped bring me through to the end of my candidature.

A Note from the Author

In such a wide ranging project as this, involving a field station which has been developed over many years, it is necessary to clarify the contributions made by the author.

The author was primarily responsible for:

(1) The complete analysis of the data collected from June 1984 to November 1990, as discussed in Chapter 3.

(2) Full maintenance (data collection, detector upkeep and repairs, calibration etc.) of the Buckland Park Extensive Air Shower Array from February 1988 to November 1990.

(3) The design and implementation (including full installation) of the array improvements for anisotropy work, as described in Chapter 3.

(4) The analysis of the 1978–1981 and 1984–1989 data sets for evidence of anisotropy in the primary cosmic ray flux in the energy range 3×10^{14}eV to 10^{17}eV, as discussed in Chapter 5.

(5) Searches for evidence of the emission of Ultra-High-Energy γ-rays from several southern hemisphere sources in the post-February 1988 data, as described in Chapter 6.

Abbreviations

The following abbreviations, nomenclature and assumptions have been adopted in this thesis:

E.A.S. (Extensive Air Shower)

γ-ray (Gamma-Ray)

In addition, the labelling of γ-ray energies will be that suggested by Weekes (1988), namely:

High Energy (H.E.) (3×10^{7}eV–10^{10}eV)

Very High Energy (V.H.E.) (10^{10}eV–10^{14}eV)

Ultra High Energy (U.H.E.) (10^{14}eV–10^{17}eV)

Extremely High Energy (E.H.E.) (10^{17}eV–10^{20}eV)

S.I. units and their abbreviations are generally used, including the following abbreviations for energy in terms of electron volts (eV) :

MeV ($\times 10^{6}$eV); GeV ($\times 10^{9}$eV); TeV ($\times 10^{12}$eV);

PeV ($\times 10^{15}$eV); EeV ($\times 10^{18}$eV).

Except where it is explicitly defined to be different, the primary cosmic ray flux will be assumed to refer to both particles and photons.

Chapter 1

Cosmic Rays

1.1 Introduction

Cosmic Rays are high energy particles (and photons) of extra-terrestrial origin. They contribute almost one third of the energy density of the inter-stellar medium (equivalent to that of starlight) and are therefore of great astrophysical significance. Apart from astrophysics, the study of cosmic rays has also contributed to advances in elementary particle physics, and they are currently the only source of the highest energy particles ($> 10^{15}$eV) available to man. However, even after more than three quarters of a century of investigation, many properties of the cosmic ray flux remain unresolved: in particular their origin, acceleration and composition.

Recently, exciting developments in Ultra-High-Energy (U.H.E.) γ-ray astronomy have provided new insights into the origin and acceleration of high energy cosmic rays. In spite of this progress, there remains much work to be done.

In this chapter, a brief history of cosmic ray research is given, followed by a review of the current knowledge of the cosmic ray flux and its properties.

1.2 History of Cosmic Ray Research

The discovery of cosmic rays can be traced back to the turn of the century, when it was observed that electroscopes suffered from a gradual charge leakage (Wilson 1901). It was initially believed that weak radiation from nearby objects was responsible for this effect.

However, in a series of balloon flights in 1912, Victor Hess investigated the variation with altitude of this radiation, and found that after an initial decrease up to an altitude of $\sim$ 700m, ionisation increased rapidly with height. His conclusion was that this radiation had an extra-terrestrial origin (Hess 1912), for which the term 'cosmic radiation' was coined by Millikan in 1926.

At the time, three types of ionising radiation were known, namely α –, β– and γ–radiation. Due to their energetic and highly penetrating nature, cosmic rays were believed to be gamma-rays.

Clay (1927) investigated the variation of the cosmic radiation with latitude, and found a 16% decrease in intensity from a latitude of 46°N to the equator. Compton (1932) found a similar result in the southern hemisphere. These measurements suggested that cosmic rays were not gamma-rays, but charged particles being deflected by the Earth's magnetic field. Further observations (Johnson 1933; Alvarez and Compton 1933) showed an excess in cosmic rays from the west of the zenith, suggesting that the majority of the particles were positively charged.

Cloud chambers were then employed in more detailed studies of this radiation. Skobelzyn (1929) showed that these particles appeared in individual swarms (showers), Anderson (1933) showed that these showers contained both electrons and positrons, and Rossi (1933) confirmed the existence of these showers, by observing coincidences between three non-collinear Geiger-Muller counters, using micro-second timing resolution.

By observing coincidences between widely-spaced detectors, Auger *et al.* (1938) determined these showers to have lateral extents of up to $\sim$ 300m. Such showers are

known as Extensive Air Showers (E.A.S.). They indicated the existence of primary cosmic ray particles of energies of $\sim 10^{15}$eV, much greater than had been considered possible. (Later observations of giant E.A.S. extended the energy spectrum past 10^{20}eV — Linsley 1963)

During the following twenty years, it was shown that E.A.S. consisted not only of electrons and protons, but also positrons, gamma-rays, and neutrinos, as well as the more exotic κ-mesons, λ-particles, and nucleons remaining from the primary particle. This research resulted in the discovery of many new particles, and led to the birth of elementary particle physics, which now carries out its research under the more controlled conditions of giant particle accelerators.

Through the use of improved technology (such as nuclear photographic emulsions), protons were identified in the primary cosmic radiation (Powell *et al.* 1959), as were gamma-rays (Kraushaar *et al.* 1968), heavier primaries, positrons and electrons (Giacconi *et al.* 1962), and nuclei heavier than iron (including transuranic elements) (Fowler *et al.* 1967).

Investigations into the energy spectrum and composition of primary cosmic rays have resulted in many exciting discoveries which have proved very useful to many disciplines. In the following section, the current status of these areas will be reviewed.

1.3 Properties of the Cosmic Ray Flux

The most fundamental measurements that may be made of the primary cosmic ray flux are those of the primary particle energy (the energy spectrum), the types of particles constituting the cosmic ray flux (the mass composition), and the observed arrival directions of these particles (the (an)isotropy). Below $\sim 10^{12}$eV, cosmic rays may be detected directly using balloon-borne or satellite detectors, but above these energies, only inferences can be made from the detection of E.A.S. (see Chapter 2). As a result, various properties in the low energy range are well determined (e.g. below $\sim 10^{14}$eV, the differential energy spectrum follows a negative power law with exponent -2.7, and

the mass composition is dominated by a predominantly light composition), while at higher energies, these properties are less well-defined.

The current status of energy spectrum and mass composition measurements of the primary cosmic ray flux will be briefly reviewed. The anisotropy of the primary cosmic ray flux will be discussed in some detail in Chapter 4.

1.3.1 Energy Spectrum

The energy spectrum of cosmic rays in its integral form (number (>E) m^{-2} s^{-1} sr^{-1}) is shown in Fig 1.1. This property of the cosmic ray flux has been extensively studied, and is known to within $\pm 20\%$ in the energy range 10^{14}eV – 10^{19}eV, with the exception of the region around $\sim 3 \times 10^{15}$eV, where there is a large deviation in the spectrum, commonly known as the 'knee' of the spectrum. Another deviation is believed to occur at energies above $\sim 10^{19}$eV and is known as the 'ankle' of the spectrum.

In the lower energy range (10^{12}eV – 10^{14}eV), the spectrum is most accurately known. This is a result of the relatively large particle flux at these energies, allowing direct measurements by balloon-borne or satellite detectors. In this region the energy/nucleus spectrum follows a power law with a differential slope of ~ -2.7 (differential flux expressed in terms of number m^{-2} s^{-1} sr^{-1} eV^{-1}).

In the medium energy range, (10^{14}eV – 10^{17}eV), spectrum measurements are based upon the detection of E.A.S. (see Chapters 2 & 3 for details) These measurements suffer from fluctuations in shower development and biases are introduced into the data as a result of the preferential detection of downward fluctuating (later developing) showers. This effect is most severe for proton-initiated showers (Clay 1985). This bias needs to be taken into account when deriving the energy spectrum from the observed shower size spectrum (see e.g. Nagano *et al.* 1984). Despite these uncertainties, the 'knee' of the energy spectrum is a well-established feature of the spectrum.

Around an energy of ~ 3–5×10^{15}eV, the differential energy spectrum steepens, changing slope from ~ -2.55 to ~ -3. This 'knee' could be a source effect, a propagation effect, result from changes in hadronic interactions at these energies, or be a

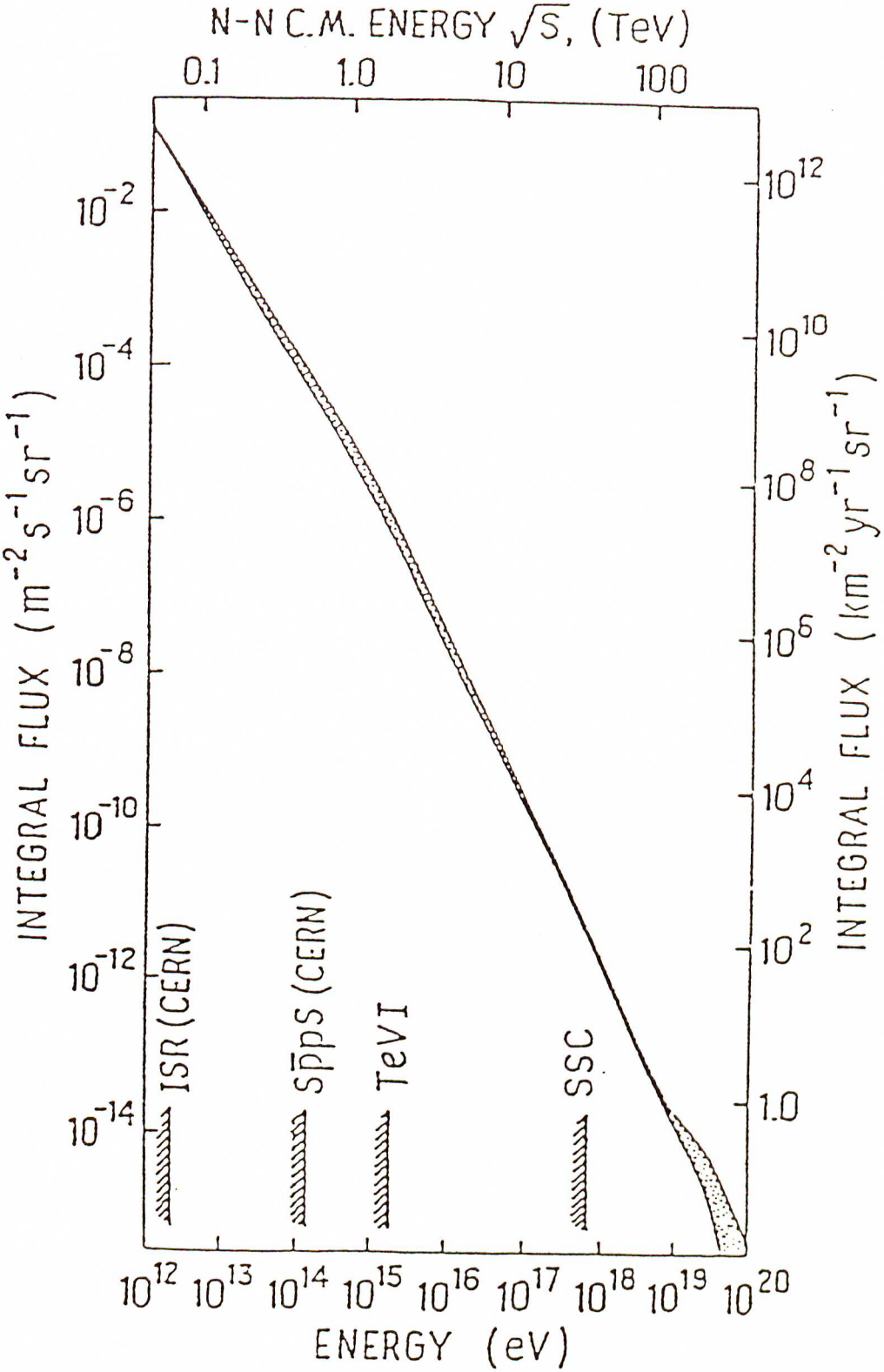

Figure 1.1: The primary cosmic ray flux (all particle) as measured at the top of the atmosphere, presented as an integral energy spectrum. The stippled regions indicate experimental uncertainties. The maximum attainable energies after present and future particle accelerators are also indicated (from Jones 1985).

combination of some or all of these effects.

An early explanation of the 'knee' was that of the 'leaky-box' model (Peters 1961). This model takes into account rigidity-dependent leakage from a local confinement region. Magnetic rigidity, R, is defined as

$$R = \frac{pc}{Ze} \tag{1.1}$$

where p = momentum

c = velocity of light

Ze = charge on the nucleus (Z = atomic number)

and is expressed in terms of Gigavolts (GV). Assuming the local confinement region to be the galactic magnetic field, cosmic rays spiral along these field lines with a radius of gyration, r_L (known as the Larmor radius — see 4.2.3), which is proportional to the rigidity.

The radius of gyration increases proportionally with R until r_L is greater than the size of the confinement region, and the particle escapes. Assuming a rigidity dependence for the 'knee', each elemental species in the primary cosmic ray flux would be expected to produce its own 'knee', progressing from a proton-induced 'knee' through to an iron 'knee' at an energy 26 times that of the proton 'knee', as demonstrated in Fig 1.2(a). Such a step-wise leakage is not observed in practice (see 1.3.2 for a discussion of the relationship of the 'knee' to the composition of the primary cosmic ray flux).

An alternative explanation for the 'knee', suggested by Karakula *et al.* (1974), proposes the dominance of particles accelerated by pulsars. Early models (e.g. Gunn and Ostriker 1969) proposed that pulsars may be able to accelerate particles up to energies $\sim 10^{16}$eV. Extrapolating the predicted power law with differential index ~ -2.5 to energies above 10^{14}eV, leads to the postulation that particles accelerated by pulsars may dominate in the region of the 'knee' (Strong *et al.* 1974) (see Fig 1.2(b)).

The discovery of U.H.E. γ-ray emission from X-ray binary sources (e.g. Samorski and Stamm 1983a; Protheroe *et al.* 1984) at energies up to $\sim 10^{16}$eV, implies the

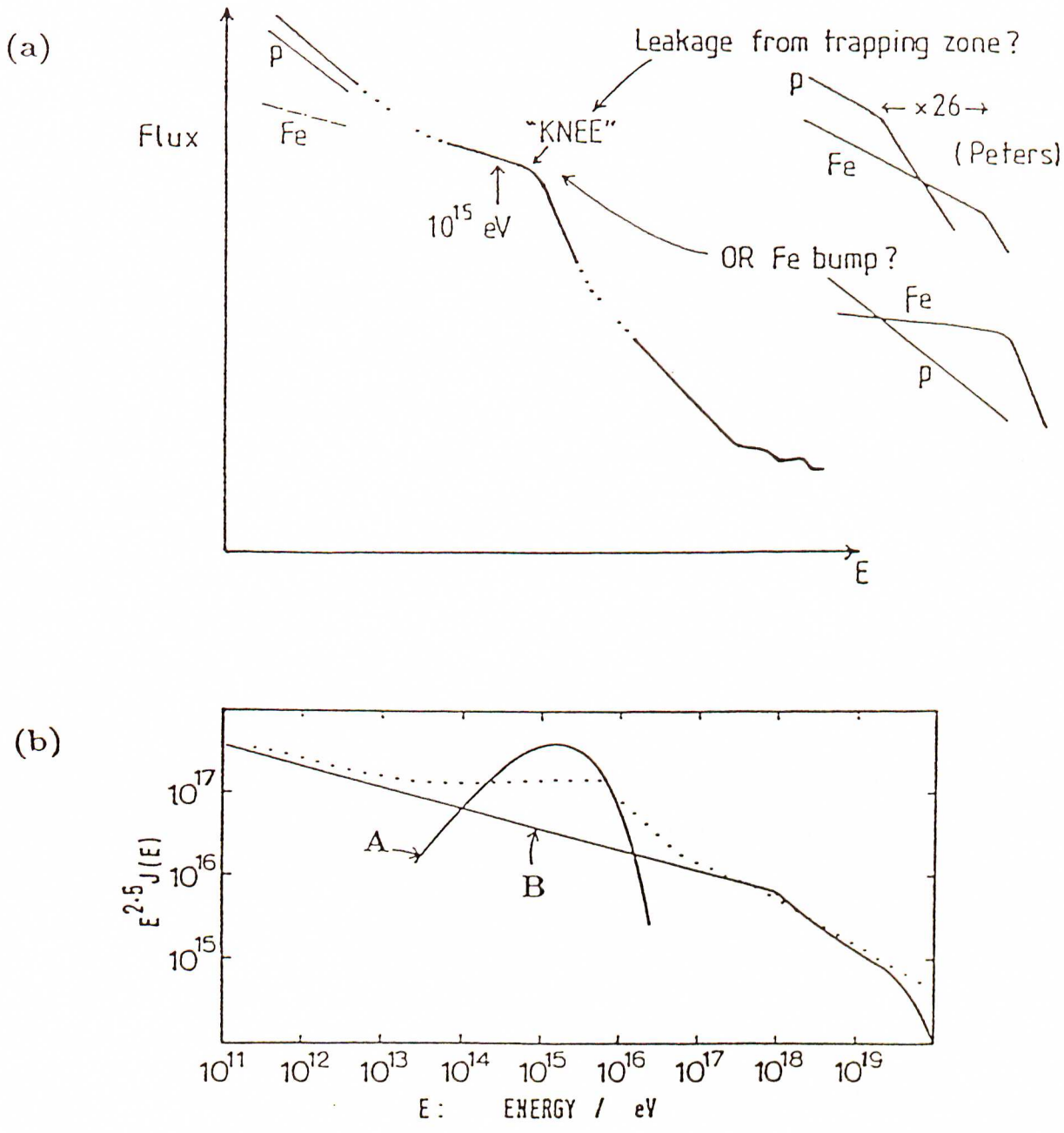

Figure 1.2: Models of the knee in the energy spectrum.

(a) The rigidity dependent escape model of Peters (1961) contrasted with an iron 'bump' model (after Hillas 1981)

(b) The superposition of a pulsar accelerated component (A), on the energy spectrum (B), with the experimentally determined spectrum dotted in (after Hillas 1975a).

acceleration of particles by these objects to energies up to at least $\sim 10^{17}$eV. Protheroe (1984a) has suggested a mechanism based upon photo-pion production in which a sharp energy absorption threshold results for a fixed source temperature. Such a feature has been observed from the γ-ray source Cygnus X-3 (Lambert *et al.* 1985). The production of the 'knee' by a break in the primary spectrum requires a sharp break (e.g. a change in the spectral index of ~ 1.5 — Clay 1988) in order to maintain consistency with both measured size spectra and E.A.S. fluctuations. The absorption feature suggested by Protheroe (1984a) could produce such a break.

In the high energy region (10^{16}eV – 10^{19}eV), the energy spectrum is essentially featureless. There is good agreement between the results of a number of groups (e.g. Akeno (Teshima *et al.* 1990), Haverah Park (Lawrence *et al.* 1990b), and Fly's Eye (Cassiday *et al.* 1990c)), and the spectrum is characterised by a differential slope of -3.0 (Kifune 1990).

The region of the energy spectrum above 10^{19}eV is of particular interest as it is the home of the 'ankle' of the energy spectrum, and any cut-off in this region has implications for both the origin and propagation of these U.H.E. cosmic rays.

Following the discovery of the 2.7K microwave background by Penzias and Wilson (1965), it was postulated (Greisen 1966; Zatsepin and Kuz'min 1966) that as a result of photo-pion production from interactions of these U.H.E. cosmic rays with the background radiation field, the primary cosmic ray flux would be severely attenuated above energies $\sim 5\times10^{19}$eV, with the effect being most pronounced at $\sim 10^{20}$eV, if the sources of these particles were at distances of the order of tens of Mpc or greater.

Early reports of the steepening of the spectrum above $\sim 4\times10^{19}$eV (Krasilnikov *et al.* 1983) have not been confirmed by other experiments. A claimed cut-off at an energy just below $\sim 10^{20}$eV (Baltrusaitis *et al.* 1985b) requires further accumulation of data before the existence and energy of such a cut-off can be established (Kifune 1990). Currently no cut-off in the energy spectrum is observed below $\sim 10^{20}$eV.

In addition, a number of groups (e.g. Fly's Eye (Baltrusaitis *et al.* 1988), Akeno (Teshima *et al.* 1990), and Haverah Park (Lawrence *et al.* 1990b)) have claimed that the

energy spectrum is somewhat flatter above $\sim 2\times10^{19}$eV (differential index of ~ -2.4 — Baltrusaitis *et al.* 1988), producing the 'ankle' in the energy spectrum. This feature may be the result of a flatter spectrum of the extra-galactic cosmic ray flux (e.g. Shapiro and Silberberg 1983). Alternatively, a propagation effect of these extra-galactic cosmic rays may explain the 'ankle'.

Hill and Schramm (1985) investigated the effect of the 2.7K microwave background on the U.H.E. cosmic ray spectrum as a result of large-scale propagation. The dominant effects were found to be photo-pion production, pair production ($\gamma \rightarrow e^+e^-$), and the red-shifting of energy. These effects result in a spectral enhancement at $\sim 6\times10^{19}$eV from the pile-up of energy degraded nucleons, preceded by a 'dip' at $\sim 10^{19}$eV produced by the combined effects of a pile-up and pair production (Hill and Schramm 1985). Haverah Park data were used to support this claim. Subsequent calculations (Hill *et al.* 1986), based upon Fly's Eye data suggest that the flattening in the spectrum above $\sim 10^{19}$eV can be interpreted as the recoil proton pile-up of the $\sim E^{-3}$ spectrum, and therefore these U.H.E. cosmic rays ($\geq10^{19}$eV) are of extra-galactic origin, having traversed a distance of at least several interaction lengths ($\sim$ 20 Mpc).

1.3.2 Composition

The relative abundances of elements (and their isotopes) in the cosmic ray flux provide useful information on the both the origin and propagation history of the cosmic ray flux.

The mass composition of the cosmic ray flux below energies of $\sim 10^{13}$eV/nucleon has been well determined through direct measurements. The standard low energy composition appears in Fig 1.3 where a comparison with solar system abundances has been made for elements with charges $Z \leq 28$ (nickel). The mass composition at these energies has been found to extend to elements with charges $Z \geq 90$ present, but the abundances of elements with $Z \geq 30$ is $\sim 10^{-4}$ that of iron (Fowler *et al.* 1987).

Fig 1.3 demonstrates the overall agreement of the relative abundances of the primary cosmic ray flux with solar system abundances apart from two notable exceptions.

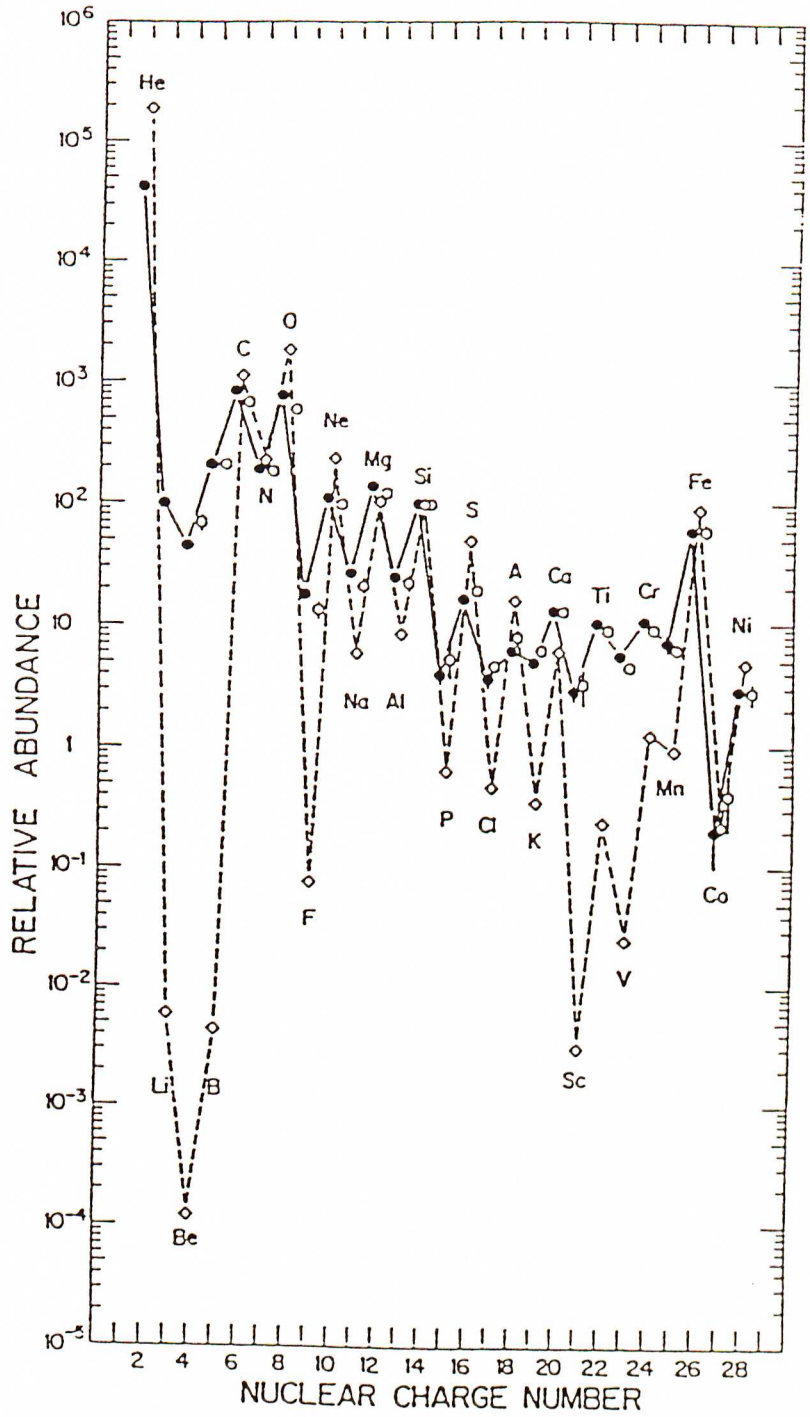

Figure 1.3: The cosmic ray elemental abundances measured at the Earth compared with solar system abundances. All abundances are relative to that of Silicon which is arbitrarily set to 100. Filled circles represent lower energy data (70 – 280 MeV/nucleon), open circles higher energy data (1 – 2 GeV/nucleon) and diamonds the solar system abundances (after Simpson 1983).

Firstly, there is an underabundance of hydrogen and helium, and this is discussed by Meyer (1985). Secondly, there is an overabundance of the light elements Li, Be, B as well as in some of the transition elements just below Fe, namely Sc, Ti, V, Cr, and Mn, relative to solar system abundances. It is widely agreed that this relative overabundance is the result of the spallation of certain primary cosmic ray nuclei (C, N, O, and Fe) as a result of interactions with the inter-stellar medium. The ratio of secondary to primary nuclei has been found to be energy dependent above $\sim 2 \times 10^9$eV/nucleon, decreasing with increasing energy (see Simpson 1983 for a discussion). This energy dependence supports the models in which cosmic ray acceleration occurs prior to propagation through the inter-stellar medium, as opposed to acceleration within the inter-stellar medium.

These secondary nuclei may be used to probe the inter-stellar medium, and their relative abundances used to estimate the amount of matter traversed between their acceleration and detection. One estimate of the matter path length, λ, which is found to decrease with energy (and hence rigidity) is given by

$$\lambda = 7.4 \pm 0.7 \text{ gcm}^{-2} \qquad 3 < \text{R} < 5.5 \text{ GV}$$

$$\lambda = (22 \pm 2)\text{R}^{-0.60 \pm 0.04} \text{ gcm}^{-2} \qquad \text{R} > 5.5 \text{ GV}$$

(Engelman *et al.* 1985)

This path length is equivalent to the escape length, λ_e, of leaky box models of cosmic ray propagation, and the energy dependence may be interpreted in terms of a rigidity dependent leakage from the Galaxy (or from a smaller confinement volume such as the local super-bubble — Streitmatter *et al.* 1983).

Knowledge of this matter path length enables spallation effects to be removed and the derivation of a source mass spectrum (see e.g. Meyer 1985). Any energy dependence in this mass composition may have significant implications (e.g. the results of Grunsfield *et al.* (1988, 1990) suggest that at energies up to $\sim 10^{14}$eV, iron becomes steadily more abundant — this is particularly important if this trend continues to higher energies).

In addition, models of the fractionation of elemental abundances may be compared

with those derived from measurements. It has been noted by Binns *et al.* (1984), that there is a significant source fractionation, ordered by the first ionisation potential of the elements. This is demonstrated in Fig 1.4, where those elements with high first ionisation potentials are depleted relative to those with low first ionisation potentials, when compared with local galactic abundances. A similar trend exists for energetic solar particles, a result which has important implications for models of cosmic ray acceleration and propagation.

Time-scales for cosmic ray propagation may also be estimated from mass compositions, due to the presence of radio-active isotopes within the cosmic ray flux. In particular, the ^{10}Be isotope possesses a half-life of $\sim 1.5 \times 10^7$ years, and comparison with the stable ^{9}Be isotope leads to a lower limit of $1\text{–}2\times10^7$ years (Simpson 1983). This age is essentially equivalent to the confinement time of the leaky box models.

At higher energies, the composition of the primary cosmic ray flux is amongst its least well-defined properties. Compositional information must be inferred from E.A.S. measurements and relies heavily upon models of E.A.S. development.

In particular, the composition in the regime of the 'knee' in the energy spectrum is subject to considerable debate. Leaky box models suggest a rigidity dependent escape of cosmic rays from the Galaxy. This would lead to a proton 'knee' at $E \sim 2 \times 10^{14}$eV, with a subsequent dominance of heavier nuclei up to an iron 'knee' at $E \sim 5 \times 10^{15}$eV. However, no early 'knee' is observed at these energies. Hillas (Watson 1985) has suggested that the best fit to shower size data corresponds to an iron 'knee' at $E \sim 2 \times 10^{15}$eV, and a proton 'knee' at $E \sim 5 \times 10^{15}$eV. If this proton 'knee' resulted from rigidity dependent leakage, the iron 'knee' must result from a different mechanism, perhaps intrinsic to the source.

Aside from the 'knee' of the energy spectrum, the overall picture of high energy cosmic ray composition is far from clear. Compositions inferred from measurements of muons in air showers (Yodh *et al.* 1984), and air Cerenkov studies of E.A.S. (Dawson *et al.* 1985) suggest a heavy-nuclei composition at $\sim 10^{15}$eV – 10^{16}eV. This is consistent (Dawson 1990) with the results obtained based upon the measurements of the

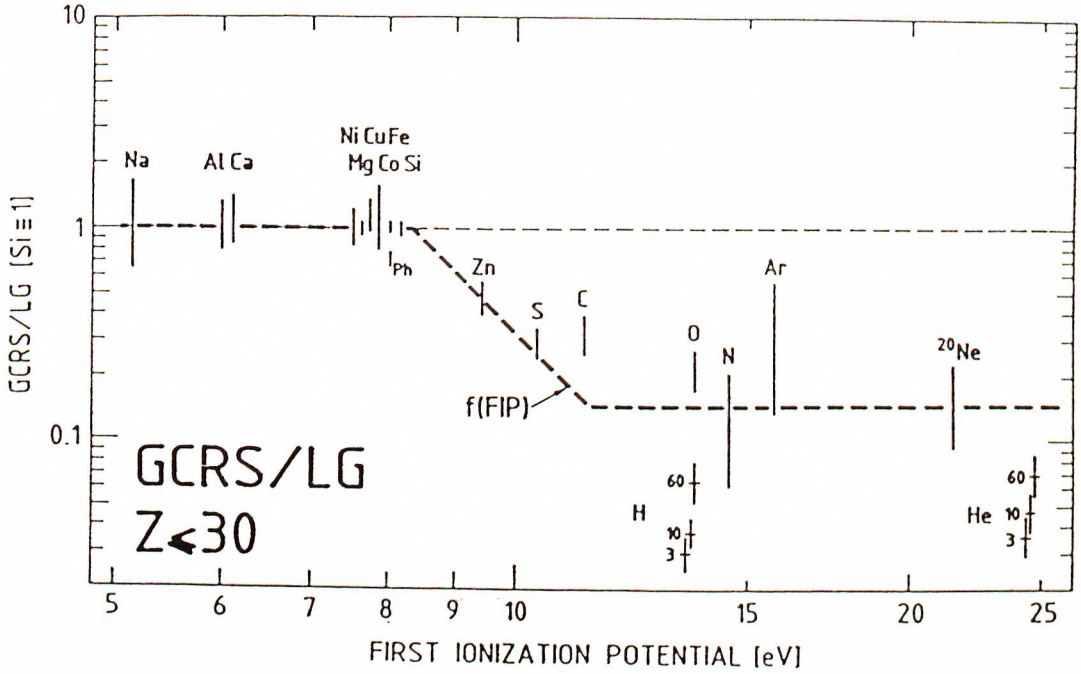

Figure 1.4: Ratio of Galactic cosmic ray source (GCRS) abundances to local galactic (LG) abundances plotted against the atomic first ionisation potential. Hydrogen and helium ratios are shown for measurements at 3, 10 and 60 GeV/nucleon. The solid dashed line is an adopted shape of the correlation between the GCRS/LG ratio and the first ionisation potential (after Meyer 1985).

elongation rate of E.A.S. (e.g. Thornton and Clay 1979) which also suggest that the composition of cosmic rays above $\sim 3 \times 10^{16}$eV is purely protons (Linsley and Watson 1981), but is in contradiction to those based upon muon multiplicities suggesting a proton-dominated composition in the energy range $\sim 3 \times 10^{13}$eV – 3×10^{15}eV (Cebula *et al.* 1990). Bimodal mass spectra consisting of 30%–40% iron, and 70%–60% protons have also been deduced from measurements of Cerenkov light pulses in the energy range 10^{17}eV – 10^{18}eV (Chantler *et al.* 1982), and investigations of muon-rich events leads to a varying heavy-nuclei fraction of $\sim$ 10% at 10^{15}eV to $\sim$ 3% at 10^{17}eV (Kifune *et al.* 1986a). Finally, muon-to-electron ratios have been used to indicate a constant mass composition over the range 10^{16}eV – 10^{19}eV (Armitage *et al.* 1987). It is only at energies above 10^{18}eV where there is general agreement on a predominantly light composition in the primary cosmic ray flux (e.g. 90 ± 10% protons at $\sim 5 \times 10^{18}$eV — Doronina *et al.* 1990).

It is obvious that a far more consistent picture of high energy cosmic ray composition is desirable, especially in the light of the dependence of interpretations of the energy spectrum, acceleration and propagation mechanisms, and anisotropies on composition.

1.4 The Acceleration of Cosmic Rays

The acceleration of cosmic rays to their observed energies involves some of the highest energy processes ever conceived and is at the forefront of both nuclear and particle physics. Attempts to model these processes, based upon mechanisms with sufficient energy output, and capable of reproducing the observed properties of the cosmic ray flux (see 1.3) date back to the earliest model of Fermi (1949). In this model, cosmic ray particles gain energy through successive collisions with clouds moving randomly within the inter-stellar medium. This mechanism is known as second-order Fermi acceleration (as $\Delta E \propto v^2$) and produces a power law spectrum. An alternative model (Colgate and Johnson 1960) proposed the acceleration of cosmic ray particles by supernova explosions. This mechanism provided an explanation of the overall cosmic ray

spectrum.

Current models of cosmic ray acceleration are based upon diffusive shock waves present in supernova remnants. These models combine features of both of the previous models (see e.g. Axford 1981). The acceleration mechanism involved, known as first-order Fermi acceleration (as $\Delta E \propto v$), is based upon the acceleration of particles as a result of their continual scattering across a shock-front, where the scattering centre possesses a non-random bulk motion (such as the boundary of the local super-bubble — Streitmatter *et al.* 1983).

This mechanism is considered to be the most likely accelerator of the majority of cosmic rays below energies of $\sim 10^{14}$eV – 10^{15}eV (Ellison 1990). Evidence for such an origin of these cosmic rays include energetics, the fact that the kinetic energy in supernovae ejecta is sufficient to provide the necessary power (assuming a 10% efficiency), the actual acceleration mechanism involved (first-order Fermi acceleration), which can give the proper spectrum, efficiency, and composition, and which has been observed to be working at heliospheric shocks (e.g. Ellison and Möbius 1987), as well as observations of external galaxies , which appear to show a correlation between cosmic ray production (deduced from synchrotron radiation observations) and the supernova rate (e.g. Duric and Slane 1990; Völk 1990; Völk *et al.* 1990).

A breakdown in supernova shock wave acceleration is expected to result in a maximum possible energy $\sim 10^{14}$eV – 10^{15}eV/nucleon (Lagage and Cesarsky 1983). This upper limit may be extended by invoking shock waves associated with the supersonic stellar winds of bright/young stars (Cassé and Paul 1980) to the region of the 'knee'. Mechanisms involving pulsars are also considered to be candidates at these energies (see e.g. Nagle *et al.* 1988 for a review).

Above the 'knee' of the energy spectrum, alternative acceleration mechanisms are necessary. Many theoretical problems remain in this region (Ellison 1990), but amongst those considered as plausible candidates are models involving accretion-related acceleration associated with neutron stars and the more exotic black holes (Fichtel and Linsley 1986). The observations of U.H.E. γ-rays from X-ray binary systems such as

Cygnus X-3 suggests that acceleration to energies $\geq 10^{16}$eV may be associated with these systems (see 1.3.1; 1.5.2; Nagle *et al.* 1988).

At energies above $\sim 3 \times 10^{17}$eV - 10^{18}eV/nucleon, it is generally considered that only extra-galactic mechanisms are capable of contributing to the cosmic ray flux (Wdowczyk and Wolfendale 1989). Sorrel (1987) dismissed statistical, Fermi-like mechanisms in this energy range in favour of direct acceleration mechanisms, based upon the electric dynamo model of Lovelace (1976), assuming suitable conditions exist within the gaseous halos of spiral galaxies in e.g. the Virgo supercluster. Another alternative involves acceleration across extra-galactic shocks associated with strong radio sources (Axford 1987). These extra-galactic models ultimately depend upon the accretion of matter onto massive black holes to provide the necessary energy.

1.5 Gamma-Ray Astronomy

Gamma-ray astronomy and cosmic rays have a strong historical link, dating back to the initial mistaken identification of the cosmic radiation as consisting of γ-rays (see 1.2). In more recent times, the relationship between γ-rays and cosmic rays has become well established. γ-rays owe their origin to cosmic rays, as they are produced when cosmic ray particles interact with the inter-stellar medium or with radiation fields. Due to their uncharged nature, which allows γ-rays to propagate directly from their production region, and the relative transparency of the inter-stellar medium to γ-rays, observations of γ-rays provide direct information on regions of high energy activity (such as X-ray binary systems, supernovae, pulsars etc.) including those responsible for the acceleration of cosmic rays, which are otherwise largely unobservable.

Following is a brief discussion of γ-ray astronomy, with particular emphasis on U.H.E. γ-ray astronomy, which is most relevant to the cosmic rays being considered.

1.5.1 History

Technological advances motivated by World War II opened up alternative regions of the electromagnetic spectrum (particularly radio and X-rays) for astronomical observation, previously the exclusive domain of the optical astronomers. Radio and X-ray observations soon revealed highly energetic processes not previously observed.

The observation of γ-rays was initially delayed by a number of factors, including their low intrinsic flux relative to the cosmic ray background, an early overestimate of the expected flux at energies of $\sim$ 100 MeV by several orders of magnitude (Morrison 1958), and the necessity of placing detectors above the majority of the Earth's absorbing atmosphere. These problems, combined with the discovery of the unusual X-ray source, Scorpius X-1 (Giacconi *et al.* 1962), left γ-ray astronomy essentially in limbo for a short period, whilst efforts were concentrated on X-ray astronomy.

High energy γ-rays ($\sim$MeV) were finally observed by a γ-ray detector aboard the Explorer II satellite (Kraushaar *et al.* 1965). Many satellite and balloon-borne detectors followed. The majority of results in this energy range to date have come from the SAS-II (e.g. Hartman *et al.* 1979) and COS-B (e.g. Swanenburg *et al.* 1981) satellites. These γ-rays were observed to originate from point sources and the galactic plane, as well as a small diffuse component assumed to be of extra-galactic origin. The up-coming Gamma Ray Observatory (G.R.O.) (see e.g. Schönfelder 1990) with its increased resolution and energy range promises further progress in exploring and identifying high energy γ-ray sources.

At V.H.E. energies and above, indirect techniques are necessary in the detection of γ-rays, due to the inability of satellite detectors to accurately measure the small flux present within a reasonable time-scale. The atmospheric Cerenkov technique has been successfully applied at V.H.E. energies in searches for γ-rays from astrophysical sources (see e.g. Weekes 1988 for a description of this technique and a general review of V.H.E. γ-ray astronomy). These sources include Centaurus A, Cygnus X-3, Hercules X-1 and the Crab Nebula (see e.g. Protheroe 1987a; Fegan 1990 for recent reviews).

1.5.2 Ultra-High-Energy Gamma-Ray Astronomy

The observation of U.H.E. γ-rays relies essentially upon the detection of E.A.S. which result from the interaction of the γ-ray with an atmospheric nucleus (see Chapter 2; Nagle *et al.* 1988).

The era of U.H.E. γ-ray astronomy is considered to have begun with the detection of U.H.E. γ-rays from Cygnus X-3 at Kiel (Samorski and Stamm 1983a), based upon E.A.S. data collected over the period 1976–1980. The Kiel observations consisted of 31 events in a $\sim 4^\circ \times 3^\circ$ bin centred on Cygnus X-3, when 14.4 were expected, corresponding to a 4.4σ excess. This was achieved using an age cut, selecting showers with ages greater than the median age of $s = 1.1$ (see 2.4). This observation was further enhanced by the 4.8 hour (orbital period known from X-ray observations) periodicity of the event arrival times (phase bin centred on phase 0.35, width 0.1, contained 12 events when 1.44 ± 0.04 were expected). The observation was subsequently confirmed by the analysis of data collected at Haverah Park (Lloyd-Evans *et al.* 1983).

Subsequently, evidence for U.H.E. γ-ray emission, based upon the periodic analysis of E.A.S. data archives, was established for a number of X-ray binary sources (e.g. Vela X-1 (Protheroe *et al.* 1984), LMC X-4 (Protheroe and Clay 1985), Hercules X-1 (Baltrusaitis *et al.* 1985a)).

Cygnus X-3 remains the most popular U.H.E. γ-ray source, due to its strong signal strength, favourable position for mid-latitude northern hemisphere observation, and unusual behaviour across the electromagnetic spectrum from radio waves to U.H.E. γ-rays (see Bonnet-Bidaud and Chardin 1988; Chardin and Gerbier 1989 for comprehensive reviews, and Ciampa *et al.* 1990 for a recent summary of observations). Several arrays have been purpose-built primarily to detect U.H.E. γ-rays from Cygnus X-3 and other similar sources (e.g. the CYGNUS array, constructed around a neutrino detector at Los Alamos — Dingus *et al.* 1988a).

The most puzzling aspect of the majority of the observations of U.H.E. γ-rays from Cygnus X-3 (and other sources) is the near-'normal' muon content of the associated E.A.S. (see 2.5.1 for a discussion). The distance to Cygnus X-3 of $\sim$ 10 kpc places

severe restrictions on the nature of possible alternative primary particles. Charged particles are excluded by the directional nature and time coherence of the signal, due to the randomising nature of the galactic magnetic field on the paths of such particles. Excluding exotic, undiscovered particles such as photinos, gluinos etc., the most likely candidates for consideration are the neutron and neutrino. However, the relatively short half-life of the neutron (898 ± 16s) requires energies $\geq 10^{18}$eV to allow time dilation to prevent decay, which effectively removes it from consideration. Furthermore, the incredibly small interaction cross-section of the neutrino would require fluxes many orders of magnitude higher than those currently considered feasible. In addition, neutrinos would interact uniformly through the atmosphere, resulting in an age distribution radically different to that observed by Samorski and Stamm (1983b).

This process of elimination leaves γ-rays as the only (currently known) realistic possibility. Such a conclusion has important implications for the origin of cosmic rays. If Cygnus X-3 emitted protons of energies $\sim 10^{15}$eV with the same efficiency as the implied fluxes of γ-rays at this energy, Wdowczyk and Wolfendale (1983a) conclude that only ~ 30 Cygnus X-3 type sources would be required to supply the Galaxy with cosmic rays at these energies. Furthermore, Hillas (1984), suggests that the strength of the observed signal from Cygnus X-3 implies a luminosity of U.H.E. particles sufficient to supply the Galaxy with the majority of cosmic rays up to an energy $\sim 10^{17}$eV, if it is assumed that Cygnus X-3 is a mono-energetic accelerator of 10^{17}eV protons. Such observations suggest one or several discrete sources for cosmic rays, as opposed to a galactic distribution of sources, as discussed in 1.4.

In addition, observations of U.H.E. γ-rays from extra-galactic sources such as the radio galaxy Centaurus A (e.g. Bird and Clay 1990a) at a distance of ~ 5 Mpc would have further implications, as fluxes of U.H.E. γ-rays at $\sim 10^{15}$eV – 10^{16}eV are predicted to be severely attenuated over these distances as a result of photon-photon interactions with the 2.7K cosmic background radiation field (e.g. Protheroe 1986).

The field of U.H.E. γ-ray astronomy is still in its infancy with many expectations not yet fulfilled. As a result largely of poor statistics, the reliance of the detection of U.H.E.

γ-rays from X-ray binary sources on periodic analysis and the serendipitous observation of transient phenomena (Fegan 1990), no truly unambiguous positive results have yet been produced. The ultimate goal of unravelling the mysteries of the sources of high energy cosmic rays will only be achieved after many problems, such as the true nature of the carriers of the signals being determined and the partially non-photonic signature of associated E.A.S. are resolved, perhaps as a result of a better understanding of the interactions of hadrons and γ-rays at these energies.

In the following chapter, the nature of the E.A.S. initiated by cosmic rays (and γ-rays) will be discussed, as this is the avenue of cosmic ray detection exploited in the work being discussed.

Chapter 2

Extensive Air Showers

2.1 Introduction

Above primary particle energies of $\sim 10^{13}$eV, the steepness of the primary cosmic ray spectrum (see Fig 1.1) results in a flux too low to allow the use of direct methods of particle detection such as satellite or balloon-borne detectors. However, the interaction of the primary particle with the atmosphere and subsequent interactions of the secondary particles and photons produced results in a shower of particles. If the primary particle energy is $>10^{14}$eV ($>10^{13}$eV for mountain altitudes), this shower reaches ground level with an observable number of coherent particles, and is known as an Extensive Air Shower (E.A.S.).

These E.A.S. provide an indirect window to the highest energy radiation and particles produced in the universe. It is therefore necessary to understand the characteristics of E.A.S. in order to study the particles/photons responsible for their production. This requires a knowledge of the physical processes occurring in high energy interactions, generally beyond the range of existing particle accelerators. The interpretation of E.A.S. information is heavily reliant upon models of these interactions and the subsequent propagation of these particles through the atmosphere.

In this chapter, the present understanding of E.A.S. production and development will be discussed in terms of the three major components of an E.A.S., namely the nu-

clear (or hadron) component, the muon (or hard) component, and the electromagnetic (or soft) component. The differences between cosmic ray and γ-ray initiated E.A.S. will also be addressed.

2.2 Nuclear Component

When a high energy cosmic ray particle impinges on the atmosphere, travelling at effectively the speed of light, the first interaction it undergoes is between the particle and an atmospheric atom or molecule. The particle loses $\sim$ 50% of its energy (i.e. an inelasticity of $\sim$ 0.5 — Jelley *et al.* 1965) in this and subsequent interactions. The nucleus itself does not gain much energy, but may lose several nucleons knocked free by the particle. The lost particle energy is channelled into the creation of new baryons and mesons. It is in this way that an E.A.S. is initiated.

For a proton primary particle, the interaction length for the initial interaction is energy dependent, and may be described by

$$\lambda_{\mathrm{p}} = 67.2 \left(\frac{E(\mathrm{TeV})}{100} \right)^{-0.065} \ \mathrm{gcm}^{-2} \qquad (2.1)$$

(Dawson 1985)

This contrasts with that of an iron primary particle, which has an interaction length essentially independent of energy, $\lambda_{\mathrm{Fe}} \sim 13$ gcm^{-2} (Westfall *et al.* 1979). This greater depth (on average) for a proton leads to greater fluctuations in shower development and hence in the depth of shower maximum, than those experienced by an iron nucleus-initiated E.A.S. (see 2.4 for a discussion of E.A.S. development).

The particles produced in this interaction may be separated into two momentum regions, namely the fragmentation and central regions, the former containing the remnant of the primary particle and other leading particles (the nuclear component), and the latter corresponding to small momenta in the centre-of-mass (CM) reference frame in which the majority of new particle production takes place.

The hadronic interactions occurring result mostly in the production of pions, with a small percentage of kaons and other heavier hadrons also produced. Pions occur in

three species (π^+, π^-, $m_{\pi\pm} \sim 140$ MeV; π°, $m_{\pi^\circ} \sim 135$ MeV) which are produced in approximately equal numbers in E.A.S. With a rest half-life of $t_{\frac{1}{2}} \sim 8 \times 10^{-17}$s, the neutral pions produced (π°) rarely interact before decaying through photo-production (i.e. $\pi^\circ \rightarrow \gamma\gamma$), contributing to the electromagnetic component of the E.A.S. (see 2.4). Charged pions possess a significantly longer half-life ($t_{\frac{1}{2}} \sim 2.6 \times 10^{-8}$s) and may interact or decay, depending largely upon the altitude (and corresponding atmospheric density) of their creation. In the latter case, the relatively stable muon ($\mu^\pm$) is produced, contributing to the muon component of the E.A.S. (see 2.3) (i.e. $\pi^+ \rightarrow \mu^+ + \overline{\nu}_\mu$, $\pi^- \rightarrow \mu^- + \nu_\mu$).

Kaons are produced at $\sim$ 10% the rate of pion production in E.A.S., with all four species (K^+, K^-, $m_{K\pm} \sim 494$ MeV; K°, $\overline{K}^\circ$, $m_{K^\circ,\overline{K}^\circ} \sim 497$ MeV) present. The two neutral kaon species are generally considered in terms of their charge parity eigenstates, namely

$$|K_S^\circ> = \frac{1}{\sqrt{2}}\left(|K^\circ> + |\overline{K}^\circ>\right), \text{ and } |K_L^\circ> = \frac{1}{\sqrt{2}}\left(|K^\circ> - |\overline{K}^\circ>\right)$$

(e.g. Eisberg and Resnick 1985)

which are differentiated in terms of their decay modes. It is assumed that half of the neutral kaons produced will be in each of these two states. These states decay through a number of channels to produce pions, muons, and electrons, therefore contributing to both the muon and electromagnetic components of E.A.S. (i.e. $K_S^\circ \rightarrow \pi^+\pi^-, \pi^\circ\pi^\circ$; $K_L^\circ \rightarrow \pi^\circ\pi^\circ\pi^\circ, \pi^+\pi^\circ\pi^-, \pi^\pm\mu^\mp\nu_\mu, \pi^\pm e^\mp \nu_e$). As in the case of pions, charged kaons may interact or decay ($t_{\frac{1}{2}} \sim 1.2 \times 10^{-8}$s), producing muons or pions (i.e. $K^+ \rightarrow \mu^+\overline{\nu}_\mu, \pi^+\pi^\circ$; $K^- \rightarrow \mu^-\nu_\mu, \pi^-\pi^\circ$).

In addition to pions, muons, and electrons, neutrinos (and anti-neutrinos) are also produced in cosmic ray E.A.S. interactions but, due to their incredibly small interaction cross-sections, play no further role in E.A.S. development.

The production of the muon and electromagnetic components of E.A.S., fed by pion and muon decay from the nuclear component, are ultimately dependent upon a number of factors, including the inelasticity of the interacting particle, the multiplicity of the interaction (<n>, the number of particles created), and the interaction cross-

sections (expressed in reciprocal form as the mean free path). Various models have been proposed, involving different values for these parameters.

The earliest models of high energy cosmic ray interactions were based upon statistical-hydrodynamical ideas (e.g. Fermi 1951). A more successful model (the C.K.P. (Cocconi, Koester and Perkins) + isobar model — see Feinberg 1981) explained pion production in terms of 'fireballs', based upon the model of Cocconi *et al.* (1961).

The energies of cosmic ray particles that initiate E.A.S. are essentially beyond the range of current (man-made) accelerators (CM energy < 1.8 TeV, corresponding to a cosmic ray particle energy $< 4\times10^{14}$eV). As a result, it is necessary to invoke 'scaling' models, based upon the hypothesis of Feynman (1969), in order to extrapolate results obtained by particle accelerators under controlled conditions up to the cosmic ray particle energies being considered.

Three forms of scaling have been distinguished, namely

(i) Limiting Fragmentation (Benecke *et al.* 1969)

(ii) Feynman Scaling (Feynman 1969)

(iii) Radial Scaling (Yen 1974)

Limiting fragmentation applies in the limit $\sqrt{S} \rightarrow \infty$ (CM energy), and only to those secondary particles with a significant fraction of the available CM momentum. This case follows from both Feynman and radial scaling in this limit.

Ideally, scaling should hold at infinite energies. However, it is generally assumed that achieved accelerator energies are sufficiently high to reach the limiting case, with scaling believed to set in at energies as low as $\sim 10^{11}$eV (e.g. Bøggild *et al.* 1971).

For the inclusive case (i.e. a two nucleon interaction, in which the products are a hadron plus numerous unobserved particles), the Lorentz invariant cross-section is generally expressed in terms of the CM energy E_o, the transverse momentum of the particle p_t, and a dimensionless variable x, namely

$$E_o \frac{d^3\sigma}{dp^3} = f(x, p_t, S) \tag{2.2}$$

Scaling assumes that these cross-sections are independent of the energy for a given

value of x. An alternative interpretation of scaling is that the number of high energy particles with fractional energies $x \geq 0.1$ produced in nucleon-nucleon interactions is independent of the primary energy, where x is defined as below.

For Feynman scaling,

$$x = x_F = \frac{p_t}{p} \tag{2.3}$$

where p is the maximum possible momentum of the particle. For radial scaling,

$$x = x_R = \frac{2E_o}{\sqrt{S}} \tag{2.4}$$

These cases differ only in the central region, corresponding to relatively low energy particles, where the predictions of radial scaling are more accurate. In the limit $\sqrt{S} \rightarrow \infty$, these cases produce identical results, and predict multiplicities to behave as

$$< n > \propto \ln E \tag{2.5}$$

The early statistical model of Fermi (1951) predicts

$$< n > \propto E^{\frac{1}{4}} \tag{2.6}$$

while other models predict multiplicities as high as

$$< n > \propto E^{\frac{1}{2}} \tag{2.7}$$

(e.g. Chantler *et al.* 1982)

which is the limiting case where the secondary particles share the energy equally in the CM system.

Following the scaling hypothesis (Feynman 1969), observations in both cosmic ray studies (e.g. Yodh *et al.* 1972, Dawson *et al.* 1986), and accelerators (Armaldi *et al.* 1977) suggested that the interaction cross-sections were not constant, but increased with energy ($\propto \ln^2 S$), a result recently confirmed at $\sqrt{S} = 1.8$ TeV by Amos *et al.* (1989) using the Fermilab Tevatron, leading to the conclusion that the inclusive cross-section is not invariant, and therefore the application of Feynman scaling is not valid in this context.

For scaling to be valid at $\sim 10^{15}$eV, it has been suggested (Olejniczah *et al.* 1977) that the primary mass composition of the cosmic ray beam would have to be very different to that at lower energies. As discussed in 1.3.2, there is evidence for an increasing dominance of iron with energy, and the extrapolation of these lower energy data suggest that iron should dominate the composition at $\sim 10^{15}$eV which would be consistent with minimal scaling violation (Yodh *et al.* 1984). It has been shown (Hillas 1979) that models assuming both an increasing nuclear cross-section and an increasing iron content in the primary beam with energy explain a range of E.A.S. properties (though not all of the observed properties) when based upon radial scaling. More recent work by Ren *et al.* (1988) using emulsion chambers suggests that the assumption of Feynman scaling in the fragmentation region and a heavy enriched primary composition ($\sim$ 14% protons, $\sim$ 40% iron) is compatible with experimental results at $\sim 10^{16}$eV.

In contrast to these results, Wdowczyk and Wolfendale (1983b, 1987) suggest that 10^{15}eV E.A.S. data are consistent with a proton-dominated composition, and propose a scale-breaking model (SBM) with similar composition to that observed at lower energies. Wdowczyk and Wolfendale (1987) quote recent accelerator results in support of such scaling violation. The overall situation is somewhat confused by the fact that the observable parameters of E.A.S., from which much of this information is derived, are more sensitive to the primary mass spectrum than to the interaction model in question (e.g. Chantler *et al.* 1982). It is also confused by the use of differing Monte Carlo models used by each group (see e.g. Holynski 1990 for a summary of these problems). Only when the use of a standard Monte Carlo model by all groups occurs will some of these controversies be solved (Holynski 1990).

In the case of a nucleus-initiated E.A.S. (as opposed to the proton-initiated case considered so far), the superposition model of de Beer *et al.* (1966) is generally applied, in which the primary particle of energy E, and mass number A, is considered to behave as A individual protons, each with energy E/A. This model does not take into account the shielding of nucleons in the nucleus which, as a result, leads to the overestimation of the rate of shower development and the underestimation of fluctua-

tions in shower development (Dixon *et al.* 1974). This model is, however, considered sufficient as a means for the calculation of average shower characteristics (Tomaszewski and Wdowczyk 1975).

The nuclear component of E.A.S. consists of the primary particle, plus those secondary particles produced in the fragmentation region, and from subsequent interactions. Those hadrons surviving to ground level possess only a small transverse momentum, and are therefore found within a few metres of the E.A.S. 'core' (defined by the trajectory of the initiating cosmic ray particle). This narrow distribution results from the relatively large masses and energies of these particles which effectively minimises any Coulomb scattering (in addition to the transverse momentum of creation). These particles comprise $\sim$ 1% of the E.A.S. particle number at ground level, but are nevertheless important, as they provide a continual energy flow into the muon and electromagnetic components until ionisation and other energy loss processes begin to dominate (see 2.4).

2.3 Muon Component

Muons are charged, sub-atomic particles ($\mu^{\pm}$, $m_{\mu^{\pm}} \sim 106$ MeV) produced in E.A.S., mostly as a result of the decay of charged mesons ($\pi^{\pm}$, $K^{\pm}$ — see 2.2). Small contributions to the muon content of E.A.S. are also made by pair production (i.e. $\gamma \rightarrow \mu^{+}\mu^{-}$, threshold $\sim$ 212 MeV), and the photo-production of pions (i.e. $\gamma \rightarrow \pi^{+}\pi^{-}$), which subsequently decay to produce low energy muons. The contribution of the latter process is predicted to become significant for primary particle energies $> 10^{18}$eV (McComb *et al.* 1979).

The mean lifetime of muons in the rest frame is $t_{\frac{1}{2}} \sim 2.2 \times 10^{-6}$s (Barish-Schmidt *et al.* 1976), implying that those travelling with a Lorentz factor > 20 will reach sea-level before decaying. Less energetic muons will decay in flight, contributing to the electromagnetic component of the E.A.S. (i.e. $\mu^{+} \rightarrow e^{+} + \nu_e + \overline{\nu}_{\mu}$, $\mu^{-} \rightarrow e^{-} + \overline{\nu}_e + \nu_{\mu}$).

Muons belong to the class of subatomic particles known as leptons, which do not

interact through the strong force with other particles. They possess small interaction cross-sections for both radiation and pair production processes. Their charged nature results in ionisation being the dominant energy loss mechanism in traversing the atmosphere ($\sim$ 2 MeV $(gcm^{-2})^{-1}$ — Allan 1971). Thus, high energy muons (E > 2 GeV), which result from the decay of pions produced early in the shower survive to sea-level, conveying important information about the early E.A.S. particle interactions to sea-level, revealing compositional information at energies well above those accessible by satellite or balloon-borne detectors (see e.g. Elbert and Gaisser 1979; Elbert and Sommers 1987).

The attenuation length of the muon component in E.A.S., λ_μ ($\sim$ 1000 gcm^{-2}), is approximately five times that of the electromagnetic component (Hara *et al.* 1983), as a result of the small energy loss rate. This implies that the muon flux observed at sea-level is essentially an integral of the muon production over the entire shower path, containing not only information on the development of the nuclear cascade. Also, it is affected to only a minor degree by fluctuations in shower development. This is in contrast to the electromagnetic component (see 2.4), where sea-level particles are the products of relatively recent, local interactions, not related to the overall E.A.S. development, but strongly affected by fluctuations in shower development.

The lateral spread of muons measured at ground level is a result of the transverse momentum of the parent pions and kaons, combined with the height of production. The magnitude of the transverse momentum itself is small, but the large height of production results in a large lateral spread with a median value of $\sim$ 300m (Allan 1971). The sea-level lateral distribution function is much flatter than that of the electromagnetic component (see 2.4) and is given by

$$\rho_\mu(N,r) \propto r^{-\frac{3}{4}} \left(1 + \frac{r}{k(s,\theta)}\right)^{-\frac{5}{2}} \qquad (2.8)$$

Greisen (1960)

where k is a function of both the shower age (s) (see 2.4) and zenith angle (θ) (Hara *et al.* 1983).

Muons are numerically smaller in E.A.S. than the electromagnetic component (typically $\sim$ 10% and 90% respectively for primary energies E $>$ 10^{14}eV), but with an average sea-level energy of $\sim$ 5 GeV (median $\sim$ 1 GeV) compared with $\sim$ 200 MeV (median $\sim$ 30 MeV) for the electromagnetic component (Allan 1971), the muons in a typical shower carry more total energy at sea-level than the electromagnetic component.

The large penetrating power of muons compared with the electromagnetic component of E.A.S., (leading to the description as the 'hard' component) requires measurements to be made by particle detectors covered by a sizable thickness of dense material in order to shield out the less-penetrating electromagnetic component. This is usually achieved by locating the detectors underground, either burying them or locating them in mines, utilising the overburden of rock or soil as a shield.

In the case of lower energy primary cosmic rays (e.g. 10^{11}eV $<$ E $<$ 10^{14}eV), the muon component is the only component of the E.A.S. to reach sea-level in observable numbers. These so-called 'unaccompanied' muons comprise the majority of the particle flux at sea-level, with the total flux being

$J = (1.44 \pm 0.09) \times 10^{-2}$ cm^{-2}s^{-1}

~ 1 cm^{-2}min^{-1} (Allkofer *et al.* 1975)

Knowledge of this flux is useful in calibrating both detector counting rates and particle numbers (see 3.3.1).

The strong penetration of muons also results in a relatively broad zenith angle dependence of the flux, given by

$$J(\theta) \propto \cos^n \theta \tag{2.9}$$

where $n = 2.1 \pm 0.1$ (Crookes and Rastin 1971) (c.f. $n \sim 8$–9 for the electromagnetic component — see 3.4.1).

2.4 Electromagnetic Component

The electromagnetic component of E.A.S. is the most numerous comprising $\sim$ 90% of the particles in E.A.S. detected at ground level corresponding to primary cosmic ray particle energies $> 10^{14}$eV. Below this energy (comprising the bulk of the primary cosmic ray flux — see Fig 1.1), the electromagnetic component of the corresponding E.A.S. is absorbed high in the atmosphere, leaving only unaccompanied muons to reach ground level (as discussed in 2.3).

In contrast to the nuclear cascade, the processes involved in the production of the electromagnetic cascade are relatively well understood (e.g. Rossi and Greisen 1941). The decay of neutral pions ($\pi^\circ \rightarrow \gamma\gamma$) created by the nuclear cascade of the E.A.S. (see 2.2) is the major source of the electromagnetic component. Each γ-ray photon produced will undergo pair production ($\gamma \rightarrow e^+e^-$) in the presence of an atmospheric nucleus. These secondary electrons[1] subsequently interact through either collisions (the ionisation or excitation of an atmospheric atom), or by radiation (Bremsstrahlung 'braking radiation' in which photon emission results from particle acceleration in the field of a nucleus). The secondary photons thus produced will then interact through either further pair-production, Compton scattering, or the photo-electric effect. A succession of these interactions (predominantly pair-production and Bremsstrahlung initially) results in a cascade of particles and photons with the multiplication of particles and the degradation of particle/photon energy after each interaction. This cascading process continues until the size of the E.A.S. has reached a maximum, after which particle loss rates begin to outweigh particle creation rates.

For electrons, this occurs when the average particle energy drops below the critical energy (E_c), where Bremsstrahlung and ionisation energy loss rates are identical, with $E_c \sim 80$ MeV (Rossi and Greisen 1941). Above this energy, electrons have a mean free path of one radiation length, $X_o = 37.15$ gcm^{-2} (Linsley 1985b). Below this critical energy, ionisation becomes the dominant energy loss process for electrons, and the shower

[1] electrons will be assumed to imply electrons and positrons for the remainder of this section.

size rapidly decreases. Similarly, as the average energy per photon drops, Compton scattering, and then the photo-electric effect become progressively more dominant than pair-production, with a critical energy $E_c \sim 20$ MeV (Rossi and Greisen 1941), above which pair-production is dominant, with a mean free path of $\frac{9}{7}X_o$. The similarity of the mean free paths of these mechanisms is not pure coincidence, but is a reflection of their similar nature when treated by the theory of quantum electrodynamics (Q.E.D.).

A simple model of an electromagnetic cascade (Allan 1971), based solely upon Bremsstrahlung and pair-production processes above shower maximum (known as 'Approximation A' — Rossi 1952), has been found to provide useful results. In this model, it is also assumed that the mean free path of both of these processes are the same, and equal to X_o. The initiating γ-ray photon of energy E_o triggers an electromagnetic cascade in which the energy is subdivided equally amongst the secondary particles[2] resulting from both of these processes. The shower unit, X_r, is defined to be the distance in which there is a 50% probability of either of these processes occurring. Thus

$$\exp\left(\frac{-X_r}{X_o}\right) = 0.5 \tag{2.10}$$

which may be expressed more conveniently as

$$X_r = X_o \ln 2 \tag{2.11}$$

The number of particles present is therefore doubled, and the average energy per particle halved after every shower unit (~ 30 gcm^{-2}). Thus, after n interactions, the expected number of secondary particles would be

$$N = 2^n \tag{2.12}$$

with an average particle energy E, given by

$$E = \frac{E_o}{2^n} \tag{2.13}$$

[2]It will be assumed that within the discussion of this model the term 'particles' will refer to both particles and photons.

This multiplication of particles, and subdivision of energy continues until the shower maximum is reached. This occurs when this average particle energy equals the critical energy, E_c, i.e.

$$E = \frac{E_o}{2^n} = E_c \tag{2.14}$$

and hence

$$N_{max} = \frac{E_o}{E_c} \tag{2.15}$$

At this stage, ionisation energy losses become comparable with those resulting from Bremsstrahlung, and ionisation losses begin to dominate, resulting in a rapid decline of the particle flux. For the secondary photons, Compton scattering cross-sections become important, as do photo-electric cross-sections at a yet lower energy.

Combining Eq 2.11 with Eq 2.14, the depth of maximum, X_{max}, may be given by

$$X_{max} = nX_r = X_o \ln\left(\frac{E_o}{E_c}\right) \tag{2.16}$$

Despite the relatively simplistic nature of this model, the estimate for X_{max} has been found to be 'remarkably accurate' (Allan 1971). In addition, several important and essentially correct conclusions may be drawn, which are borne out by more detailed models. These include the initial exponential growth of the cascade, the proportionality of shower size at shower maximum N_{max} with the initial photon energy, E_o, the proportionality of the depth of shower maximum, X_{max}, with $\ln E_o$, and the rapid attenuation of particles beyond shower maximum.

However, such a model is still an oversimplification of the real situation. It does not take into account the distribution of particle energies at a given depth which in reality is such that lower energy particles become more abundant (Rossi 1952), while in the model they are assumed to be equal. In addition, random fluctuations in particle numbers are ignored, when they are, in fact, a significant factor in shower development (see e.g. Clay 1985). Ionisation is a significant though not dominating factor in shower development prior to shower maximum and should also be included.

Through the use of such models, the development of the electromagnetic component as it propagates through the atmosphere has been studied. Including an ionisation

factor of $\sim$ 80 MeV per radiation length prior to shower maximum (known as 'Approximation B' — Rossi 1952) leads to the relatively accurate description of the longitudinal development derived by Greisen (1956), with particle number, N_e, being described as a function of the initiating photon energy E_o, and the atmospheric depth of observation, t, by

$$N_e(E_o, t) = \frac{0.31}{\sqrt{t_{max}}} \exp(t[1 - \ln s]) \tag{2.17}$$

where

$t_{max} = \ln \frac{E_o}{E_c}$ (depth of maximum),

and $s = \frac{3t}{t+2t_{max}}$ (shower age),

with all depths expressed in terms of radiation lengths.

The shower age, s, characterises an electromagnetic cascade (e.g. Rossi and Greisen 1941; Cocconi 1961), and describes the state of shower development. Shower age is defined to be zero at the start of development, monotonically increasing to a value of one at shower maximum, and continuing to increase past shower maximum, reaching a value of two when one particle remains. Typical experimentally observed ages of E.A.S. electromagnetic components lie within the range (0.5 - 2.0) (e.g. Stamenov 1987).

Past shower maximum, the electromagnetic cascade is attenuated with an attenuation length, $\lambda_{em} \sim 130$ gcm^{-2} (Cocconi 1961).

The electromagnetic component of an E.A.S. initiated by a cosmic ray particle (as opposed to a photon) is considered to be approximated by the superposition of such electromagnetic cascades, continually fed into the E.A.S. through the production (and subsequent decay) of neutral pions (π^o) by the nuclear cascade. This leads to a more gradual development and decay compared to a photon-initiated shower (see 2.5 for a more detailed discussion of these differences), with a deeper shower maximum, and an attenuation length, $\lambda_{cr} \sim 200$ gcm^{-2} (e.g. Bird and Clay 1990b).

2.4.1 Lateral Distribution

Whereas the longitudinal development of E.A.S. provides more direct information than the study of the lateral distribution of E.A.S. particles, only experiments such as the Fly's Eye (e.g. Cassiday 1985) image the former distribution directly. For the majority of E.A.S. experiments, the detection and interpretation of E.A.S. at ground level is based upon the sampling of the lateral spread of E.A.S. particles at a number of discrete points, in terms of both arrival times and particle numbers. From these measurements, it is possible to deduce information about both the E.A.S. and the initiating primary particle, through the determination of shower parameters such as the shower 'core' position (x, y), the shower age (s), and the shower size (N_e). To achieve this, a model of the lateral distribution is necessary.

The most important contribution to the lateral spread of the electromagnetic component is made by Coulomb scattering. The angle of scatter $\delta\theta$, is related to the particle energy E, and the thickness of scatterer δt, by the relation

$$< \delta\theta^2 >= \left(\frac{E_s}{E}\right)^2 \delta t \tag{2.18}$$

(Rossi and Greisen 1941)

where $E_s = 21$ MeV (Cocconi 1961). This leads to the natural unit of lateral displacement, the Moliére unit, r_o, given by

$$r_o = X_o \frac{E_s}{E_c} = 9.5 \ \ \mathrm{gcm}^{-2} \tag{2.19}$$

which is obviously altitude dependent, in converting to metres.

It is clear from this argument that the angle of scatter is inversely proportional to energy, implying that lower energy particles will be found further from the shower 'core' and, due to the longer trajectories produced by the multiple scattering, these particles will tend to lag longitudinally behind the higher energy particles in the shower-front.

This leads to the representation of an E.A.S. as possessing a shallow disk shape with a radius of curvature $\sim$ 1 km, moving through the atmosphere at essentially the speed of light. The thickness of the shower-front is typically $\sim$ 2m, but increases with

distance from the shower 'core' as a result of the variable multiple scattering of these particles. It has been suggested (Linsley 1983) that the dispersion of these more distant particles can be utilised to determine shower size, the corresponding primary particle energy, and core distance, for large showers through the use of mini-arrays (see e.g. Sokolsky 1987 and references therein).

For E.A.S. initiated by primary cosmic rays of energy $\sim 10^{15}$eV, shower maximum will occur fairly high in the atmosphere (e.g. Thornton and Clay 1981), and at sea-level the E.A.S. will have developed well past maximum, with a useful lateral extent of $\sim$ 100m.

Lateral distribution functions, describing the density of E.A.S. particles (particles per m^2), as a function of distance from the shower core, r, (and the shower size N_e) have been found to be of the form

$$\rho(N_e, r) = \frac{N_e}{r_o^2} f\left(\frac{r}{r_o}\right) \tag{2.20}$$

where $f\left(\frac{r}{r_o}\right)$ is known as the lateral structure function.

The most commonly applied lateral distribution function (although its application has recently come under question) is the NKG function (Nishimura-Kamata-Greisen) which is an empirical approximation by Greisen (1956) to the theoretical expression for a purely electromagnetic cascade of Nishimura and Kamata (1951). The structure function of the NKG function is given by

$$f_{\mathrm{NKG}}\left(\frac{r}{r_o}\right) = C(s)\left(\frac{r}{r_o}\right)^{s-2}\left(\frac{r}{r_o}+1\right)^{s-4.5} \tag{2.21}$$

where the coefficient, $C(s)$, is defined as

$$C(s) = \frac{\Gamma(4.5-s)}{2\pi\Gamma(s)\Gamma(4.5-2s)} \tag{2.22}$$

The Moliére radius, r_o, is assumed to have the value of $r_o \sim$ 79m at sea-level (Greisen 1960), although Greisen (1956) showed that the lateral spread of the E.A.S. is influenced by atmospheric conditions two radiation lengths higher in the atmosphere than those at the level of sampling, implying that this value of the Moliére unit may need to be modified.

A variety of techniques are employed to determine the basic E.A.S. parameters (s, N_e, (x, y), (θ, ϕ) (arrival directions)) by fitting the NKG function (or a similar lateral distribution function) to the data. This usually involves firstly reducing the dimensionality of the problem (e.g. determination of the arrival direction (θ, ϕ) firstly using fast-timing — see 3.3.1; 3.3.2), and then applying some sort of minimisation technique to determine the parameters corresponding to a best fit to the data (see Erlykin 1990 and references therein for a summary of the techniques currently employed).

Deficiencies in the NKG function have been revealed by both experimental and theoretical results, primarily in the value of the Molière radius and the usage of a single age parameter.

The results of calculations by Hillas and Lapikens (1977), and more recently by Fenyves *et al.* (1988) suggest that the electromagnetic lateral distribution function is somewhat narrower than that of the NKG function, corresponding to a median radius $\sim 0.5 r_o$. This is supported by the work of Lagutin *et al.* (1979), who suggest an age dependence of the median radius, given by

$$r_m = (0.78 - 0.4s) r_o \tag{2.23}$$

and van der Walt (1988), who suggests a similar dependence,

$$r_m = (1.254 - 0.499s) r_o \tag{2.24}$$

The general result that the lateral distribution function of the electromagnetic component of E.A.S. is narrower than that suggested by the Moliére radius is now generally (but not universally) accepted (see Erlykin 1990 and references therein).

Capdevielle and Gawin (1982) suggest that using the NKG function leads to a contradiction between the longitudinal age (the 'correct' age of the shower), and the lateral age (the age deduced from the lateral distribution), with the lateral age being consistently smaller. They suggest the use of a local age parameter, $s(r)$, from which the longitudinal age parameter may be deduced. van der Walt (1988) suggests the application of techniques such as the maximum likelihood method as opposed to those

suggested by Capdevielle and Gawin (1982) due to the inability of the latter to take into account zero densities recorded.

The overall situation involving the relationships between these shower parameters is still far from clear, requiring further theoretical and experimental work (Erlykin 1990).

2.5 Gamma-Ray Initiated Showers

It is appropriate within a discussion of E.A.S. to review the criteria and current status of both theoretical and experimental results in differentiating hadron-initiated E.A.S. from photon-induced E.A.S. Any successful technique for doing so will assist in increasing the appalling signal-to-noise ratio present in U.H.E. γ-ray astronomy, resulting from the comparatively strong and almost uniform flux of hadron-induced showers.

Apart from primary cosmic ray particles, U.H.E. γ-rays[3] are also capable of initiating an E.A.S., which should be an electromagnetic cascade of the type discussed in 2.4. The absence of a nuclear component providing a continual flow of energy into this electromagnetic component, combined with the small photo-nuclear cross-sections leads to the expectation that such photon-initiated E.A.S. should be characteristically different to hadron-initiated E.A.S. Most notably, the muon content and shower age would be expected to differ. Following is a discussion of a number of methods used to improve the signal-to-noise ratio of U.H.E. γ-ray initiated E.A.S. from the hadron-initiated E.A.S. background, highlighting the current conflicts between theory and experiment, and even between different experiments.

2.5.1 Muon Content

It has long been expected that γ-ray initiated E.A.S. should be less efficient at producing muons than hadron-initiated E.A.S. by a factor of ~ 10 (e.g. Maze and Zawadski 1960; Karakula and Wdowczyk 1963; Braun and Sitte 1965; Wdowczyk 1965). This re-

[3]It will be assumed for the majority of this discussion that U.H.E. γ-rays are responsible for the observed signals. See 1.5.2 for a brief discussion of the alternatives.

sults from the 'standard' picture of particle interactions in which the photo-production cross-section is approximately 200 times smaller than the proton inelastic cross-section in air at several GeV, and based upon the assumption that both of these cross-sections increase logarithmically with the interaction energy (Stanev 1986).

Early experimental investigations (e.g. Firkowski *et al.* 1961; Kamata *et al.* 1968; Gawin *et al.* 1968) confirmed the existence of such muon-poor showers which were attributed to γ-rays. However, it was also realised that other explanations may be invoked to explain muon-deficiencies, such as extreme upward fluctuations in neutral pion (π°) multiplicities, leading to a larger electromagnetic component (Maze *et al.* 1969). These early observations have recently been confirmed by the Tien Shan group (Nikolsky *et al.* 1987), who also included a hadron deficiency criteria in their analysis in order to primarily detect U.H.E. γ-ray initiated E.A.S. These events were found not to be coincident with Cygnus X-3 or the Crab Nebula (two suspected strong sources of U.H.E. γ-rays), but appear as a diffuse flux originating primarily at high galactic latitudes. Unfortunately, the low number of actual events detected prevents any significant conclusions being drawn.

Contrary to these results, the E.A.S. attributed to γ-rays from Cygnus X-3 observed by the Kiel group (Samorski and Stamm 1983a), contained a relatively high muon content for γ-ray initiated showers, $\sim$ 77% that of 'normal' E.A.S. (Samorski and Stamm 1983b). Similarly, excess events detected from the direction of the Crab Nebula (Dzikowski *et al.* 1983) were also found to contain a relatively high muon content, $\sim$ 60% that of 'normal' E.A.S.

These experimental results prompted contemporary calculations using updated hadronic interaction models (e.g. Gaisser *et al.* 1983), which essentially confirmed the early result of $\sim$ 10% of the muon content for γ-ray initiated E.A.S. compared to proton-initiated E.A.S. in the primary energy range (10^{15} – 10^{17}eV) (Edwards *et al.* 1985; Stanev *et al.* 1985). More recent Monte Carlo simulations (Stanev *et al.* 1990) suggest that in the shower size range, 4×10^4 – 2×10^5, fluctuations in muon numbers act to increase the differences in muon content. It was concluded that it should be very

hard for a photon-initiated shower to imitate a proton-initiated shower (Fegan 1990). By way of partial explanation, Stanev *et al.* (1985) suggested that $\sim 1/3$ of the observed muon content may result from γ-rays penetrating the heavy detector shielding and being registered as muons.

More recently acquired results continue to contradict one another as well as theoretical predictions. The Akeno group detected events from the direction of Cygnus X-3, modulated by the 4.8 hour binary period, only after applying a muon-poor cut to their data (Kifune *et al.* 1986c). Reducing the significance of this cut reduced the significance of this signal. The phase of emission and intensity were also in contradiction to the earlier observations of Cygnus X-3 (Samorski and Stamm 1983a, 1983b; Lloyd-Evans *et al.* 1983), but are consistent with TeV and more recent PeV observations (see e.g. Protheroe 1987a). Furthermore, the BASJE collaboration reported excesses from Vela X-1 and Centaurus X-3 based upon the detection of muon-poor E.A.S. (Suga *et al.* 1985).

In contradiction to these observations are the results of the Cygnus group (Yodh 1988) who have detected an anomalously high muon content from Cygnus X-3 (Dingus *et al.* 1988a) at a significant, but not compelling statistical level, and pulsed emission from Hercules X-1 (Dingus *et al.* 1988b) of a higher significance containing a muon content an order of magnitude higher than that expected from conventional V.H.E. and U.H.E. γ-ray E.A.S. To date, the experimental situation remains confusing, and it is not currently obvious how to incorporate all of these observations into a consistent theory. Hopefully, the CASA (Chicago Air Shower Array) (Gibbs *et al.* 1990), due to be on-line in early 1991, with its unprecedented angular resolution, and the associated Michigan muon detector, will provide a resolution to some of these inconsistencies.

Several explanations have been proposed for the anomalously high muon content observed by Samorski and Stamm (1983b) and Dingus *et al.* (1988a, 1988b). The most obvious conclusions are that our understanding of interactions at PeV energies is severely deficient, or that the primary particles involved are not γ-rays (see 1.5.2 for a brief discussion of this latter possibility).

The observation of pulsed emission from Hercules X-1 at TeV energies implies a rest mass < 1.3 MeV (Fegan 1990) for the particles responsible, based upon time dilation dispersion effects. However, Hillas (1985) showed that if the mean free path for photo-production by γ-rays is increased above $\sim$ 1 TeV, then several anomalies, including the muon content of these E.A.S., can be explained. Along these lines, Drees and Halzen (1988) (and Halzen 1990) have proposed a theory invoking the gluon content of high energy photons, suggesting this effect may produce a dramatically larger photo-production cross-section than 'conventional' theories at energies > 10 TeV, and thus may explain the high muon content in some γ-ray initiated E.A.S. Nagle *et al.* (1988) suggest that there are still some problems to be overcome before this effect can be claimed with any confidence.

2.5.2 Shower Age Parameter

The development of an U.H.E. γ-ray initiated E.A.S. is essentially that of an electromagnetic cascade, as described in 2.4. The U.H.E. γ-ray initiated E.A.S. will develop and be attenuated faster than the electromagnetic component of a corresponding hadron-initiated E.A.S., as the latter is continually replenished during its passage through the atmosphere by the decay of neutral pions produced by the nuclear component throughout the atmosphere. In addition to this effect, the mean free path for γ-rays upon entering the atmosphere is smaller than that for protons. Hence, on average, γ-ray E.A.S. are expected to be initiated earlier and to maximise earlier in the atmosphere, resulting in 'older', flatter lateral distributions at ground level, than for comparable hadron-initiated E.A.S. of the same shower size. Gawin *et al.* (1968) found that the muon-poor showers they detected possessed a mean age of $\sim$ 1.4, compared to $\sim$ 1.2 for 'normal' showers. However, the origin of these E.A.S. could not be attributed to γ-rays with certainty.

Age cuts have been applied, and in some cases been crucial, to the reported excesses in emission from a number of U.H.E. γ-ray sources. Samorski and Stamm (1983b) found a DC excess in events from Cygnus X-3, based upon an age cut, selecting E.A.S. with

shower ages $s \geq 1.1$. It is interesting to note that the confirming observation of Cygnus X-3 (Lloyd-Evans *et al.* 1983) was made without an age cut. The Akeno observation (Kifune *et al.* 1986c) did not produce a significant result when an age cut was applied, but it is possible that this may reflect a triggering bias inherent in the array, resulting in the exclusion of older showers. Similarly, an age cut $s \geq 1.3$ was necessary in order to obtain a phase enhancement in the periodic emission from Vela X-1 by Protheroe *et al.* (1984). van der Walt (1987) also obtained a maximum signal from Vela X-1 with a similar age cut. Additional observations by the BASJE collaboration of Vela X-1 and Centaurus X-3 were based upon both muon and age cuts (Suga *et al.* 1985), as were the observations of Cygnus X-3 by Tonwar *et al.* (1988), and the recent observations of the Crab Pulsar at 200 TeV (Gupta *et al.* 1990), and Cygnus X-1 at 100 TeV (Khristiansen *et al.* 1990). The actual value of the age cut applied is obviously dependent upon the altitude (atmospheric depth) of detection.

In the observation of U.H.E. γ-rays from LMC X-4 (Protheroe and Clay 1985), no age cut was applied due to the relatively large zenith angles of the source. This broadens the age distribution, causing an increased overlap with the age distribution of the background cosmic rays, rendering the age cut less useful.

The validity of applying age cuts in order to enhance a signal has been questioned by Fenyves (1985) whose Monte Carlo simulations suggested that the age parameter cannot be used to effectively discriminate between U.H.E. γ-ray initiated E.A.S. and cosmic ray particle initiated E.A.S. Hillas (1987) and Cheung and MacKeown (1988) confirmed these results with other simulations, suggesting that the average age of U.H.E. γ-ray initiated E.A.S. may be slightly less than that of cosmic ray particle initiated E.A.S. of the same primary energy. The results of Nikolsky *et al.* (1987) are interesting in light of these calculations, as their observations of muon-poor showers not only agree with those made two decades previously, but also consisted of E.A.S. with an average age slightly smaller than 'ordinary' E.A.S. In addition, calculations also indicate that photon-induced showers posses a narrower age distribution as a result of the small value of the radiation length (~ 37 gcm^{-2}), compared to the interaction

lengths of protons and pions ($\sim 80 - 120$ gcm^{-2}) (Fegan 1990).

Hillas (1987) also suggested that age selection may be a disguised zenith angle selection, but re-examination of the Vela X-1 data by Edwards (1988) found no zenith angle bias in comparison to background events.

Overall, it must be concluded that, contrary to current theoretical predictions, the preferential selection of older showers in certain instances seems to enhance the signal-to-noise ratio significantly. It is perhaps comforting to note that these theoretical predictions also fail to reproduce the experimentally observed cosmic ray E.A.S. age distributions (Tonwar *et al.* 1988).

Due to the rather uncertain and controversial nature of the methods just discussed to increase the signal-to-noise ratio in U.H.E. γ-ray signals, significant emphasis is placed on improving this ratio through more conventional (and well understood) methods, such as improving the angular resolution of the array being used, and searching for a periodic modulation of the signal.

2.5.3 Angular Resolution and Period Searches

The most direct method in which to search for evidence of U.H.E. γ-ray emission is to search for an excess of E.A.S. events from a given direction in the sky, above the nearly uniform background of cosmic ray E.A.S., thus utilising the neutral nature of the source radiation. To date, however, only a minority of sources have been detected directly as an excess of events, and these only marginally (e.g. Cygnus X-3 (Samorski and Stamm 1983a, 1983b), Crab Nebula (Acharya *et al.* 1990)), due to the intrinsically weak flux of photons which results in poor sampling statistics, combined with relatively poor angular resolutions.

Improving the angular resolution by a factor of two has the impact of reducing the background by a factor of four, so optimising the angular uncertainty of the E.A.S. array being used is critical. Edwards (1988) has reviewed the major factors contributing to

the angular resolution of an E.A.S. array in terms of array and detector design, and data analysis techniques. The angular resolution of an E.A.S. array may also be significantly improved, especially for larger E.A.S. by replacing the standard plane shower-front fit used to determine the E.A.S. arrival direction (see 3.3.2) with a curved shower-front fit, which more accurately approximates the true shower-front shape (see e.g. Ciampa 1988).

Despite such improvements to the angular resolution (and hence signal-to-noise ratio), the detection of DC excesses of events remain conspicuous by their absence in significant numbers. If no DC excess is detected from a suspected source (and even in the cases when such an excess is detected), one must search for emission modulated by a source period for the cases where such emission is considered possible (e.g. pulsars or X-ray binary systems).

To date, the majority of claimed U.H.E. γ-ray detections have been based upon the detection of a periodic modulation in emission, based mostly upon ephemerides determined by measurements at other wavelengths (e.g. radio (pulsars), and X-ray (X-ray binary systems) wavelengths). Such methods assume similar production methods, or similar mechanisms operating to produce such a modulation (usually a rotational or orbital period of some type). In at least one case, this assumption has been found not to be valid (Hercules X-1, where the period observed by three different groups differs by 0.16% from the observed X-ray period — see Protheroe 1987a). In addition, there is a strong reliance on emission over a limited range in phase in order to increase the sensitivity, and the necessity of a well-determined ephemeris (period P, and its time derivative $\dot{P}$) in order to avoid smearing the phase of emission, when considering the long time intervals over which such studies are carried out. Light-curve information is also useful in determining the appropriate circular statistical test to be applied (see e.g. 6.2.2; Protheroe 1987b for a discussion).

2.5.4 Summary

The current status of the differentiation between U.H.E. γ-ray and cosmic ray initiated E.A.S. remains unclear. Theoretical and experimental results are in conflict in both the use of muon-poor cuts, where theory predicts a muon-deficiency not observed by some experiments, and cuts based upon the E.A.S. age parameter, where recent calculations suggest E.A.S. age cuts are essentially useless, despite the reliance of some observations on such a cut. The most powerful (and non-controversial) techniques in U.H.E. γ-ray astronomy remain the optimising of E.A.S. array angular resolutions, and the use of known source periodicities.

The characteristics of E.A.S. have been discussed in some detail. In the following chapter, the Buckland Park E.A.S. Array used to collect the data upon which this work is based, will be described in detail.

Chapter 3

The Buckland Park Extensive Air Shower Array — Development and Data Analysis.

3.1 Introduction

The instrument used in the gathering of data used for this thesis was the the University of Adelaide's Extensive Air Shower (E.A.S.) Array, located at the Department of Physics and Mathematical Physics' field station at Buckland Park.

Buckland Park is located in rural surrounds approximately 40 km North of the city of Adelaide, at a latitude of 34°38′ South and a longitude of 138°28′ East. It resides on a coastal plain, near sea-level, at an atmospheric depth of $\sim$ 1030 gcm^{-2}.

The array provides information on E.A.S. through the detection of particles within those showers. Detectors, ranging in area from 0.25 to 2.25 m^2, have 'slow' and/or 'fast' photomultipliers. The 'slow' photomultipliers allow the determination of particle density, and the 'fast' photomultipliers enable fast-timing measurements of the shower-front. Fast-timing measurements allow arrival directions of the showers to be determined. Density measurements allow the determination of shower size and core position, and hence an estimate of the energy of the initiating particle.

3.2 Buckland Park — A Brief History

The original Buckland Park E.A.S. Array began operation in 1972, consisting of components from an array previously operated at Penticton, British Columbia, by the University of Calgary.

It has subsequently experienced several stages of development, each new phase being associated with a change in direction of investigations. A brief discussion of the history of the array and its development follows.

3.2.1 The Original Array

The Buckland Park E.A.S. Array initially consisted of eight particle detectors, each containing a $1m^2 \times 50$ mm slab of plastic scintillator (type NE102), which was viewed by a 'slow' photomultiplier[1] mounted 530 mm below (see 3.3.1 for details of detector operation). This arrangement was enclosed in a light-tight box, internally coated with highly reflective white scintillator paint (type NE560; see Clay and Gregory 1978), to maximise photon detection. Each of these 8 detectors was housed in a semi-permanent 'hut', located at the positions A-H in Fig 3.1. The five central detectors also possessed a 'fast' photomultiplier[2] to provide fast-timing information. The initial array had an enclosed area of $\sim 8100m^2$, a sea-level size threshold of $\sim 2x10^5$ particles, an event rate of $\sim 10^{-3}$ Hz, and an angular resolution of $\sim 2°$.

3.2.2 Development

In 1977, three new detectors (I, J, K — see Fig 3.1) were added to the array, increasing the collecting area for large showers by a factor of ~ 4 (Crouch *et al.* 1981) and providing an upper size threshold of $\sim 10^7$ particles. Each of these detectors were pyramidal in shape (Clay and Gregory 1978), containing a $1m^2 \times 10$ mm slab of plastic scintillator (type NE110), viewed 500 mm above by a 'slow' photomultiplier.

[1] type RCA8055, diameter 120 mm

[2] type Philips XP1040, diameter 120 mm

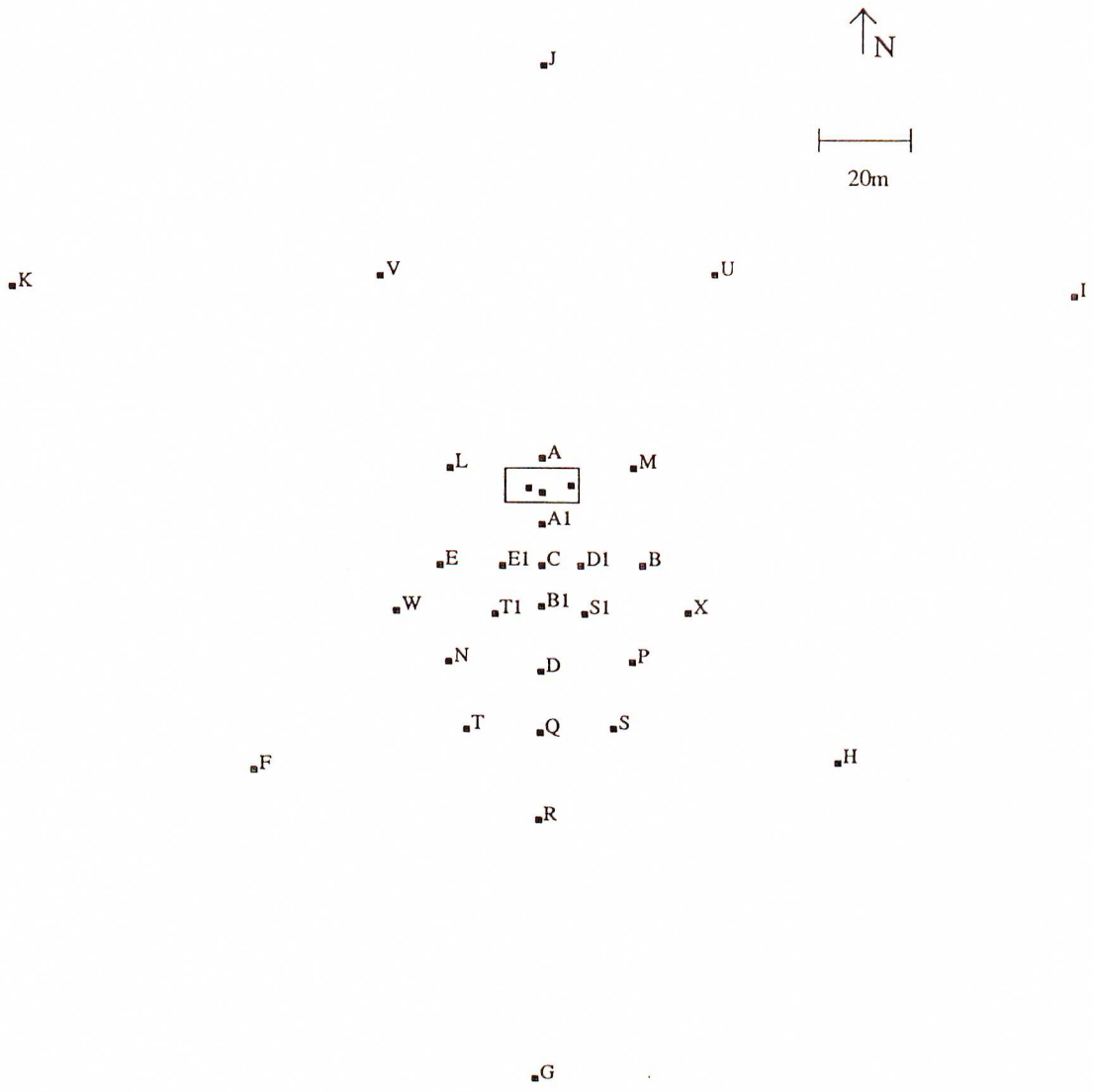

Figure 3.1: The layout of the Buckland Park Extensive Air Shower Array for the period 1984–1989. The three unlabelled detectors are (left to right) RB2, BFD, RB1. They were all contained within the ATCO Electronics Hut (large rectangle). The detector specifications and arrangements are given in Fig 3.2 and Table 3.1.

Detector Label	Type (Fast/Slow)	Position x (m)	Position y (m)	Size (m^2)	Trigger (Fast[4]/Slow[5])	Detector Arrangement[1]
A	F,S	0	22	1	F,S	1
B	F,S	22	0	1	F,S	1
C	F,S	0	0	2.25	F,S	6
D	F,S	0	-22	1	F,S	1
E	F,S	-22	0	1	F,S	1
F	S	-61.5	-43.2	1	—	1
G	S	0	-107.2	1	—	1
H	S	64.8	-40.7	1	—	1
I	S	116	55	1	—	2
J	S	0	130	1	—	2
K	S	-114	56.6	1	—	2
L	F[2],S	-20	20	1	S	3
M	F[2],S	20	20	1	S	3
N	F[2],S	-20	-20	1	S	5
P	F[2],S	20	-20	1	S	5
Q	F[2],S	0	-34.6	1	S	3
R	F[2],S	0	-53	1	S	1
S	F,S	16	-33.8	1	F,S	3
T	F,S	-16	-34	1	F,S	3
U	S	37.6	59.6	1	S	3
V	S	-35.1	59.3	1	S	3
W	F[2],S	-31.3	-9.6	1	S	5
X	F[2],S	32	-9.8	1	S	5
A1	F,S	0	8.5	2.25	F,S	6
B1	F,S	8.5	0	2.25	F,S	6
D1	F,S	0	-8.5	2.25	F,S	6
E1	F,S	-8.5	0	2.25	F,S	6
S1	F[3]	9.4	-10	1	—	3
T1	F[3]	-10.1	-10	1	—	3
RB1	F[3]	6.3	16.4	0.25	—	4
RB2	F[3]	-2.9	15.9	0.25	—	4
BFD	F[3]	0	15	1	—	3

Table 3.1: Detector Specifications for the Buckland Park Extensive Air Shower Array (1984–1989).

Notes:

(1) see Fig 3.2 for detector arrangements.

(2) detector modified to include timing photomultiplier (1986).

(3) timing detector added to array June 1986.

(4) all fast trigger detector thresholds at the 2-particle level.

(5) all slow trigger detector thresholds at the 6-particle level.

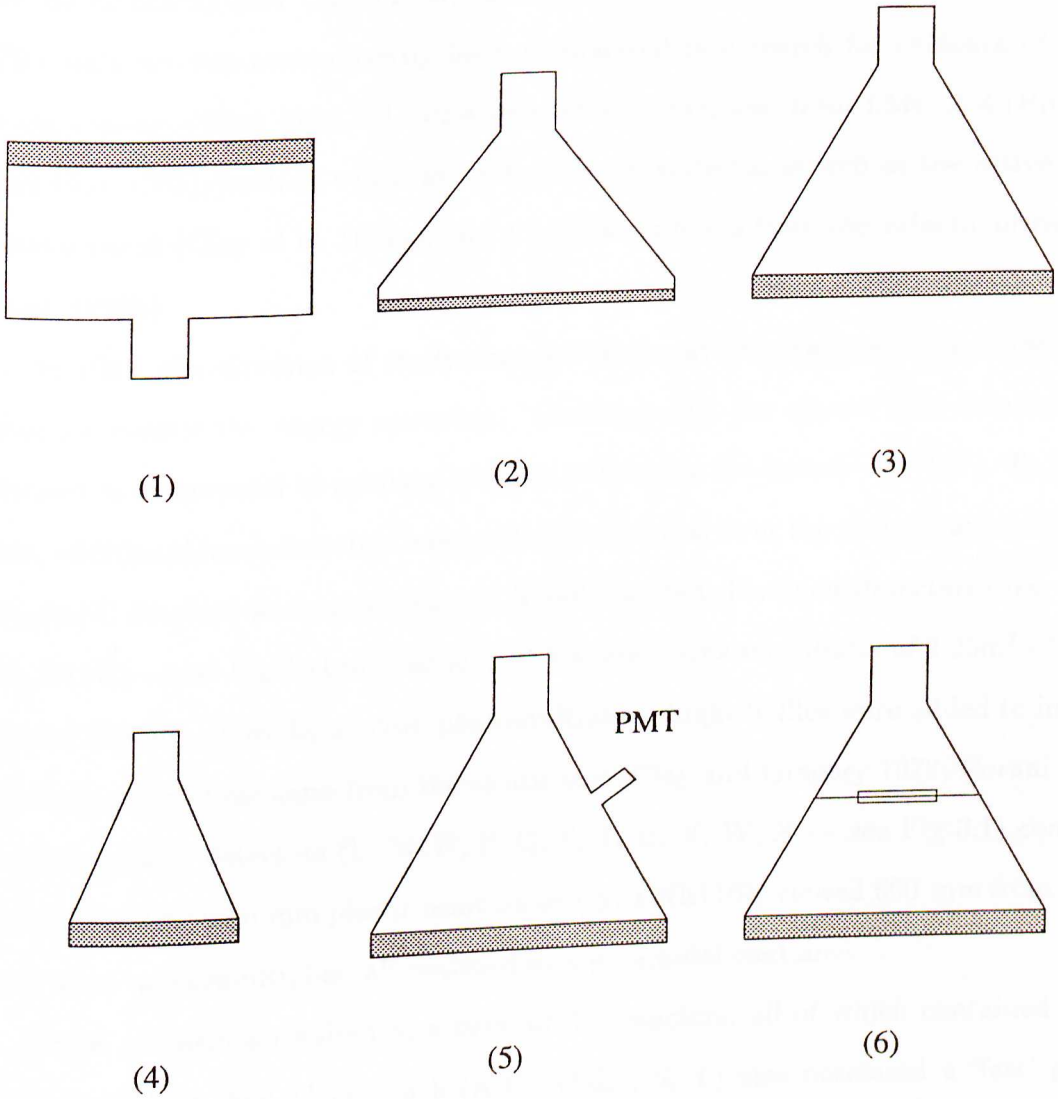

Figure 3.2: The types and relative sizes of detectors used at Buckland Park during the period 1984–1989. The numbers refer to the last column of Table 3.1. The shaded region indicates the scintillator. All photomultipliers are mounted inside the boxed region except for detector type (5) where the side-mounted photomultiplier is a small timing tube added during early-1986. Detector (6) has a light baffle between the scintillator and photomultiplier to improve the uniformity of response (Corani 1986).

This configuration was used to collect the 1979–1981 data set (Gerhardy 1983; Gerhardy and Clay 1983). Anisotropy investigations were carried out on this data set by Gerhardy and Clay (1983), along with a study of the shower size spectrum. This data set has more recently been re-analysed in a search for evidence of U.H.E. γ-ray emission from Vela X-1 (Protheroe et al 1984), and from LMC X-4 (Protheroe and Clay 1985), both of which are X-ray binary systems, as well as the active galaxy Centaurus A (Clay *et al.* 1984a), and a general emission from the galactic plane (Clay *et al.* 1984b).

In 1981, the direction of study changed to an investigation into the 'knee' of the primary cosmic ray energy spectrum. Consequently, the shower size threshold was lowered to correspond to primary energies well below the knee ($\sim 10^{15}$eV). To achieve this, additional inner detectors were added to the array over the period 1981–1984. The original C detector was repositioned at R and inverted. Five new detectors (new C, A1, B1, D1, E1 — see Fig 3.1) were added, with a larger area scintillator of $2.25\text{m}^2 \times 50$ mm, viewed 700 mm above by a 'slow' photomultiplier. Light baffles were added to improve the uniformity of response from the scintillator (Clay and Gregory 1978; Corani 1986). Additional new detectors (L, M, N, P, Q, S, T, U, V, W, X — see Fig 3.1) consisted of a slab of $1\text{m}^2 \times 50$ mm plastic scintillator (type NE110), viewed 600 mm from above by a 'slow' photomultiplier, all enclosed in a pyramidal container.

These extensions resulted in a total of 27 detectors, all of which contained 'slow' photomultipliers, and 11 of which (A-E, A1-E1, S, T) also possessed a 'fast' photomultiplier. They were all housed in semi-permanent 'huts', thermally insulated using sheets of glass wool and a covering of double-sided reflective thermal insulation known as sisalation.

The 'new' array lowered the effective size threshold to $\sim 3 \times 10^4$ particles (Prescott *et al.* 1983; Clay *et al.* 1985), through new triggering requirements, and the event rate increased from $\sim 10^{-3}$ Hz to $\sim 10^{-1}$ Hz. The angular resolution of the array near threshold was $\sim 6°$, but overall it was similar to that of the 1979–1981 data set (Ciampa *et al.* 1986). The resulting data set (June 1984 - June 1986), was used in

an unsuccessful search for U.H.E. γ-ray emission from X-ray binary systems (Edwards *et al.* 1989). It also comprises the initial portion of the data set analysed by the author in the search for anisotropies in the incident cosmic ray flux (see Chapter 5).

By 1986, the general emphasis in cosmic ray research had shifted towards searching for sources of U.H.E. γ-ray emission. As a consequence, the array was again upgraded, to improve its suitability for these investigations. Angular resolution is a key factor in such searches, and to improve this, a number of additional timing detectors were added during early-to-mid 1986, principally to provide a longer baseline, but also to provide independent timing information for the reconstruction of shower arrival directions (Ciampa 1988).

Five new detectors (S1, T1, RB1, RB2, BFD) were added to the central region of the array, to provide further fast-timing information. Three of these detectors (S1, T1, BFD) contained a $1m^2 \times 50$ mm slab of scintillator, viewed from 600 mm above by a 'fast' photomultiplier[3]. RB1 and RB2 contained smaller $0.25m^2$ x 50 mm slabs of scintillator, viewed 350 mm from above by a 'fast' photomultiplier[4]. In addition to these new detectors, eight existing detectors had 'fast' tubes added to them (L, M, N, P, Q, R, W, X). Fig 3.2 illustrates the various types of enclosures and photomultiplier arrangements used at Buckland Park.

For this configuration, the event rate remained unchanged to that of the 1984–1986 array as the triggering criteria remained unaltered. However, the angular resolution of the array was improved by the availability of additional timing information. The 1986–1988 data set was used in a further, more successful search for U.H.E. γ-ray emission from both X-ray binary systems and an active galaxy (Ciampa *et al.* 1988b; Ciampa and Clay 1989; Ciampa *et al.* 1989), as well as the recent SN1987A (Bird *et al.* 1987; Ciampa *et al.* 1988a; Bird *et al.* 1989).

In addition to the work purely involving the scintillator array, other studies have been carried out using the array. These include studies of the lateral distribution of

[3]type Phillips XP2040, diameter 120 mm

[4]type RCA 6199, diameter 30 mm

Cerenkov radiation from cosmic ray showers (Kuhlmann and Clay 1981; Dawson 1985), the temporal variation of the Cerenkov radiation associated with E.A.S. (Liebing *et al.* 1981), as well as the development of E.A.S., using Cerenkov radiation (Thornton and Clay 1979, 1981)

The array remained as described until May 1989, forming a 5 year data set. It is this data set upon which the majority of the anisotropy analysis in Chapter 5 is based. The array was then shut down whilst a new power supply and data acquisition system were installed and several detectors repositioned, as well as new ones being added. The development of the array post-May 1989 is discussed in 3.5.

3.3 Buckland Park (1984–1989)

The configuration of detectors comprising the Buckland Park E.A.S. Array during the period 1984–1989 is shown in Fig 3.1. Details of the individual detectors are presented in Table 3.1 in conjunction with Fig 3.2.

Apart from the detectors BFD, RB1 and RB2 (installed in 1986), the array was symmetrical about the north-south axis, but not so about the east-west axis. This asymmetry, along with the prevailing triggering conditions (see 3.3.1), resulted in the slightly non-uniform azimuth angle exposure distribution (see 3.4.1). The non-uniform distribution of detectors used resulted from simulations carried out prior to each development stage, in order to maximise the array response to the target regions of the shower size spectrum (and hence primary particle energy spectrum) of interest.

Following is a discussion of the methods employed to obtain data using the array and the subsequent analysis and interpretation of these data. Although the author was not responsible for the design and operation of the array prior to March 1988, details of the array operation are necessary in both understanding the characteristics of the data produced, and in modifying the system to introduce a new operating system, include extra detectors, and alter the array sensitivity.

3.3.1 Data Acquisition

The acquisition (and analysis) of data from Buckland Park can be considered in terms of the two types of measurements made, namely those of the incident shower direction (fast-timing measurements), and the total shower size (particle density measurements).

Detectors

Detection of E.A.S. at Buckland Park depends exclusively upon the detection of the electromagnetic component of those showers, using particle detectors. These detectors consist of a slab of plastic scintillator, viewed by a photomultiplier, contained in a light-proof box.

When a charged particle passes through the scintillator, the atoms within the scintillator are excited and ionised. These atoms then de-excite through photo-emission. The emitted photons may then be detected by the photomultiplier. The photomultiplier converts the detected light to a pulse of electric charge through the photo-electric effect. These electrons are focussed and accelerated by an electric field to a dynode. The resultant collision produces significantly more electrons which are subsequently focussed and accelerated to the next dynode. After multiplying through a series of stages (typically 10–15), this flow of electrons reaches the anode. This results in a significant current at the anode which is proportional to the intensity of light detected. The maximum sensitivity of the phototubes was matched to the maximum emission of the scintillators employed, corresponding to a wavelength of 420 ± 30 nm in order to maximise photon detection.

Particle detection using this method is a secondary process, resulting in a loss of resolution in information due to statistical fluctuations in both photon and photo-electron numbers. These fluctuations must be taken into account in any interpretation of the resultant data, and in simulating these processes.

Fast Timing Measurements

In order to estimate the arrival direction of an incident E.A.S. as accurately as possible, a fast-timing system was employed, based upon the method of Bassi *et al.* (1953). This involves the use of phototubes with 'fast' (and consistent) rise-times of ~ 2 ns or better (e.g. Philips XP2040) to record the passage of a shower-front through each scintillator. These photomultipliers contain 14 dynodes, and operate at a voltage of $\sim$ 2100V, resulting in gains $\geq 10^7$.

Output pulses from these tubes are passed along 50Ω cable to the ATCO electronics hut. Large bandwidth RG8 cable is used in order to both minimise signal attenuation and to preserve the shape of the photomultiplier pulse. This signal is then passed through a discriminator set at the 2-particle level which corresponds to a rate of $\sim$ 100 Hz. It then encounters a fixed delay ($\sim$ 50–200 ns), before triggering the stop of the appropriate T.D.C. (time-to-digital converter – LeCroy type 2228A) channel.

During 1986, these discriminators were replaced by 'double discriminators' in order to reduce timing uncertainties, resulting from photomultiplier pulse 'jitter', for the 1m^2 detectors to < 1 ns (Clay and Ciampa 1986). These discriminators have two channels, one set at the 2-particle level which, when triggered, gates the other channel, which is set at a much lower threshold and slightly delayed thus triggering the discriminator earlier in the rise of the signal, improving the resolution of the recorded time.

From this timing information, the relative arrival times of the shower-front at different detectors can be deduced, and the E.A.S. arrival directions can then be estimated from these measured time differences (see 3.3.2).

Particle Density Measurements

The amount of light emitted by the scintillator is directly proportional to the number of particles passing through it. Therefore, to measure the number of particles, the total number of photons emitted (i.e. the light intensity) must be measured.

This is achieved using a 'slow'-response phototube, operating at a voltage of $\sim$ 900V (a 'fast'-response photomultiplier is unnecessary), whose output passes to an on-site

charge-sensitive preamplifier which effectively integrates over the input pulse. The interior of these detectors are painted with highly reflective paint (NE560) to maximise photon detection. The resultant signal then has an amplitude proportional to the integrated charge which in turn is proportional to the number of particles passing through the scintillator.

This pulse propagates along a 50Ω RG58A cable, passing through a line receiver which inverts and shapes the pulse, before it reaches a peak-sensing A.D.C. (analogue-to-digital converter – LeCroy type 2259A). From this information, the number of particles passing through the scintillator (and hence particle density) may be deduced (see 3.3.2 for details).

Miscellaneous Electronics

Apart from the timing and density information supplied by the detectors, additional information is required for the analysis of the data.

A clock was used to record the absolute arrival time of each event as accurately as possible. Prior to June 1987, the clock used was accurate to within one second, being latched with the VNG radio signal transmitted by Telecom Australia. At this time, Telecom Australia discontinued this service, and the clock was replaced by an Omegarec Clock based upon the Omega Navigational System. This clock possesses superior accuracy ($\sim 5-10$ ms) making possible investigations corresponding to typical pulsar rotation periods (Ciampa 1988).

A barometric pressure sensor and atmospheric temperature sensor were located in a meteorological box and were used to record the prevailing atmospheric conditions. In addition, temperature sensors were sited within a detector (C), and in the ATCO electronics hut in order to monitor any temperature effects of the detectors and electronics.

All of the above electronics were connected to a home-made data logger with the clock being read at every event, and pressure and temperatures being sampled every fifteen minutes.

Array Triggering

The flux of detectable particles at the Earth's surface is ~ 1 cm^{-2}min^{-1}. The majority of these particles are muons, associated with E.A.S. whose electromagnetic component has been absorbed by the atmosphere (see 2.3). In order to detect the electromagnetic component of the E.A.S. which do reach ground level, the lateral extent of these showers is used and coincidences between neighbouring detectors within ≤ 100 ns are required for an event trigger.

Simulations were used to determine the exact trigger requirements, as array shower size exposure is dependent upon the shower parameters required (Corani 1986). For the period in question, the coincidence requirements for an event were 2 out of 11 'fast' signals at the 2-particle level, combined with a 2 out of 19 coincidence of the 'slow' signals at the 6-particle level (Edwards 1988; Ciampa 1988). This triggering requirement was found to minimise 'false' detections resulting from random coincidences, and resulted in an array threshold of $\sim 3 \times 10^4$ particles (Clay *et al.* 1985).

Once an event trigger took place, the transfer of data to the recording system was initiated.

Data Recording

A schematic diagram of the data recording system employed at Buckland Park during 1984–1989 is shown in Fig 3.3. The A.D.C.s and T.D.C.s, as well as a LeCroy type 2251 Scaler and a home-made data logger used to interface clock and meteorological information were contained in a Kinetic Systems CAMAC (Computer Automated Measurement And Control) crate. This crate acted as an interface between the detectors and the recording system, which consisted of a G.P.I.B. bus connected to a Data General Nova 4S Mini-Computer with a tape drive.

To activate data transfer upon a valid event (i.e. a 'fast' and 'slow' trigger), the following process took place. Every 'fast' trigger that took place was used to start the T.D.C.s, and gate the A.D.C.s. If a 'slow' trigger did not occur within the preset time of $\sim 3\mu$s, a reset was generated, resetting both the A.D.C.s and T.D.C.s. If a

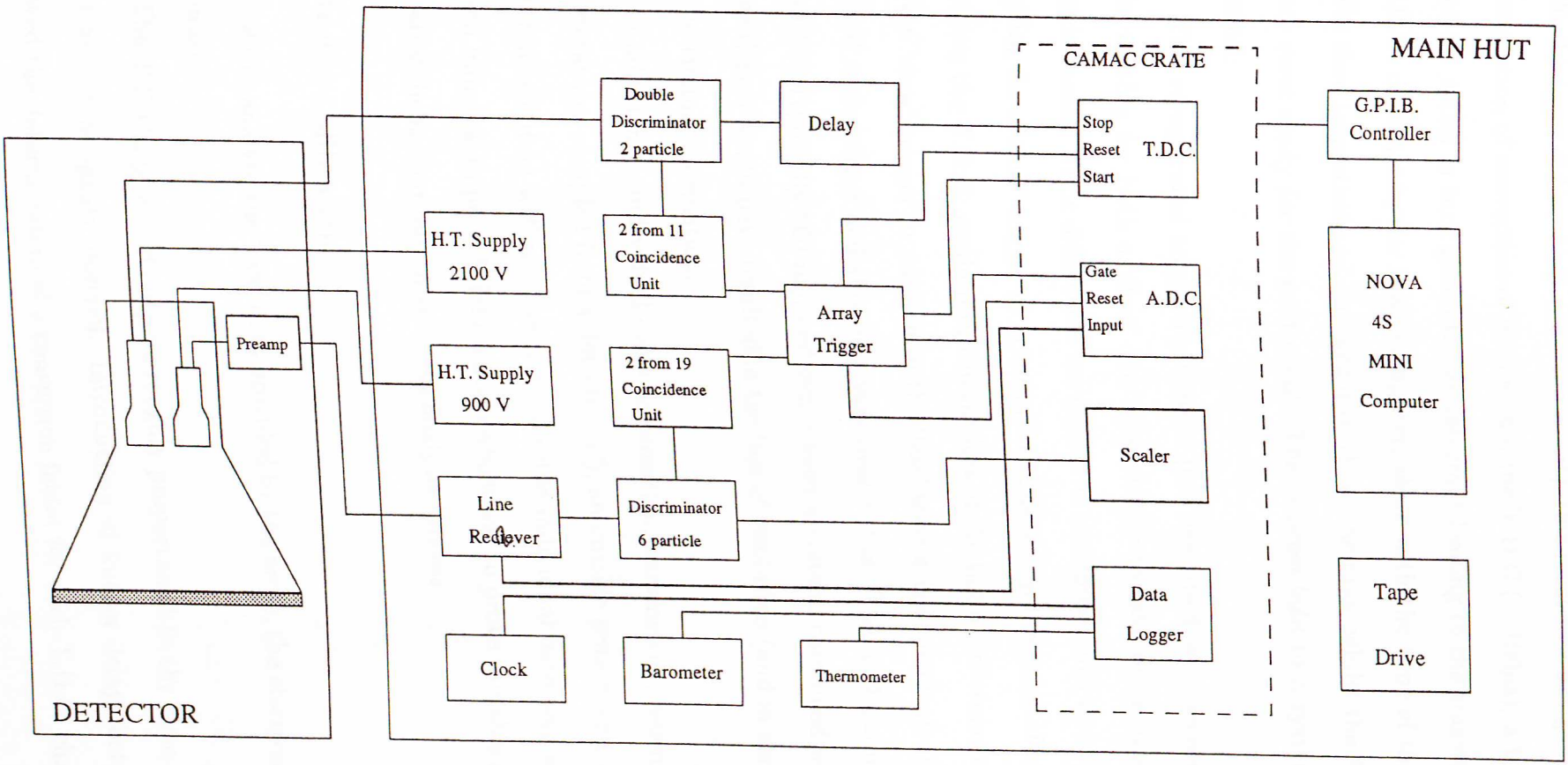

Figure 3.3: A schematic diagram of the components used in processing the data at Buckland Park 1984–1989.

'slow' trigger did occur (i.e. a valid event), this reset was not generated, and upon the completion of conversion of data within the T.D.C.($\sim 100\mu$s), a L.A.M. (Look-At-Me) was set which in turn generated an interrupt leading to the transfer of the A.D.C. and T.D.C. contents to the Nova computer, along with the time of the event. These data were then formatted and dumped directly to the tape, whilst the A.D.C.s and T.D.C.s were reset ready for the next event. This process lead to a system dead time of ~ 1 second.

The complicated triggering system just described was necessary, as opposed to just waiting for both a 'slow' and 'fast' trigger to take place, due to the fast-timing requirements. Time differences are measured in nanoseconds and the delay involved in waiting for a 'slow' trigger to occur in coincidence (in the order of microseconds) before starting the T.D.C. would result in the loss of the timing information. The arrival time of the 'slow' trigger in relation to the 'fast' trigger is dependent upon which detectors caused each trigger and this may vary over $\sim 1\mu$s. The T.D.C.s used had ranges less than this (typically 500 ns), and hence such a system, combined with the necessity of large delays would have resulted in the loss of resolution (and in some cases, total loss) of the timing information.

In addition to individual event information, barometric pressure and atmospheric temperatures sampled from a detector (C), an outside sensor, and a sensor within the electronics hut as well as rates from selected individual detectors were sampled every fifteen minutes, to provide information which was to prove valuable in both monitoring the array behaviour and in the data analysis process.

Detector Calibration

In order to analyse the 'raw' data provided by the array, the electronics firstly required calibration.

The T.D.C.s provided outputs roughly proportional to the time delay between the start and stop signals received. Introduction of known delays between these inputs allowed the determination of a conversion factor for each T.D.C. channel from T.D.C.

output to time (in ns). The T.D.C. channels were found to be approximately linear, and regular checks found the constants involved to be stable over time.

Calibrating the A.D.C.s in terms of the number of particles detected required more work. The pulse height spectrum obtained from a 'slow' detector using a Multi-Channel Pulse Height Analyser (M.C.A.) is shown in Fig 3.4. The spectrum (above the noise) is due almost entirely to the passage of single muons, associated with E.A.S. whose electromagnetic components have been absorbed by the atmosphere. This distribution approximates a Landau distribution and contains a peak, known as the Single Particle Peak (S.P.P.). This S.P.P. is a very good approximation to the mean pulse height for vertical single muons. This results from two factors:

(1) the ratio of the mean to the mode in the Landau distribution applicable here is 1.3 (White and Prescott 1968)

(2) the S.P.P. of vertical muons is a factor 1.3 less than that of omni-directional muons (detected here) (Clay and Gregory 1978).

It is these single vertical muons which are taken as the standard particle measurements. Using a M.C.A., the voltage corresponding to the S.P.P. was measured. Using this measurement, the number of particles corresponding to an A.D.C. output was calculated using

$$N = \frac{A \times (A.D.C. - Ped)^B \times Slope}{S.P.P. - Intercept} \qquad (3.1)$$

(Corani 1986)

where A, B and the slope and intercept were experimentally determined parameters for each A.D.C. channel, and the pedestal value the 'zero' value for each A.D.C. channel. Particle densities were then estimated by dividing the number of particles by the detector area ($1m^2$ in most cases).

Calibration of the A.D.C.s in order to determine A, B, slope and intercept was routinely carried out with the relationships involved being found to be almost linear, and stable over time. The pedestal value was easily found by examining the raw A.D.C. data for the minimum non-zero value recorded by each A.D.C. channel.

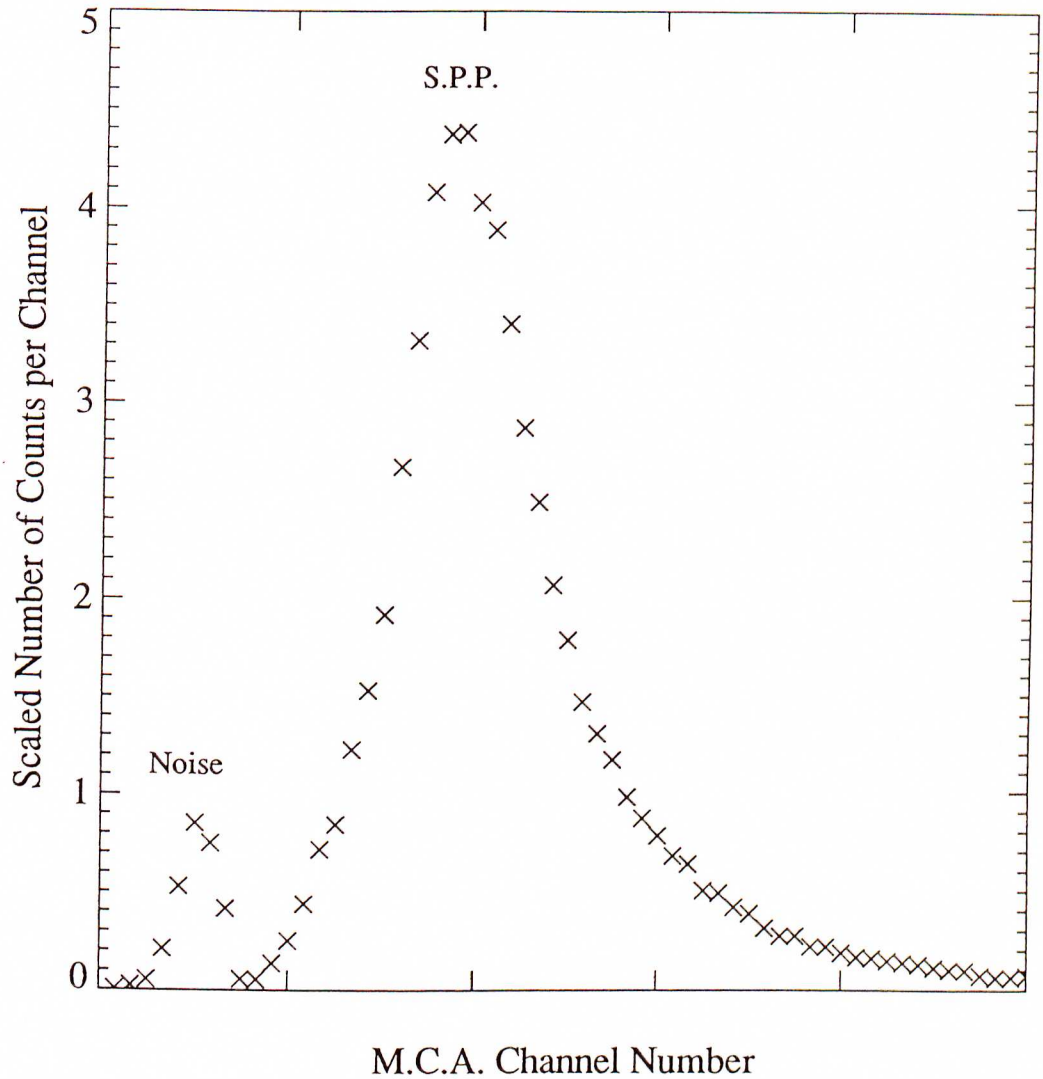

Figure 3.4: A pulse-height spectrum obtained from detector R, used for calibrating the data for density measurements. In this case, the noise peak is small, but it may be up to 10 times as large as the single particle peak, and in a 'noisy' detector may swamp the single particle peak.

3.3.2 Data Analysis

Initial analysis of the data (predominantly directional analysis) was carried out using the University of Adelaide's VAX 785 mainframe computer. During 1988, a Sun 4/280 File-server and associated Sun 3/60 Workstations were installed within the Department of Physics and Mathematical Physics as part of an upgrade of the campus-wide computer network. These provided vastly improved facilities in terms of disk space, CPU time and available processing power.

Timing Differences

The first step in the analysis of the data involves the determination of the arrival directions of the incident E.A.S. in terms of local co-ordinates (zenith (θ), azimuth (ϕ)). To achieve this, the technique of fast-timing is used (Bassi *et al.* 1953), relying on the determination of the relative times of arrival of the shower-front at the detectors. It is therefore necessary to know the relative arrival times between detectors for each E.A.S.. Inherent in the electronics and cables used to carry and process the timing signals are delays which contribute to the measured time differences. The absolute time differences may vary with time, and are not in themselves measured, but may be inferred from the data set itself.

Assuming that (to a first order) cosmic rays comprise an isotropic flux at the Earth at the energies being considered ($> 10^{14}$eV), on average, the mean E.A.S. direction is the zenith (i.e. $\theta = 0, \phi = 0$). As a result, the mean timing differences sampled over a sufficiently large number of events (i.e. several weeks data), provide an excellent estimate for these timing differences. This may be expressed for the difference between the ith and the jth detector as

$$\overline{t_{ij}} = \overline{t_i - t_j} = \frac{1}{N}\sum_{l=1}^{N}[t_i(l) - t_j(l)] \tag{3.2}$$

where N is the number of events used in calculating the mean (typically 10^4–10^5). Care must be taken when using this approach, as false signals, resulting from particles not correlated with the event will distort this mean. This effect was investigated for

the Buckland Park analysis (Edwards 1988), and a suitable algorithm was developed which was applied to this data analysis.

The standard error of the calculated mean timing differences for the difference between the i^{th} and j^{th} detector is given by

$$S_{ij} = \frac{\sigma_{ij}}{\sqrt{N}} \tag{3.3}$$

where σ_{ij} is the standard deviation of the timing distribution for times between the i^{th} and the j^{th} detectors. To a good approximation, σ_{ij} is approximately proportional to the distance between the detectors. For the further spaced detectors of the array, a better estimate of the delays involved was obtained by 'stepping' between the detectors using intermediate detectors. Such an analysis was carried out (Edwards 1988; Ciampa 1988), with the result that the use of 'step' differences was found to improve S_{ij} by up to a factor greater than $\sqrt{2}$. Stepped differences were used in the calculations of timing differences.

In practice, typically a months data were used in determining these timing differences. Deviations between successive data tapes ($\sim 3-4$ days data) were in general found to be ≤ 1 ns. Knowledge of these timing differences allowed the directions of the incident E.A.S. to be calculated.

Arrival Direction Determination

In determining the E.A.S. arrival direction, an index detector with respect to which all times will be measured is firstly chosen. Starting at the 'centre' of the array a search is carried out working away from the centre of the array, until a detector with a recorded time is found.

The relative time of arrival of the shower-front at detector i (t_i), with respect to the time of arrival at the index detector (t), is given by

$$t_i = t - \overline{t - t_i} \tag{3.4}$$

The arrival direction is then determined by assuming that the shower-front is planar, and that it propagates through the atmosphere with a velocity c, and then fitting

the appropriate shower-front to the data. This fit is achieved using a least squares minimisation on the following function:

$$\chi^2 = \sum_{i=1}^{N} w_i[c(t_i - t_0) - lx_i - my_i]^2 \tag{3.5}$$

where

x_i, y_i are the co-ordinates of the ith detector,

t_i is the relative time for the ith detector relative to the index detector as given by Eq 3.4

t_0 is the timing offset

$w_i = 1$ if the detector triggered a valid time

$= 0$ otherwise

l, m are the x and y direction cosines of the E.A.S. direction.

The timing offset, t_0, is a free parameter, so that the fitted shower-front is not constrained to pass through the index detector at time zero. Minimisation with respect to l, m, t_0 is achieved using matrix methods (Edwards 1988), assuming all detectors lie in the same horizontal plane. The third direction cosine may then be found using

$$n = \sqrt{1 - l^2 - m^2} \tag{3.6}$$

The E.A.S. arrival direction may then be determined in local co-ordinates using the following equations:

$$\theta = \tan^{-1}\left(\frac{\sqrt{1-n^2}}{n}\right) \tag{3.7}$$

$$\phi = \frac{\pi}{2} - \tan^{-1}\left(\frac{m}{l}\right) \tag{3.8}$$

The variation in the vertical heights of the detectors is then taken into account by correcting the relative arrival times for this displacement, using the following relationship

$$t_i = t_i - \frac{z_i \cos\theta}{c} \tag{3.9}$$

where z_i is the z co-ordinate of the ith detector measured with respect to some arbitrarily determined zero. χ^2 is then minimised and the process repeated until the direction converges.

The 'goodness of fit' parameter, σ, used to measure the fit of the planar shower-front, is given by

$$\sigma = \frac{\sum_{i=1}^{N_t} w_i[c(t_i - t_0) - lx_i - my_i - nz_i]^2}{N_t - 3} \tag{3.10}$$

where N_t is the number of times contributing to the arrival direction calculation. As a result of the restriction on N_t, a significant number of showers were found to be unanalysable due to an insufficient number of times.

The finite thickness of the shower-front, combined with the subtle curvature of the shower-front limit the usefulness of the planar shower-front fit. The resolution for such a fit is somewhat coarse ($\sim 5°$, depending upon the number and positions of timing detectors triggered). To improve the estimated arrival direction, these factors may be taken into account once the core position of the shower size has been determined.

Shower Parameter Determination

Once the arrival direction (θ, ϕ) of a shower has been determined, it is possible to estimate other shower parameters, the most important of these being N_e , the shower size, (x_c, y_c), the shower core position, and s, the shower 'age'.

The first step in carrying out this parameterisation is the conversion of the raw A.D.C. numbers in the data files to densities. (see 3.3.1). This is achieved using small data files containing the relevant information (namely the S.P.P. and Pedestal values as well as detectors to be removed from the analysis).

The parameters x_c, y_c and s are determined by fitting the NKG lateral distribution function (see 2.4.1) to the derived detector densities and arrival direction. From these three parameters, the shower size, N_e can then be determined. The fit is achieved using the maximum likelihood method (Bevington 1969), maximising

$$\ln P(x_c, y_c, s) = \sum_{i=1}^{n} [d_i^o \ln(d_i^c) - (d_i^c - \ln(d_i^o!))] \tag{3.11}$$

where d_i^o is the observed density, from the i^{th} detector, and d_i^c is the corresponding calculated density for that detector, from the fit.

An alternative fit is available using the χ^2 goodness-of-fit parameter :

$$\chi^2 = \sum_{i=1}^{n} \frac{(d_i^o - d_i^c)^2}{\sqrt{d_i^o d_i^c}} \tag{3.12}$$

This method has the advantage of being an absolute (and hence comparable) measure of fit, whereas the maximum likelihood parameter is dependent on the densities being used, and so cannot be directly compared, from event to event. However, χ^2 has the disadvantage of not allowing the inclusion of detectors measuring zero particles, thus eliminating useful information. It is also a less efficient algorithm than the maximum likelihood method (see e.g. Poirier *et al.* 1987).

Work carried out by Corani (1986) found that the χ^2 goodness-of-fit parameter also resulted in a hut-seeking effect. Core positions were found to be artificially placed on or near huts recording the highest particle density, resulting in an adverse effect on the shower size and age estimation. The introduction of the maximum likelihood method was found to reduce this problem (although not entirely eliminating it) to the point where the effect on the derived shower size was minimal in comparison to uncertainties due to statistical fluctuations in sampling etc.

In practice, the MINUIT minimisation package (James and Roos 1975) is employed to minimise $-\ln P$ (identical to maximising $\ln P$). As a compromise measure, χ^2 is calculated for the final fit in order to provide some comparable measure of the goodness of fit for each event.

Once the shower core position has been estimated, it is possible to take into account errors in the estimated direction as a result of the planar shower-front approximation.

Shower-Front Thickness and Curvature

Linsley (1985a) has investigated the average dispersion in the arrival times of E.A.S. particles detected by scintillators, and derived the following empirical relation to take into account the shower-front thickness:

$$\sigma_t = \sigma_0(1 + \frac{r}{r_t})^b \tag{3.13}$$

where

$\sigma_0 = 1.6$ ns

$r_t = 30$m

$b = 1.5$

The contribution to the timing uncertainty can be approximated (assuming a Poisson particle distribution in the shower-front) by

$$\delta t = \frac{\sigma_t}{\sqrt{n}} \tag{3.14}$$

where n is the number of particles detected.

The intrinsic instrumental uncertainty also needs to be taken into account. The following weighting factor is used to allow for these effects (substituted into Eq 3.5):

$$w_i = [(\frac{c\delta t}{r_i})^2 + \theta^2_{instr}(i))]^{-1} \tag{3.15}$$

(Ciampa 1988)

σ_{instr} = instrumental resolution

r_i = distance to the core from the ith detector in the plane of the shower.

The effect of shower-front curvature is less well understood. The radius of curvature of the shower-front is believed to be ~ 1 km for E.A.S. corresponding to primary particle energies $E \geq 10^{14}$eV (Greisen 1960).

An extensive investigation into shower-front curvature was carried out at Buckland Park, with the limited ($r_i \leq 60$m) timing information available (Ciampa 1988). The resultant correction derived from the data was

$$t_i' = t_i - 0.14 r_i \tag{3.16}$$

where t_i is the observed time of arrival as defined by Eq 3.4, and

t_i' is the corrected time in order to fit a plane shower-front.

(i.e. a lag of 0.14 ± 0.05 nsm^{-1} was found experimentally).

Correcting the data using Eq 3.16 once the shower core position has been determined, the arrival direction is then recalculated on the assumption of a planar shower-front. Such corrections were found to halve the angular uncertainty of the array (Ciampa 1988).

More recently, an alternative approach has been attempted. Computer simulations based upon the derived result (Eq 3.16) have been carried out to determine the angular corrections necessary for all possible permutations of core position and azimuth and zenith angles. This method has the advantage of not requiring the raw timing information and differences, but only the core position and arrival direction. Such corrections have been applied in searches for U.H.E. γ-rays from astrophysical sources (see e.g. Meyhandan and Clay 1991).

The author was responsible for the complete acquisition and analysis of data from March 1 1988 onwards. Prior to this, arrival directions had been calculated by previous postgraduate students (Edwards 1988; Ciampa 1988), along with a very limited number of shower size and core fits.

The major stumbling block had been computer CPU time availability and, to a lesser extent, disk space. Fitting shower sizes and cores consumes approximately three seconds of CPU time per event, requiring $\sim 30\%$ efficiency in computing to prevent a backlog occurring due to the $\sim 10^{-1}$ Hz event rate. Only a small percentage of this time had been available on the VAX 785 accessible to the department, and as a result, the complete analysis of all of the recorded events had not been attempted.

With the installation of the Sun 4/280 in the department, and similar machines around campus, complete analysis became feasible. The author was responsible for carrying out this task, and the shower size and core fitting to the five years of data was completed in just under five months.

The results of this analysis, the array characteristics will now be presented and discussed.

3.4 Array Characteristics (1984–1989)

In order to determine the effectiveness of the array, it was important to compare the analysed data with expected behaviour. This not only provides a test on the array

performance (and the analysis procedures), but also provides information about the cosmic ray flux.

The five year data set (1984–1989) considered here has been divided into two separate data sets (1984–1986) and (1986–1989). The major difference between these data sets is the increase in the number of timing detectors from 11 to 24, the new detectors coming on-line during June 1986. Whilst the triggering conditions were not changed, the availability of additional timing information allowed the acceptance of more events (the requirement being that a minimum of three non-collinear, 'physical' times were available). This effect was most evident in the azimuth angle distributions (see 3.4.1).

The 1984–1986 data set was used in a search for U.H.E. γ-rays from astrophysical sources (Edwards 1988; Edwards *et al.* 1989). A total of 4.38×10^6 events were recorded between June 21 1984 (JD 244 5872.6) and June 23 1986 (JD 244 6604.6). The array had an on-time efficiency of 75% during this period, the off-times due to power failures and equipment breakdown as well as routine maintenance. Directions were initially assigned to 3.87×10^6 events, corresponding to 88% of the total. Subsequent shower size and core fitting resulted in 2.86×10^6 events corresponding to 65% of the total.

The early part of the 1986–1989 data set, used in another search for U.H.E. γ-rays from astrophysical sources (Bird *et al.* 1987; Ciampa 1988; Ciampa *et al.* 1988a, 1988b; Bird *et al.* 1989; Ciampa and Clay 1989) consisted of 3.30×10^6 events recorded between June 24 1986 (JD 244 6605.6) and March 1 1988 (JD 244 7221.6). Over this period the array was operational for 76% of the time, the main source of down-time being power-failures (requiring the resetting of the array), and a period of $\sim$ 40 days during which the Nova mini-computer suffered an undiagnosed, intermittent problem, which resulted in effectively no data collection. Directions were assigned to 92% of these events (3.03×10^6 events). Subsequent shower size and core fitting resulted in 2.31×10^6 events corresponding to 70% of the total.

The remaining portion of the data set collected from March 1 1988 (JD 244 7221.6) to 16 May 1989 (JD 244 7663.6) consisted of 1.40×10^6 events. Significant disruptions to this data set were experienced due to further problems with the Nova mini-computer.

90% of these events had directions assigned (1.26×10^6 events) and subsequent shower size and core fitting resulted in 1.01×10^6 events corresponding to 72% of the original total.

Overall, 9.08×10^6 events were recorded by the Buckland Park E.A.S. Array during the period June 21 1984 (JD 244 5872.6) to May 16 1989 (JD 244 7663.6), directions were assigned to 8.16×10^6 events (90%), and shower sizes and cores were fitted to 6.18×10^6 events (70%).

In the following distributions, only those events that were satisfactorily analysed were included. Satisfactory analysis required the following conditions on the derived shower parameters to be satisfied:

$\sigma < 10$ (timing goodness-of-fit)

$|x|, |y| < 100$m (core positions)

$\chi^2 < 6$ (shower size and core goodness-of-fit)

$0.55 < s < 1.95$ (shower age).

3.4.1 Arrival Directions

Azimuth Angle Distribution

The azimuth angle distributions for the two data sets being examined are shown in Fig 3.5.

The 1984–1986 distribution demonstrates a strong first and second harmonic modulation with amplitudes of 1.3% and 2.9% respectively. Clearly, showers from the north, and, to a lesser extent, those from the south are slightly more predominant than those from the east and the west. A similar effect was observed in the 1979–1981 data set (predominantly second harmonic amplitude of $\sim$ 4% — Gerhardy 1983). Edwards (1988) suggested that this effect resulted from the asymmetry of the array, especially in the 'fast' and 'slow' trigger detectors, which extended further in the north-south direction than the east-west direction.

The addition of fast-timing tubes to the array during early 1986 (Ciampa 1988) led

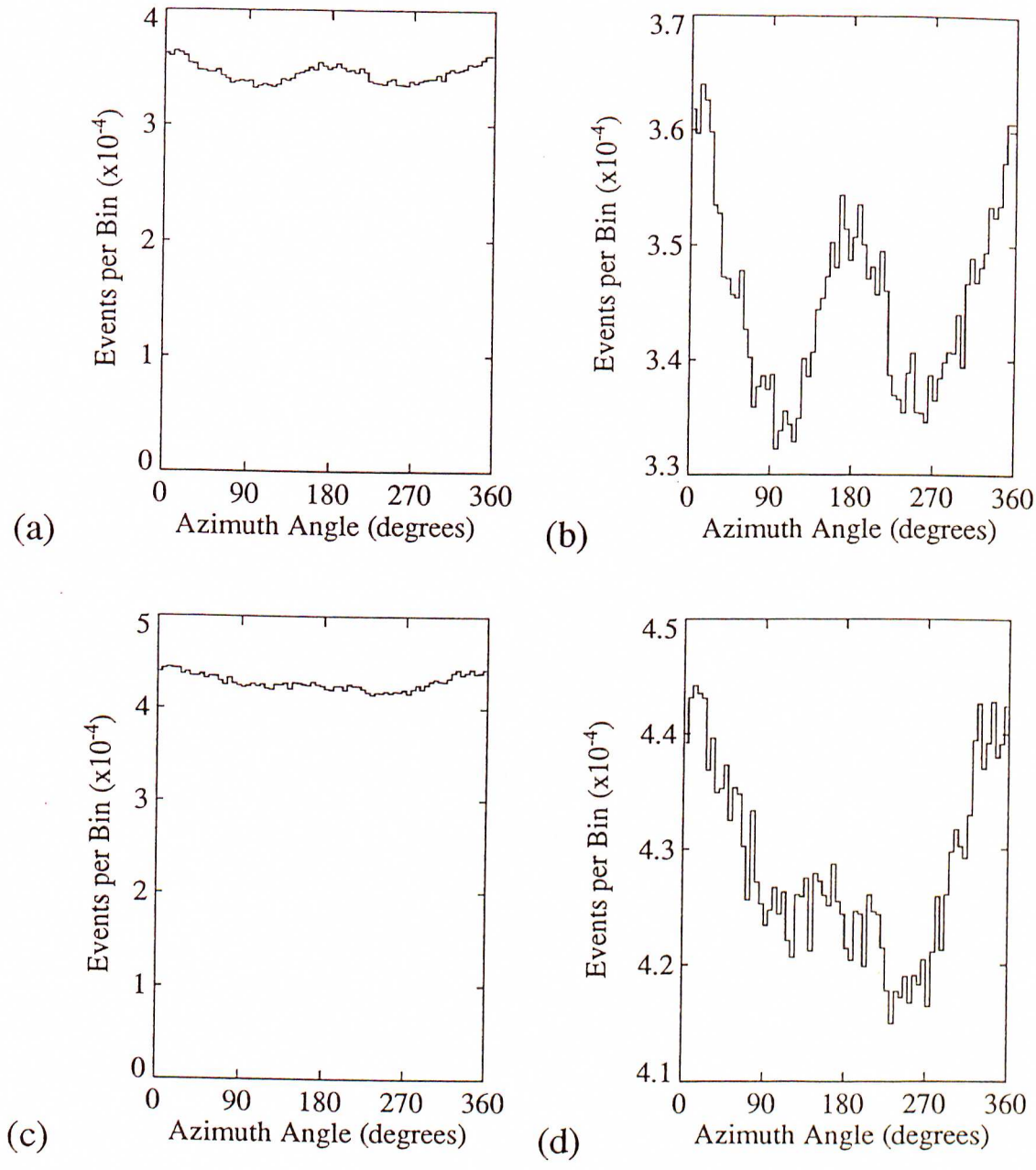

Figure 3.5: The calculated azimuth angle distributions of the arrival directions of E.A.S. detected at Buckland Park during 1984–1989.

(a), (b) 1984–1986 data set

(c), (d) 1986–1989 data set

to the partial removal of this second harmonic effect in the 1986–1989 data set. This allowed the analysis and acceptance of more east-west showers. However, the array still demonstrated a first harmonic, favouring northerly showers (Harmonic amplitudes of 2.2% and 1.1% respectively).

Development of the array during 1989–1990 lead to the removal of this effect, and a near-uniform azimuth angle distribution was achieved (see 3.6.2).

Zenith Angle Distribution

The zenith angle distributions for the two data sets are presented in Fig 3.6. The study of zenith angle distributions provides information on how E.A.S. develop, and how they are attenuated by the atmosphere.

The number of events initially increases with zenith angle as the viewed solid angle increases ($\propto \sin\theta$), and reaches a peak at typically 20°. Above this angle, the number of events decreases as atmospheric absorption (dependent upon $\sec\theta$) becomes increasingly important.

The number of events per steradian is conventionally described by

$$\Phi(\theta) = \frac{dN(\theta)}{d\Omega} \propto \cos^n\theta \tag{3.17}$$

(Hayakawa 1969)

where n is in the range 6–10, but is approximated by a constant value of 8.3 (Greisen 1956). This value for n leads to a predicted peak in the zenith angle distribution at $\theta \sim 19°$, which is in agreement with the distributions presented in Fig 3.6.

Plots of the data in terms of the number of events per steradian appear in Fig 3.7(a), (c). Fits of the data to $\cos^n\theta$ curves for $n = 8$ and $n = 9$ have been superimposed. The lower value of n $(= 8)$ fits the data at low zenith angles, but as zenith angle is increased it is clear that a progressively higher value of n is needed.

An alternative representation of the zenith angle distribution may be produced by considering $\log_{10}\Phi(\theta)$ as a function of $\sec\theta$ (Kalmykov *et al.* 1973), namely :

$$\log_{10}\Phi(\theta) = C\sec\theta + D \tag{3.18}$$

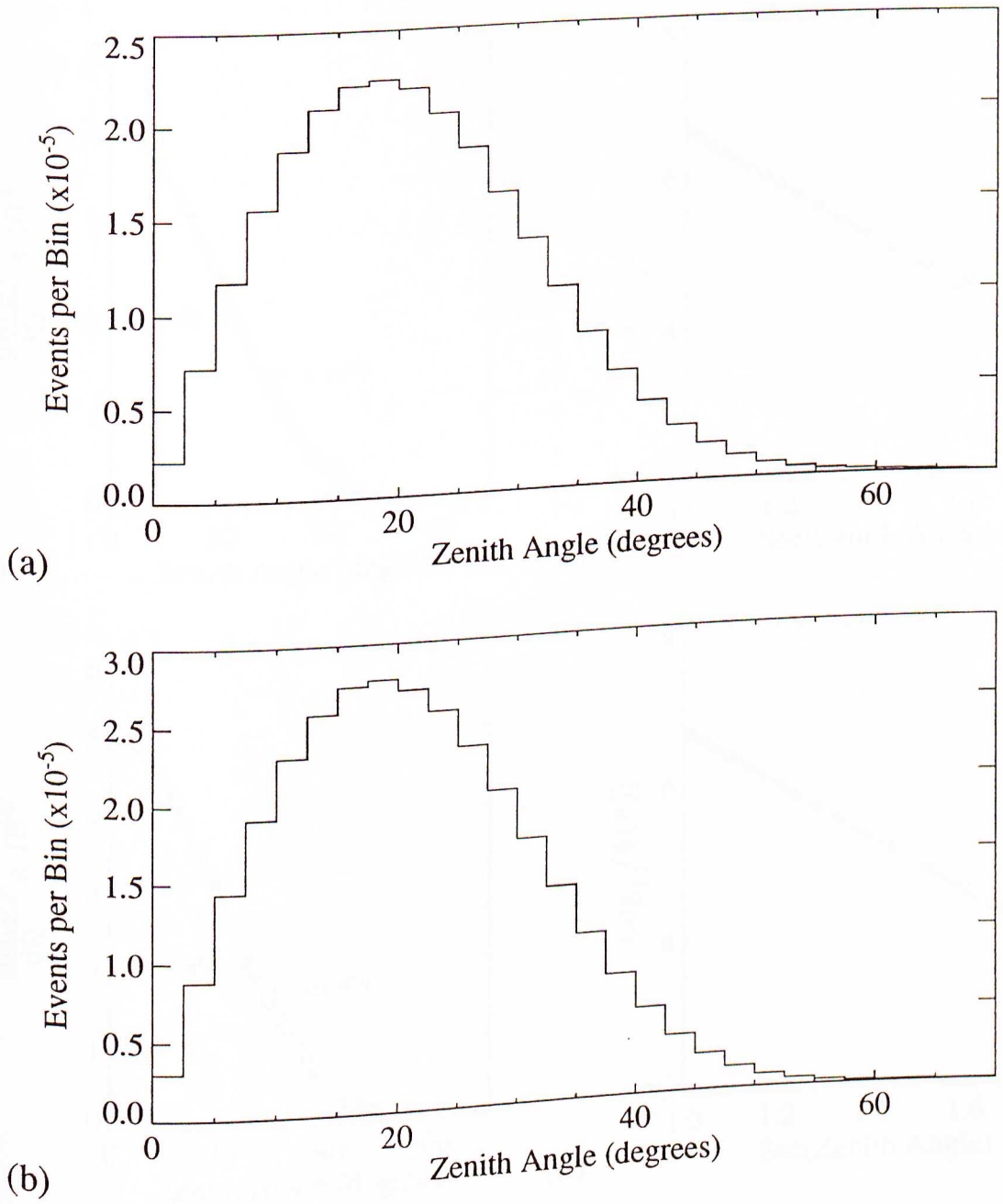

Figure 3.6: The calculated zenith angle distributions of the arrival directions of E.A.S. detected at Buckland Park during 1984–1989.
(a) 1984–1986 data set
(b) 1986–1989 data set

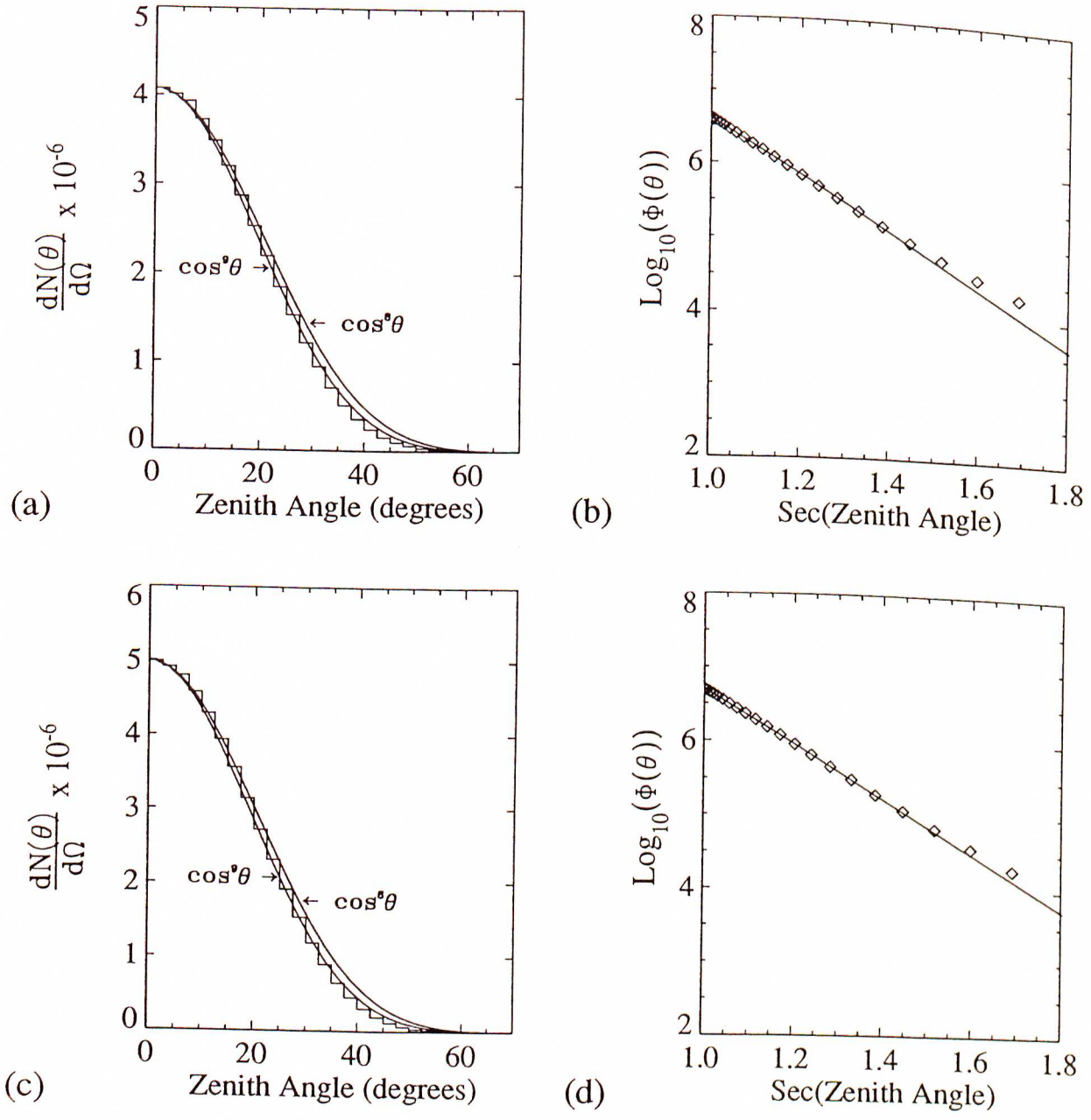

Figure 3.7: The zenith angle distributions in terms of solid angle exposure. Curves of $\cos^8\theta$ and $\cos^9\theta$ have been superimposed for comparison in (a), (c) (see text). (b) and (d) show the alternative fit, $\log_{10}\Phi(\theta)$ versus $\sec\theta$. The solid lines are good fits for $\sec\theta \leq 1.4$, and have slopes ~ -3.70.

(a), (b) 1984–1986 data set

(c), (d) 1986–1989 data set

To a first order, and ignoring shower fluctuations, the constant C should be given (at sea-level) by $1030(1-\gamma)/2.3\lambda$, where γ is the negative index of the cosmic ray differential spectrum, and λ is the shower attenuation length (Ciampa and Clay 1988). Typical values for γ ($\sim$ 2.5–3) and λ ($\sim$ 185 gcm^{-2}) give $|C| \geq 3.5$.

Monte Carlo simulations of E.A.S. detection with the Buckland Park E.A.S. Array were carried out by Ciampa and Clay (1988). Investigating the relationship between $\log_{10}\Phi(\theta)$ and $\sec\theta$, they found it to be close to a linear relationship, but was dependent upon the values of γ and λ chosen, as well as the primary composition. By assuming values of $\gamma = -2.5$, and $\lambda = 185$ gcm^{-2} (Clay and Gerhardy 1982), values for C of -3.6 and -4.1 were obtained for compositions of protons and iron nuclei respectively. Examining a portion of the observed zenith angle distribution obtained by Ciampa (1988) with the Buckland Park E.A.S. Array, the relationship was found to be linear in values of θ up to $\theta \sim 40°$, with $|C| \geq 3.6$, beyond which the influence of the muon component in E.A.S. results in a deviation from this linear fit (Kalmykov *et al.* 1973; Armitage *et al.* 1973). These results were found to be consistent with a composition not dominated by a heavy nuclei flux, with Ciampa and Clay (1988) quoting a value for C of -3.66 ± 0.03 for $\sec\theta \leq 1.4$.

Examining the two data sets considered here, the second consisting partially of the data used by Ciampa (1988), the distributions of $\log_{10}\Phi(\theta)$ vs. $\sec\theta$ were found to be well-fitted by slopes of -3.71 ± 0.02 and -3.70 ± 0.02 respectively for $\sec\theta \leq 1.4$ (see Fig 3.7(b), (d)). These results may be interpreted as indicating a predominantly light component of composition at $\sim 10^{15}$eV, in agreement with the results of Ciampa and Clay (1988) and Ciampa (1988).

Overall, these results indicate that the zenith angle distribution behaviour is in agreement with that expected.

Once the arrival directions of the E.A.S. have been determined in local co-ordinates (zenith (θ), azimuth (ϕ)), knowledge of the latitude and longitude of the array together with the arrival time of the E.A.S. in local sidereal time (derived from Universal Time

and longitude), allows the conversion of these co-ordinates to equatorial co-ordinates (declination (δ), right ascension (α)).

Declination Distribution

The declination distributions of the data are presented in Fig 3.8. These distributions demonstrate the region of the sky to which the array is exposed, and indicate that the array is sensitive to declinations in the range $-80° < \delta < 15°$, centred roughly upon the latitude of the array ($\sim -35°$).

This distribution highlights the importance of situating E.A.S. arrays at a variety of latitudes, as there is negligible overlap between observations made in the southern and northern hemispheres. The construction of arrays such as SPASE (the South Pole Air Shower Experiment — Hillas 1989) is one such example of an attempt to fill the gaps in exposure.

Right Ascension Distribution

The complete right ascension distributions for the two data sets are presented in Fig 3.9. The interpretation and subsequent analysis of the non-uninformities in this distribution which result from a number of effects will be discussed in detail in Chapter 5.

3.4.2 Shower Parameters

Shower Size Distribution

Fig 3.10 displays the fitted shower size distributions of the array from 1984–1989. Shower sizes were derived using the maximum likelihood method on the NKG function (see 2.4.1). The core distance range of these showers was restricted to lie well within the physical extremities of the array ($|x|, |y| < 100$m), in order to minimise errors resulting from poor sampling statistics and fluctuations. In addition, limits on the shower age parameter were applied to the data $0.55 < s < 1.95$ (these limits are considered physically reasonable for a sea-level array — see e.g. Ciampa 1988).

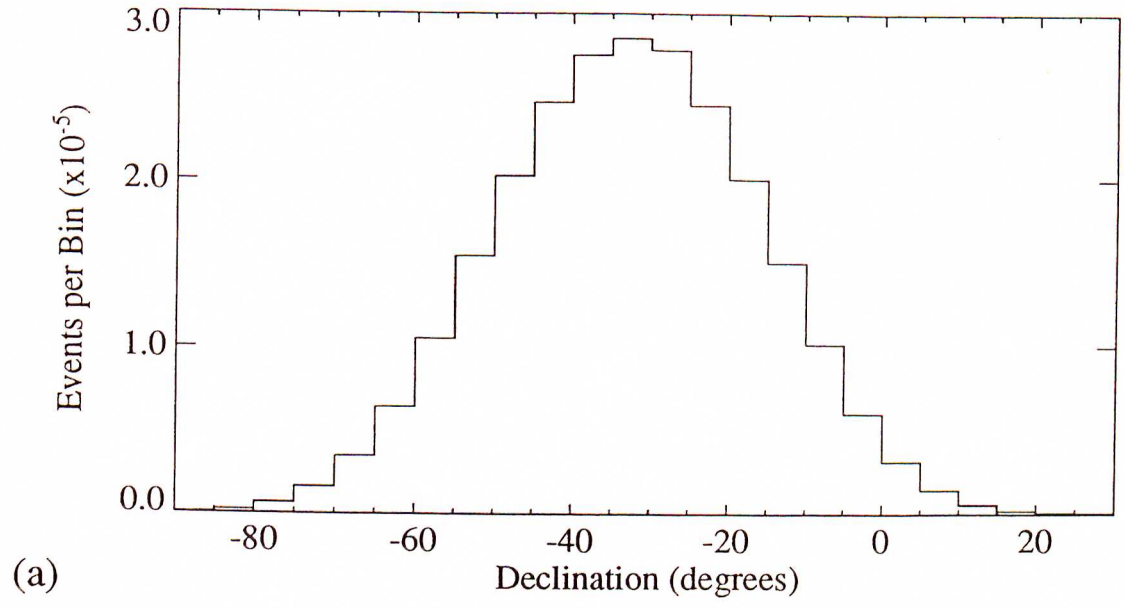

(a)

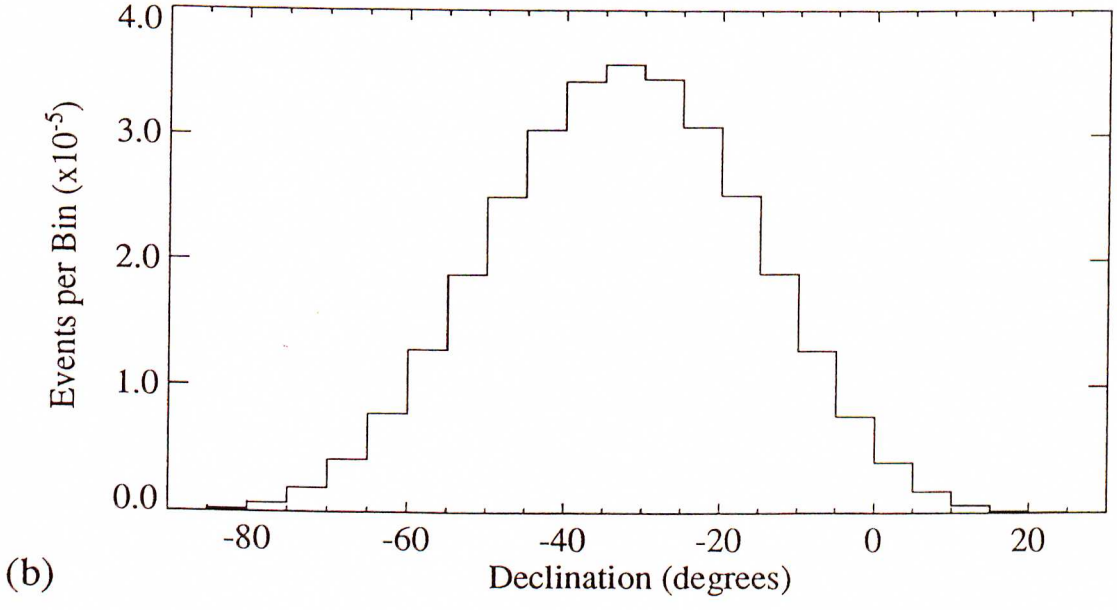

(b)

Figure 3.8: The calculated declination distributions of the arrival directions of E.A.S. detected at Buckland Park during 1984–1989.
(a) 1984–1986 data set
(b) 1986–1989 data set

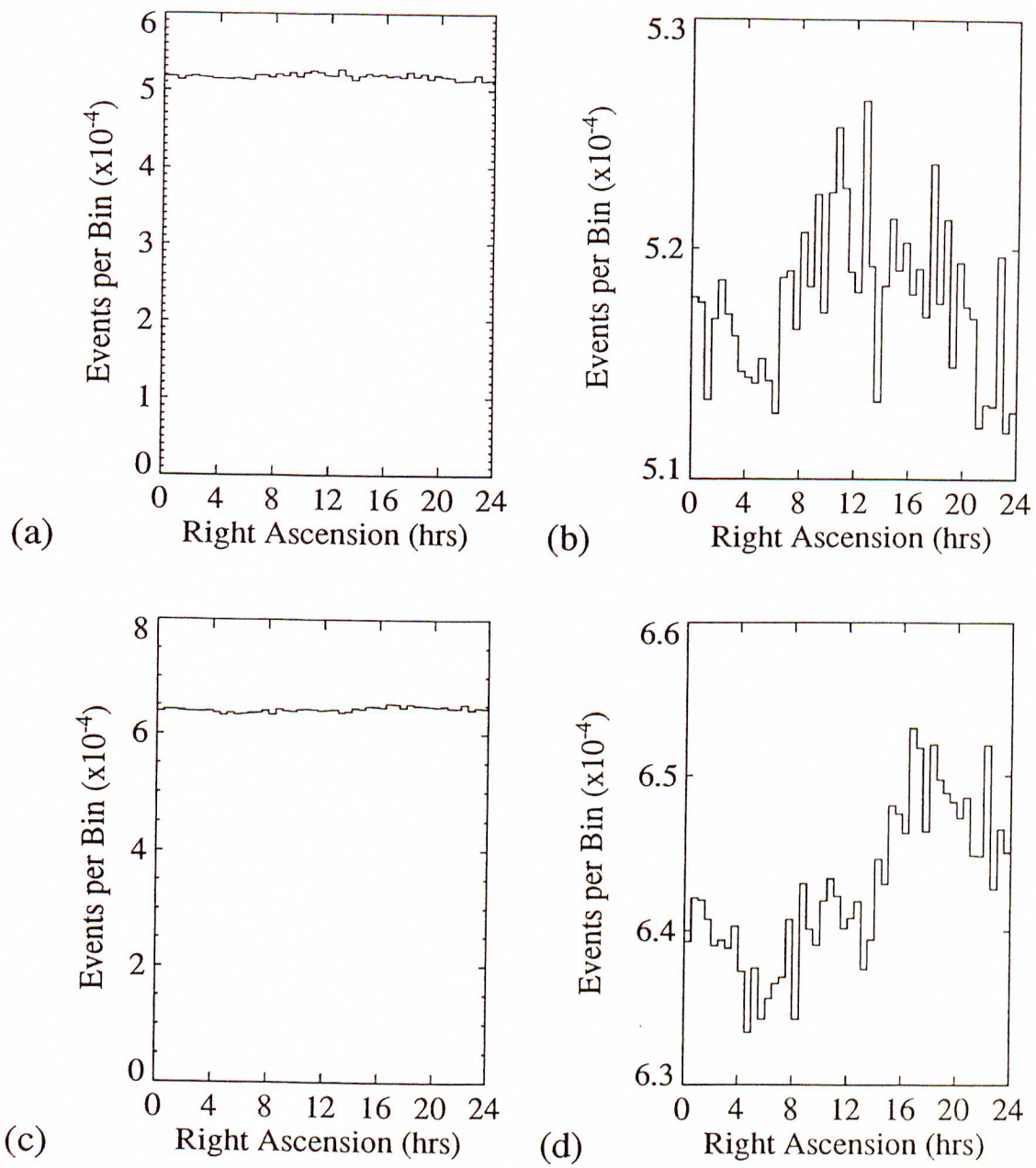

Figure 3.9: The calculated right ascension distributions of the arrival directions of E.A.S. detected at Buckland Park during 1984–1989.
(a), **(b)** 1984–1986 data set
(c), **(d)** 1986–1989 data set

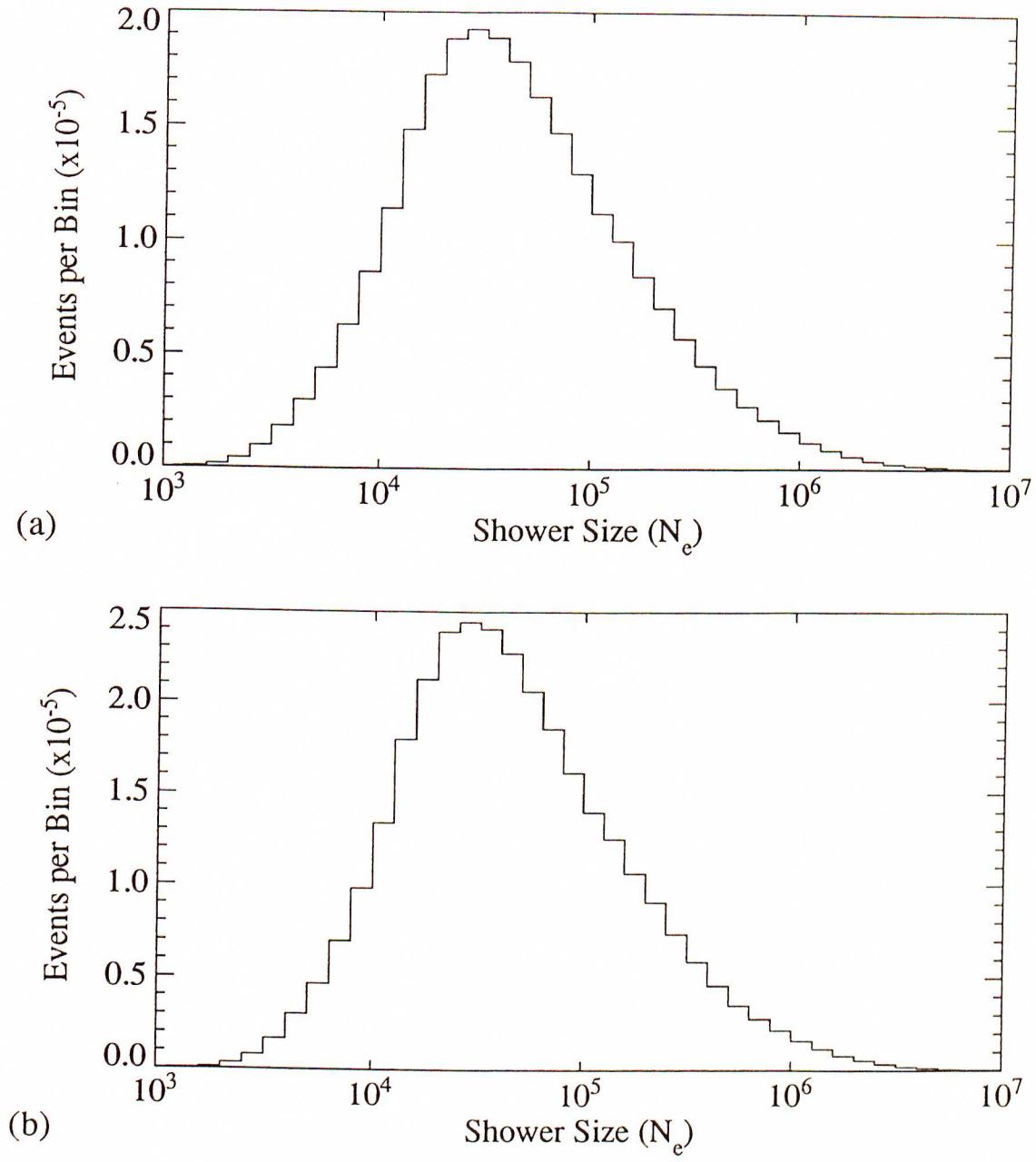

Figure 3.10: The derived shower size distributions for the two data sets analysed.
(a) 1984–1986 data set
(b) 1986–1989 data set

Analysis resulted in a loss of 28% of these events due to these limitations, or the failure of the minimisation to converge. It was these results which were then applied to the anisotropy analysis described in Chapter 5.

Simulations of the array in this form were carried out to estimate the behaviour of the array. A comparison of the simulated and measured size spectra is presented in Fig 3.11. The simulated results were produced by firstly choosing a primary energy from a standard source spectrum (integral indices of $\gamma = -1.58$ for primary energies below $E \sim 3 \times 10^{15}$eV, and $\gamma = -2.02$ for primary energies above $E \sim 3 \times 10^{15}$eV) along with arrival direction and random core position from the appropriate distributions. The shower size at maximum was then calculated by dividing the primary particle energy by 10^{10}, which was then converted to a sea-level shower size using the data compiled by Protheroe and Patterson (1984) (see 5.4.1; Fig 5.12) taking into account atmospheric attenuation and zenith angle. The number of particles in each detector was then calculated and fluctuated as discussed in 3.5.2, and then used to determine if the array triggered.

The resultant size spectrum is in reasonable agreement with the observed size spectrum (see 3.6.3 for a possible explanation of the deviations). In addition, the predicted rate of events for the array ($\sim$ 7 events per minute) was also in agreement with the experimental rate. A similar simulation was carried out for the post-1989 array and will be discussed in 3.6.3.

Integral Shower Size Spectrum

A useful check on our data analysis procedure was provided by the derivation of an integral sea-level shower size spectrum. Such spectra have been previously determined by other experiments (e.g. Nagano *et al.* 1984).

To calculate such a spectrum, it was first necessary to determine the areas of 100% triggering probability of the array. This was necessary in order to avoid underestimating the shower flux due to variations in detection efficiency. These regions were determined using simulations of the array, and the following conservatively chosen

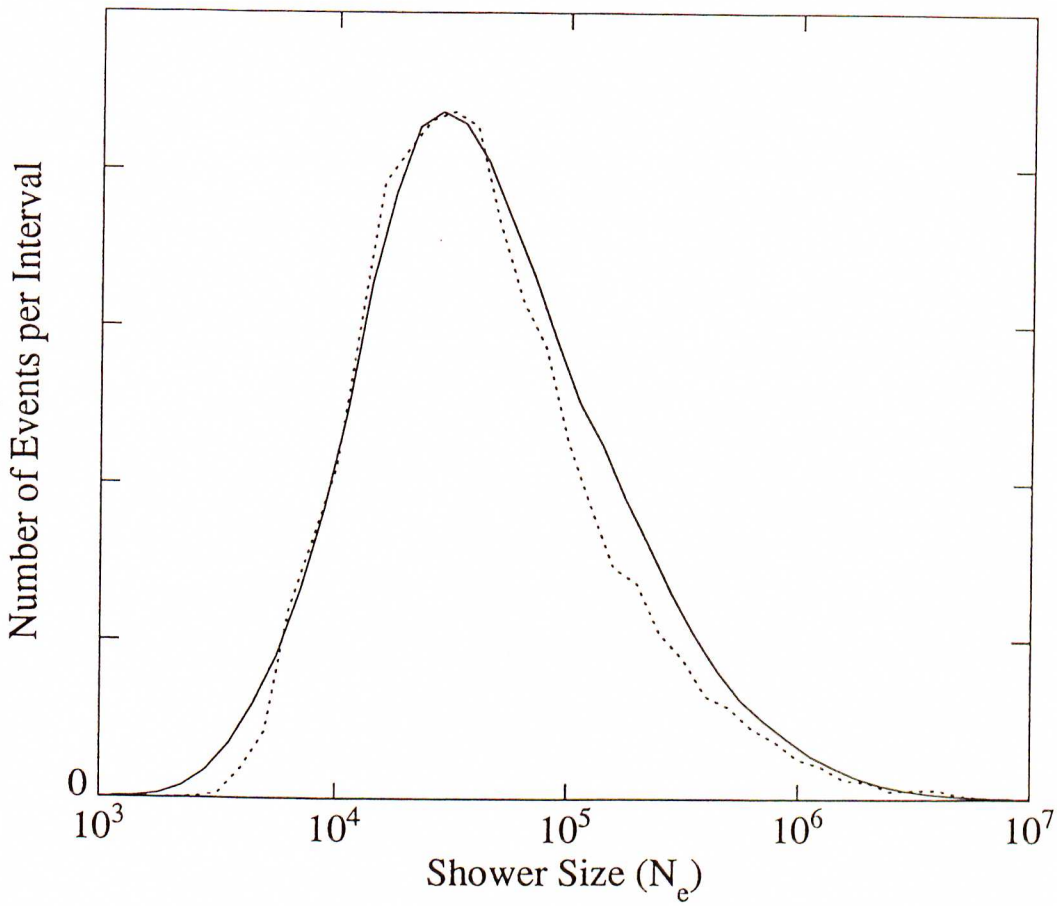

Figure 3.11: Comparison of the observed shower size spectrum (solid line) with that simulated (broken line) for the 1984–1989 data set (see text for simulation details).

areas were used:

Shower Size	Perimeter of Region (m)	Area (m^2)
$3 \times 10^4 < N_e < 10^5$	$\|x\| < 17 \quad -31 < y < 18$	1666
$10^5 < N_e < 5 \times 10^5$	$\|x\| < 27 \quad -47 < y < 26$	3942
$N_e > 5 \times 10^5$	$\|x\| < 61 \quad -67 < y < 52$	14518

A vertical integral shower size spectrum was produced and appears in Fig 3.12. The shaded region indicates the range of values suggested by the compilation of Hillas (1980). The experimental data points agree with this compilation.

Events were binned into both size and zenith angle (2° intervals) bins within these constraints. The consideration of zenith angles is important as atmospheric path length increases with zenith angle, resulting in a more severe attenuation of the E.A.S. Integral rates were determined by dividing by the array area, solid angle viewed, and the exposure time, and then integrating.

The overall integral shower size spectrum for all of the zenith angle ranges considered (0°–40°) appears in Fig 3.13. The knee of the primary energy spectrum manifests itself clearly at $\sim 10^{5.7}$ particles. For showers with vertical sea-level shower sizes below $\sim 3 \times 10^5$ particles, the spectrum may be described by a power law function of the form

$$I(> N_e) = 10^{-\beta} \left(\frac{N_e}{10^5}\right)^{-\gamma} \mathrm{m}^{-2}\mathrm{s}^{-1}\mathrm{sr}^{-1} \tag{3.19}$$

with $\beta = 5.7 \pm 0.1$, $\gamma = 1.65 \pm 0.08$ (Bird and Clay 1990b).

These parameters are in agreement with previously determined values (Hillas 1975b) and the rate of events above a measured sea-level size of 10^5 particles agrees well with the compilation of Nagano *et al.* (1984).

Using those data it was also possible to measure the atmospheric attenuation of E.A.S. as a function of atmospheric depth. Assuming that the integral rate of showers at a given size is constant, the apparent decrease in shower size with increasing zenith angle is a result of further attenuation of the shower, due to the atmospheric absorption of particles resulting from the larger path length. Using constant intensity cuts, it was

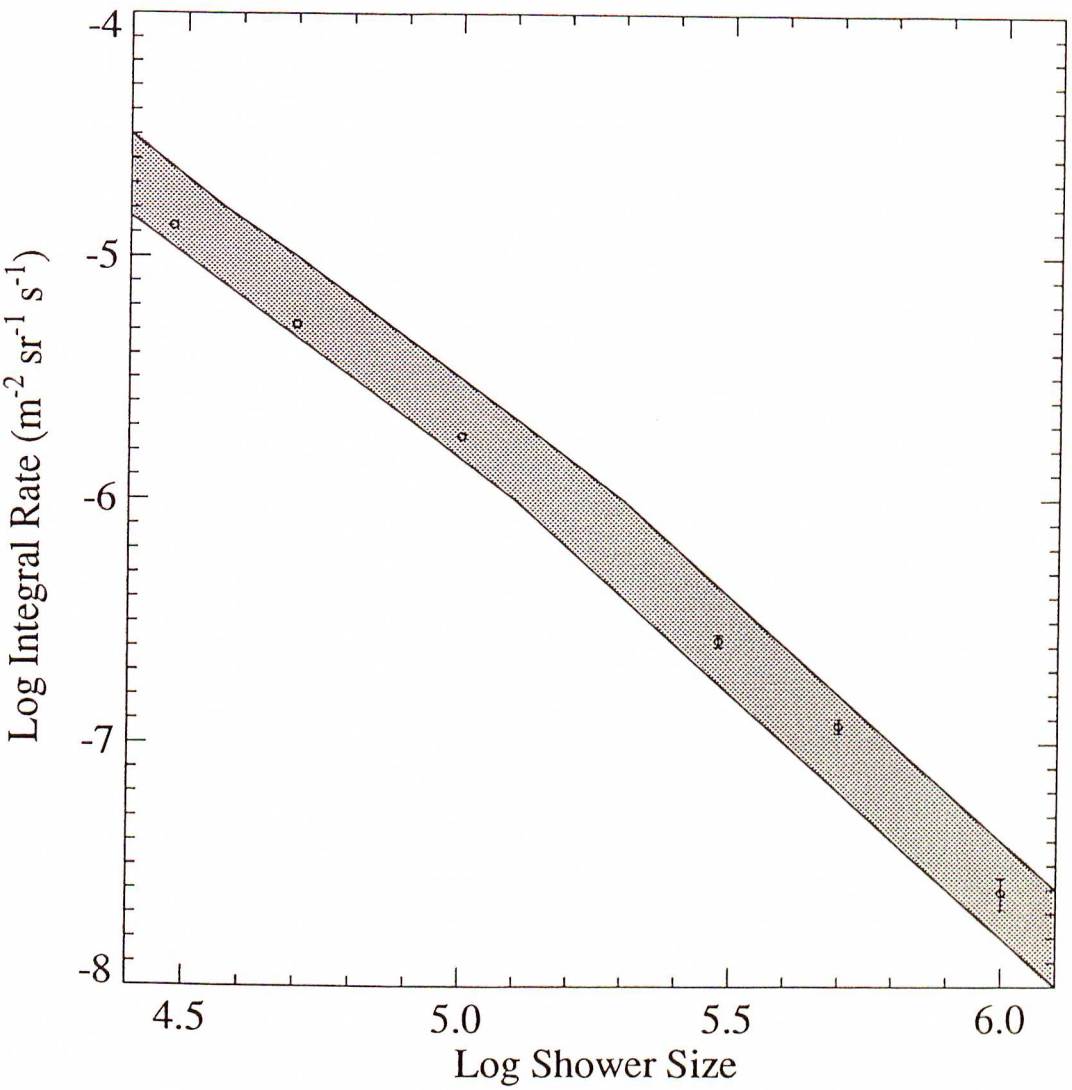

Figure 3.12: The integral vertical shower size spectrum derived from Buckland Park measurements. The shaded area indicates the region suggested by the compilation of Hillas (1980).

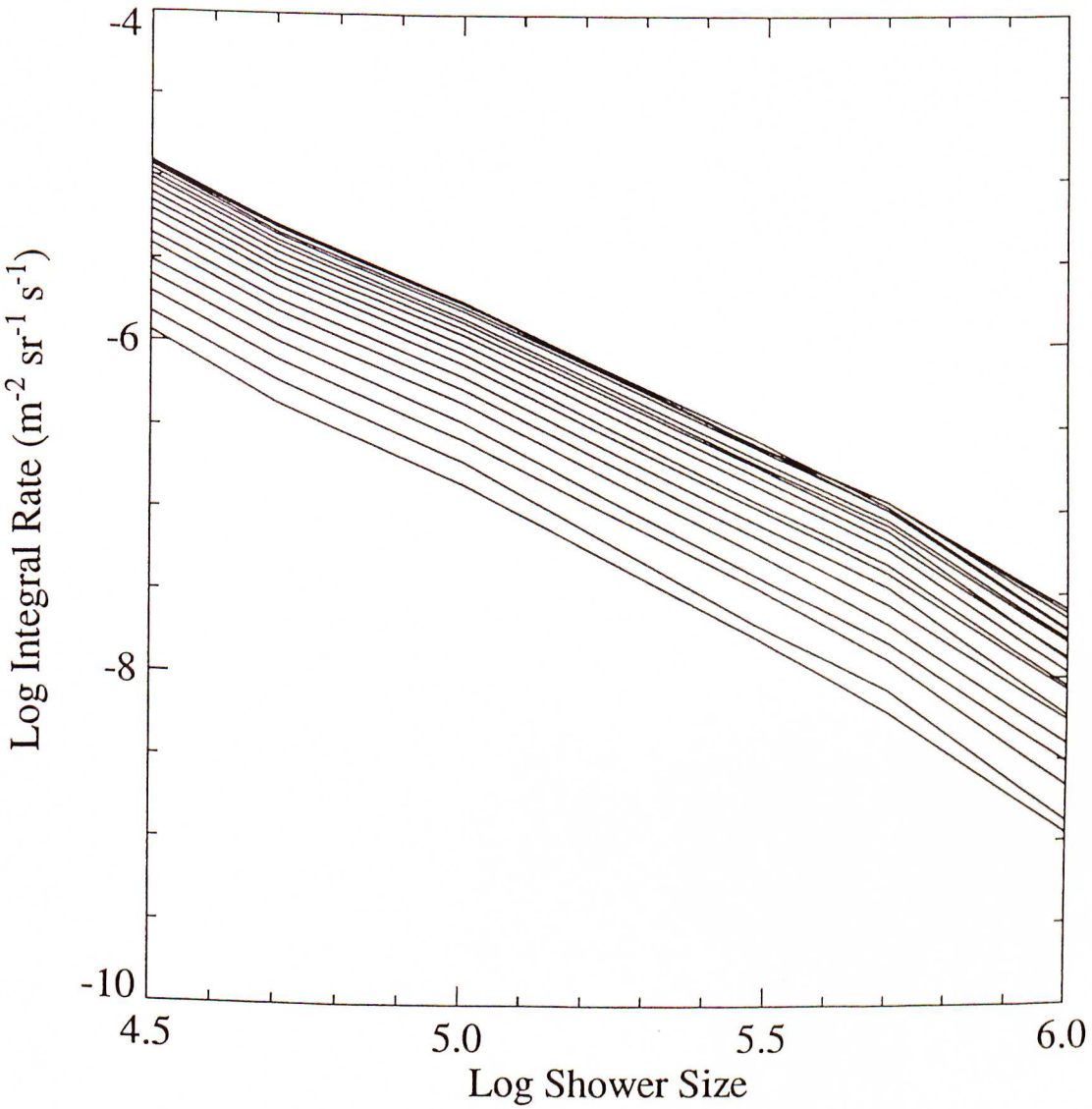

Figure 3.13: Integral shower size spectrum measured at Buckland Park. The lines correspond to zenith angles ranging from 0 to 40 degrees in 2 degree intervals. Constant intensity cuts on this diagram provide a measure of shower attenuation in the atmosphere (See Fig 3.14)

possible to estimate shower size attenuation. Fig 3.14 shows fits to shower size attenuation for selected vertical shower sizes. Between depths of 1030 gcm^{-2} and 1400 gcm^{-2}, the attenuation is a good approximation to exponential with a characteristic length of ~ 200 gcm^{-2}. (Bird and Clay 1990b)

There appears to be a systematic change in this length from 192 ± 6 gcm^{-2} at a vertical size of $10^{5.4}$ particles to 215 ± 8 gcm^{-2} at $10^{5.9}$ particles (see Fig 3.13). This is consistent with an effect discussed by Ashton *et al.* (1975) whose compilation suggests a systematic increase in characteristic length with size of ~ 40 gcm^{-2} per decade in the size range 10^5 to 10^7 particles.

Shower Age Distribution

Apart from the shower size, the NKG function contains another parameter, known as the shower age (see 2.4), which is related to the relative development of the E.A.S. when it reaches the detectors. This parameter was fitted to the showers along with the shower size and core position. The resulting distributions are shown in Fig 3.15. The mean age of these distributions is ~ 1.20, consistent with measurements from other arrays.

The same data set as that used for the integral size spectrum shows a progressive reduction in age with shower size of 0.1 ± 0.04 per decade over the range $10^{4.5} - 10^{5.5}$ particles, with a mean value of 1.32 ± 0.02 at a size of $10^{5.5}$ particles (Bird and Clay 1990b). This latter value agrees well with earlier Buckland Park results above $10^{5.5}$ particles (Clay *et al.* 1981; Gerhardy 1983), and the rate of change with size is similar to that obtained in the compilation of Asakimori *et al.* (1983).

Overall, these results suggest a particularly rapid change of age with size through sizes close to the knee of the primary energy spectrum.

3.4.3 Event Time-Spacing Distribution

The time spacing of successive cosmic ray events is generally considered to be approximately random, as a result of both the distribution of sources, and the randomising

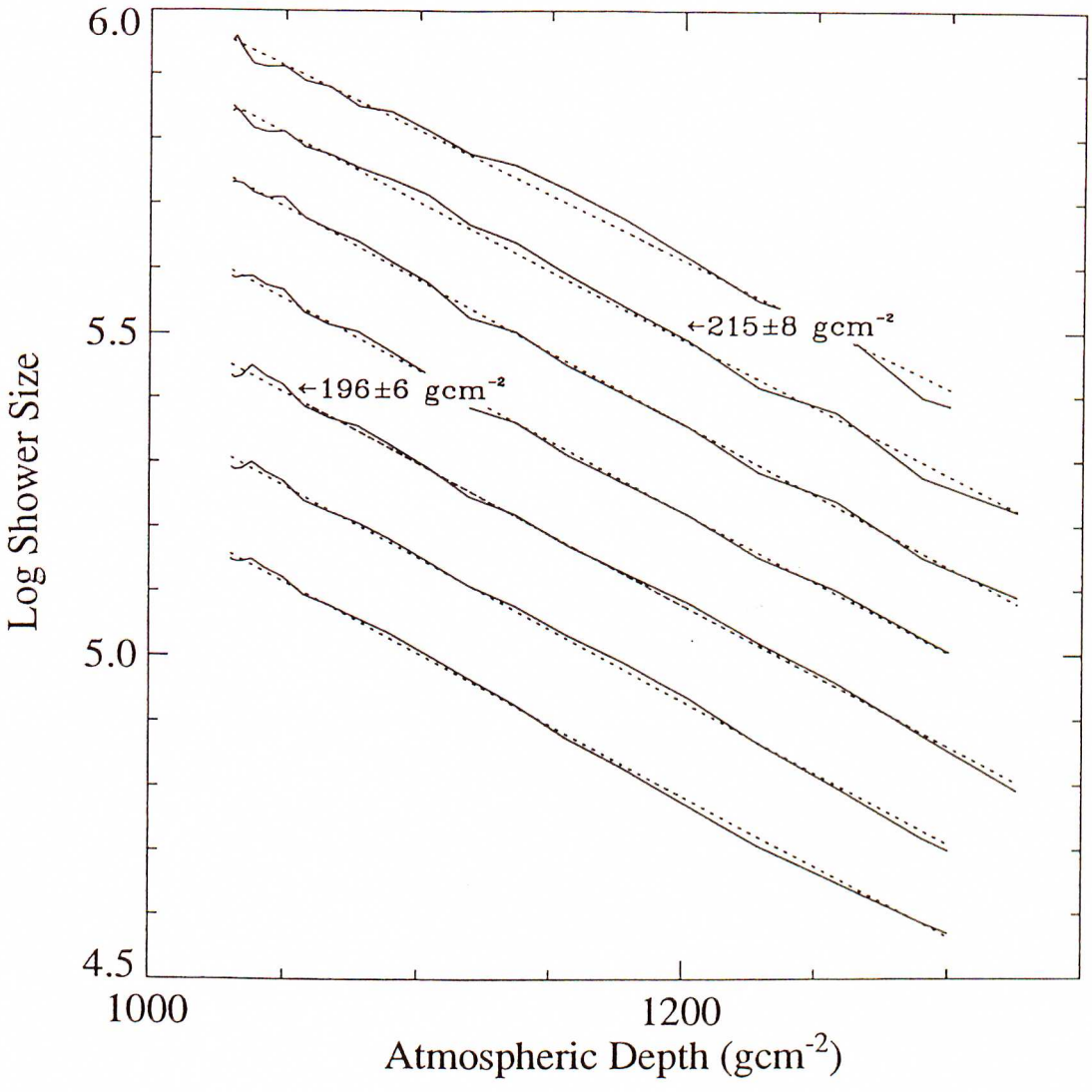

Figure 3.14: The attenuation of showers detected at Buckland Park, using the constant intensity cuts described in the text. Dashed lines indicate least squares fits to the lines and the numbers indicated correspond to the data referred to in the text.

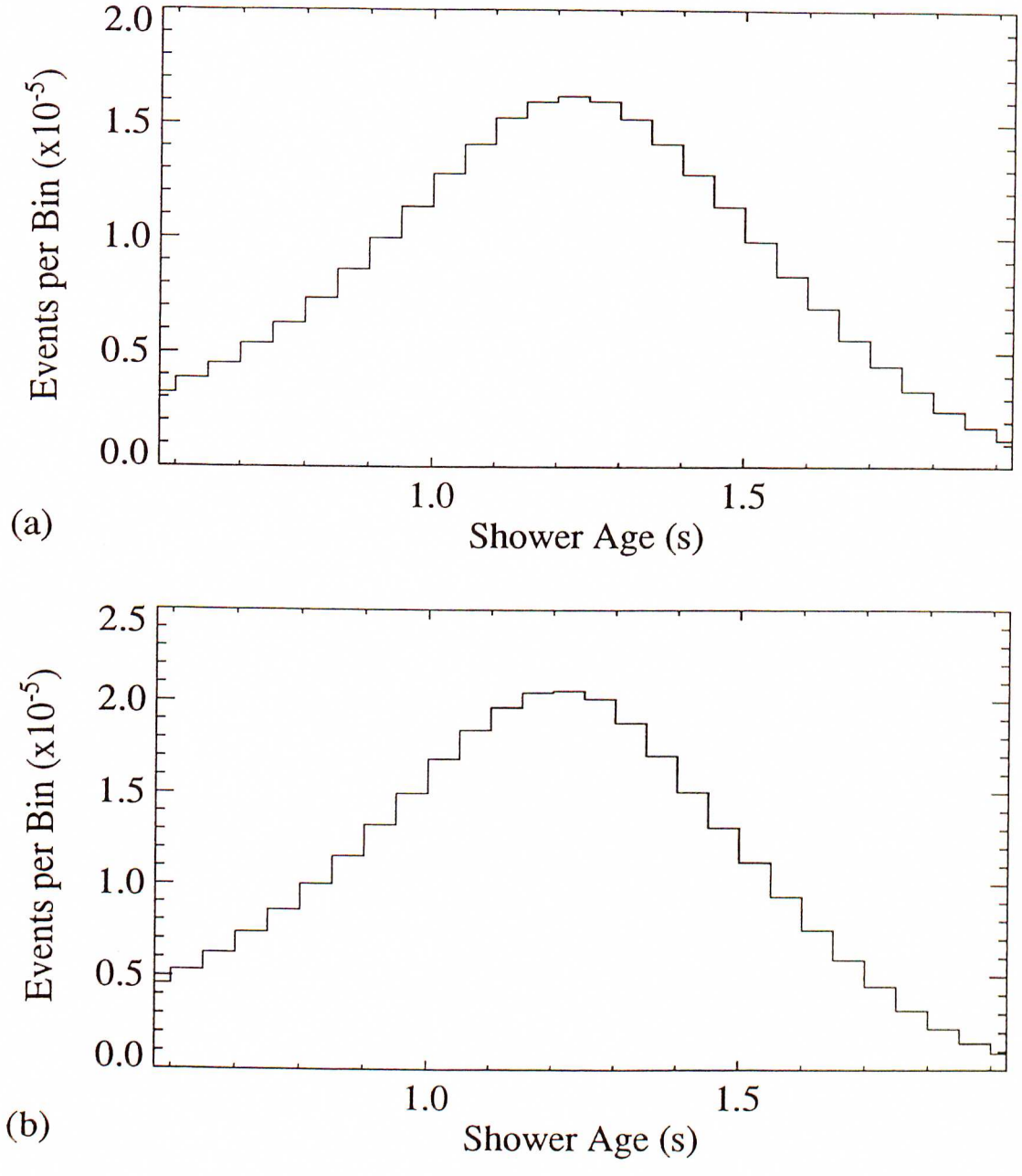

Figure 3.15: The derived shower age distributions for the two data sets analysed.
(a) 1984–1986 data set
(b) 1986–1989 data set

effect of the galactic magnetic field on charged cosmic ray particles as they propagate through the inter-stellar medium.

For such random events, the probability distribution of successive arrival times obeys Poisson statistics (see e.g. Bevington 1969), and is given by

$$p(t) = k \exp(-Rt) \tag{3.20}$$

where R is the mean event detection rate. This leads to a predicted distribution for the number of event spacings between a time t, and time $t + dt$, given by

$$N(t, dt) = N_{\circ} R \exp(-Rt) dt \tag{3.21}$$

where $N_{\circ}$ is the total number of events detected.

Using such an analysis, Bhat *et al.* (1979, 1980) identified an excess of small event time-spacings (< 25 seconds) corresponding to $\sim 12\%$ of the total number of events, suggesting a non-random component in the flux of cosmic ray primaries at energies just above 10^{14}eV. This non-randomness was interpreted as the emission of neutral particles (including γ-rays), by objects such as pulsars and γ-ray bursters, which could maintain coherence while propagating through the inter-stellar medium without being affected by the galactic magnetic field. Subsequent investigations failed to confirm this observed excess, apart from a 1% excess in muon detection rates in time-spacings < 37 seconds reported by Badino *et al.* (1980).

Several investigations into the event time-spacing distribution of cosmic ray events have been carried out using the Buckland Park E.A.S. Array (e.g. Clay and Gerhardy 1980; Clay and Dawson 1981; Bruce *et al.* 1985), all reporting results consistent with random expectations. It is therefore appropriate to examine the data to be used in the anisotropy analysis of Chapter 5 for such a randomness, a necessity for the successful application of an anisotropy analysis.

The event time-spacing distributions of cosmic ray events derived from the analysed events of the 1984–1986 and 1986–1989 data sets with the previously discussed parameter cuts imposed appear in Fig 3.16. The array dead-time (~ 0.5s) manifests

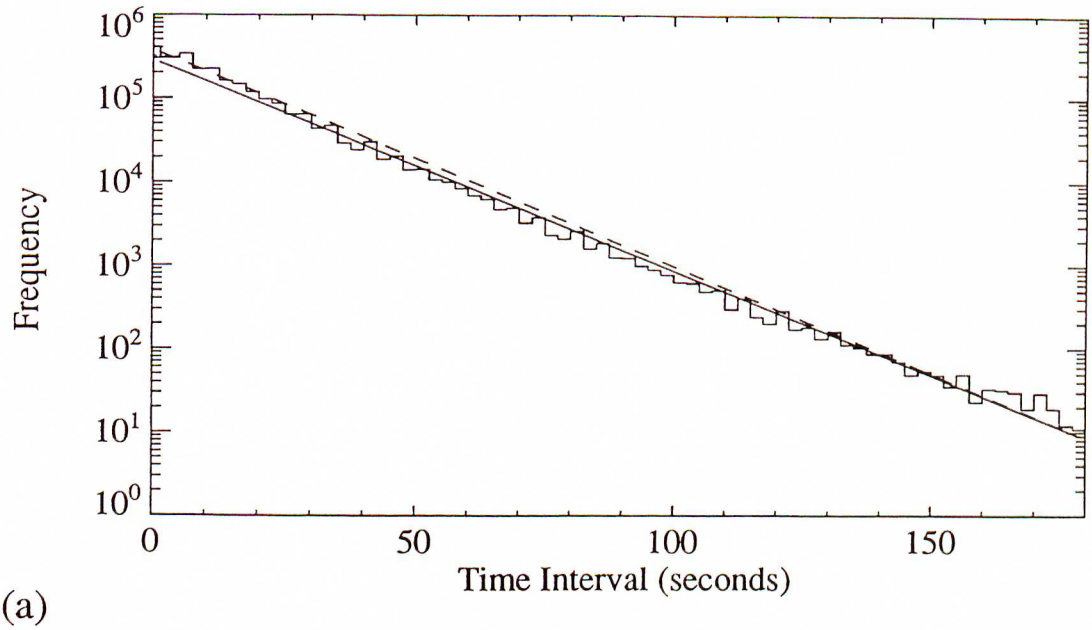

(a)

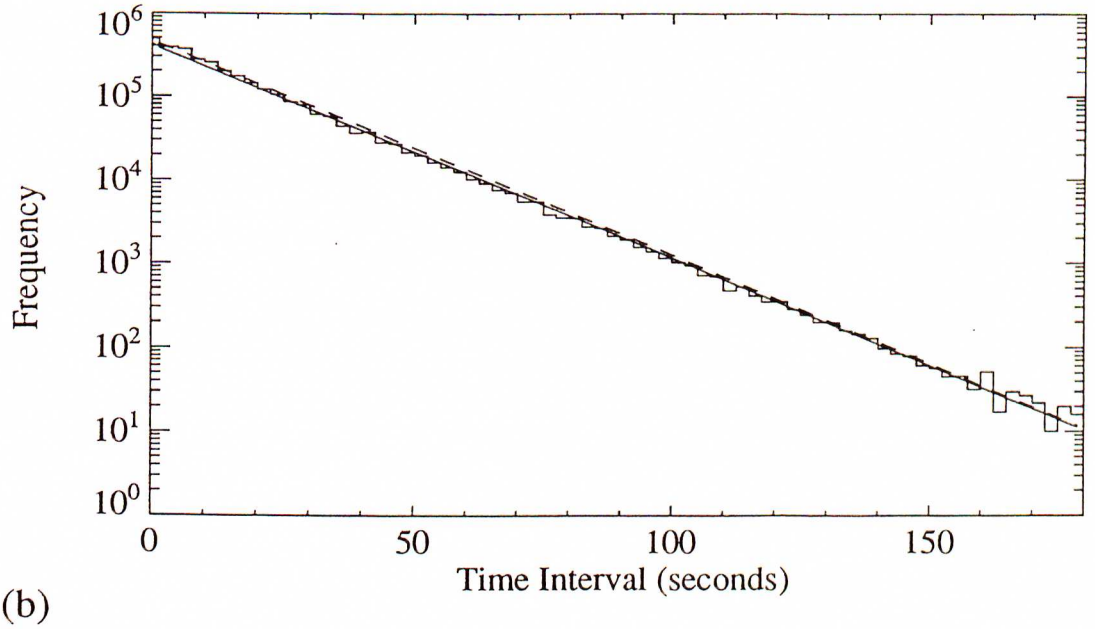

(b)

Figure 3.16: The event time-spacing distributions for the two data sets under consideration (see text for discussion).

(a) 1984–1986 data set

(b) 1986–1989 data set

itself as a slight deficiency of events in the initial bin (bins are 2.5 seconds wide) which has been corrected for. For the 1984–1986 data set, the experimentally determined spacing is 14.7 seconds (represented by the dashed line in Fig 3.16(a). The solid line in Fig 3.16(a) is the line of best fit to the histogram, corresponding to an average event spacing of 15.1 $\pm$ 0.1s. From this diagram, it is clear that there is a problem with the 1984–1986 data set, as the histogram appears to be slightly concavely curved, suggesting the presence of a non-uniformity in the analysed event rate over this period. The problems associated with this data set for the anisotropy analysis will be discussed in some detail in 5.3.1. The 1986–1989 data set, with an experimentally determined average analysed event spacing of 15.4 seconds (represented by the dashed line in Fig 3.16(b)), has a corresponding fitted average spacing of 15.5 $\pm$ 0.1 seconds and fits the predicted distribution well (within the experimental limits of 1σ), and is therefore suited to an investigation into the primary cosmic ray flux. It is this data set upon which the majority of the anisotropy analysis discussed in Chapter 5 was based. The time event-spacing distribution of the 'new' array will be examined in 3.6.1.

3.5 Development of Buckland Park (1989–1990)

The decision to again upgrade the Buckland Park E.A.S. Array (see 3.2.2 for details of previous development) was based upon a number of factors (see Bird and Clay 1989 for a brief summary and description).

The lowering of the array threshold to $\sim 3 \times 10^4$ particles in 1984 (Clay *et al.* 1985) in order to study the cosmic ray flux below the knee of the primary energy spectrum had resulted in a dramatic ($\sim$100-fold) increase in the array event rate, the majority of these E.A.S. having sea-level sizes below 10^5 particles. It was decided that a sufficient number of events had been collected in this lower end of the size spectrum, and in order to ease the data analysis procedure, it was decided to increase the array threshold to $\sim 10^5$ particles. In addition, the collecting area for E.A.S. above this size was to be increased through the addition of detectors in order to collect a larger number of these

events. The addition of further spaced detectors (with timing capability) would also allow investigations into both shower-front curvature at large distances, and the so-called Linsley effect (Linsley 1983) which requires spacings of several hundred metres from the shower core.

Apart from these purely scientific factors, the data recording system, most notably the NOVA 4S Mini-computer was showing signs of age. The NOVA had become very erratic and unreliable by early-to-mid 1989. The installation of a 'modern' multi-tasking computer would also have the advantage of allowing continuous data collection without constant breaks required for tape-changing and other computer-related maintenance.

During the latter half of 1989, Buckland Park was essentially shut down whilst the electronics and recording system was rewired and updated, along with the addition of eight new detectors, and the relocation of four existing detectors. A discussion of this development and the behaviour of the 'new' array follow in the remainder of this chapter.

3.5.1 Detector Design and Construction

In order to upgrade the Buckland Park E.A.S. Array, it was necessary to construct additional detectors. These detectors were to be kept simple and portable.

A prototype detector was initially constructed, based upon a rectangular water tank of dimensions (1100 mm×1100 mm×700 mm), with a side-mounted lid. A $1m^2$ NE102-type scintillator[5] (50 mm thick) was placed in the tank after being painted with highly reflective white scintillator paint (NE560), in order to direct the majority of the emitted photons upwards. The side lid was then closed and sealed.

A 2 inch diameter hole was punched in the top of the detector and the single photomultiplier[6] to be used in these detectors inserted through this hole. This tube

[5] $1m^2$ has been found to be the optimum scintillator size for the dual purposes of timing and density measurements. Ideally, smaller sizes are used for timing measurements and larger sizes used for density measurements, but $1m^2$ has been found to be adequate for both.

[6] RCA type 8575, with a typical rise-time of 2 ns, and a peak sensitivity at a wavelength of 385 nm.

was supported by the 'base', consisting of a socket and dynode chain, constructed within a small die-cast box, and mounted exterior to the detector to simplify maintenance. The 'top' of the detector was reinforced with a 1/8 inch thick sheet of aluminium to assist in supporting the base. The arrangement was made light-tight through the use of gaskets, an opaque sealant, and Wotan cloth tape, and appears in Fig 3.17.

The dual tasks of fast-timing and particle density measurements to be performed by this detector have contradictory requirements. Fast-timing requires the accurate measurement of the arrival time of the first light produced by the shower-front, whereas density measurements require the detection of the majority of the photons emitted by the scintillator in order to be accurate. This is normally achieved by using a pyramidal shaped detector, with its inside coated with reflective paint. Extraneous light signals resulting from reflections can confuse timing signals and these detectors are normally coated black inside to minimise these reflections. As a compromise measure, the insides of the detector were left the natural galvanised iron colour, and the detector was found to behave satisfactorily for both purposes.

Due to the dual purpose of the photomultiplier signal, it was not possible to use an on-site charge-sensitive preamplifier to produce a suitable signal for the A.D.C. as is the case with the existing detectors. Such a preamplifier would absorb the photomultiplier signal, eliminating the possibility of obtaining accurate timing information. As an alternative, a voltage-sensitive preamplifier was designed and constructed, to be sited within the ATCO Electronics Hut. To minimise signal attenuation *en route*, large bandwidth 50Ω RG8 cable was to be used to carry the photomultiplier signal to the central hut. A splitter would then be used to divide this signal with one output passing to the preamplifier and the other going to the timing channel.

Signals from timing tubes are in general noisier than those from 'slow' tubes, and no S.P.P. was apparent in the ungated pulse-height spectrum (swamped by noise). The gated pulse-height spectrum produced with the aid of a gating detector clearly showed a S.P.P. However, it is impractical to have either a gating scintillator located at each detector, or to transport such a scintillator from detector to detector. Instead, in order

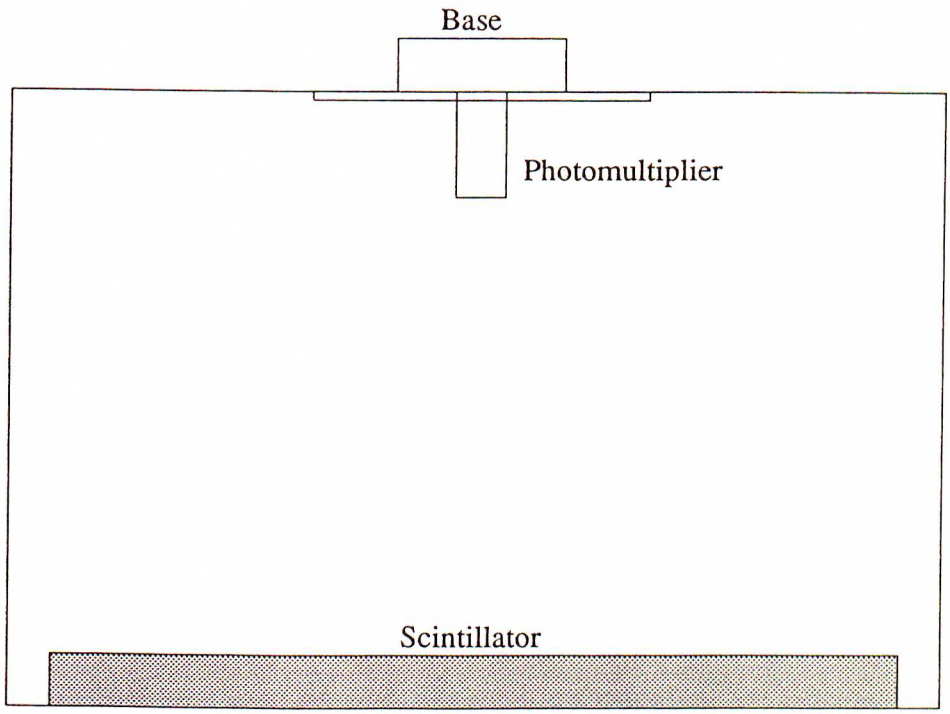

Figure 3.17: Design of the new detector, eight of which were installed at Buckland Park during the development of the array. See text for design and construction details.

to estimate the S.P.P. for these detectors, rates from a detector with a known S.P.P. were used to determine the number of counts expected above the 1, 2, 3, 4, 5 & 6 particle levels in a given time (averaged over 5 minutes). These numbers were then used to determine the M.C.A. channel number corresponding to the 3, 4, 5 & 6 particle levels, and linear regression was then used to determine the S.P.P. channel to be used in converting the recorded A.D.C. voltage to particle number for these detectors using Eq 3.1.

The prototype detector was installed next to detector M to supplement timing information, and was found to behave satisfactorily. Consequently, eight additional detectors were constructed to be used in the improvement of the Buckland Park E.A.S. Array.

Before these detectors could be placed in the field however, their optimum positions needed to be determined. This was achieved through the use of computer simulations which will now be discussed.

3.5.2 Simulations

The design of an E.A.S. array is a balance of conflicts between the close detector spacing necessary to determine shower parameters such as core and shower size accurately, and a wider spacing which allows a larger collecting area and hence detects a larger number of showers, as well as providing a larger baseline for timing measurements. In addition to this conflict, there is a need to take into account the presence of the existing array.

In deciding positions for the new detectors, and subsequently the new array triggering conditions, it was first necessary to make the following decisions :

(1) the larger central detectors A1, B1, D1, E1 would be relocated from their central location to the extremities of the array, to provide both timing and density information on the larger showers.

(2) Deployment of the new detectors would be to the south[7] of the current array,

[7]A small swamp/lagoon forms to the immediate north of the array in winter, which would cause problems in detector access and maintenance. In addition, the majority of the existing detectors were

separated by $\sim$ 100m in order to maximise detection and analysis of E.A.S. with sea-level shower sizes of 10^5 particles and above.

This would lead to a raising of the threshold through the removal of those detectors primarily responsible for the triggering of the array on small showers (i.e. well below 10^5 particles), and increase the collecting area for larger showers ($\geq 10^5$ particles) through the addition of the new detectors.

It was then necessary to carry out several simulations in order to

(1) determine the optimum positions of these detectors within the given constraints, and

(2) determine the appropriate triggering conditions given the detector positions determined in (1) to maximise the collecting area for larger showers whilst minimising the array sensitivity to smaller showers.

Detector Positions

The twelve new detector positions were determined by computer simulations using the following method.

Shower sizes and core positions were chosen, and the corresponding particle densities at each site were calculated using the NKG function (see 2.4.1). These numbers then had random fluctuations introduced to simulate the actual measurement fluctuations assuming Poisson statistics. This was achieved using the Normal approximation to the Poisson distribution (see e.g. Bevington 1969), which gives accurate results for particle numbers greater than 6, but leads to an underestimate for those numbers below 6. This results from the fact that the Landau distribution is somewhat narrower than the Poisson distribution. These 'observed' densities were then used to reconstruct the shower using the MINUIT package as discussed in 3.3.2. For each configuration of detectors, core location and shower size, this procedure was repeated ten times, and the mean core location, mean shower size and rms core error were calculated.

Only vertical showers were considered in these simulations as it had been previ-

located south of the array origin.

ously determined that the core errors for inclined showers are not significantly different (Crouch 1979). In addition, most attention was placed upon the rms core error, as it had previously been determined that greater inaccuracies were introduced by typical core errors than shower size errors (Crouch 1979).

Within the constraints considered, the array model progressed through several stages until the configuration shown in Fig 3.18 was reached. The new detectors are labelled 1,...,8 and detectors A1, B1, D1, E1 were repositioned as shown. Detector 4 is located $\sim$ 15m southwest of its optimum position due to complications in laying cables across/below the array access road. The detectors were initially placed within 5m of their optimum positions, and accurate positions were determined from an aerial photograph provided by the South Australian Department of Lands.

Once the detector positions had been decided upon, it was then necessary to determine the new array triggering criteria.

Array Triggering

The triggering probability at a point on the array (for a given shower size) was found as follows. The density at each detector was calculated using the NKG function. A random Poisson fluctuation was then introduced, to estimate the actual number of particles observed by the scintillator, as previously discussed. This number was then compared with the threshold set for each detector in question. If a 2-fold coincidence was found for both the 'slow' and 'fast' triggering schemes, an event was recorded. This process was repeated on a 5m$\times$5m grid, centred on the array, whose size was related to the shower size (e.g. up to $\sim$ 1.4 km for a sea-level shower size of 10^8 particles).

In this way, the triggering probability $P(N_e, x, y)$ was determined for each shower size and core location for each triggering scheme considered. The total collecting area of the array as a function of shower size, $A(N_e)$, may then be calculated as

$$A(N_e) = \int\int P(N_e, x, y) dx dy \tag{3.22}$$

It is this number which was used to compare different triggering schemes in order to

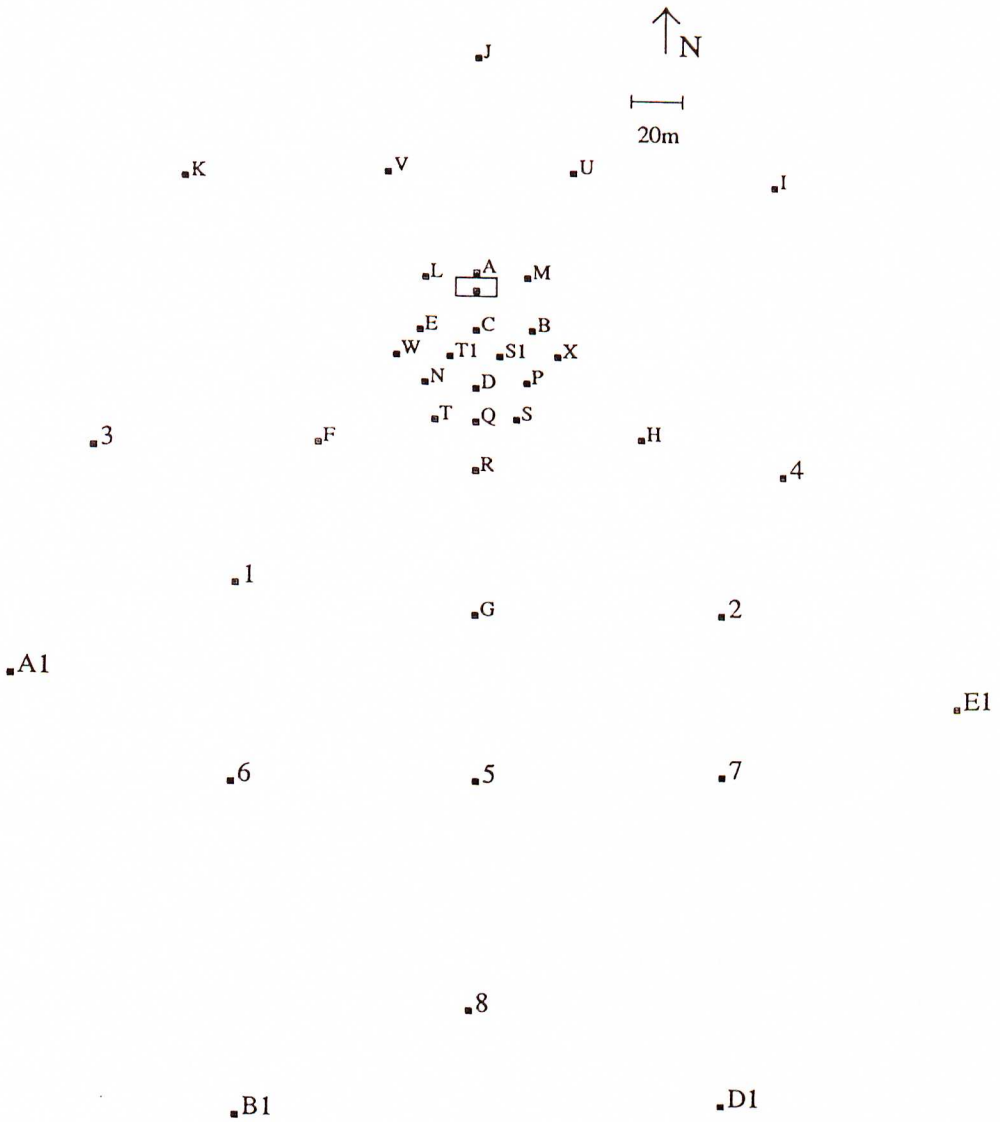

Figure 3.18: The layout of the Buckland Park Extensive Air Shower Array from 1990 onwards. The unlabelled detector is BFD contained within the ATCO Electronics Hut (large rectangle). The detector specifications are given in Table 3.2.

Detector Label	Type (Fast/Slow)	Position x (m)	Position y (m)	Size (m^2)	Trigger (Fast/Slow)	Threshold (particles)
A	F,S	0	22	1	F,S	8
B	F,S	22	0	1	F,S	8
C	F,S	0	0	2.25	F,S	6
D	F,S	0	-22	1	F,S	8
E	F,S	-22	0	1	F,S	8
F	S	-61.5	-43.2	1	S	4
G	S	0	-107.2	1	S	4
H	S	64.8	-40.7	1	S	4
I	S	116	55	1	—	—
J	S	0	130	1	—	—
K	S	-114	56.6	1	—	—
L	F,S	-20	20	1	S	6
M	F,S	20	20	1	S	6
N	F,S	-20	-20	1	S	6
P	F,S	20	-20	1	S	6
Q	F,S	0	-34.6	1	—	—
R	F,S	0	-53	1	F,S	6
S	F,S	16	-33.8	1	F,S	6
T	F,S	-16	-34	1	F,S	6
U	S	37.6	59.6	1	S	6
V	S	-35.1	59.3	1	S	6
W	F,S	-31.3	-9.6	1	—	—
X	F,S	32	-9.8	1	—	—
S1	F	9.4	-10	1	—	—
T1	F	-10.1	-10	1	—	—
BFD	F	0	15	1	—	—
1	F (S)	-93	-97	1	F,S	4
2	F (S)	96	-106	1	F,S	4
3	F (S)	-148	-46	1	—	—
4	F (S)	120	-54	1	—	—
5	F (S)	1	-170	1	F,S	4
6	F (S)	-94	-172	1	—	—
7	F (S)	97	-167	1	—	—
8	F (S)	0	-258	1	—	—
A1	F,S	-179	-133	2.25	—	—
B1	F,S	-91	-298	2.25	—	—
D1	F,S	99	-293	2.25	—	—
E1	F,S	189	-141	2.25	—	—

Table 3.2: Detector Specifications for the 'new' Buckland Park E.A.S. Array (1990). Detector types are as in Table 3.1. Detectors 1–8 are of the type described in the text (and in Fig 3.17). F (S) indicates that the one tube (RCA type 8575) is used for both timing and particle density measurements. New/relocated detectors are listed below the solid line. All fast trigger detector thresholds are at the 2-particle level, and the slow trigger detector threshold levels are given in the last column.

maximise the array performance.

Two approximations were made in carrying out this simulation. Firstly, only vertical showers were considered. This approximation leads to an underestimate of the triggering area, as the apparent detector spacing within the plane of the shower-front is reduced with increasing zenith angle. However, in making comparisons between triggering schemes, this affected each simulation similarly and was therefore not considered important. Secondly, the approximation of the Poisson distribution to a Normal distribution as previously discussed leads to an additional underestimate of the triggering area.

In choosing the detectors and thresholds to be used in the triggering schemes, one must be careful of introducing selection effects which may bias the resultant data. Most importantly, in regions where the triggering probability is less than 50%, shower size may be overestimated through the preferential triggering of showers with upward fluctuations in the mean number of particles detected. This effect may be reduced dramatically by firstly avoiding the use of small detector thresholds (< 4 particles) in the array trigger, and secondly, using detectors well within the physical confines of the array in the array trigger. In this case, if an upward fluctuation causes a trigger, there should be a sufficient number of densities recorded to minimise this overestimation.

It is for this reason that the larger (2.25m^2) detectors A1, B1, D1, E1 were placed on the extremities of the array. Their larger collecting area makes them less susceptible to large fluctuations in particle number compared to the smaller 1m^2 detectors for the corresponding particle density.

In designing the new triggering criteria, symmetry was also taken into account in order to minimise the low-order harmonics in the azimuth angle distribution for the 'old' array (see 3.4.1).

On the basis of these assertions and simulations, new triggering conditions were determined to optimise event detection above $\sim 10^5$ particles, and to minimise shower detection below $\sim 5 \times 10^4$ particles.

Figs 3.19–3.22 demonstrate the triggering contours for the 'old' and 'new' array,

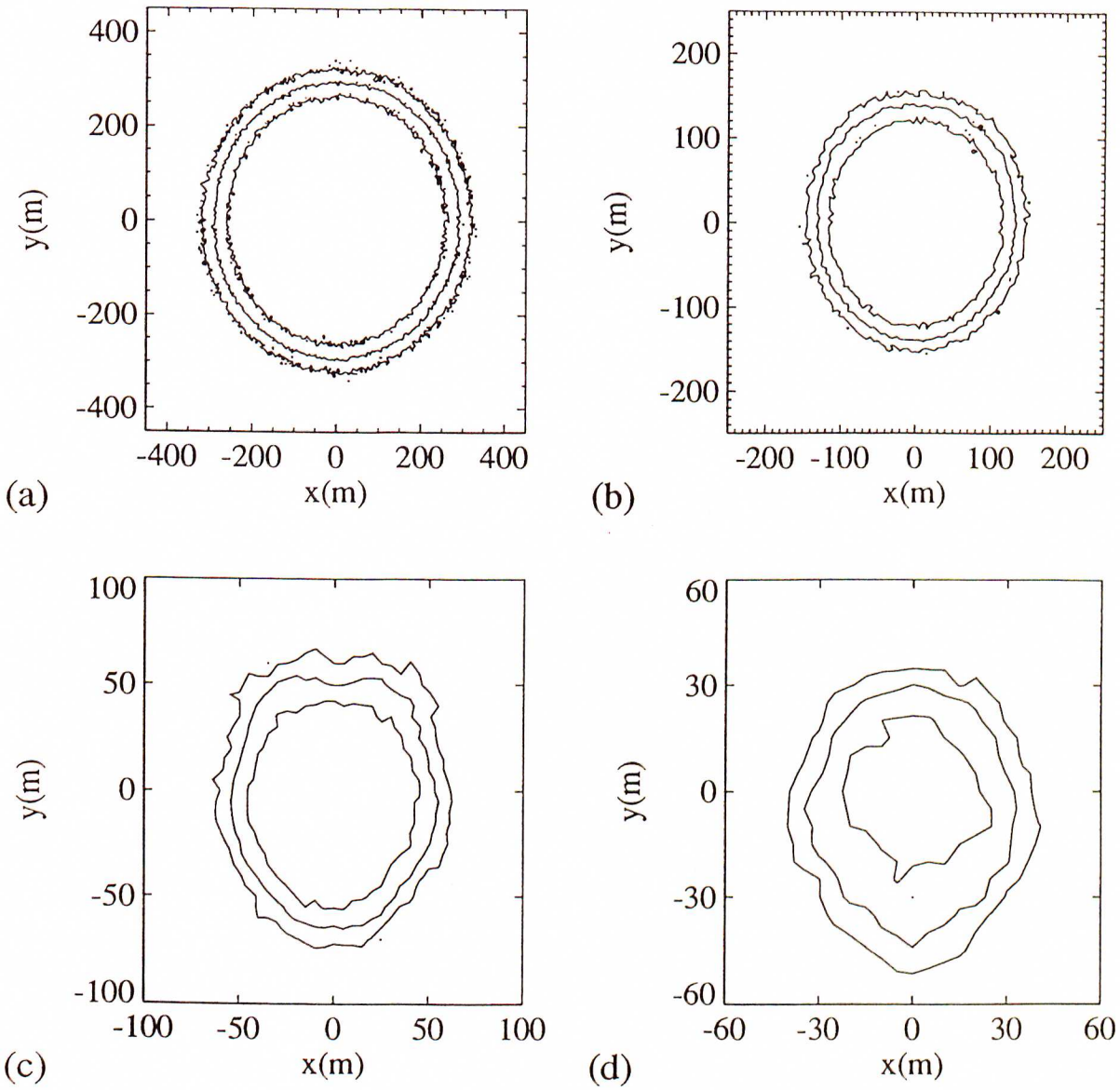

Figure 3.19: Triggering Contours of the Buckland Park E.A.S. Array for the period 1984–1989. Contours shown are 100%, 50% and 10% percentiles, and correspond to the following sea-level shower sizes.

(a) 10^7 particles
(b) 10^6 particles
(c) 10^5 particles
(d) 3×10^4 particles

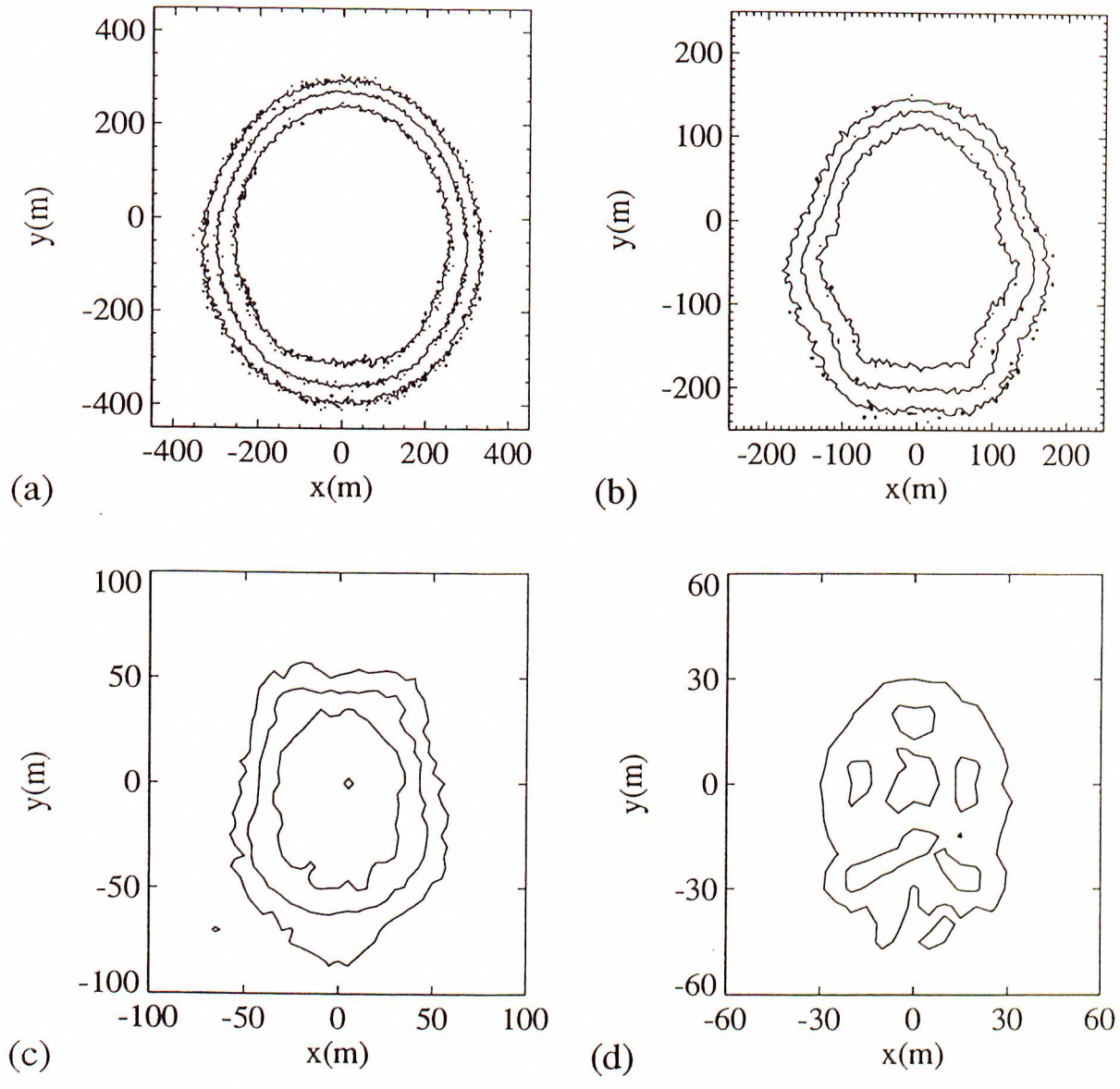

Figure 3.20: Triggering Contours of the Buckland Park E.A.S. Array for the new array (1990). Contours shown are 100%, 50% and 10% percentiles, and correspond to the following sea-level shower sizes.

(a) 10^7 particles
(b) 10^6 particles
(c) 10^5 particles
(d) 3×10^4 particles

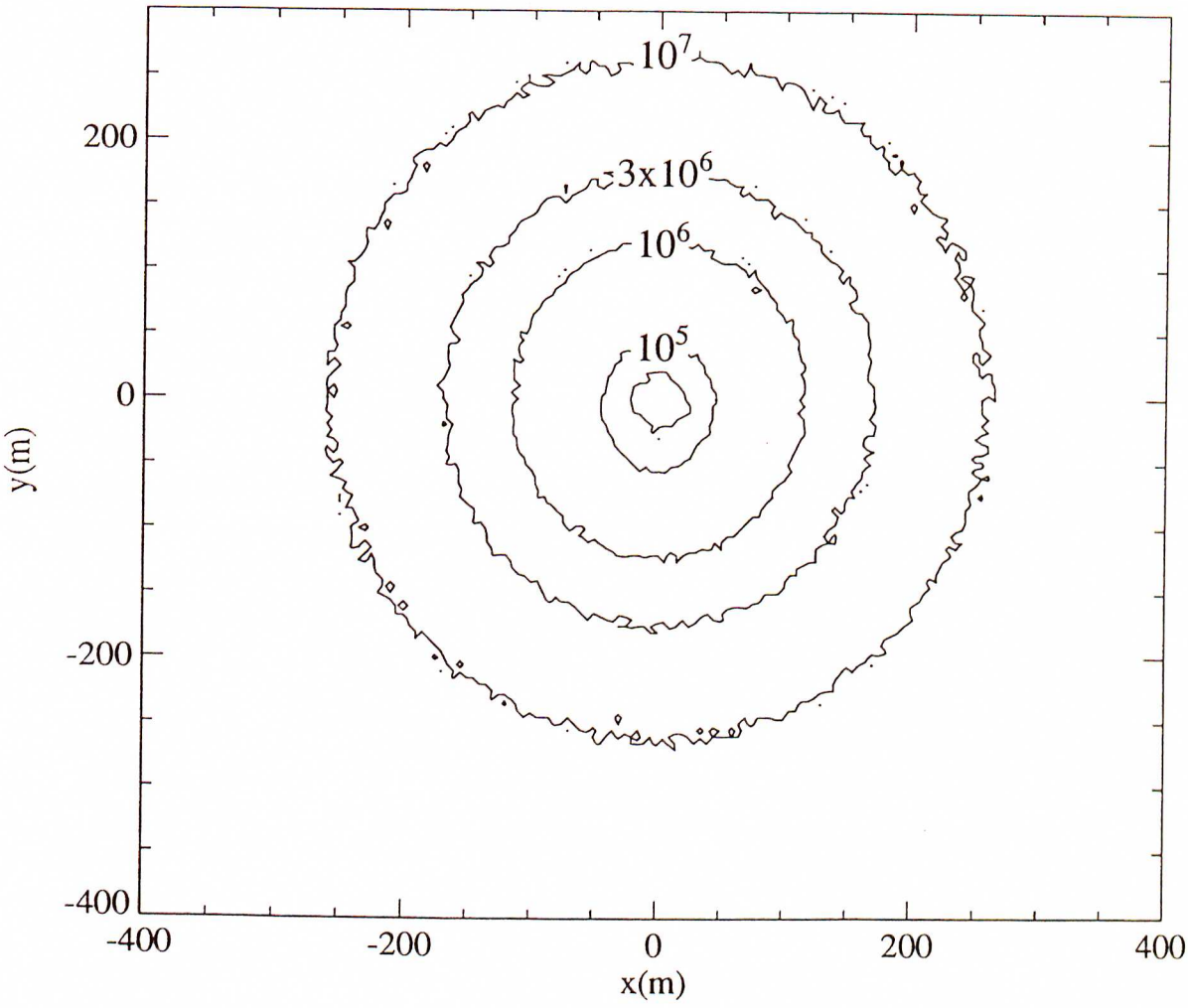

Figure 3.21: 100% contours for the detection of the marked shower sizes with the 'old' array (The smallest region corresponds to a sea-level shower size of 3×10^4 particles).

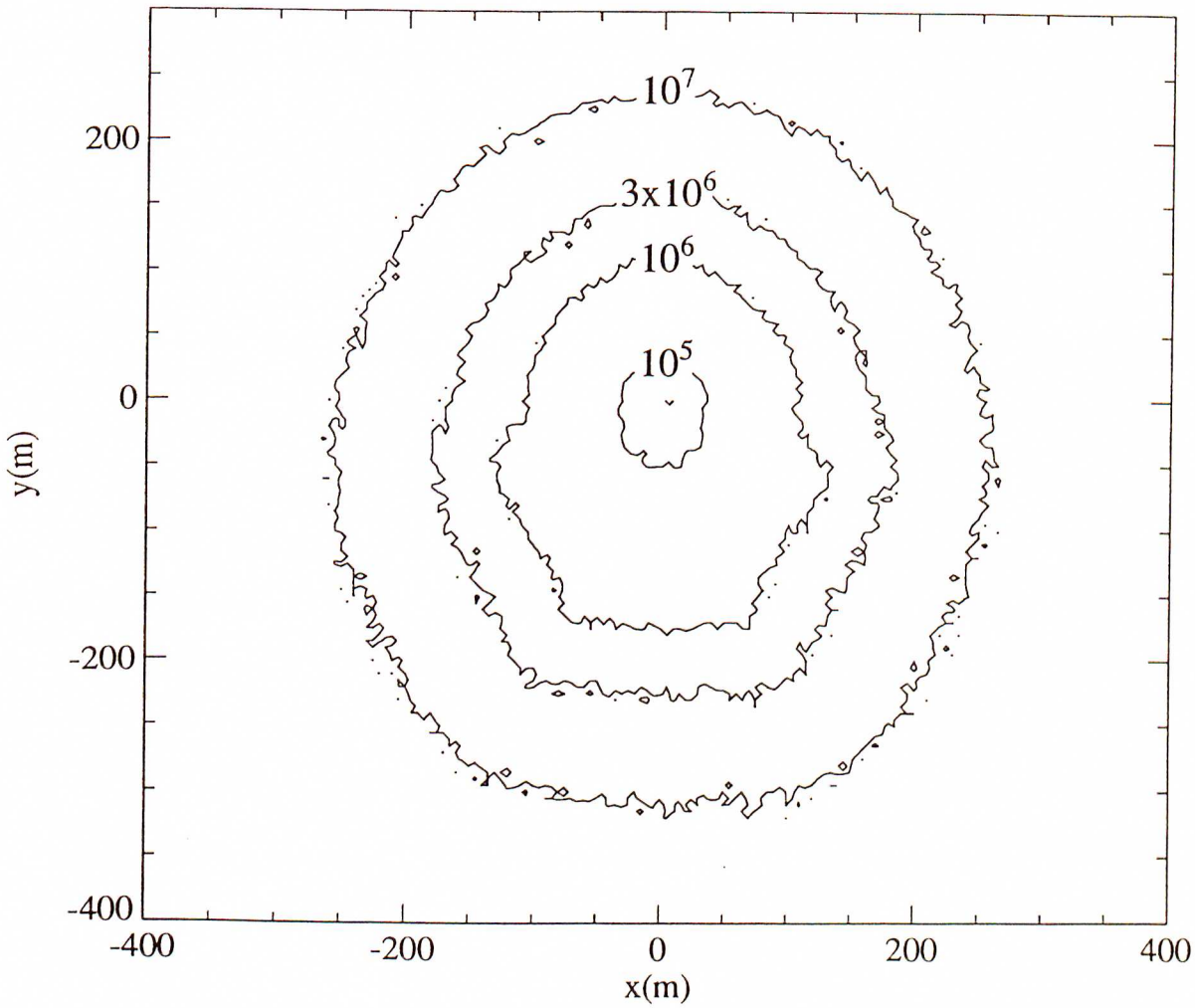

Figure 3.22: 100% contours for the detection of the marked shower sizes with the 'new' array.

and Fig 3.23 shows a comparison of the 'old' and 'new' collecting areas of the array as a function of shower size. This information was used to estimate the shower size spectrum as discussed in 3.4.2, and will be considered in comparison with the observed shower size spectrum in 3.6.3 (see Fig 3.33).

It must be noted that uncertainties resulting from instrumental errors were not included in these simulations, and this fact must be taken into account when comparing the observed array behaviour with that simulated.

3.5.3 Detector Installation and Associated Electronics

The new detectors were initially designed to stand exposed in the paddocks of Buckland Park[8], supported by wooden sleepers. They were firstly insulated with glass-wool insulation, then covered with heavy-duty black plastic, secured with fibreglass-reinforced tape. As a final measure of protection, the detectors were covered by a large, heavy-duty tarpaulin, secured to the ground using eight heavy-duty pegs. However, following the results of three months of exposure to the elements of the coastal plains of Buckland Park, it was decided that sturdier protection was required, and garden sheds of the type used for the existing detectors were constructed around these detectors in late 1988.

The high voltage necessary for the operation of these detectors was carried by 50Ω RG58A cable, whereas the signals were carried to the electronics hut along 50Ω RG8 cable, which possesses a smaller attenuation, and larger bandwidth. Upon reaching the ATCO Electronics Hut, the signal was split using a suitably terminated splitter. One output of this splitter was passed to the timing electronics, whilst the other output was passed to the particle measurement electronics.

Each timing signal was passed through a discriminator set at the 2-particle level ($\sim$ 100 Hz), before passing through a delay set typically at $\sim 1\mu$s, before reaching the STOP of the appropriate T.D.C. channel. The 12-channel T.D.C. used for the eight

[8]the existing detectors were housed in small 'garden' sheds.

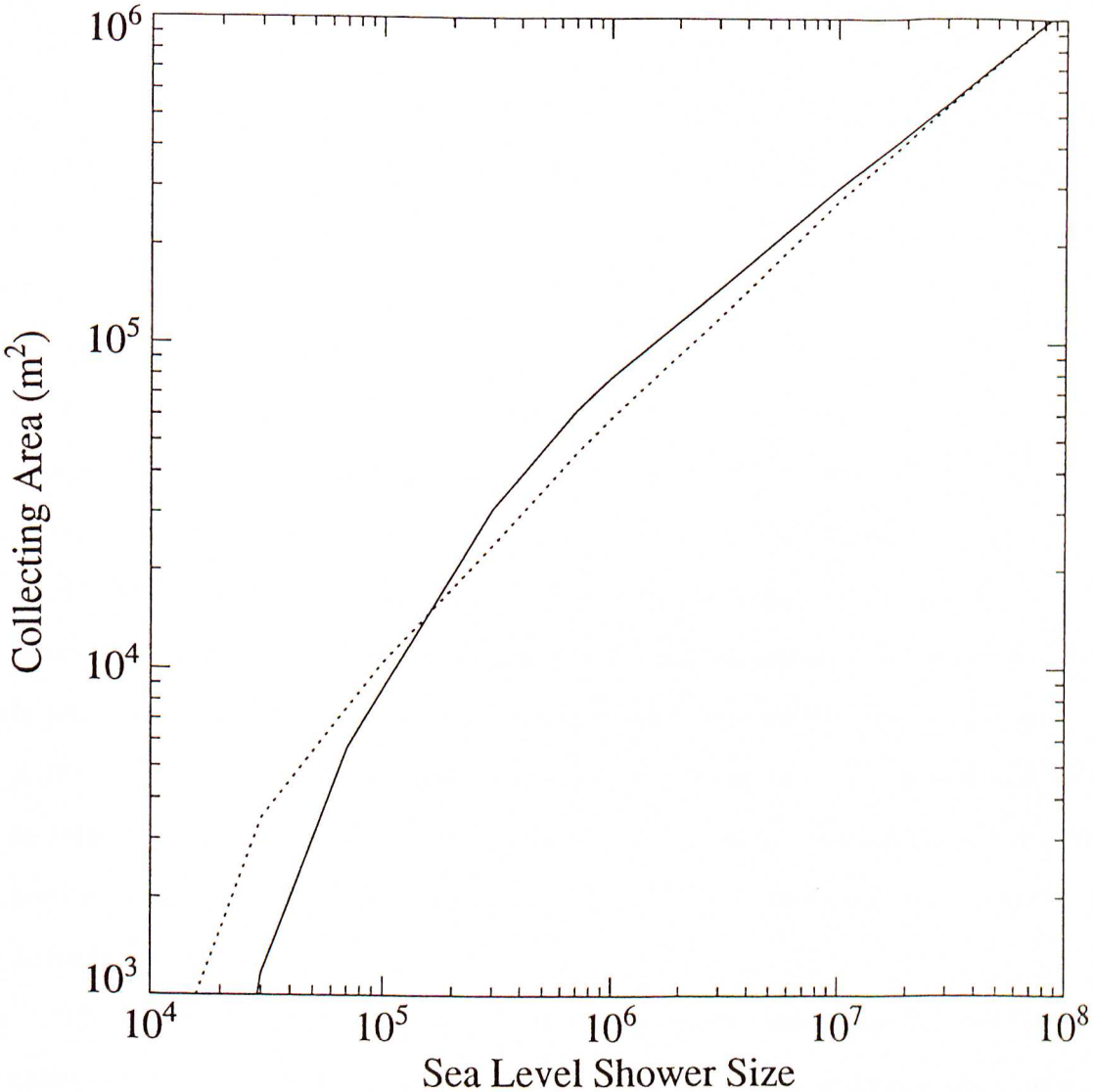

Figure 3.23: Collecting areas as a function of sea-level shower size for the 'new' array (solid line), and the 'old' array (broken line).

new detectors and four relocated detectors was constructed by the Electronics Services Group within the Department of Physics, and was designed to have a 1μs range with 0.5 ns resolution. This range was found to be inadequate, and the T.D.C. was altered to provide a 4μs range with a 1 ns resolution. The fast-timing signals from detectors A1, B1, D1 & E1 were also passed through delays of $\sim$ 1μs before stopping the appropriate T.D.C. channel.

In addition to the timing information, three of these detectors (1, 2, & 5) contributed to the 'fast' (and 'slow') trigger (see Table 3.2). The 'fast' trigger of the 'old' array was based upon coincidences within $\sim$ 100 ns from the 'fast' detectors in question. However, including these new detectors required an increase in this time to $\sim$ 1μs for the further spaced detectors in the array 'fast' trigger (1, 2, 5 & R) due to delays resulting from both shower propagation and cable lengths. The appropriate discriminators were altered to produce 1μs length output pulses. The raw times recorded by the new T.D.C. are shown in Fig 3.24, and show behaviour consistent with the triggering criteria.

The other output of the splitter was passed to a voltage-sensitive preamplifier which effectively integrated over the input pulse, providing an estimate of the particle density. It was then passed to a line receiver and inverter before terminating in the appropriate A.D.C. channel. The calibration of these 'slow' channels were checked and adjusted fortnightly to maintain consistency in particle measurements from these detectors. In addition, detectors 1, 2, & 5 contributed to the 'slow' trigger of the array at the 4-particle level (see Table 3.2).

The installation of the new detectors and associated electronics as well as the relocation of A1, B1, D1, E1 was carried out during late 1989, and occurred concurrently with the upgrading of the array data recording system, which will now be discussed.

3.5.4 Data Recording and Array Control System

By 1988, it had become apparent that the NOVA 4s Mini-computer used to control the Buckland Park E.A.S. Array was due for replacement. This, combined with the requirement for continuous data sets not broken by tape changes every 3–4 days (see

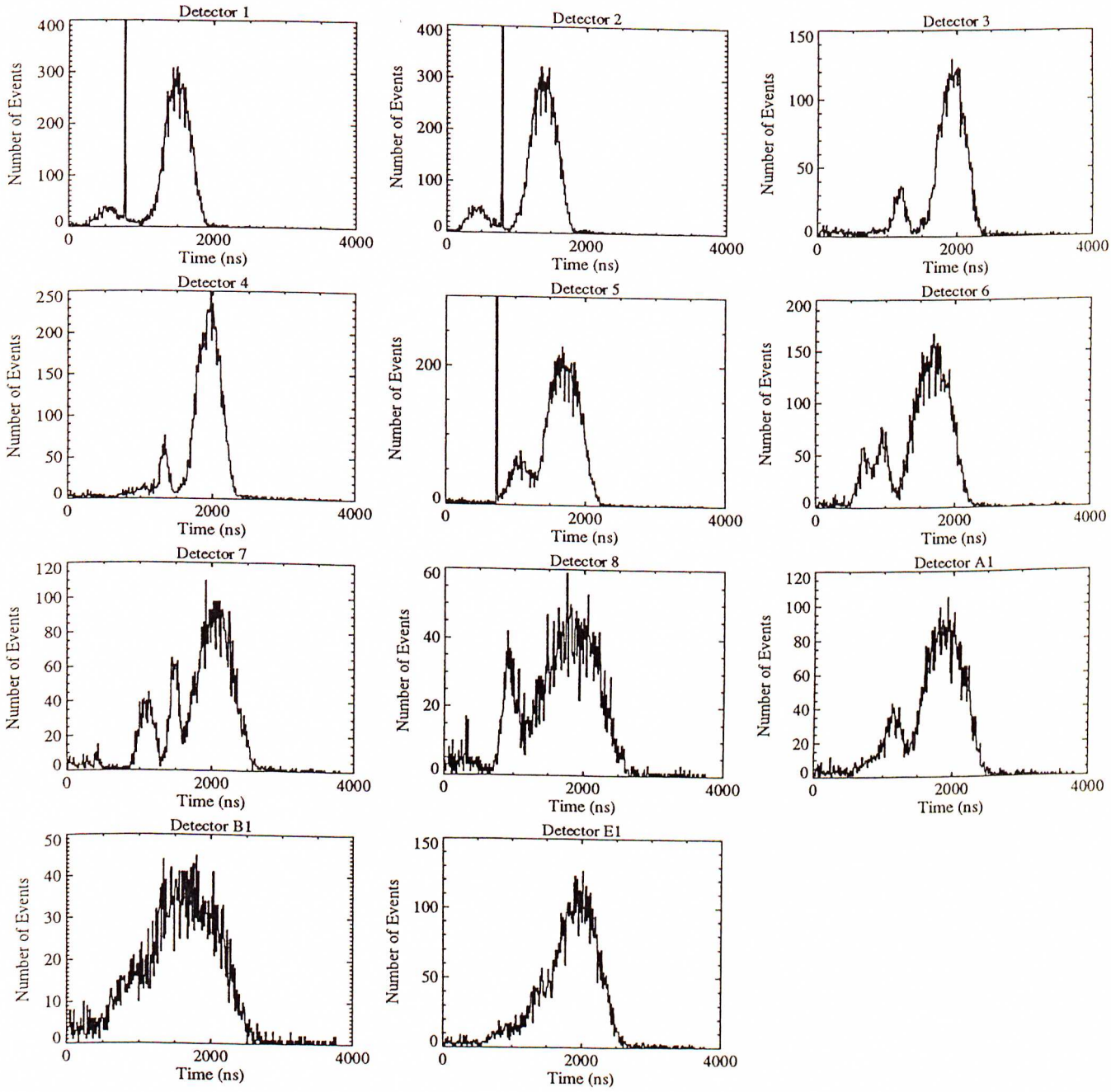

Figure 3.24: Raw times collected by the new and relocated detectors during the month of July 1990. The spikes in the distributions for detectors 1, 2 & 5 correspond to events where these detectors have triggered the array and hence the time is approximately the same. The distributions show a Gaussian shape typical of differences between separate detectors (some display several overlapping). This results from the large spacing of these detectors relative to the separation of the other 18 timing detectors. No times were available for detector D1 due to the failure of one channel in the T.D.C.

Chapter 5) lead to the purchase of a Motorola MVME133 System, based upon the V.M.E. bus, with a 68020 processor, and including a G.P.I.B. interface, operating under the VERSADOS operating system. This is a multi-tasking, multi-user computer and was planned to allow more efficient array operation.

Unfortunately, despite a lengthy effort, we were unable to make use of the G.P.I.B. controller interface on the V.M.E. We did, however, have access to an I.B.M.-P.C. G.P.I.B. interface, and an operating system was designed using an Olivetti M-24 personal computer (P.C.) as an intermediatry.

Upon an event (i.e. a 'fast' and 'slow' trigger), a L.A.M. (Look-At-Me) was generated by the # 1 T.D.C. The P.C. would then acknowledge this and proceed to read the time, pressure and temperature information, followed by the three A.D.C.s, four T.D.C.s and two scalers before resetting the entire crate ready for the next event. These data were then buffered into memory on the P.C. from which they were transferred to the V.M.E. over a serial line, where it was suitably formatted and dumped to hard disk. Data were stored in two hour files to minimise data loss resulting from power failures (which Buckland Park suffered from frequently).

This system reduced the array dead-time to ~ 300 ms, a significant reduction from the previous dead-time of ~ 750 ms. This dead-time was deemed acceptable in light of the reduced event rate (from $\sim 10^{-1}$ Hz to $\sim 5 \times 10^{-2}$ Hz).

The program operating on the P.C. was designed and written to be flexible, requiring only minimal changes in order to facilitate future changes in the array operating conditions (e.g. extra devices in the CAMAC crate), unlike the previous, relatively inflexible operating systems.

The V.M.E. possessed a 70 Megabyte hard disk of which 50 Megabytes was available for data storage. The array recorded ~ 3 Megabytes of data per day, requiring data retrieval approximately once a fortnight (in comparison to twice a week under the previous operating system). Data were dumped onto streamer tape, which was used to transfer array data to the mainframe computers at the University of Adelaide. This transfer of data from the array was carried out without interrupting array operation,

allowing the collection of continuous data sets (apart from power failures, equipment breakdown, and occasional maintenance).

Detector Monitoring

With the advent of the new operating system at Buckland Park, as well as improved computing facilities on campus, it became feasible to monitor the behaviour of each photomultiplier tube at Buckland Park. This was achieved in the following way. Each tube signal was passed through a discriminator set at a pre-determined level (2–8 particle level). Some use was made of the discriminators used in the 'slow' and 'fast' triggers. These discriminator outputs were fed to a channel of a scaler (LeCroy type 2551, 12-channel, 24-bit) which counted the number of NIM pulses received. These scalers were read and reset after every event, and from this information average rates for the detectors were determined. Anomalous detector behaviour would appear as irregular changes in detector rate over time.

Unfortunately, this required upwards of 50 scaler channels, with only 24 available. This problem was overcome with the construction of 4-way, 12-channel electronic switch by the Electronic Services group. An event trigger output was used to switch the channels being fed to a scaler after each event, along with a signal to identify the position of the switch. This allowed the monitoring of all but three tubes and proved invaluable in assessing both array performance and individual detector behaviour. A typical rates output is shown in Fig 3.25. 'Dead' or misbehaving detectors were easily identified using these plots, greatly simplifying array maintenance.

Power Supply

In addition to extending the array and installing a new computer system, a new high voltage power supply for the detectors was installed in early 1988. The 'old' array relied upon four high voltage power supplies (Fluke type 412B) whose outputs fed 10 or 12 channel home-made voltage fan-outs, which were used to control the voltages supplied to the detectors. Such an arrangement provides no direct measurement of the voltages

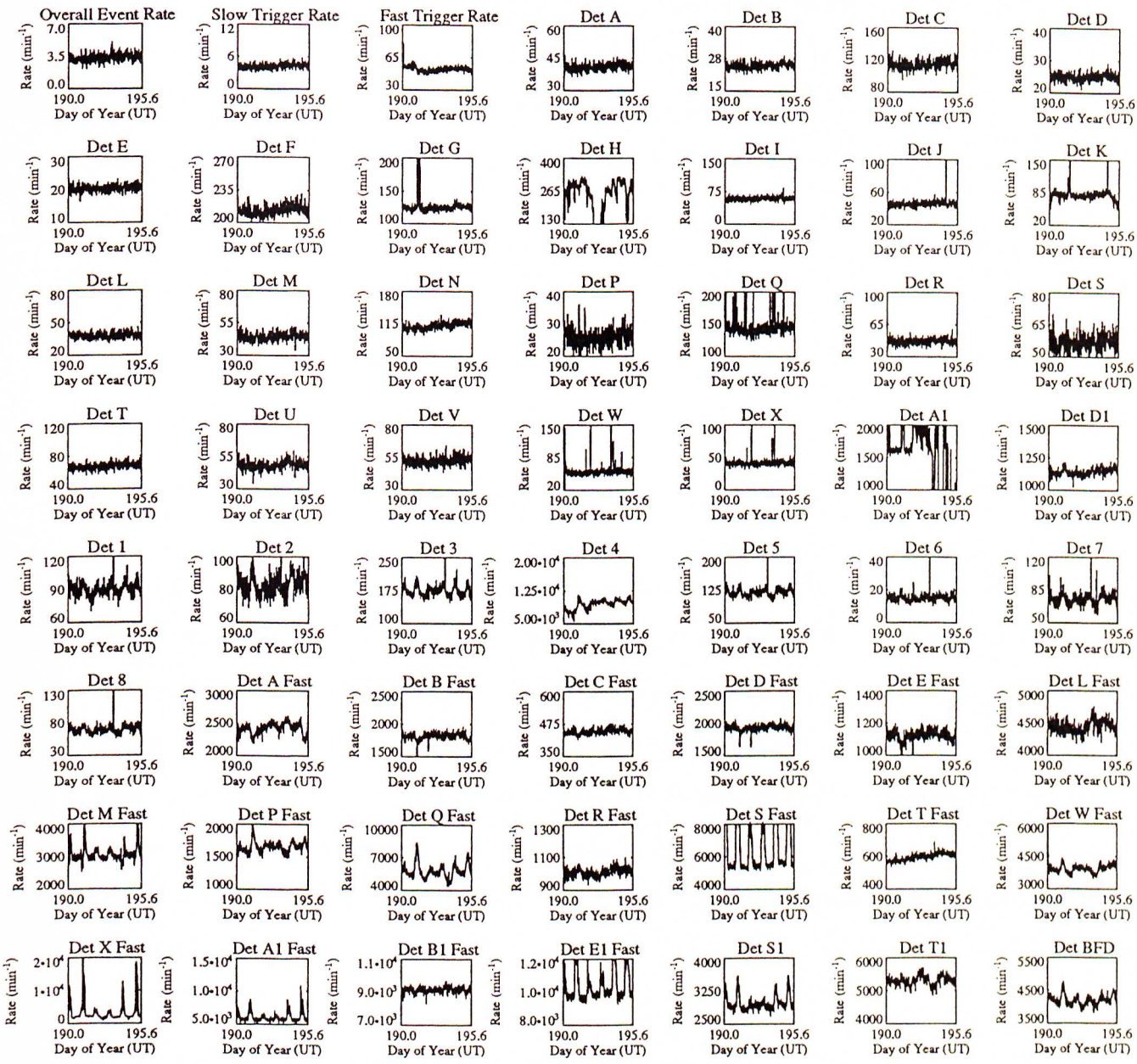

Figure 3.25: A typical rates plot used to monitor array performance and individual detector behaviour. In the period presented here (approximately 5 days), detector A1 (slow tube) shows a failure. In addition, several of the fast tubes demonstrate light leaks. Overall, the array performed satisfactorily over this period, with a constant overall event rate, and constant fast and slow trigger rates.

applied to each detector, and adjusting the voltage of one detector tended to affect the others associated with that fan-out. This arrangement was replaced by a LeCroy System 1440 Power Supply. This is a micro-processor controlled high voltage supply, and provides 64 individually controlled high voltage channels, giving an exceptional level of control on individual detectors. This supply was connected to a spare serial line on the V.M.E. and was accessed via the V.M.E.. The array performance was found to improve as a result of the ability to fine tune the individual photomultiplier voltages.

It was found that this Power Supply was particularly sensitive to the 'rough' electricity supplied to Buckland Park. A power conditioner (Sola type 63–26–735, 3.5 kVA) was installed on the computer control systems phase of the supply and the problem was eliminated.

Modem

During early 1990, a modem line was installed to Buckland Park. Due to the relative remoteness of the array to the university, and the lack of a full-time station manager, determining the status of the array generally required a 40 minute road trip to visit the array. The installation of the V.M.E. made modem access possible (the Nova computer had no such facility). A 2400 Baud modem was connected to the remaining serial line of the V.M.E. allowing remote access to the system.

This connection allowed Buckland Park to be monitored from Adelaide providing the following facilities :

— confirmation of array operation.

— the ability to remotely alter the detector voltages.

— information on the remaining disk space.

— the remote monitoring of individual detector behaviour.

The last of these was the most important, resulting from the installation of the previously discussed scaler switch, as it was possible to determine if any detectors were misbehaving or had failed before venturing out to Buckland Park. Previously, these could only be deduced *in situ*, or after the data had been returned to Adelaide and

analysed.

The modem also provided a link in the opposite direction, allowing the access of mainframe computers at Buckland Park for communication and analysis purposes, significantly reducing the isolation of Buckland Park.

The modem connection does not currently allow direct transfer of the raw data due to the slow transfer speed (currently 2400 Baud). However, this option remains open for future development when high-speed modems (a factor of 10 or so faster than those currently available) become available at a reasonable cost.

The final teething problems associated with the upgrading of Buckland Park E.A.S. Array had been eliminated by the end of May 1990. Data were collected routinely from May 30 1990 onwards (apart from down-times resulting from power failures and equipment breakdowns).

The analysis of these data, and the behaviour of the array from this time to November 1990 will be presented in the remainder of this chapter, and compared to that expected from simulations and previous work.

3.6 Array Characteristics (1990)

The 'new' Buckland Park E.A.S. Array officially began data collection on May 30, 1990 (JD 244 8042.6). The data presented in the remainder of this chapter were collected from this date to November 1, 1990 (JD 244 8197.5). During this time, the array operated continuously, apart from down-times due to power failures and equipment breakdowns, with a total of 4.75×10^5 events successfully triggering the array at a mean event rate of $\sim 5.6\times10^{-2}$ Hz, approximately half that of the 'old' array (see 3.4). Directions were initially assigned to 4.49×10^5 events, corresponding to 95% of the total, and shower sizes, ages and core positions were successfully fitted to 3.73×10^5 events, corresponding to 78% of the total number of events triggered, after the appropriate limits had been applied (see 3.6.2). These percentages are higher than those for the

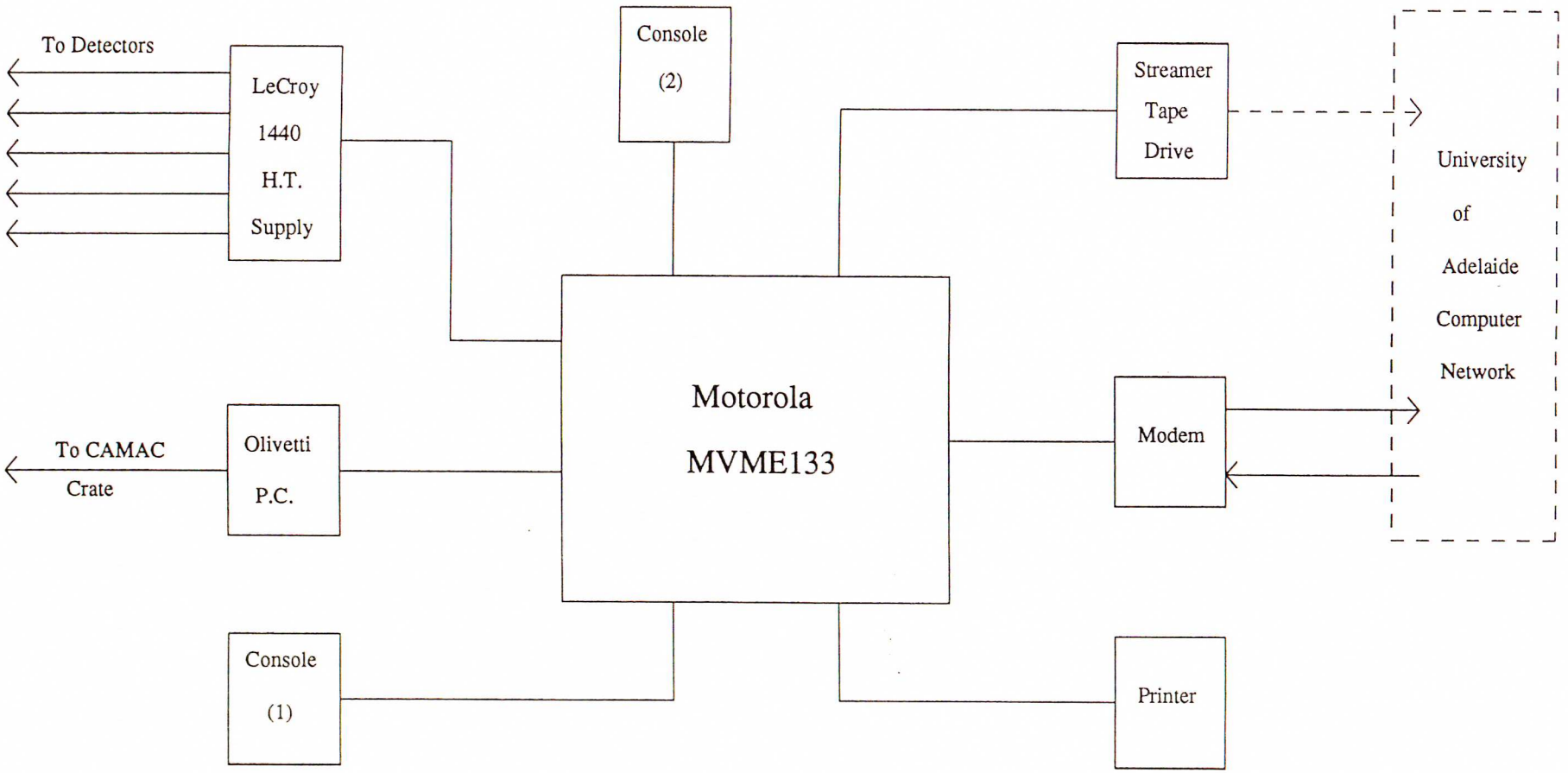

Figure 3.26: A schematic diagram of the array control system installed at Buckland Park by the author.

'old' array analysis (90% and 70% respectively) due to better shower-front sampling resulting from the altered triggering conditions, which raised the array threshold (see 3.6.3), increasing the average number of particles detected, thus improving the sampling statistics.

Following is a discussion of the characteristics of the 'new' array, based upon the data collected, which will be referred to as the 1990 data set.

3.6.1 Event Time-Spacing Distribution

As discussed in 3.4.3, the examination of the event time-spacing distribution of recorded cosmic ray events is an important test for both the uniformity of the data collected and general array performance and behaviour. It is therefore appropriate to examine the data collected by the 'new' array for such a 'randomness' in the event time-spacing distribution.

The event time-spacing distribution derived from the raw data of the 1990 data set is presented in Fig 3.27. The array dead-time ($\sim$ 0.3s) manifests itself as a deficiency in the initial bin. The experimentally determined mean event spacing is 17.42 seconds, and the solid line in Fig 3.27 corresponds to this mean event-spacing and the total number of events triggered (taking into account the array dead-time), as predicted by Eq 3.21. The dashed line indicates the line of best fit to the histogram, which corresponds to an average event spacing of 17.6 $\pm$ 0.3s. Clearly, both of these lines fit the experimental distribution well within the experimental limits (1σ), and it is concluded that there is no evidence for a non-random component in the primary cosmic ray flux over the period and energy range under investigation.

Such a uniformly random distribution is necessary in order to accurately determine upper limits to the anisotropy of the primary cosmic ray flux, for which the modifications to the array were primarily designed. Clearly, the 'new' array is suited for such anisotropy work over a large time-scale, based upon this distribution, and the arrival distributions which follow (a similarly uniform distribution was also found for the analysed event time-spacings).

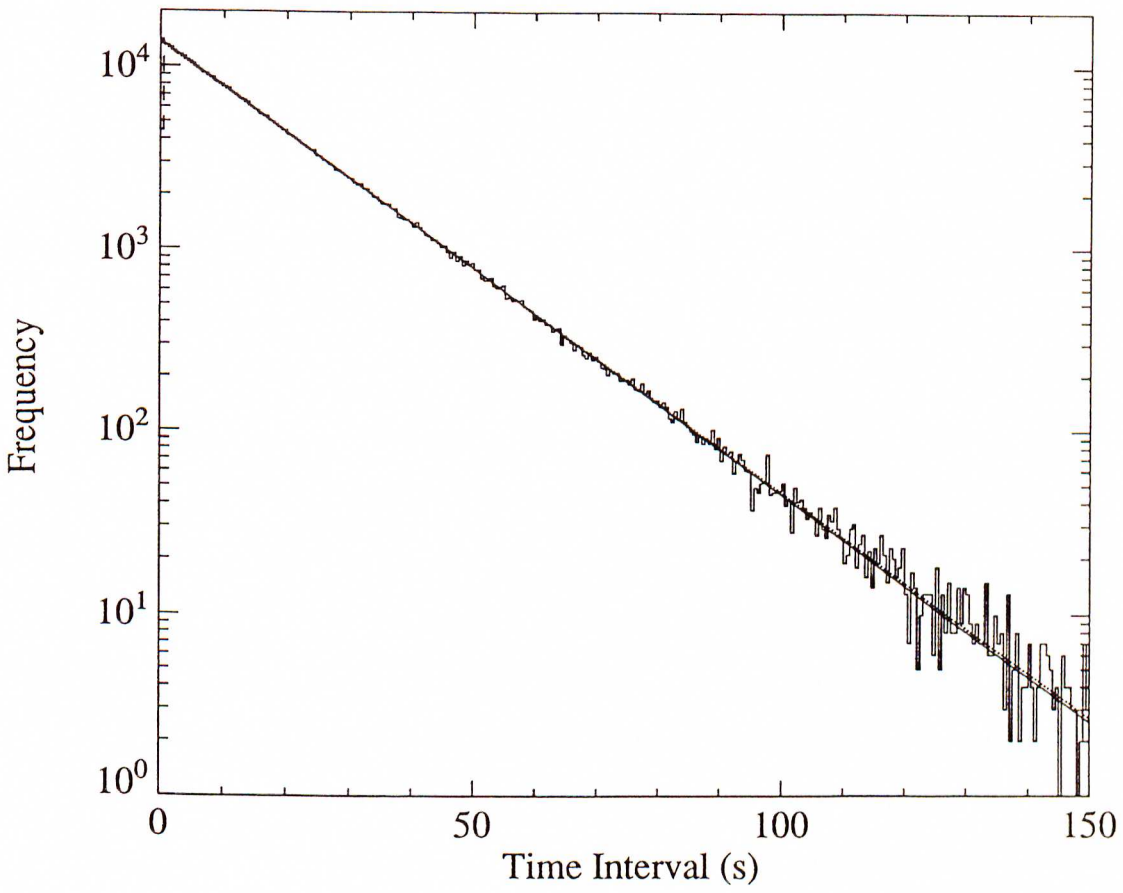

Figure 3.27: Event time-spacing distribution for the 1990 data set. The dip in the first bin results from the array dead time of ~ 0.3s. The solid line indicates the best line of fit as predicted by Poisson statistics for truly random arrival times, corresponding to an average event time spacing of 17.42s. The dotted line indicates the line of best fit to these data, and corresponds to an average event time spacing of 17.6 ± 0.3s. Clearly there is no evidence for a deviation from randomness in these data.

3.6.2 Arrival Directions

The addition of eight new fast-timing detectors (1–8), and the relocation of four detectors with fast-timing capability (A1, B1, D1, E1), resulted in significantly extended baselines for the determination of E.A.S. arrival directions through the use of the fast-timing technique (see 3.3.1).

The 'stepped' timing differences algorithm discussed in 3.3.2 required modification in order to include these new baselines, to allow the estimation of the inherent time differences between pairs of detectors necessary for effective fast-timing analysis. This is particularly important for the new, relatively widely-spaced detectors, where only a small percentage of events will trigger two widely-spaced detectors (e.g. separated by several hundred metres), resulting in a poor estimate for the timing difference between distant pairs of detectors. Incorporating 'stepping' between neighbouring detectors, which are more likely to both trigger in an event, provides a larger sample from which an improved estimate for the inherent timing differences between widely-spaced detectors may be determined.

It was also necessary to modify an algorithm developed by Edwards (1988) and Ciampa (1988), which serves to reject 'bad' times on the basis of either being 'unphysical' (i.e. not physically possible, resulting from a signal not associated with the shower-front), or that the removal of the time significantly improves the shower-front fit, as estimated by σ, defined in Eq 3.10. This modification was necessary as the previous maximum possible timing baseline ($\sim$ 60m), was increased several times ($\sim$ 300m), implying that both shower-front curvature and the so-called 'Linsley effect' (Linsley 1983) become increasingly important, requiring changes in the parameters for determining a 'bad' time.

These modifications reduced the average value of σ (as defined in Eq 3.10) from $\sigma \sim 6.5$ to $\sigma < 4.0$ for a plane shower-front fit, which was deemed acceptable. Curved shower-fronts have also been fit to these data for the purpose of U.H.E. γ-ray astronomy, as discussed in Chapter 6.

The distributions of E.A.S. arrival directions calculated using these modifications

will now be discussed. In these distributions, the limits discussed in 3.4 were applied, with the exception of E.A.S. core positions, which have new limits applied :

$|x| < 140\text{m}$

$-240\text{m} < y < 140\text{m}.$

Azimuth Angle Distribution

The azimuth angle distribution for the 1990 data set appears in Fig 3.28, in both full and high resolution formats. The strong first and second harmonic effects present in the 1984–1989 azimuth angle distribution (see 3.4.1; Fig 3.5) have been reduced with the previously significant first harmonic effectively removed (from $\sim 2\%$ to 0.3%), and the previous second harmonic marginally reduced (from 1.1% to 0.8%), primarily as a result of widening the array in an east-west direction, and extending it in a southerly direction. The remaining asymmetry in the distribution results from the longer north-south baseline ($\sim 400\text{m}$) than the east-west baseline ($\sim 300\text{m}$) of the array.

Zenith Angle Distribution

The zenith angle distribution for the 1990 data set is presented in three alternative forms in Fig 3.29. As discussed in 3.4.1, the zenith angle distribution provides useful information on the primary particle composition, as well as on E.A.S. development and attenuation.

The raw data for the zenith angle distribution are shown in Fig 3.29(a) and demonstrate the initial rise in events with solid angle ($\propto \sin\theta$), followed by a decrease with increasing zenith angle as atmospheric attenuation effects become increasingly important ($\propto \sec\theta$). The peak of the distribution occurs just below a zenith angle of 20°, which is consistent with previously determined values (see 3.4.1).

The number of events per solid angle as a function of zenith angle ($\Phi(\theta)$, as defined in Eq 3.17), appears in Fig 3.29(b). As in Fig 3.7(a), (c), fits of the data to $\cos^n\theta$ have been superimposed for $n = 8, 9$. It is clear that $n = 8$ is a good fit at low zenith angles, but a progressively higher value of n is required with increasing zenith angle (as was

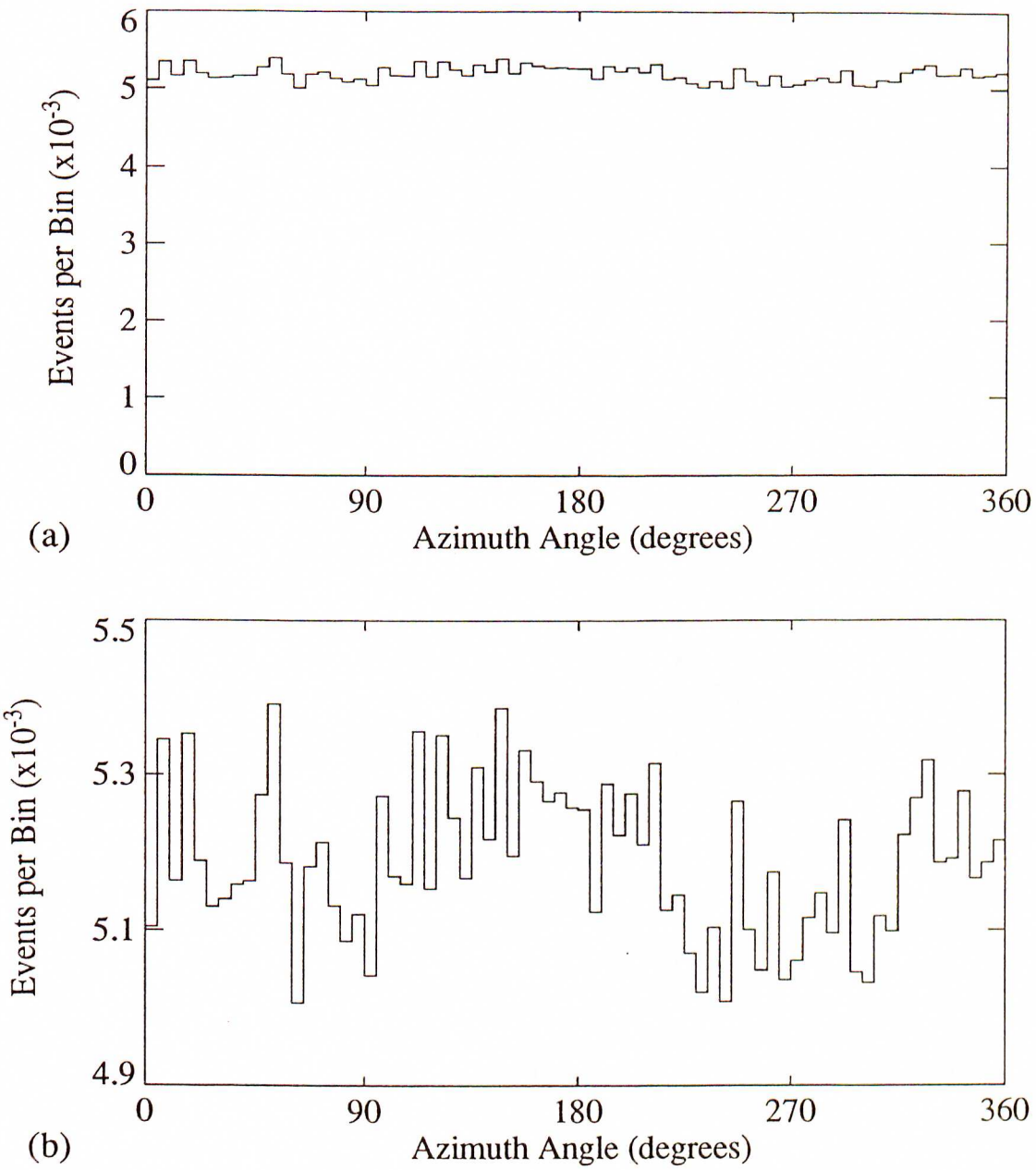

Figure 3.28: The calculated azimuth angle distribution of the arrival directions of E.A.S. from the 1990 data set in both **(a)** full, and **(b)** high resolution formats.

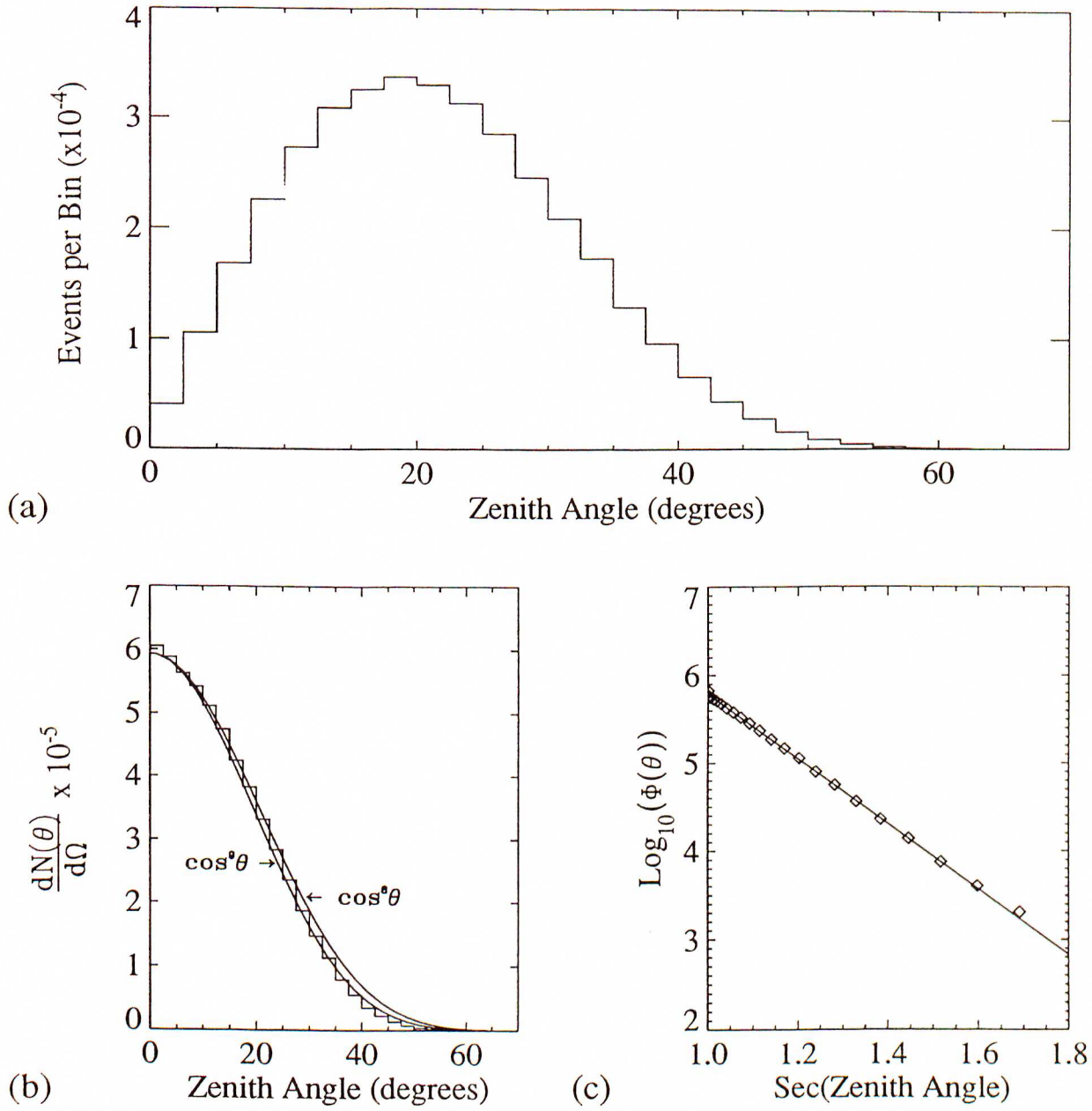

Figure 3.29: The calculated zenith angle distribution of the 1990 data, using three alternative methods of presentation (as used in Figs. 3.6, 3.7).

(a) The raw data, binned in intervals of 5 degrees.

(b) The zenith angle distribution in terms of solid angle exposure, with curves of $\cos^8\theta$ and $\cos^9\theta$ superimposed for comparison (see text).

(c) The alternative $\log_{10}\Phi(\theta)$ versus $\sec\theta$ fit to the data, as discussed in the text. The solid line is a good fit for $\sec\theta \leq 1.4$, and has a slope of ~ -3.69.

the case in 3.4.1).

Fig 3.29(c) shows the alternative presentation of the zenith angle distribution in terms of $\log_{10}\Phi(\theta)$ versus $\sec\theta$, as discussed in 3.4.1. The line of best fit to these data (for $\sec\theta \leq 1.4$) has a coefficient $C = -3.69 \pm 0.03$, where C is defined in Eq 3.18. This value of C is consistent with previous results, and suggests a predominantly light component of composition in the primary cosmic ray flux at $\sim 10^{15}$eV (see 3.4.1).

Overall, these results show that the zenith angle distribution behaviour is in agreement with that expected.

Declination Distribution

The derived declination distribution of the 1990 data set is shown in Fig 3.30. The shape of this distribution is very similar to that of the 'old' array (see Fig 3.8), with the exception of a slight enhancement of southerly E.A.S. in the range $-45° < \delta < -35°$, relative to northerly E.A.S. Overall, the array declination sensitivity remains essentially the same as the 'old' array, with an effective range $-80° < \delta < 15°$.

Right Ascension Distribution

The right ascension distribution for the 1990 data set is included here for completeness (Fig 3.31). Variations in this distribution result primarily from the overall non-uniform sidereal on-time exposure of the array during the period in question. Techniques for removing or allowing for this non-uniformity of exposure will be discussed in detail in Chapters 4 & 5.

3.6.3 Shower Parameters

The shower size (N_e), and the shower age (s), were estimated by fitting the NKG function (see 2.4.1), using the maximum likelihood method as discussed in 3.3.2. Only modifications in data format were necessary in order to accommodate the extra/modified detectors.

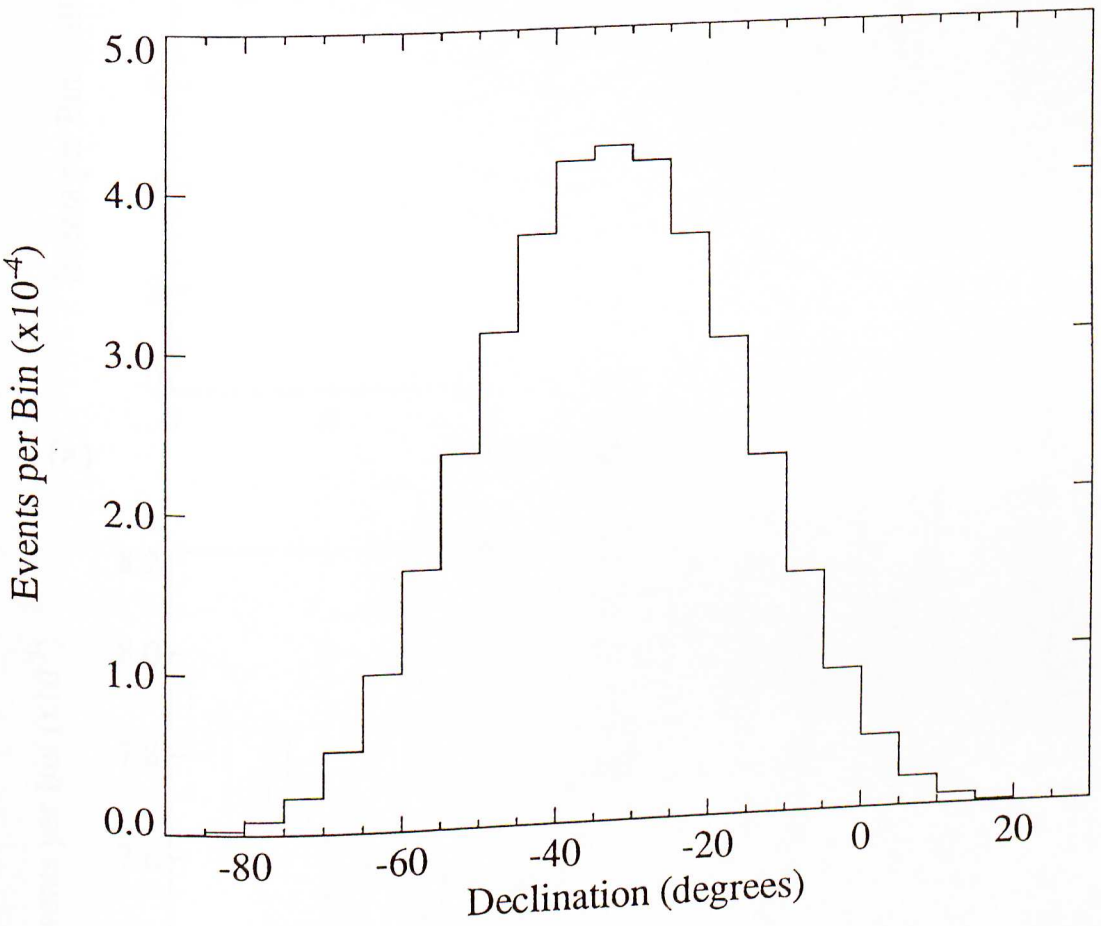

Figure 3.30: The calculated declination distribution of the arrival directions of E.A.S. from the 1990 data set.

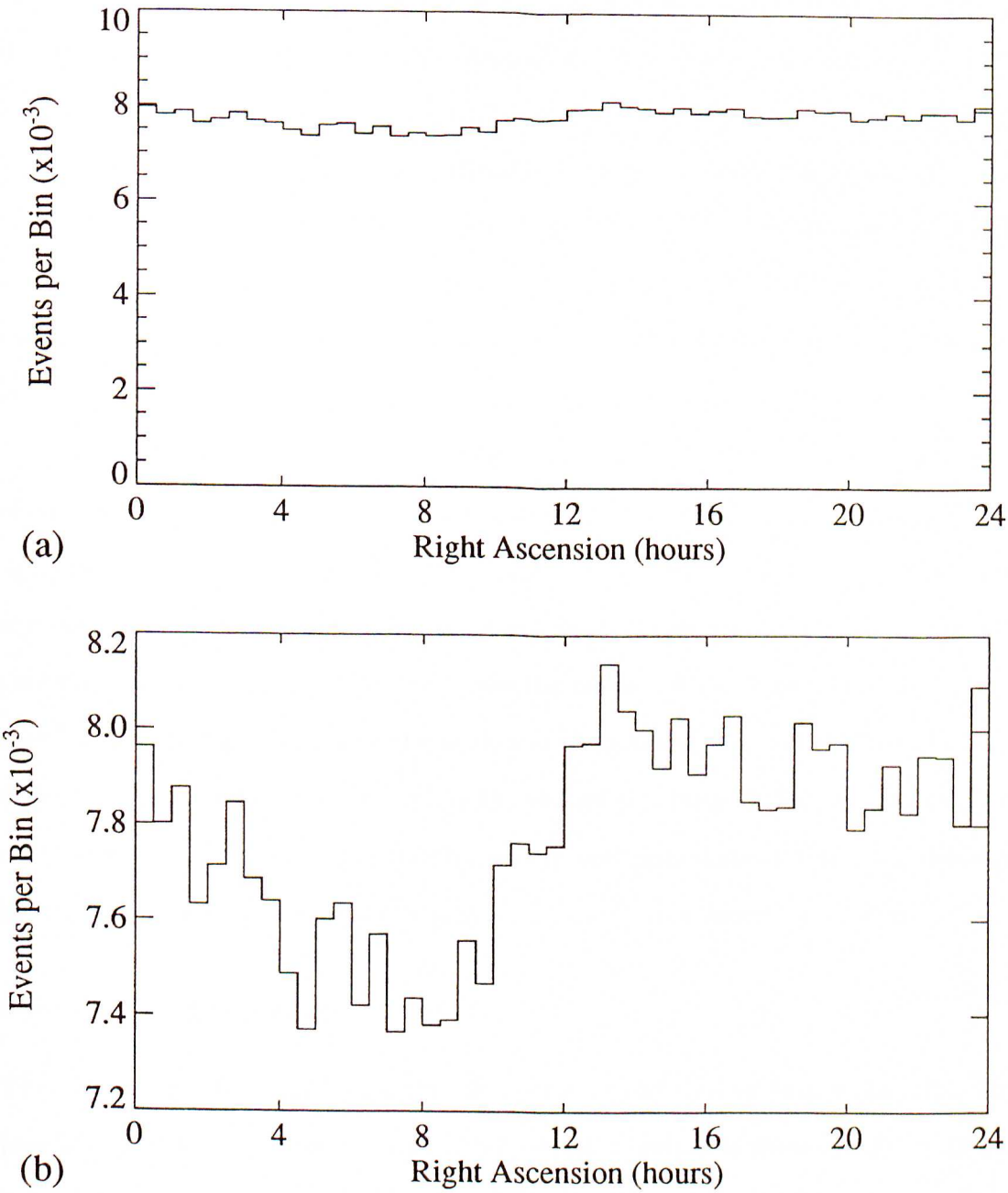

Figure 3.31: The calculated right ascension distribution of the arrival directions of E.A.S. from the 1990 data set in both **(a)** full, and **(b)** high resolution formats.

Shower Size Distribution

The calculated shower size distribution for the 1990 data set is displayed in Fig 3.32(a). In modifying the array, the shower size threshold was significantly increased in order to reduce the event rate. The steepness of the shower size spectrum (see 3.4.2; Fig 3.12) resulted in an approximate halving of the event rate (from $\sim 10^{-1}$ Hz to $\sim 5.6 \times 10^{-2}$ Hz), when the array threshold was increased by a factor of ~ 3, from $\sim 3 \times 10^4$ (Clay *et al.* 1985) to $\sim 8 \times 10^4$ particles. The mean shower size of this distribution is 1.1×10^5 particles, compared to 4.5×10^4 particles for the 'old' array. The tail of the spectrum is significantly broader, an indication of the increase in collecting area in the shower size range 10^5–10^7 particles, as indicated in Fig 3.23.

As discussed in 3.4.2, a simulation was carried out in order to estimate the behaviour of the 'new' array. The predicted event rate of ~ 3 events per minute is in good agreement with the experimental trigger rate of $\sim 5.6 \times 10^{-2}$ Hz. The simulation results are compared to the experimentally determined shower size spectrum in Fig 3.33. In general, there is good agreement between the predicted and experimentally determined spectra in both the position of the peak and the general shape of the distribution. The differences between the two spectra in the shower size range $\sim 2 \times 10^5 - 2 \times 10^6$ particles may be the result of sampling fluctuations in the more distant detectors, inadequacies in the simulation of these fluctuations, or in the source spectrum chosen.

Shower Age Distribution

The shower age distribution for the 1990 data set, derived by fitting the NKG function (see 2.4.1) to the observed densities and arrival direction is shown in Fig 3.32(b). The general shape of this distribution is similar to those of the 'old' array (see Fig 3.15), but possesses a slightly higher mean ($s \sim 1.23$ compared to $s \sim 1.20$). This remains consistent with comparable measurements from other arrays.

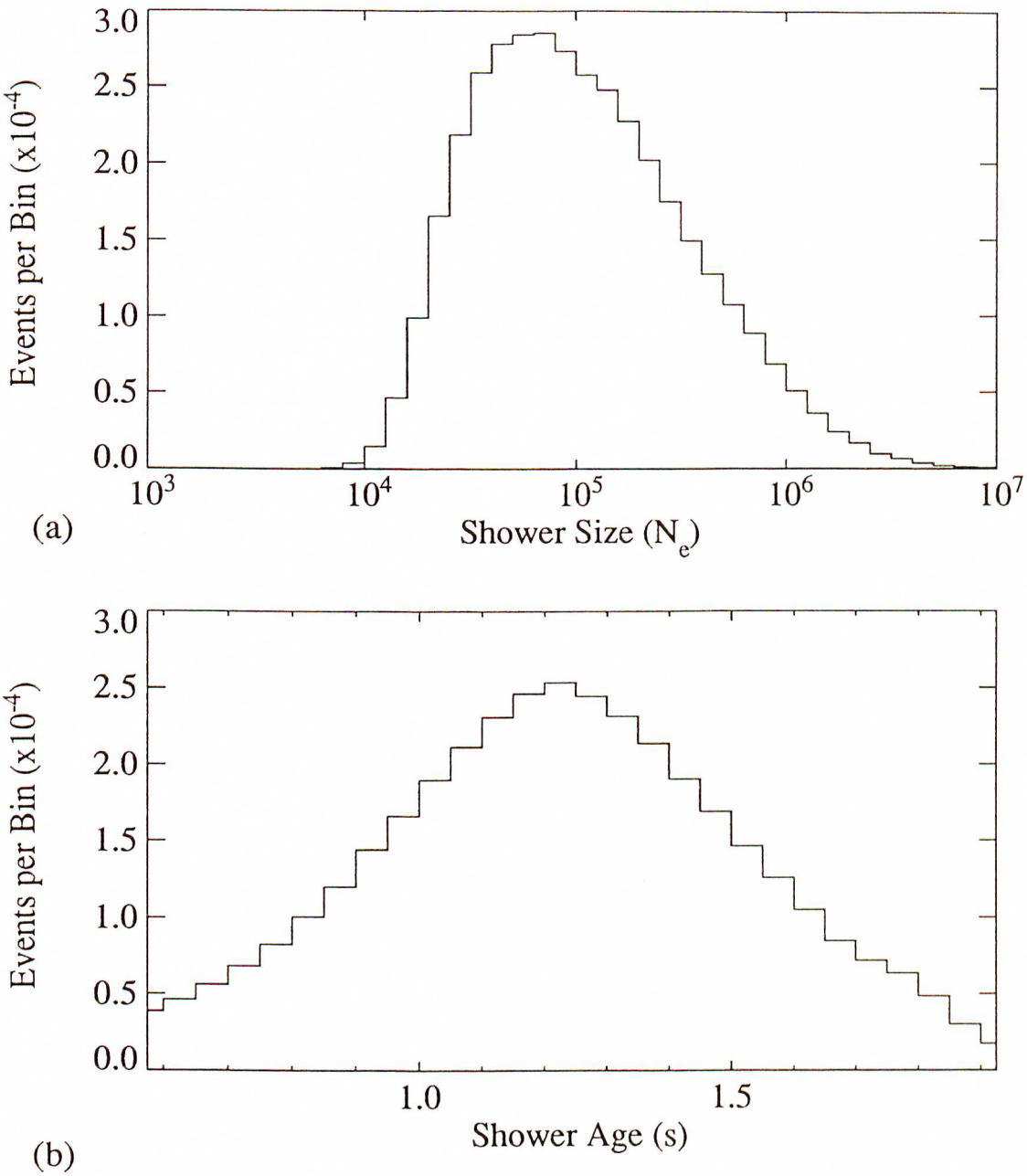

Figure 3.32: The derived shower parameter distributions for the 1990 data set.
(a) Shower Size (N_e)
(b) Shower Age (s)

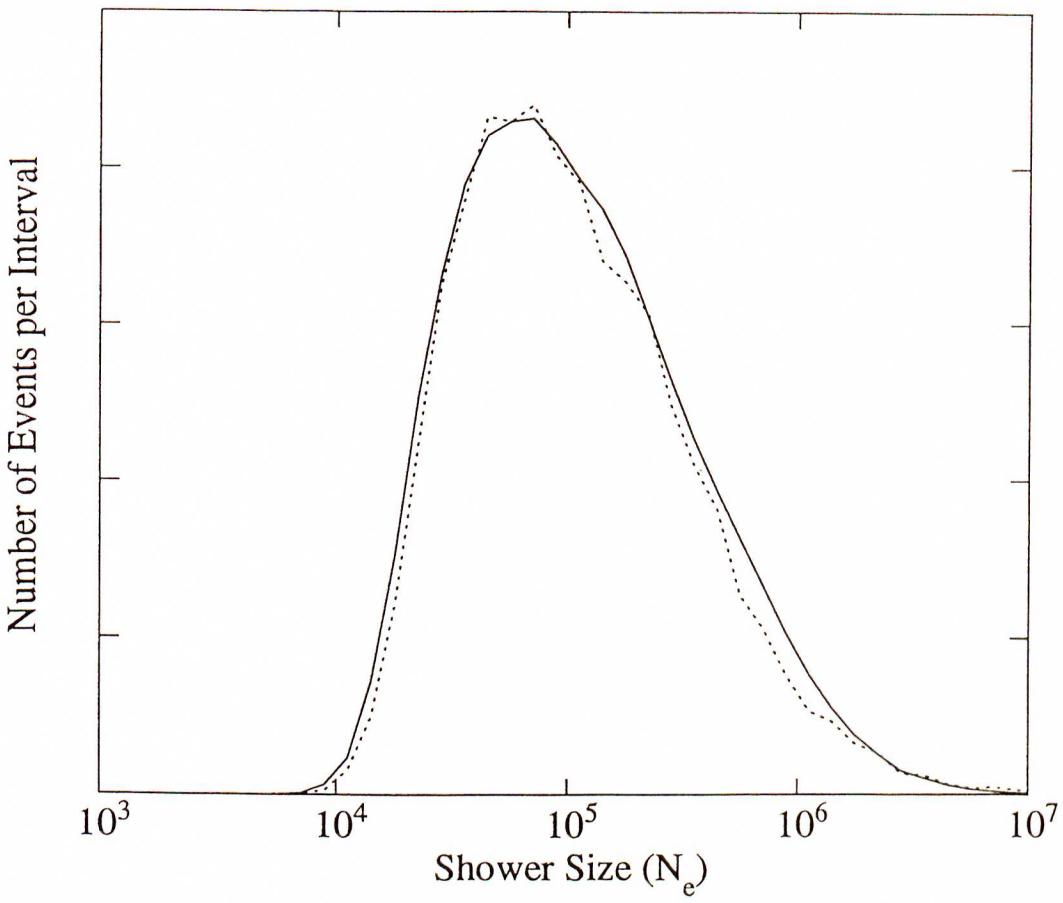

Figure 3.33: Comparison of the observed shower size spectrum (solid line) with that simulated (broken line) for the 1990 data set (see text for simulation details).

3.6.4 Summary

The overall characteristics of the 'new' array, derived from the 1990 data set are in good agreement with those predicted and/or expected. In particular, the essentially random event time-spacing distribution and the near uniform azimuth angle distribution together with the increased shower size threshold, and increased collecting area above $N_e \sim 10^5$ particles, indicate that the 'new' Buckland Park E.A.S. Array is ideally suited for long-term investigations into the anisotropy of the primary cosmic ray flux at primary energies of $\sim 10^{15}$eV and above.

3.7 Conclusion

In this chapter, the Buckland Park E.A.S. Array has been described in considerable detail. The history of its development, and its previous performance have been outlined, with specific emphasis on the collection and analysis of the 1984–1989 data set to be used in anisotropy analyses to be discussed in the remainder of this thesis.

In addition, the author has designed, simulated, and implemented major modifications to all aspects of the array, with the primary goal of a long-term investigation into the anisotropy of the primary cosmic ray flux detected at mid-southern latitudes at primary energies $\sim 10^{15}$eV and above. The performance of the array to November 1990 suggests that it is suited to such an investigation.

In the following chapter, an extensive review will be carried out into the anisotropy of the primary cosmic ray flux at energies $> 10^{11}$eV, encompassing both theoretical and experimental results to date.

Chapter 4

The Anisotropy of Cosmic Rays

4.1 Introduction

Investigations into the preferred arrival directions of primary cosmic rays (anisotropy) have been carried out for more than forty years. Such measurements provide the most direct method of approaching the question of galactic versus extra-galactic origin of cosmic rays, as well as providing useful information about the particle sources and subsequent propagation. However, it is only in recent times that a consistent picture has emerged at primary energies greater than $\sim 10^{12}$eV, where heliospheric effects cease to become important.

The primary cosmic ray flux in the energy range 10^{12}eV to 10^{16}eV has been found to be isotropic to within $\sim 1\%$ (see e.g. Fichtel and Linsley 1986). Such isotropy, combined with spurious effects introduced into the data by solar and atmospheric effects, has both required experiments to collect a large number of events to improve statistics, and advanced analysis techniques to remove or allow for these effects. The resulting isotropy is presumably largely due to the randomising effect of the magnetic field within the Galaxy.

Before a detailed discussion of Cosmic Ray Anisotropy is undertaken, the Galactic Magnetic Field will be discussed.

4.2 The Galactic Magnetic Field

The Galaxy possesses a magnetic field which, on a large-scale, appears to be ordered, at least locally. The field lines are thought to be frozen within the partially ionised gas of the inter-stellar medium. The origin of the field remains somewhat of a mystery[1]. Superimposed upon the large-scale field of strength $\sim$ 2–3 μG, is a small-scale random field of comparable strength, varying in dimensions from a few to hundreds of parsecs (Manchester 1974).

Accurate measurements of the field are restricted to regions within $\sim$ 3 kpc of the sun, and are generally within the galactic plane. Towards the galactic centre, and away from the galactic plane, measurements become increasingly uncertain.

The larger of the small-scale regions are thought to be associated with 'magnetic bubbles' formed as a result of matter being swept up by shock waves, possibly as a result of supernovae (Vallée 1984). They have been associated with regions such as the North Polar Spur and the Gum Nebula (Broten *et al.* 1985) (see Fig 4.1).

Outside the galactic plane, it is thought that a halo field exists, but its structure and strength are still the subject of speculation.

4.2.1 Measurement Techniques

There are a number of techniques available for determining magnetic field strengths for astronomical purposes. Two of the most commonly used are Faraday Rotation and Starlight Polarisation which will now be briefly discussed. (see Verschuur 1979; Heiles 1976 for a comprehensive review of these techniques).

Faraday Rotation

Plane-polarised electromagnetic radiation travelling through a plasma will suffer rotation of the plane of polarisation (Faraday Rotation). The magnitude of this rotation,

[1] Fritz Zwicky suggested as a hypothesis for its origin : *Dixitque Deus, fiat lux campusque magneticus* (And God said, "Let there be light and magnetic field")

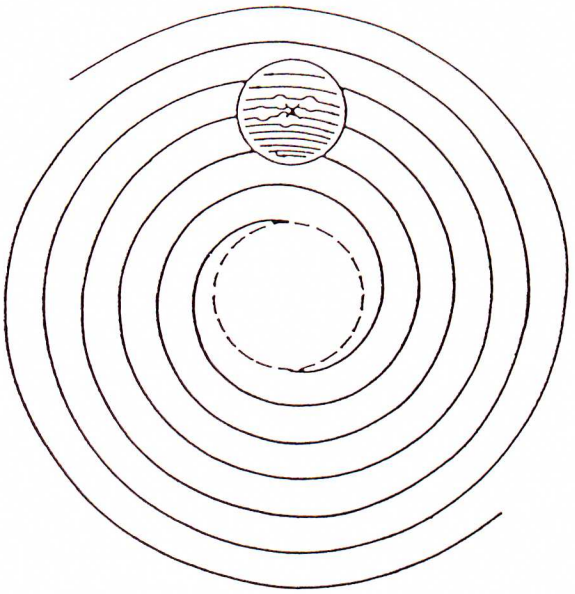

(a)

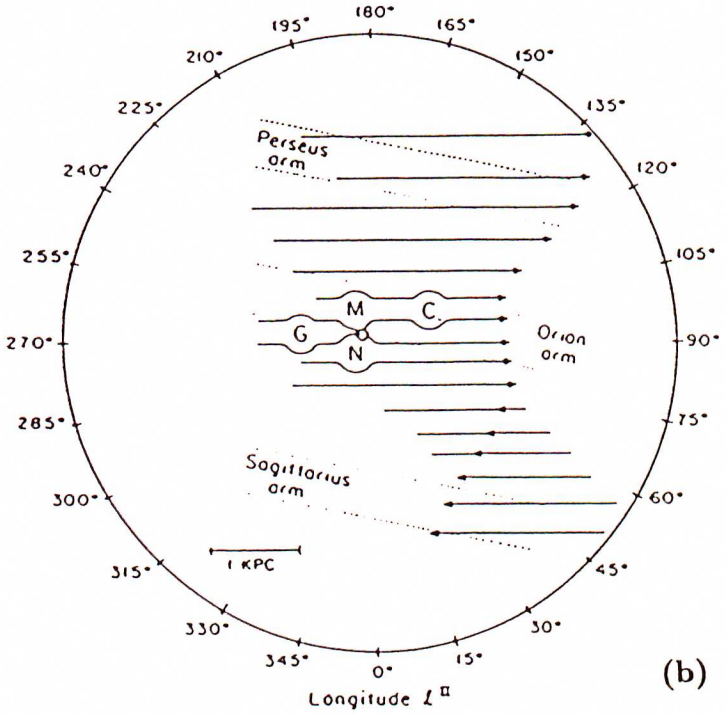

(b)

Figure 4.1: Proposed Galactic Magnetic Field Structures
(a) Large-Scale Field (after Ruzmaikin et al 1988a)
(b) Local Field (after Vallée 1984)
(N-North Polar Spur, C-Cetus Arc, G-Gum Nebula, M-Monogem Ring)

over a path of length l (in pc) through such a plasma is given by

$$\Delta\theta = \frac{\lambda^2 e^3}{8\pi^2 c^3 \varepsilon_o m_e^2} \int_0^l n_e B_{||} dl \tag{4.1}$$

$$= 8.1\text{x}10^5 \lambda^2 \text{ RM}$$

where

dl is in parsecs,

$B_{||}$ is the component of $\vec{B}$ parallel to the line of sight in Gauss,

n_e is the thermal electron density in cm^{-3},

λ is the wavelength observed in m, and

R.M. is the rotation measure, defined as $\int n_e B_{||} dl$

Since $\Delta\theta$ may be $> 2\pi$, several measurements, corresponding to different wavelengths are necessary to determine $\Delta\theta$ uniquely. Furthermore, such rotations are only observable at radio wavelengths.

Calculation of $\vec{B}$ from Eq 4.1 requires knowledge of n_e, the thermal electron density along the line of sight. In the case of pulsars, which emit linearly polarised radio waves, this may be determined by measuring the Dispersion Measure.

Pulsars emit short pulses of radiation at many frequencies. Different frequencies (ν) travel through a magnetised plasma at different velocities, and the time taken to travel a distance l is given by

$$T = \frac{l}{c} + \frac{e^2}{8\pi^2 \varepsilon_o m_e c \nu^2} \int_0^l n_e dl \tag{4.2}$$

where $\int n_e dl$ is known as the Dispersion Measure.

Multi-frequency measurements from pulsars allow both the Rotation and Dispersion Measures to be calculated. Hence, an average magnetic field ($B_{||}$) along the line of sight can be calculated, viz

$$< B_{||} > = 1.232 \frac{\int n_e B_{||} dl}{\int n_e dl} \quad \mu\text{G} \tag{4.3}$$

This method has obvious limitations. It requires the presence of a plasma of reasonable electron density ($\geq 10^{-4}\text{cm}^{-3}$) (and that variations in this density are understood),

and is unable to take into account field reversals along the line of sight. Nevertheless, by progressively measuring $< B_{||} >$ from pulsars with increasing distance, a picture of the local magnetic field can be produced.

Polarisation of Starlight

Starlight (initially unpolarised) may be partially polarised by the Davis-Greenstein effect (Davis and Greenstein 1951). This involves the scattering of light from elongated dust grains of size $\sim \lambda$ in the inter-stellar medium.

These dust grains align themselves to their lowest energy state in the presence of a magnetic field, which is parallel to the field. Provided this occurs over a large enough region of space, the $\vec{E}$ field of this scattered light will predominantly be polarised along the grain axis and hence parallel to the magnetic field.

This method provides no information about the magnetic field strength, nor is it capable of measuring field structure on a scale < 10 pc, which is important for the propagation of cosmic rays below $\sim 10^{16}$eV. (For these scales, the constancy of the inter-stellar wind, within a distance of a few parsecs from the Sun has been interpreted as evidence for a similar constancy in the local magnetic field (Kiraly *et al.* 1979). Such a measurement is based on spectral analysis of inter-stellar absorption lines — see e.g. McClintock *et al.* 1978).

Other Techniques

Other techniques include the observation of synchrotron radio emission produced by relativistic cosmic ray electrons passing through magnetic fields. This tends to give an indication of global field properties, but relies on knowledge of the distribution of cosmic ray electrons throughout the Galaxy.

Zeeman splitting of the 21 cm absorption line of neutral hydrogen also provides information on magnetic field strength, but only for those regions of relatively high density.

Results

Rotation and Dispersion Measure data from both pulsar and extra-galactic radio sources suggest a local longitudinal field in the direction of galactic longitude $l \sim 90°$, within the plane of the Galaxy, with a strength of 2–3 μG (Manchester 1974; Heiles 1987; Lyne and Smith 1989). Matthewson and Ford (1970) used 6000 stellar measurements to propose a longitudinal field in the direction $l \sim 80°$, from the apparent alignment of polarisation vectors. They also showed that these lines lie parallel to the galactic plane. The discrepancy with the former results is most likely due to the different regions and depths sampled by the two techniques.

A recent analysis of rotation measures by Rand and Kulkarni (1989), used 116 pulsars within 3 kpc of the Sun. From this survey they derived a longitudinal field of strength 1.6 ± 0.2 μG in the direction $l = 96° \pm 4°$. They also observed a field reversal at a distance of 600 ± 80 pc towards the galactic centre. This field strength applies only to the uniform component of the local field and so is not necessarily inconsistent with the previous larger estimates.

4.2.2 Models of the Galactic Magnetic Field

In modelling the galactic magnetic field, it is assumed that the field lines are frozen within the partially ionised gas of the inter-stellar medium. Such an assertion has consequences for both the radial and galactic latitude dependence of the field. In particular, the field outside of the galactic plane (the galactic halo) will depend upon the extent to which the trapped lines can bulge outside of the disk, as a result of turbulence, cosmic ray pressure, and galactic winds. This implies that the magnetic field strength will fall off more slowly with increasing distance from the plane, than the inter-stellar gas density, but that the field strength in an extended halo will be small (see 4.2.4 for a discussion of the halo field). This assertion also leads to the conclusion that the small-scale, irregular structure of the field is probably a result of the motion of the gas trapping the field lines.

Any model must also take into account the origin and/or generation of the galactic magnetic field as well as observations. Various origins have been suggested, including the relic field theory (Hoyle 1958; Piddington 1964), and production by the ejection of magnetic fields by stars (e.g. Michal and Yahil 1973). However, the most likely generation mechanism is the dynamo effect, resulting from the motion of ionised gas within the Galaxy (see Ruzmaikin *et al.* 1988a, 1988b for a review). This results in a large-scale circular/spiral field configuration.

The two most common models for the large-scale field are the Bisymmetric Spiral (BSS) models and the concentric ring (Circular) models (see Sofue *et al.* 1986 for a review). These models are supported by observations of similar-type spiral galaxies which exhibit these types of large-scale fields (Sofue *et al.* 1986).

In the BSS models, the magnetic field is basically one in which the field follows the direction of the spiral arms. A model suggested by Thielheim and Langhoff (1968), and used in simulations of cosmic ray propagation (see e.g. Karakula *et al.* 1971; Smith and Clay 1990), decreases in strength with distance from the galactic plane with a scale height of 175 pc, and from the galactic centre (outside $\sim$ 2 kpc), with a scale length of 10 kpc. The field also reverses in direction at the galactic plane.

Such a model fits in well with pulsar rotation measures, and has been improved over the years, taking into account improved measurements and local field information (e.g. Sofue and Fujimoto 1983, 1985; Lyne and Smith 1989). However, Rand and Kulkarni (1989) have suggested that a circularly symmetric field has a better fit to the observational data than the BSS model. At present there is no resolution to this contradiction in opinions, but the BSS field appears to be the more favoured, at least as far as cosmic ray propagation simulations are concerned.

4.2.3 Propagation of Cosmic Rays

Charged cosmic ray particles spiral around magnetic field lines, with a radius of gyration, the Larmor radius, given by

$$r_L = \frac{1.08E}{ZB} \quad \text{parsecs} \tag{4.4}$$

where Z = charge in units of e (1.6×10^{-19}C), E = energy in PeV (10^{15}eV), B = magnetic field strength in microgauss (μG).

This is illustrated in Fig 4.2 where the radii of gyration for both protons and iron nuclei in the presence of a 3μG field have been plotted as a function of particle energy. From this diagram, it is obvious that only for the highest energy cosmic rays (above $\sim 10^{18}$eV, where $r_L \sim$ galactic radius) can measured arrival directions be associated with the source direction. At lower energies, the galactic magnetic field acts to effectively randomise the arrival directions measured. These directions are, however, related to the structure of the 'local' magnetic field, particularly for energies below $\sim 10^{15}$eV.

Simulations have been carried out on the propagation of cosmic rays through the Galaxy and their interactions with the galactic magnetic field (e.g. Thielheim and Langhoff 1968; Karakula *et al.* 1971; Berezinsky and Mikhailov 1985; Smith and Clay 1990), and these will be discussed in more detail in 4.4.1

4.2.4 Halo Field of the Galaxy

Whether or not there exists a magnetic halo field within the halo of our galaxy (even a relatively weak field) is a long-standing question (Baldwin 1959). It is important as it has implications for the containment of cosmic rays within the Galaxy, and hence is related to the question of the origin and propagation of high energy cosmic rays.

If there is a negligible field within the halo, then many of those particles whose Larmor radius is greater than the galactic thickness (see Fig 4.2) can be assumed to have an extra-galactic origin. This would result in a rather large anisotropy at these

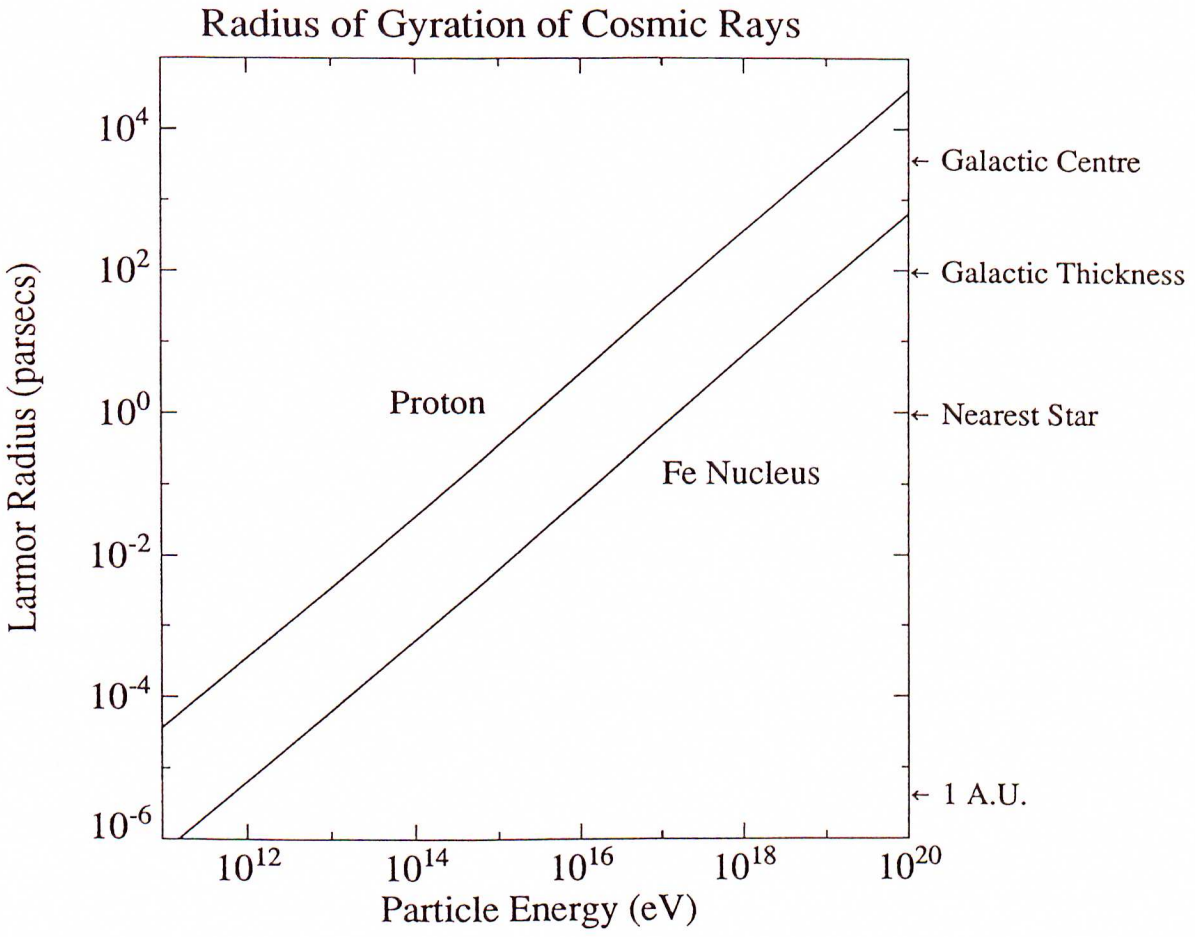

Figure 4.2: The radii of gyration for a proton and an iron nucleus in a $3\mu G$ field.

energies (Smith and Clay 1990), which is currently not observed (see e.g. Fichtel and Linsley 1986).

Alternatively, if an ordered magnetic field within the halo does exist, then those particles leaving the galactic plane may later return, possibly many times, due to deflection within this field. This would result in a reduced anisotropy as the trajectory of the particle becomes randomised (Smith and Clay 1990).

Therefore, the presence or lack of a halo field has a direct link to anisotropy measurements of cosmic rays at the higher energies.

Observations

Observations of the galactic halo are difficult, due to the relative sparseness of matter, and the large fields of view necessary to come to any conclusive results.

Work has been done in the ultra-violet region of the spectrum, in search of a galactic halo (mostly gas). York (1982) has reviewed these observations with the conclusion that there is evidence for a moderate extension of the Galaxy to $|z| \leq 10$ kpc, (where z is the distance from the galactic plane) which co-rotates, but no firm figures are available.

An alternative method of investigation is to examine the halos of other spiral galaxies of a similar type to our own. Such an investigation has been summarised by Sofue *et al.* (1986), and more recently by Duric and Bloemen (1990). Non-thermal radio emission has been detected, significantly extended from the disk planes of several edge-on galaxies, indicating the presence of magnetic halos.

Work done within the Galaxy relies largely on the rotation measures of extragalactic sources (the pulsar distribution only extends to $z \sim 500$ pc). Assuming a layer ~ 3 kpc thick and an electron density of $\sim 10^{-3}\mathrm{cm}^{-3}$, the halo field strength is estimated to be of the order of a few microgauss (Sofue *et al.* 1986).

It was decided to examine this result in more detail in order to investigate the effect that a halo field would have on rotation measures.

Simulations

Simulations were carried out on models of a uniform halo magnetic field, to determine the effect such a field would have on rotation measures.

Two models of electron density were used :

(1) Sofue and Fujimoto (1983) used a model for electron density to simulate rotation measures and then compare them with measured rotation measures to verify their galactic magnetic field model. The model chosen for halo field simulations was the better fit of the two suggested, namely

$$n_e(r,z) = 0.03\left(\frac{R_\odot}{r}\right)\exp\left[-\left(\frac{z}{d_e}\right)^2\right] \tag{4.5}$$

where

$4 \leq r \leq 15$ kpc

$R_\odot$, the sun's distance from the galactic centre was taken to be 10 kpc,

d_e, the scale height of the electron density distribution was taken to be 750 pc, and

z is the distance above (below) the galactic plane.

(2) Manchester and Taylor (1981) suggested a model for electron density, based upon the observations of 330 pulsars, mostly in the galactic plane. This worked well close to the plane but in their model as $z \to \infty$, $n_e \to 0.025$ cm^{-3}, which is believed to be incorrect at large values of z (see e.g. Harding and Harding 1982). This was modified by adding an overall z-scale factor of $d_e = 750$ pc.

The resulting model is

$$n_e(r,z) = \left[0.025 + 0.015\exp\left(-\frac{|z|}{0.07}\right)\right]\left(\frac{2}{1+r/R_\odot}\right)\exp\left(-\frac{|z|}{d_e}\right) \tag{4.6}$$

(all distances in kpc)

Other models do exist (e.g. those of Harding and Harding 1982; Guseinov *et al.* 1981), but the two chosen above were found to best fit the observed data with the models used for fields within the Galaxy.

Both of these distributions were used on three, fairly simple models of halo fields.

(1) A spiral field extended in the z direction (away from the galactic plane) with no attenuation.

(2) A divergent radially directed field.

(3) A non-divergent radially directed field.

In carrying out these simulations, the calculation technique used to derive the resultant rotation measures is that described by Sofue and Fujimoto (1983). Their suggested galactic magnetic field model was used as a 'background' field for comparison purposes, but the results obtained were largely independent of the type of 'background' model used.

For model (1) electron density distribution, the variations in Rotation Measure resulting from the introduction of the halo fields reached values of 20–30 radm^{-2} near the galactic plane, but were minimal for galactic latitudes greater than 20°, even when the halo field strength was $\sim 5\mu$G. (Typical Rotation Measures for distant (non-local) objects are of the order of 300 radm^{-2} or greater). The largest results were found for the radially divergent halo field, but were not significantly different from those produced by the other fields.

This is perhaps largely a result of the the model for electron density being used, where $n_e \rightarrow 0$ ($< 10^{-4}$ cm^{-3}) for $|z| \geq 4$ kpc, with the halo field only being introduced for $|z| > 1$ kpc (the generally accepted height at which the halo field is to be introduced).

For model (2) electron density, which is a broader distribution than (1), the magnitudes of the rotation measures appear to be largely independent of the type of magnetic field chosen.

A halo field of 1μG introduces a maximum change in the estimated Rotation Measure of ~ 10 radm^{-2} for small galactic latitudes. These reach up to ~ 100 radm^{-2} for a 5μG field.

In addition to these simulations, two others were attempted.

A random magnetic field of constant magnitude was found to have a minimal effect on the rotation measures for fields up to a strength of $\sim 5\mu$G.

Ultra-violet astronomical observations (see York 1982 for a review) suggest that there exists a galactic halo of electrons with $n_e \simeq 10^{-4}$ cm^{-3} out to $z \sim 10$ kpc. Setting

the electron density distributions to have this minimum value had no detectable effect on the previous simulation results.

In conclusion, little is known about , the magnetic field and electron density in the Galaxy in general, and we are particularly ignorant in the region outside of the galactic plane (within the halo). As a result, simulations of various halo fields will be dependent upon the electron density model assumed. Using the results of the simulations here, it is suggested that there could exist an ordered field in the galactic halo, of magnitude $\sim 3\mu$G (comparable to that in the galactic plane), whose effect upon rotation measures is within the uncertainty of these measurements. In addition, there may be a randomly oriented field of strength $\leq 5\mu$G which would have a similarly negligible effect on these measurements. The results quoted here are upper limits to the halo field strength in the Galaxy, derived from the previously discussed simulations. To lower these limits, more detailed models and simulations will be necessary, along with higher resolution experimental data, in order to determine the strength and structure of the halo magnetic field (assuming a measurable field exists).

4.3 The Anisotropy of Cosmic Rays

The degree of anisotropy of the cosmic ray flux is defined by

$$\delta = \frac{I_{max} - I_{min}}{I_{max} + I_{min}} \tag{4.7}$$

where I_{max} is the maximum cosmic ray intensity measured and similarly I_{min} is the minimum cosmic ray intensity measured.

The experimental and analytical techniques involved in the determination and subsequent interpretation of the anisotropy of the cosmic ray flux will be discussed in the remainder of this chapter.

4.3.1 Harmonic Analysis

Traditionally, anisotropies are quoted in terms of Fourier amplitudes and phases (mostly the first and second harmonics) of the cosmic ray intensity as a function of right ascension. This application of harmonic analysis has been criticised in the past (e.g. Kiraly and White 1975; Kiraly *et al.* 1975), in favour of χ^2 tests. However, its application may be justified on a number of grounds.

The most important of these is the fact that the sinusoidal analysis carried out is of the same form as the variations in sidereal and solar time being investigated. In addition, this technique allows easy testing for spurious variations introduced in both solar and sidereal time. Furthermore, the majority of anisotropy experimental results published have been presented in this form and allow easy comparison of results between experiments. Other methods do exist (e.g. galactic plane plots), and these will be discussed in 4.3.3.

Whatever analysis technique is applied, equal exposure on all regions of the sky is a necessity (or alternatively, any uneven exposure needs to be taken into account). This is most easily achieved by considering bands of constant declination. Even exposure in sidereal time guarantees even exposure in right ascension (apart from atmospheric effects). Even exposure in a range of declinations is not easily achievable due to the effect atmospheric attenuation has on shower detection (see Fig 3.6).

The theoretical aspects of harmonic analysis are based on ideas introduced by Lord Rayleigh (1880). Chapman and Bartels (1940), and Linsley (1975a, 1975b) have discussed this work in more detail, with Linsley's work dealing in particular with the application to cosmic ray anisotropy analysis.

If we assign each event with a vector of equal magnitude, and phase in terms of its right ascension, then the amplitude of the resultant vector can by defined by

$$r = \sqrt{a^2 + b^2} \tag{4.8}$$

where

$$a = \frac{2}{N}\sum_{i=1}^{N} cos\psi_i, \qquad b = \frac{2}{N}\sum_{i=1}^{N} sin\psi_i \tag{4.9}$$

ψ_i is the phase of the ith event, and

N is the total number of events being considered.

The overall phase, ψ, may be defined by

$$\psi = \psi' \qquad \text{for } b > 0, a > 0$$

$$\psi = \psi' + \pi \qquad \text{for } a < 0$$

$$\psi = \psi' + 2\pi \qquad \text{for } b < 0, a > 0$$

where $\psi' = \tan^{-1}(b/a)$, $\frac{-\pi}{2} < \psi' < \frac{\pi}{2}$. (A similar definition applies to the second and higher harmonics).

Harmonic analysis of the cosmic ray data can be carried out by sorting the data into h bins of right ascension, each bin containing n_i events. The components a and b can then be defined as

$$a = \frac{2}{N}\sum_{i=1}^{h} cos(n_i\psi_i), \qquad b = \frac{2}{N}\sum_{i=1}^{h} sin(n_i\psi_i) \tag{4.10}$$

with r and ψ being defined as before.

Once an amplitude and phase have been obtained, a significance must be assigned to the resultant vector. For a large number of events (N), and randomly distributed phases (ψ_i) (i.e. random events), the probability distribution function for the displacement vector R, is given by

$$p(R) = \frac{R}{2N}\exp\left(\frac{-R^2}{4N}\right) \tag{4.11}$$

Integrating, this gives the probability of obtaining a resultant greater than or equal to R as

$$P(\geq R) = \exp\left(\frac{-R^2}{4N}\right) \tag{4.12}$$

$$= \exp(-k_o) \tag{4.13}$$

with k_o defined by

$$k_o = \frac{R^2}{4N} \tag{4.14}$$

This may be related to the fractional result $\vec{r}$ obtained by putting $\vec{R} = N\vec{r}$ (Linsley 1975b), and hence

$$k_o = \frac{r^2 N}{4} \tag{4.15}$$

In general, $\vec{r} = \vec{s} + \vec{x}$, where $\vec{r}$ is the measured vector, $\vec{s}$ is the true source vector (assumed to be non-zero in cosmic ray work), and $\vec{x}$ represents other contributions. Ideally, $\vec{x}$ will represent just the Rayleigh fluctuations. In reality, there will be other spurious factors contributing to $\vec{x}$ (see 4.3.2; 5.2.3 for a discussion of these factors). We will assume that these effects have been eliminated for the present discussion.

If $k_o \gg 1$, then $\vec{x}$ is unimportant and $P_{s,\theta}$ (the probability distribution that a measurement of amplitude r and phase ψ, had s in ds, and θ in $d\theta$) will approach normal distributions with P_s normal about $s = r$, with dispersion $\sigma_r = (2/N)^{\frac{1}{2}}$, and P_θ normal with dispersion $\sigma_\theta = (2k_o)^{-\frac{1}{2}} = \sigma_r/r$. However, $k_o \gg 1$ is rarely achieved in cosmic ray work.

As $k_o \rightarrow 1$, $\vec{r}$ tends to overestimate $\vec{s}$, and for $k_o \geq 1.5$, $< s >$ can be approximated by

$$< s >= r\left(1 - \frac{1}{2k_o}\right)^{\frac{1}{2}} \qquad \text{Linsley (1975a)} \qquad (4.16)$$

For values of $k_o < 1.5$, the approximation breaks down due to the tendency of $\vec{r}$ to underestimate $\vec{s}$. Fig 4.3 shows expectancy and confidence levels for the ratio (s/r) (calculated by Linsley 1975b) as well as the 95% error in θ.

Clay (1987) has carried out simulations for both purely random events, and a random distribution with an introduced anisotropy, and concludes that the threshold value for the detection of a broad anisotropy (180° wide) is $k_o \sim 0.4$.

The previous discussion has assumed the values of r and ψ are tainted only by Rayleigh fluctuations. Unfortunately, it is not possible in general, to get pure first and second harmonics directly from the measurements. To obtain estimates of r and ψ from the measured fluxes, it is first necessary to allow for (and hopefully eliminate) spurious effects which may have been introduced into the data in its collection.

4.3.2 Spurious Effects

In the majority of air shower anisotropy experiments carried out to date, it has been assumed that year-round measurements are made. This is a simplifying assumption

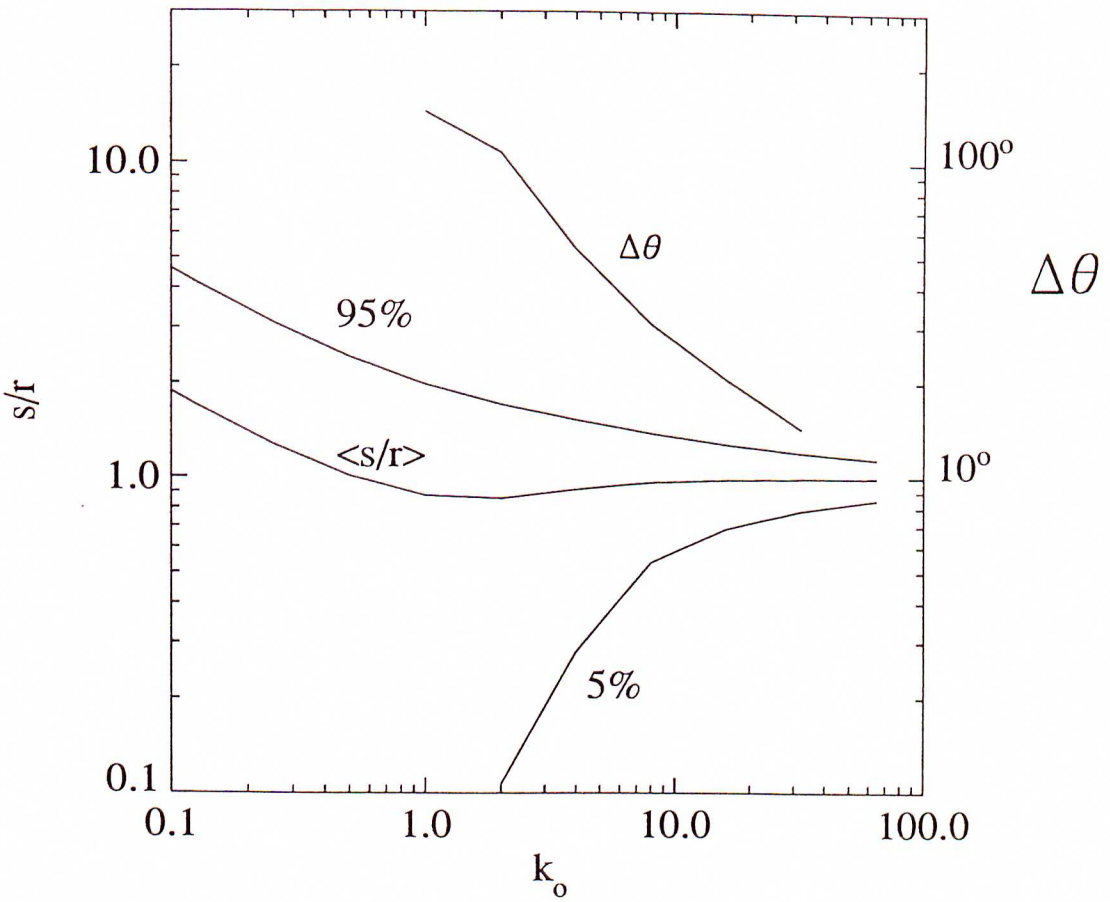

Figure 4.3: The best estimate and 5% and 95% confidence limits for the ratio of genuine to measured amplitude (s/r). $\Delta\theta$ is the 95% confidence interval for the phase. (from the data of Linsley 1975b).

and, as a result, any solar period effects, assuming there is no annual modulation, will be averaged out and do not need to be taken into account.

If this is not the case, then these effects will contribute to a spurious sidereal component. The consideration and elimination of these components will be discussed in 5.2.3. Their causes are, in many cases, known and will now be discussed.

Production of Spurious Effects

Any measured anisotropy will be a contaminated version of the true galactic (and extra-galactic) anisotropy. There are a number of known effects which may either alter the value of anisotropy measured, or add to the anisotropy, distorting the resultant observations. These effects may be either atmospheric, or extra-terrestrial in nature.

The Compton-Getting Effect (Compton and Getting 1935) is responsible for the known extra-terrestrial effects. It results from the motion of an observer through the cosmic ray gas, which is assumed to be in equilibrium, and produces a maximum in intensity in the direction of motion. The magnitude of the resulting anisotropy will be given by

$$\delta = (2+\gamma)\frac{v}{c} \qquad \text{Thambyapillai (1974)} \qquad (4.17)$$

where γ is the exponent of the differential rigidity spectrum.

The first of these effects is the co-rotation anisotropy, which is a result of the motion of the solar magnetic field with respect to the Earth. At low enough rigidities (corresponding to energies $< 10^{11}$eV/Nucleon) , it may be assumed that the cosmic ray gas is frozen in the solar magnetic field (Thambyapillai 1974). Hence, as it sweeps past the Earth, overtaking the orbital motion of the Earth, a maximum will be generated. However, this is rigidity dependent, and is not significant at the energies being considered ($> 10^{14}$eV).

We can also consider the orbital motion of the Earth with respect to the cosmic ray gas stationary with respect to the sun. Such an effect should be energy independent, with an amplitude of $\sim 0.05\%$ (for $\gamma = 2.6$), the maximum occurring at 06.00 hr local solar time (outside of the magnetosphere). There is no evidence for any annual

modulations in these effects (Thambyapillai 1974), and so they shouldn't contribute to produce spurious sidereal anisotropies, provided measurements are made over a full year. When this isn't the case, the resultant solar period modulation must be taken into account (see 5.2.3 for details).

Another, more subtle Compton-Getting effect results from the motion of the solar system with respect to the local inter-stellar medium, considered to be stationary in the rotating galactic frame. Hillas (1982) has estimated the first harmonic resulting from this effect at low energies to be $\sim 0.03\%$ at 18.6 hr in right ascension. It applies at all energies where the cosmic ray gas is in equilibrium and contributes to a real sidereal anisotropy, which cannot be removed by averaging over a year, or any other technique employed to remove solar period related effects.

Within the atmosphere, periodic changes in atmospheric conditions, such as temperature with solar time will affect the detected shower rate. Similarly, aperiodic, chaotic effects, such as barometric pressure, and the height and temperature of various pressure levels may also contribute to variations in the measured flux. Any annual modulation of such effects may also result in spurious sidereal components. The elimination of these atmospheric effects for the present analysis will also be considered in 5.2.3.

Anti-Sidereal Analysis

One such technique developed to remove spurious effects resulting from solar period effects is the anti-sidereal analysis procedure of Farley and Storey (1954). In this technique, it is assumed that there are only two natural frequencies in the variations in the cosmic ray flux, namely the sidereal variations resulting from any genuine flux anisotropy, and solar variations produced by e.g. diurnal temperature fluctuations.

Amplitudes (and phases) are calculated for sidereal, solar and anti-sidereal (24 hr, 4 min) periods, and these vectors may then be algebraically combined to eliminate these effects from the data (see e.g. Gerhardy 1983).

This method has several limitations. For the vector combination to be effected,

data covering a full year is required which, for a remote field station (such as Buckland Park) is difficult to achieve. This presents problems in considering periods of less than one year in length. It also assumes that there is no annual phase modulation of the solar vector. Pollock (1978) has provided a detailed solution for the latter problem, by introducing vectors corresponding to other periods, further removed from the solar and sidereal periods.

The data analysed by the author for anisotropies has been treated with an alternative technique for removing solar period effects which will be discussed in detail in Chapter 5.

4.3.3 Alternative Methods of Data Analysis and Presentation

The application of harmonic analysis in anisotropy investigations has the drawback that, in its simplest form, it only searches for variations as a function of right ascension, averaging over the entire investigated interval of declinations. These regions are rather wide in most E.A.S. experiments and as a result not all of the information concerning the arrival directions of cosmic rays is used. This has the effect of diluting any anisotropy which has a phase dependent on declination. As an example, the galactic plane, which it is believed should show up in anisotropy analyses, varies in a complicated manner with right ascension and declination (see e.g. Lang 1974).

One solution is simply to calculate first and second harmonics for each declination band being considered (in the cases where the declination information is available). Unfortunately, this compromise results in poorer statistics due to the smaller number of events being considered.

Astley *et al.* (1981) have suggested an alternative method of analysis. Their method is based upon the assumption that any genuine anisotropy should be somehow correlated with the galactic plane (see 5.5 for a definition of galactic co-ordinates). It can be equally suited to any other hypothesis defining the arrival directions of cosmic rays in some way.

In this technique, narrow strips of declination are considered, and the contribution

as a function of galactic latitude is calculated, being weighted by assuming there is a uniform distribution of showers as a function of right ascension. The ratio N_{obs}/N_{exp} can then be calculated as a function of galactic latitude. A least squares fit may then be applied, the slope of the resulting line being known as a latitude gradient. Applying this technique to different energy ranges, a description of the latitude gradient as a function of energy may be obtained providing information on the preferred arrival directions of high energy cosmic rays as a function of galactic latitude and primary energy. This method is only applicable when there is a significant anisotropy ($> 1\%$), and is therefore only applied to the highest energy cosmic rays ($> 10^{17}$eV). Results in this energy regime will be considered in 4.5.3 (and for the present data set in 5.5.1).

4.4 The Production of Anisotropies

As discussed in 4.2.3, for all but the highest energies, the observed arrival directions of cosmic ray particles will be governed by both the structure of the local magnetic field, and the distribution and properties of the particle sources. Measurements of anisotropies can be used to infer information about both of these effects, as models of cosmic ray sources and propagation can be used to predict anisotropies of the flux.

The first detailed model of cosmic ray propagation including the effects of the galactic magnetic field was proposed by Davis (1954). Using a field of similar structure, but somewhat stronger than that currently postulated, tentative agreement was found with the anisotropy estimates available at that time. A more recent model (Hillas and Ouldridge 1975) assumed a source spectrum and, assuming a leaky box model of confinement, produced a model which matched the observed variation of anisotropy with energy. Unfortunately, the model suffers from several problems, the most important being the assumption of a single power law production spectrum for the source over the entire energy range considered (10^{11}eV – 10^{19}eV). A more detailed model was proposed by Bell *et al.* (1974), which involved galactic diffusion governed by both magnetised gas clouds and the large-scale magnetic field. However, its usefulness was limited by

the necessity of specific configurations of the scattering fields in order to produce an adequate result.

A number of models of cosmic ray origin and propagation for energies above 10^{15}eV were tested by Lloyd-Evans *et al.* (1979). It was found that all of the models disagreed with observations in at least part of the energy range. It was also noted that the two most prominent features of the energy spectrum (the 'knee' at $\sim 10^{15}$eV, and the 'ankle' at $\sim 10^{19}$eV), appear to be associated with changes in the behaviour of the measured anisotropy. Above the knee, there appears to be a more rapid increase in amplitude with energy and the phase also varies more rapidly. The onset of very large anisotropies (or at least large upper limits) were observed at $\sim 10^{19}$eV. These effects have several interpretations, depending largely upon the composition of the primary cosmic ray flux at these energies.

More recent models and interpretations will be considered in 4.5.2, 4.5.3

4.4.1 Simulations

Simulations of the production of cosmic ray anisotropies have been carried out for more than twenty years (e.g. Thielheim and Langhoff 1968), in order to interpret measurements of anisotropies in terms of origin and propagation models. In general, simulations have only been carried out for primary energies above $\sim 10^{17}$eV. Below this energy, particles tend to travel in helical paths, following the magnetic field lines (parallel to the spiral arms in general) of the Galaxy. Trajectories of protons within the Galaxy are simulated by tracing the paths of anti-protons leaving the Earth, following their paths until the particle leaves the Galaxy. An estimate of the lifetime of the particle within the Galaxy is then possible.

Early simulations were carried out by Thielheim and Langhoff (1968), Thielheim *et al.* (1971), and Karakula *et al.* (1971) with similar results. The major conclusion was that the majority of particles with energies $> 10^{18}$eV are of extra-galactic origin in order to be consistent with observed anisotropies. A purely galactic origin, providing the particles could be contained, would result in a large anisotropy which is currently

not observed.

More recent simulations by Berezinsky *et al.* (1979) and Berezinsky and Mikhailov (1985) examining the 10^{17}eV – 10^{19}eV region have been interpreted as suggesting that the observed anisotropy component can be considered to be a result of interactions with a galactic halo, and are of galactic origin. They suggest that extra-galactic sources meet problems in explaining both the measured particle flux and anisotropy amplitude. However, if the anisotropy measurements are considered only as upper limits (see e.g. Clay 1987), then these results can be brought into line with an extra-galactic source consistent with the previous results of Karakula *et al.* (1971)

Smith and Clay (1990) have carried out the most recent simulations to date, and argue that for primary energies greater than 10^{18}eV, the predicted anisotropy for uniformly distributed sources results in an anisotropy much greater than the currently observed 10%. It is further suggested that the anisotropy at these energies may be greatly below this value, in which case a galactic source model would fail completely. Smith and Clay (1990) suggest a dominating extra-galactic source distributed broadly and uniformly would be necessary to give the appropriate anisotropy. The results of these simulations assume a predominantly proton composition at these energies, which tend to be favoured by current observations (Clay 1985). If this is found not to be the case, then a revision of these conclusions would be necessary.

Results of simulations are unanimous in suggesting an extra-galactic source for U.H.E. cosmic rays to be consistent with the currently available observations, many of which must be considered only as upper limits. Further anisotropy and composition measurements at these energies are necessary in order to determine some of the finer details of these results.

4.5 Anisotropy Measurements

Measurements of the preferred arrival directions of cosmic rays have been attempted for more than forty years, and have progressed from relatively crude but effective counting

experiments to the current generation of E.A.S. arrays. These experiments and their results and significance will be considered in the remainder of this chapter (Fig 4.4 is a compilation of the measurements to be discussed).

4.5.1 Low Energy Measurements

The minimum energy at which useful sidereal anisotropies can be measured, and distinguished from solar modulation effects is $\sim 10^{11}$eV. This lower limit may vary significantly over the solar cycle, reaching $\sim 3 \times 10^{11}$eV at times of high solar activity, and dipping below 10^{11}eV during quiet times (Jacklyn 1986). Measurements of galactic cosmic ray anisotropies in the low energy range (10^{11}eV – 10^{14}eV) have been recently reviewed by Jacklyn (1986). Elliot (1979) has also provided a useful summary of anisotropy results in this energy range.

In this lower energy range, the primary cosmic ray flux may be monitored by the detection of the secondary penetrating muon component of air showers by underground or shielded muon detectors (the less penetrating electromagnetic component does not reach sea-level at these energies). These high energy muons result from the decay of pions produced early in the shower, and may be detected at depths of up to $\sim$ 500 m.w.e. (equivalent depth of water in metres). Detectors may be shielded significantly to prevent the detection of less penetrating shower particles. Around 10^{13}eV, the method of detection changes to small air shower arrays, situated at mountain altitudes.

The muon monitoring experiments usually determine the flux through the measurement of event rate, recorded as a function of both solar and sidereal time. Directionality is provided by atmospheric collimation, resulting in angular uncertainties typically $\sim$ 0.5 steradians. Atmospheric variations may be essentially eliminated by using a pair of cosmic ray detectors operating simultaneously, sensitive to events arriving from a small range of directions, and pointing in opposite directions (usually East-West), but at similar zenith angles. These detectors are equally affected by the prevailing atmospheric conditions, and therefore the flux anisotropy may be obtained by the vector difference of the individual detector results, which should then be free of atmospheric

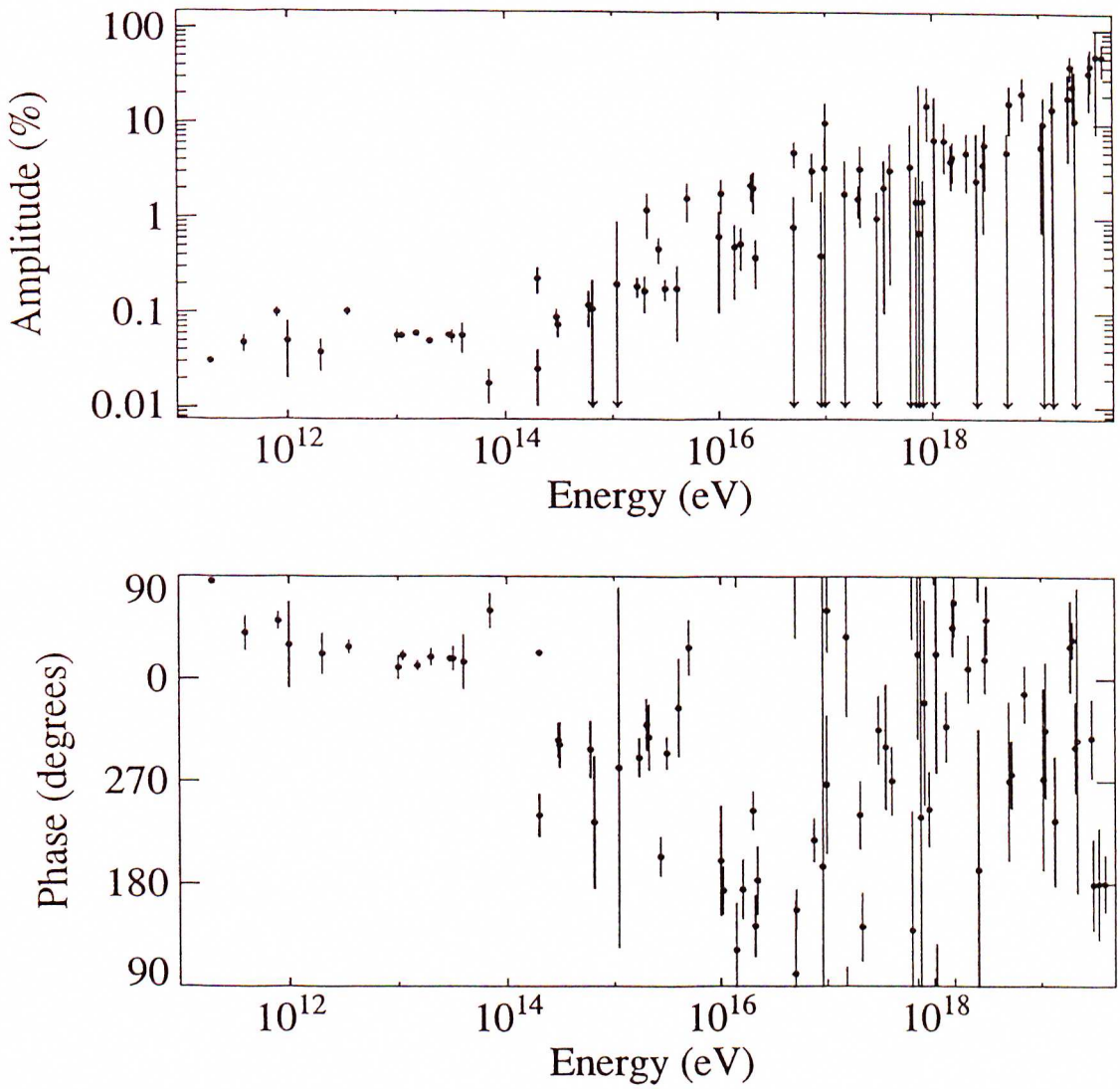

Figure 4.4: A compilation of anisotropy measurements (first harmonic amplitude and phase). (See Figs 4.5, 4.7, & 4.8 for more detail and references).

effects.

Below 10^{12}eV, statistically significant first harmonic results have been obtained with amplitudes of the order of 0.04% through the use of underground muon telescopes in both hemispheres (Hobart (Fenton 1976; Humble and Fenton 1977), London (Davies *et al.* 1979)). However, large variations evident in the measured anisotropy were found to be well correlated with changes in the interplanetary magnetic field. Sekido *et al.* (1976), through the use of air Cerenkov Telescopes, found results in excellent agreement with those above. However, solar effects were once again found to be prominent. It has been suggested (Wolfendale 1977), that the actual anisotropy outside of the heliosphere at these energies may be different to that measured as a result of the disturbing effect of the interplanetary magnetic field.

For primary particle energies above 10^{12}eV, the effect of the interplanetary magnetic field on anisotropy measurements is expected to be minimal (see e.g. Jacklyn 1986 and references therein). However, measurements made by the Poatina muon telescopes (Fenton and Fenton 1976) give some indication that there is still a contribution by the interplanetary magnetic field at a median energy of $\sim 1.5 \times 10^{12}$eV. Despite a significant sidereal first harmonic (0.05%), some correlation with the direction of this field was found.

Measurements carried out at Baksan (USSR) (Andreyev *et al.* 1987) operating at a median energy of $\sim 3 \times 10^{12}$eV showed no such correlation. Similarly, measurements carried out in Utah (Bergeson *et al.* 1979) at a comparable energy show no correlation. Bergeson *et al.* (1979) applied a Discrete Fourier Transform to their underground muon detector measurements to obtain an anisotropy comparable in both phase and magnitude to those previously discussed (see Fig 4.5 for comparisons).

In the decade above 10^{13}eV, anisotropy measurements have been dominated by the air shower experiments of Baksan (see e.g. Andreyev *et al.* 1987), and Mt. Norikura (see e.g. Nagashima *et al.* 1989), with a small contribution from Musala Peak (Gombosi *et al.* 1975).

The experiment carried out at Baksan (latitude 43°N) involved the counting of

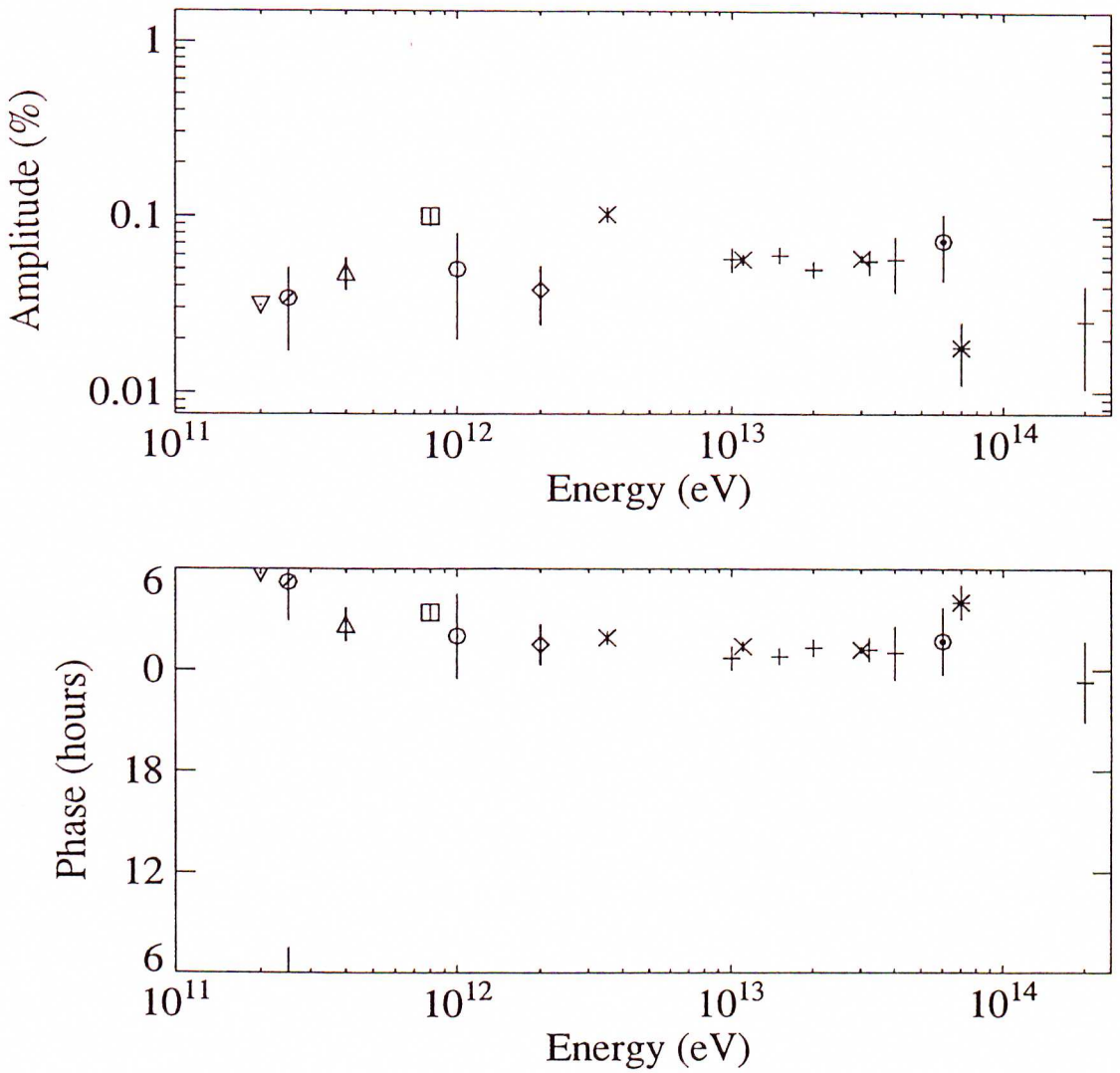

Figure 4.5: A compilation of low energy anisotropy measurements (first harmonic amplitude and phase).
(+) Nagashima *et al.* (1990), Sakakibara (1976, 1979)
(∗) Fenton *et al.* (1990)
(◯) Fenton and Fenton (1976)
(◇) Bergeson *et al.* (1979)
(△) Davis *et al.* (1979)
(□) Bercovitch and Agrawal (1981)
(×) Alexeenko *et al.* (1981), Andreyev *et al.* (1987), Alexeenko and Navarra (1985)
(▽) Fenton (1976)
(⊘) Sekido *et al.* (1976)
(⊙) Gombosi *et al.* (1975)

coincidences between four sets of air shower detectors corresponding to a mean energy of $\sim 10^{13}$eV (Alexeenko *et al.* 1981). Atmospheric collimation was used for directionality, and the data were corrected for barometric pressure variations. The resultant first harmonic amplitude and phase ($0.057 \pm 0.004\%, 1.4 \pm 0.3$ hr) agree well with those measured at Mt. Norikura ($0.060 \pm 0.003\%, 0.8 \pm 0.3$ hr) (Nagashima *et al.* 1990) (see Fig 4.5).

Measurements made at Mt. Norikura (latitude 36°N) collected over two decades (1970–1989) similarly relied on three-fold and four-fold coincidence counting rates, resulting in a mean energy of $\sim 1.5 \times 10^{13}$eV (Nagashima *et al.* 1989). In addition, results from an East-West pair of detectors operating simultaneously were found to be in agreement with those obtained from the omni-directional detectors. The only significant solar diurnal variation measured was that expected from the Compton-Getting effect, indicating that atmospheric effects are unimportant for this experiment. Nagashima *et al.* (1989) conclude that the measured sidereal anisotropies at these energies are of a galactic origin. Annual variations in the measured sidereal vectors were found, presumably resulting from heliomagnetospheric modulation, and this modulation showed a correlation with the polarity reversal of the polar magnetic field of the Sun (Nagashima *et al.* 1989).

Earlier measurements carried out at Musala Peak in Hungary (Gombosi *et al.* 1975) also indicated a significant sidereal anisotropy at a median energy $\sim 6 \times 10^{13}$eV ($0.073\%, 1.7$ hr).

An array operating at Liawenee in Tasmania since 1982 is situated at a conjugate latitude to Mt. Norikura with the intention of employing the bi-hemisphere comparative method to determine the relative contributions of uni-directional and bi-directional diurnal components (see Jacklyn 1986 and references therein). No such results are available at present for this method, but operating as a single detector, recent results obtained at 7×10^{13}eV ($0.018 \pm 0.007\%, 4.0 \pm 1.0$ hr) (Fenton *et al.* 1990) are small compared with results obtained at 4×10^{13}eV and below which amplitudes are consistently of the order of 0.06%. A further result from Mt. Norikura ($0.025 \pm 0.015\%$)

(Nagashima *et al.* 1990) at a slightly higher energy (2×10^{14}eV) confirms this lowering of the anisotropy around 10^{14}eV.

A summary of low energy anisotropy measurements is presented in Fig 4.5. Data presented are uncorrected for the Compton-Getting effect of the solar motion through the inter-stellar medium. Second and higher order harmonic measurements have also been made, in order to provide further information on the structure of the galactic flux anisotropy. The majority of these measurements have been found to be nearly consistent with isotropy although a few recent results have been found to be indicative of a bi-directional flow (see Jacklyn 1986 for a discussion).

The demonstration of the existence of the observed finite anisotropy has taken decades of painstaking work. Unfortunately, these data provide no direct information about the primary particle origin at these energies, due to the small Larmor radii of these particles (10^{-5}–10^{-2} pc). The relative consistency in both amplitude and phase with energy up to an energy of $\sim 5 \times 10^{13}$eV indicates that the mode of propagation of these cosmic rays changes little over this energy range, and may be interpreted as indicating a uniformity in the local inter-stellar magnetic field over these scales.

The conventional view was that the measured anisotropy was constant at $\simeq 0.05\%$ up to energies of $\sim 10^{15}$eV, and then increased with energy (see e.g. Kifune 1990). The recently observed dip in the anisotropy around 10^{14}eV (Fenton *et al.* 1990; Nagashima *et al.* 1990), and supported by preliminary results from Akeno (Murakami *et al.* 1990) is contradictory to this conventional view, and requires a revision of the interpretation of anisotropies at these energies.

4.5.2 Medium Energy Measurements

In the medium energy range (10^{14}eV – 10^{17}eV), the effects of the sun and the inter-planetary magnetic field are negligible. This energy range is entirely the province of E.A.S. experiments, with many measurements having been made at both sea-level and mountain altitudes. However, due to the steep energy spectrum of the primary cosmic ray flux, resulting in a decrease in flux of ~ 100 for every decade in energy, arrays with

large collecting areas, operating for lengthy, continuous periods are necessary in order to give a result above that which would be expected simply due to cosmic rays arriving from completely random directions.

Linsley and Watson (1977) completed a comprehensive survey of anisotropy determinations in this energy range, between 1951–1965, based upon the work of Sakakibara (1965). They considered 42 results from 20 independent experiments. The majority of these experiments were air shower rate counting experiments, relying on atmospheric collimation for directional information. Only a few of the later experiments, working at the top end of this energy regime used the now commonly employed technique of fast-timing (see 3.3.1) for directionality. Energy resolution in the majority of these experiments was also crude, based on the mean number of shower particles, the determination of which was based essentially upon coincidences.

At the lower end of this range, atmospheric attenuation was minimised by conducting them at high altitudes (e.g. Pic du Midi at 2860 m.a.s.l. — Daudin *et al.* 1956). Despite these limitations, Linsley and Watson (1977) arrived at several conclusions, the most notable being the apparent clustering of the maxima around 17.5 hours (R.A.) when given equal weight. Such clustering will be discussed in 4.5.4. Despite the first harmonic agreement, the second harmonic phases showed no significant agreement.

The energy dependence of these results was investigated by grouping the data into decade energy ranges (A:10^{14}eV – 10^{15}eV; B:10^{15}eV – 10^{16}eV; C:10^{16}eV – 10^{17}eV) (Linsley and Watson 1977). The resultant quoted for each group was obtained by the vectorial addition of the experimental vectors, and the results are shown in Table 4.1.

In Group A, 5.8×10^7 events were collected. The majority ($\sim$ 70%) came from the counting experiment of Daudin *et al.* (1956), carried out at Pic du Midi (altitude 2860m, latitude 43°N). The experimental apparatus consisted of five trays of Geiger-Müller counters separated by distances of up to 80m. Energies were assigned by different coincidence requirements, and corrections were made for atmospheric pressure and temperature. The validity of the sidereal component was confirmed by dividing the data into half-yearly bins. The sidereal component showed a constant phase, whilst

Energy Group	Number of Events	Average Energy (eV)	Apparent Amplitude (%)	Phase (degrees)
A	5.8×10^7	3×10^{14}	0.075 ± 0.02	302 ± 20
B	1.3×10^7	1.7×10^{15}	0.19 ± 0.045	291 ± 17
C	3.7×10^5	1.6×10^{16}	0.53 ± 0.25	176 ± 27

Table 4.1 : Summary of the Linsley and Watson (1977) survey.

the solar component changed phase. The other experiments in Group A made only a minimal contribution to the amplitude, although some phase agreement existed.

In Group B, 1.3×10^7 events were considered from fifteen independent experiments. The largest contribution came from the experiment of Daudin *et al.* (1956), but significant contributions were also made by Citron and Stiller (1958), and Farley and Storey (1954, 1957). Citron and Stiller (1958) operated duplicate sets of Geiger-Müller counters at Schauinsland (altitude 1230m, latitude 48°N), the duplicate set allowing constant monitoring of the apparatus. They found a significant solar variation, but only a small sidereal effect, which changed from year to year, and could be partially explained by atmospheric effects (e.g. temperature and barometric pressure variations). An alternative view is that any genuine anisotropy may have been disguised by the atmospheric effects. The variation has since been attributed to counting statistics (Linsley and Watson 1977). Similar variations were also observed by Farley and Storey (1954, 1957) at Auckland (altitude 40m, latitude 37°S). Their earlier experiment recorded a larger but statistically less significant amplitude than their latter experiment, which had better statistics. The small contributions (statistically) of Clark (1957) and Chitnis *et al.* (1960) were important because they employed fast-timing instead of atmospheric collimation for directionality, and hence were able to assign both a right ascension and declination for each recorded event.

In Group C, the statistics were much poorer, consisting of only 3.7×10^5 events, collected by seven experiments. The most important contribution was made by the experiment of Delvaille *et al.* (1962), carried out at Ithaca, where fast-timing was used to calculate directions for energies greater than 10^{15}eV. Their array consisted of fifteen scintillators, covering an area of almost 1 km in diameter. The anti-sidereal analysis technique of Farley and Storey (1954, 1957) was applied to their results, but these corrections were ignored by Linsley and Watson (1977). They suggested that these corrections were uncertain and may have just added noise to the results. Whilst their amplitude results were inconclusive, there was consistency in their phase measurements.

Following 1965, there was a lull in medium energy measurements, which resumed

in the mid-70s. In more recent times, more results have become available as the larger arrays, constructed in the 1970s, became operational and collected significant numbers of events.

The exception to this trend is the Haverah Park Array (see e.g. Edge *et al.* 1978; Lloyd-Evans 1982; Eames *et al.* 1985) which collected data onwards from 1963. This array (recently decommissioned) used large, deep-water Cerenkov detectors, configured into sub-arrays with spacings ranging from 50m to 2 km, and operated at a threshold of $\sim 10^{15}$eV. Whilst capable of detecting events of energies E $\sim 10^{21}$eV, a significant contribution has been made in the medium energy range (Lloyd-Evans 1982), using the 50m and 150m arrays. Spurious effects were examined in great detail and the results, although only marginally significant, are in agreement with Linsley and Watson's survey (1977).

More recently, data has become available from Buckland Park (Gerhardy and Clay 1983), and Akeno in Japan (Kifune *et al.* 1986b), which is generally in agreement with previously determined results.

Medium energy anisotropy measurements have been summarised in Figs 4.6 & 4.7. Following from Linsley (1983), only those results from the Linsley and Watson survey (1977) which were corrected for atmospheric pressure effects have been included. The summary results from Linsley and Watson (1977) have also been included for comparison purposes.

Furthermore, the data have been separated into northern and southern hemisphere measurements. There is no reason, *a priori*, to expect these measurements to be compatible, as different regions of the sky (and hence the Galaxy in general) are being viewed. Northern hemisphere observations have generally been made in the latitude range 40°N–60°N, whilst southern hemisphere observations exist for the range 35°S–40°S. Taking into account atmospheric attenuation, there is essentially no overlap of the observed regions. This is especially important in the early counting experiments where declination information is unavailable. On this premise, the Group B results of Linsley and Watson (1977) must be viewed with caution, as they contain a significant

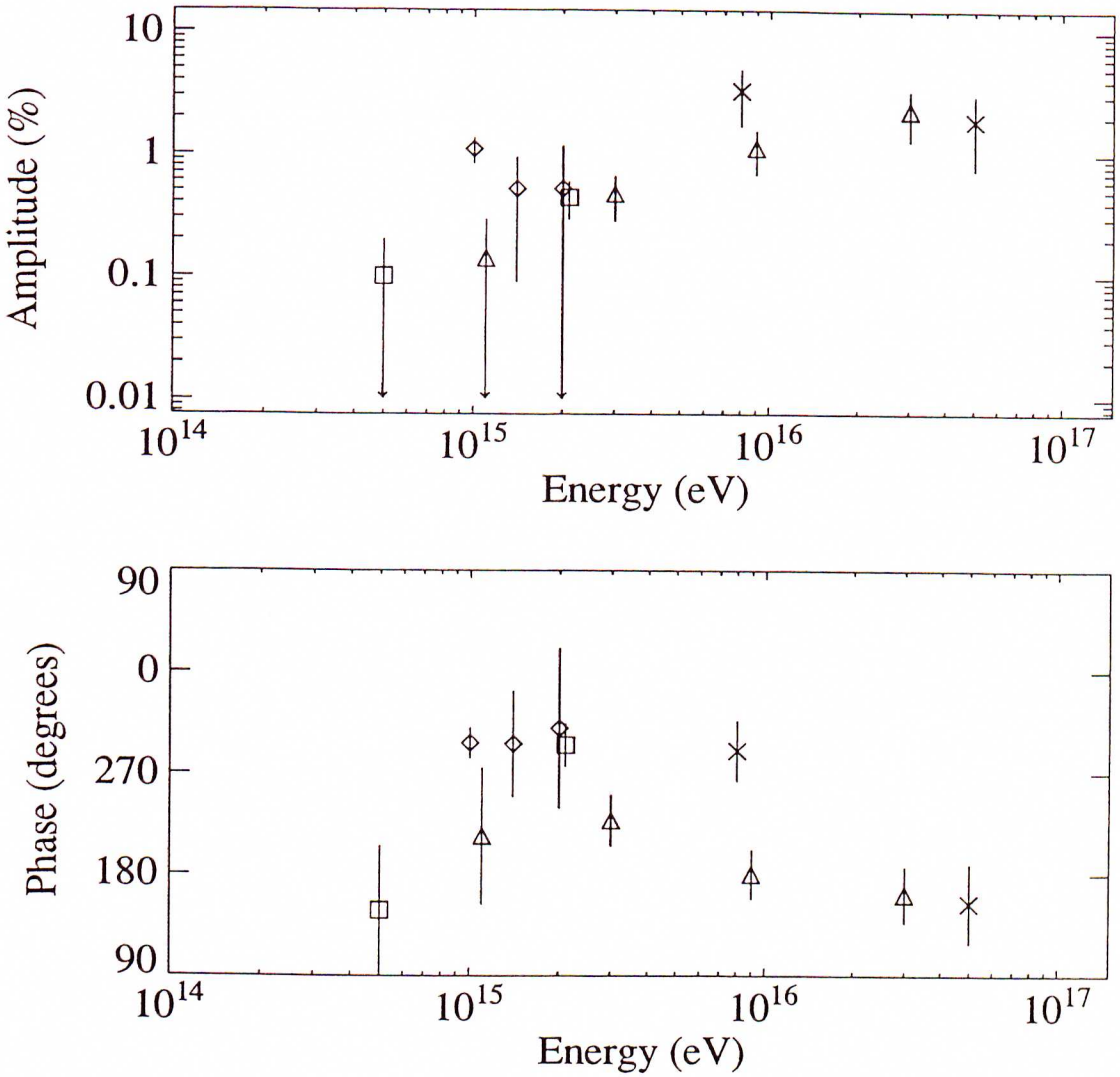

Figure 4.6: A compilation of southern hemisphere medium energy anisotropy measurements (first harmonic amplitude and phase).
(◇) Farley and Storey (1954)
(△) Farley and Storey (1957)
(×) Gerhardy and Clay (1983)
(□) Escobar *et al.* (1960)

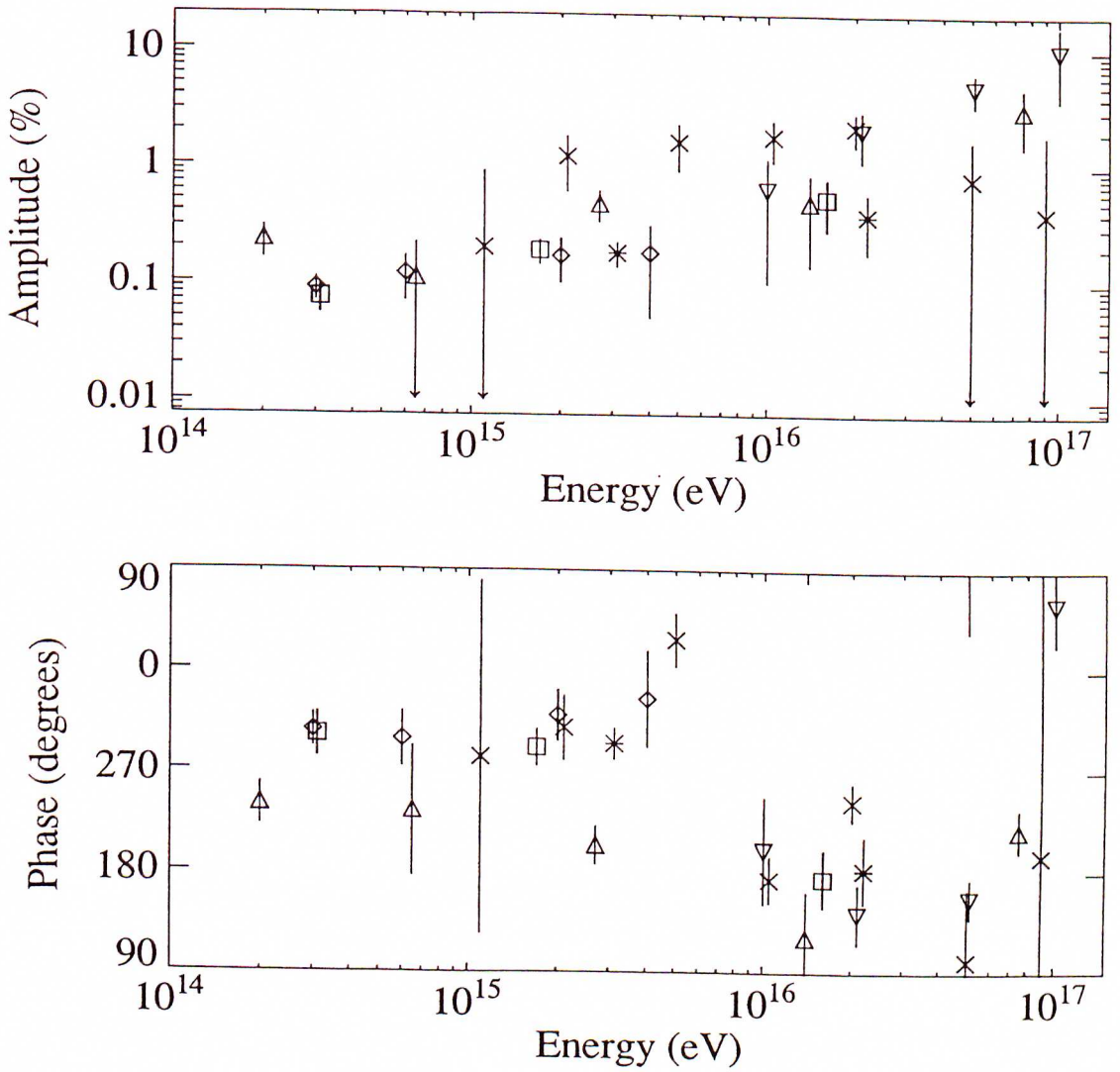

Figure 4.7: A compilation of northern hemisphere medium energy anisotropy measurements (first harmonic amplitude and phase).
(◇) Daudin *et al.* (1956)
(△) Delvaille *et al.* (1962)
(×) Kifune *et al.* (1986b)
(□) Linsley and Watson (1977)
(▽) Cranshaw and Galbraith (1954)
(∗) Lloyd-Evans (1982)

contribution from the southern hemisphere (Farley and Storey 1954, 1957).

Examining the first harmonic data in this energy regime, data below $\sim 10^{15}$eV are in good agreement with the lower energy underground experiments (apart from the recently discovered dip around 10^{14}eV — see 4.5.1) and remain approximately constant with energy in both amplitude and phase. The most prominent feature is the apparent change in both amplitude and phase with energy above $\sim 10^{15}$eV. The amplitude then appears to increase as $\sim E^{\frac{1}{2}}$ up to $\sim 10^{20}$eV. This change in behaviour of the anisotropy occurs at approximately the 'knee' of the energy spectrum (several times 10^{15}eV), and this is believed to be more than coincidental. As a result, any effect responsible for the 'knee' of the energy spectrum (e.g. a change in composition) may also be responsible for the change in behaviour of the observed anisotropy.

Conventionally, the change in both amplitude and phase at around this energy is interpreted as evidence for a galactic origin of these cosmic rays (e.g. see Kiraly *et al.* 1979). Below this energy, the cosmic rays essentially follow the galactic magnetic field lines parallel to the spiral arms of the Galaxy. As particle energy increases, their orbits deviate further and further from the plane, resulting in an increased anisotropy. This explanation has the problem of explaining the observed abruptness of the change in behaviour of the observed anisotropies. Changes in composition are necessary (Kiraly *et al.* 1979), about which little information is currently available.

Following the results of Samorski and Stamm (1983a) in their detection of U.H.E. γ-rays from Cygnus X-3, Wdowczyk and Wolfendale (1983a) suggested that U.H.E. γ-rays may be contributing significantly to the measured anisotropy, resulting in the observed phase change. This suggestion was based upon the fact that at low energies (i.e. $\sim 10^{8}$eV), the ratio of photons to protons (γ/p) is $\sim 10^{-6}$, but they possess different spectral indices ($\simeq -2.2$ and $\simeq -2.6$ respectively), resulting in a predicted (γ/p) ratio of $\sim 10^{-3}$ at 10^{15}eV. However, in order to avoid a γ-ray domination above 10^{17}eV (which is clearly not observed), it was necessary to introduce a sharp cut-off, somewhere below 10^{17}eV, perhaps as a result of photon-photon interactions close to the source. Further investigations into the true γ-ray flux are necessary to determine

the validity of this explanation.

Clay (1984) presents a somewhat alternative view. It is firstly noted that a minimum in intensity will result, using harmonic analysis, in a maximum with phase 180° different from the direction of the minimum. Therefore, if we had a general cosmic ray flow along the spiral arm (parallel to the galactic magnetic field), there would appear a maximum in intensity in the direction of the source arm (viewed in one hemisphere), and a minimum in intensity in the opposite direction (viewed in the opposite hemisphere). In this case, observations in the northern and southern hemispheres should be comparable, one set measuring the inward flow, and the other the outward flow, suggesting there should be significant agreement in phase. This is evident by comparing the observed phases in Figs 4.6 & 4.7.

Clay (1984) suggests the change in phase observed may be reconciled with a change in direction of the flow at energies around $\sim 10^{15}$eV. Below this energy, the particles are of galactic origin, and are streaming outwards along the spiral arms. This results in a maximum in the northern hemisphere (and hence a minimum in the southern hemisphere). Above this energy, the particles may be streaming inwards along the spiral arms, but following the arms less and less as the Larmor radius of their orbits increase, resulting in the observed change of phase. Phase measurements are in agreement with this hypothesis, but the source of the particles above this energy presents problems (in general an extra-galactic source needs to be invoked).

Kifune (1990) suggests that the anisotropy is probably not due to a simple global leakage of cosmic rays from the galactic disc with uniformly distributed cosmic ray sources. Instead, a nearby source, or local effects of particle propagation in the inter-stellar matter near the Solar System may have an important role, resulting in a complicated dependence of the observed anisotropy with energy.

Kifune (1990) also suggests that a change in anisotropy with energy is expected to occur naturally when cosmic rays have several types of production or propagation properties (e.g. the galactic halo and disc component of a closed galaxy model — Peters and Westergaad 1977; the emergence of a component from a local source such

as superbubbles in inter-stellar matter — Streitmatter *et al.* 1985; or superposition of nearby supernova remnants — Dorman *et al.* 1985). Overall, the change of cosmic ray composition varies from model to model, and more detailed information in this area is required.

Overall, measurements of a 'real' anisotropy at medium energies, rather than the upper limits currently observed, as well as detailed compositional information are necessary before a detailed resolution to the above problems is possible.

4.5.3 High Energy Measurements

At the highest energies ($E > 10^{17}$eV), the bulk of the data, apart from the early counting experiments of Cranshaw and Galbraith (1954, 1957) and Cranshaw and Elliot (1956), has been collected using giant air shower arrays, relying on fast timing for directional analysis. Large collecting areas and exposure times are necessary at these energies in order for a significant number of showers to be detected due to the low flux of primary cosmic rays.

Experimentally, the most important contribution has come from Haverah Park (see e.g. Lawrence *et al.* 1990a). The SUGAR array (see e.g. Horton *et al.* 1983) has also provided a significant contribution from the southern hemisphere, and will be considered in the energy regime above 10^{19}eV. Other contributions have been made by the Fly's Eye (see e.g. Cassiday *et al.* 1990a); Akeno (see e.g. Matsubara *et al.* 1990); Yakutsk (see e.g. Efimov *et al.* 1987); and Volcano Ranch (Cunningham *et al.* 1977).

The early counting experiments found no statistically significant sidereal anisotropy (although a significant solar variation was detected) (Cranshaw and Galbraith 1954, 1957; Cranshaw and Elliot 1956). Similarly, the early fast-timing experiments (Clark *et al.* 1961; Delvaille *et al.* 1962; Aguirre 1974) produced statistically insignificant anisotropy results.

Volcano Ranch (Linsley 1975c) produced results which indicated a strongly energy dependent anisotropy above 10^{17}eV from $\sim 3 \times 10^3$ events. This author suggested a time dependence in the sidereal anisotropy to explain the apparent discrepancy with

the previous results. It was also suggested this might explain the observed strong solar variations.

The Haverah Park data ($\sim 10^5$ events) suggests a general trend of an increase in first harmonic amplitude with energy, apart from a dip at $\sim 5 \times 10^{17}$eV, from 1.6% at $\sim 10^{17}$eV to $\sim$ 70% at 3×10^{19}eV. Changes in the phase of the anisotropy first harmonic are apparent at $\sim 2 \times 10^{17}$eV and $\sim 4 \times 10^{18}$eV. Data from the Yakutsk array, Fly's Eye and Akeno support these observations in general. (see Fig 4.8 for a compilation of high energy anisotropy measurements)

Variations in the anisotropy below 10^{19}eV suggest changes in the source and/or propagation distribution. The prevalent view (see e.g. Fichtel and Linsley 1986) is that cosmic rays near 10^{18}eV are predominantly of galactic origin. The Larmor radius of their orbits is comparable to the thickness of the Galaxy's magnetic disc (assuming a negligible halo). As a result, some anisotropy is expected (but not observed). Cassiday *et al.* (1990a) suggest that the observed lack of a large anisotropy may be achieved by cosmic rays from the galactic disc, if they are of a mixed chemical composition, or a composition dominated by iron nuclei. However, it is not yet possible to determine the relative contributions of these effects without definite composition data. In addition, more complete measurements of this anisotropy in the southern hemisphere would also contribute to a resolution of this problem.

Berezinsky and Mikhailov (1985) have suggested that the observed anisotropy in this energy range can be explained in a galactic model, with a regular component of the magnetic field in the galactic halo. Such a component is necessary to contain these high energy particles due to the size of their Larmor radius (exceeding the galactic thickness at around these energies). Extra-galactic models meet serious difficulties in explaining both the observed flux and anisotropy of these cosmic rays.

Above 10^{19}eV, it is necessary to combine data from several arrays due to poor statistics, resulting from the miniscule flux at these energies. Both Wdowczyk and Wolfendale (1989), and Efimov *et al.* (1990) have combined data from several arrays (Haverah Park and Sydney, Haverah Park, Sydney and Yakutsk respectively) with

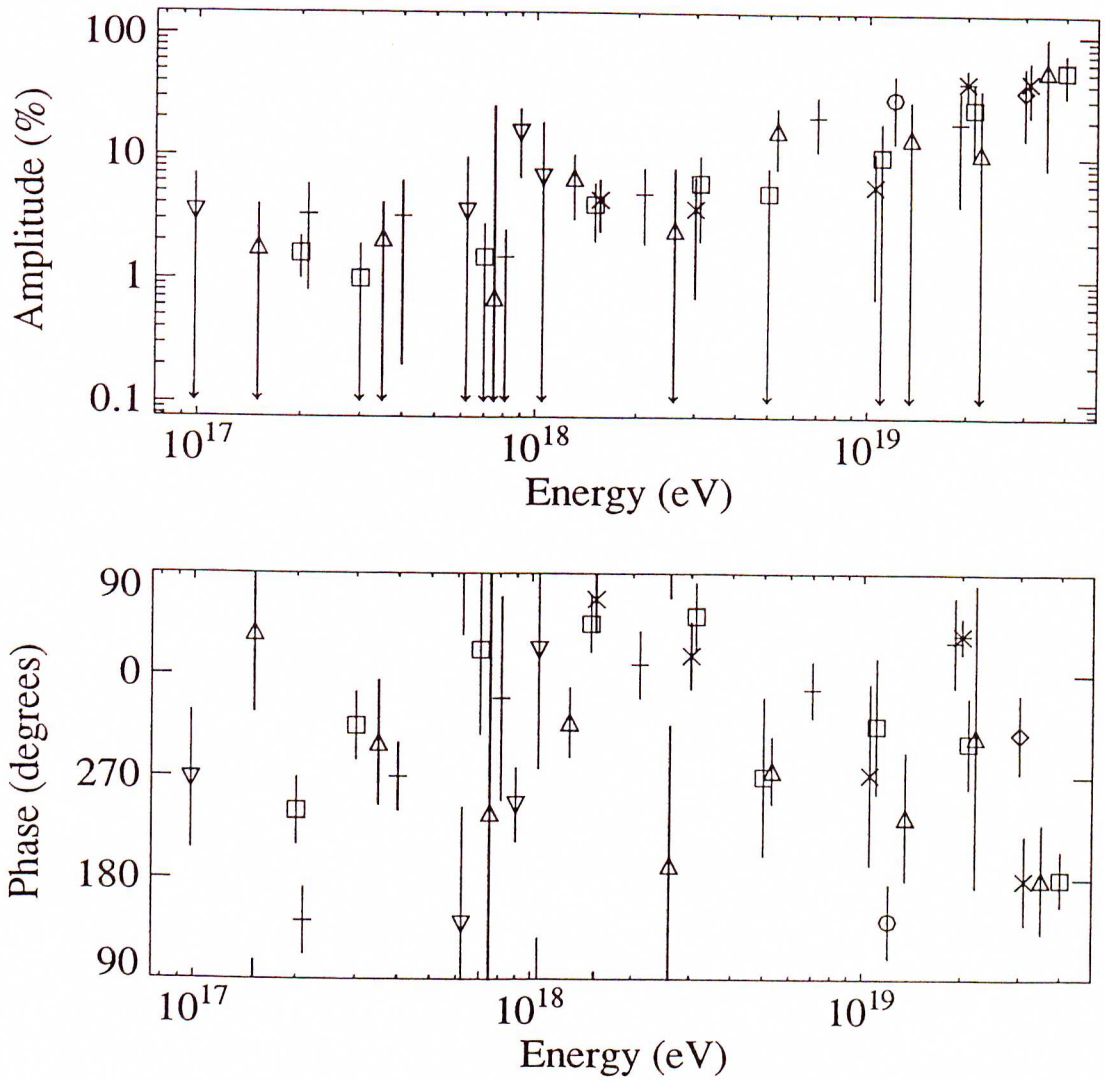

Figure 4.8: A compilation of high energy anisotropy measurements (first harmonic phase and amplitude).
(∗) Efimov *et al.* (1990)
(◇) Matsubara *et al.* (1990)
(△) Cassiday *et al.* (1990b)
(×) Eames *et al.* (1985)
(+) Efimov *et al.* (1987)
(□) Lloyd-Evans (1982)
(▽) Kifune *et al.* (1986b)
(○) Horton *et al.* (1983)

similar results.

Wdowczyk and Wolfendale (1989) suggest their results are consistent with a galactic origin below 10^{19}eV (mostly from the plane), with an abrupt switch to a non-galactic dependence around 10^{19}eV. Efimov *et al.* (1990) suggest that cosmic rays up to $\simeq 2 \times 10^{19}$eV are purely of galactic origin, and the galactic contribution continues up to $\simeq 10^{20}$eV. Furthermore, at $E > 4 \times 10^{19}$eV, they suggest that there is a significant extra-galactic contribution in the direction of the Virgo cluster.

Examining the latitude gradient for these energies (as discussed in 4.3.3) (see Fig 4.9), there appears to be a general increase in intensity of a southern hemisphere excess up to energies $\sim 10^{19}$eV. At $\sim 2 \times 10^{19}$eV, there is an abrupt change to a strong northern hemisphere excess. The disadvantage of these measurements is that the majority were carried out in the northern hemisphere. Wdowczyk and Wolfendale (1984) have argued that extrapolation of the data to large southern galactic latitudes (i.e. $b < -50°$) is invalid as a result, and they suggest that when combined with the sparse southern hemisphere data available, the results support an overall enhancement in the general direction of the galactic plane below $\sim 10^{19}$eV. Above $\sim 2 \times 10^{19}$eV, the observed northern hemisphere enhancement is considered by Wdowczyk and Wolfendale (1984) to be evidence that at least part of the cosmic ray flux at these energies is extra-galactic in origin.

High energy results, in general, are only upper limits, currently restricted by counting statistics. It is entirely possible that the actual anisotropies present may be an order of magnitude (or more) below those figures traditionally accepted. More experimental data is required in order to lower these limits and establish the strength of any 'real' anisotropy present.

4.5.4 Significance of the Results

The statistical significance of both medium and high energy measurements has been examined by Lloyd-Evans (1982), and in more detail by Clay (1987). In a review of the data available to that date, Clay (1987) plotted these compiled results in terms of

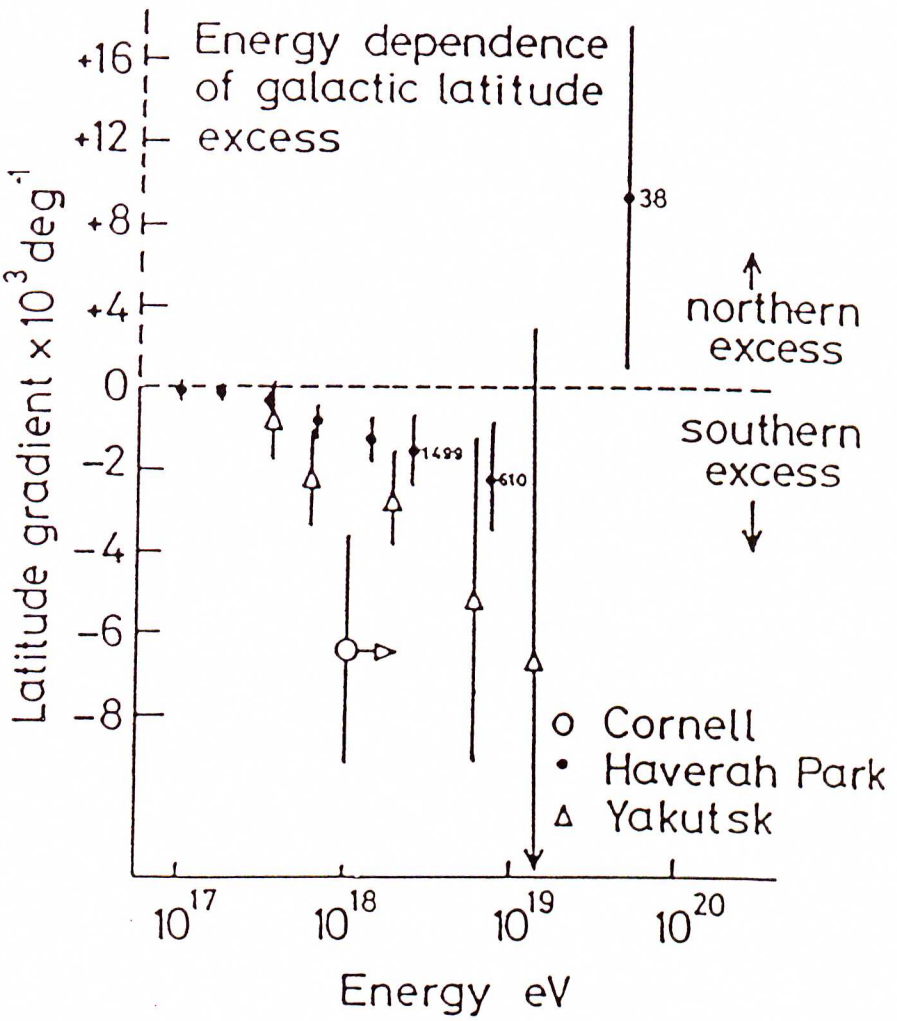

Figure 4.9: Energy Dependence of the Latitude Gradient (after Watson 1984).

their confidence level, as determined by Rayleigh statistics (see 4.3.1) (see Fig 4.10).

Many published results claim high confidence levels for the measurement of a real anisotropy, but the data set provides less convincing evidence when viewed as a whole. Clay (1987) found that whilst there was an excess of results with probability levels of more than 50%, there is no progressive deviation from the general form of random distribution with increasing event number, as would be expected in the presence of a real anisotropy. (i.e. increasing the number of events examined increases the signal to noise ratio). An investigation into the energy dependence of these results was also carried out, with the results that the individual energy ranges considered were also found to be inconsistent. Large anisotropies, measured with a small number of events and assigned a high confidence level ($> 95\%$) did not appear in experiments with higher number of events, as would be expected if there existed any real anisotropy. One such example occurred with the data set of Farley and Storey (1954), who reported a large anisotropy (1.1%) with a very high level of confidence ($> 99.99\%$) at $E \sim 10^{15}$eV. In a subsequent experiment carried out in the same energy range, and involving a larger number of events (Farley and Storey 1957), the reported anisotropy was much lower (0.14%) with a much lower confidence level (45%). Clay (1987) concluded that there exists no convincing evidence for any clear anisotropy amplitude in the data set examined. However, the data set does not exhibit the amplitude distribution expected from a random distribution of events predicted by Rayleigh statistics. It appears there exists a non-random component which, it is suggested (Clay 1987), may result from the incomplete cancellation of residual systematic effects.

In light of this view, the apparent agreement in observed phases (see Figs 4.6, 4.7 & 4.8) is puzzling. Clay (1987) has questioned the confidence limits applied to phases, in view of questionable amplitudes, and suggests that the assumption that a distribution where any possible amplitude and phase is possible is being sampled (Linsley 1975a) is false. If this is the case, then the limits suggested by Linsley (1975a) should be regarded as lower limits to the angular uncertainty.

Phases are represented as cyclic data, with the freedom to shift the data by multiples

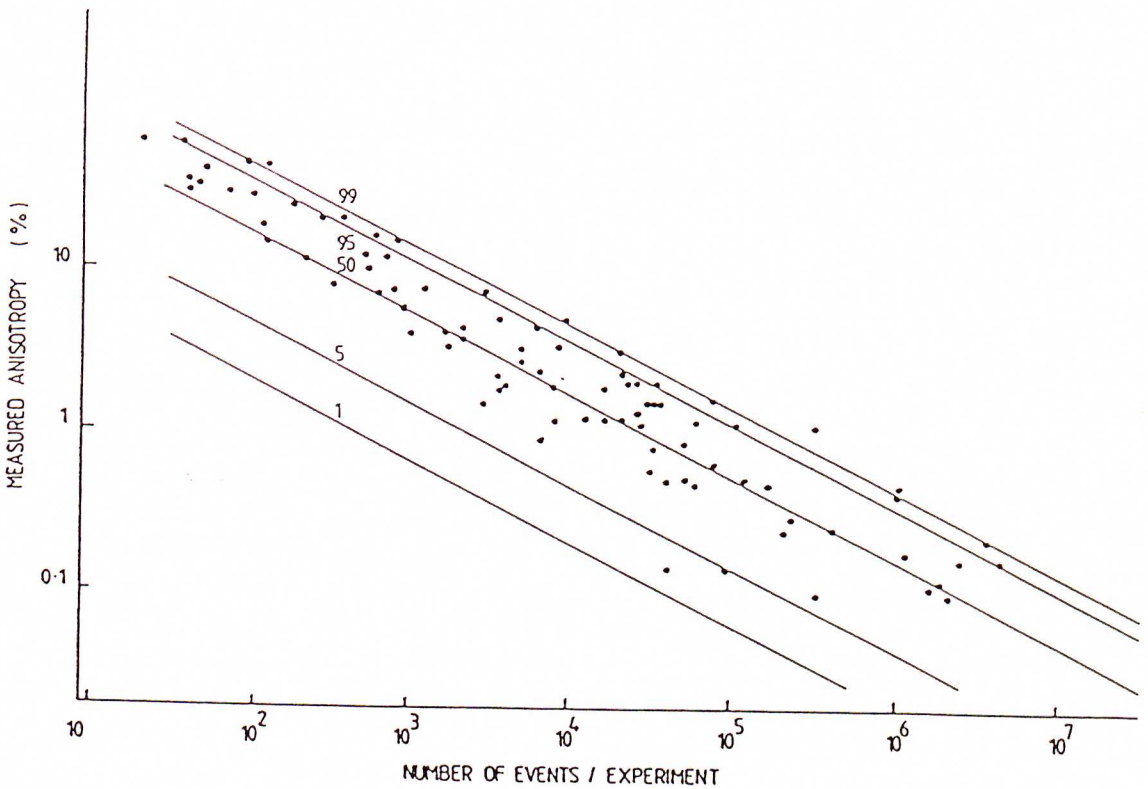

Figure 4.10: Medium and High Energy Anisotropy amplitudes as a function of number of events in the data set. The lines represent confidence levels according to Rayleigh statistics (after Clay 1987).

of 360°, in order to present the data in the most aesthetically pleasing form. Clay (1987), through the use of Monte Carlo simulations, places an 80% confidence level on the observed phase consistency, finding better fits occurred from purely random distributions 20% of the time.

The measured phases may be replotted by adding appropriate multiples of 360° as shown in Fig 4.11. This figure demonstrates only two significant changes in phase, just below 10^{16}eV, and at $\sim 2\times10^{19}$eV (and perhaps the suggestion of another at $E \sim 3 \times 10^{18}$eV). Above this energy, the phase varies fairly uniformly with energy. This suggests that many of the 'wiggles' in the standard form of phase presentation may be meaningless, and result only from the method of presentation. In the light of this discussion, along with the relatively large errors in phase, interpretations of phase changes with energy should be approached with caution.

Apart from these effects, it is also possible that, inherent in the data are experimental effects unique to a particular experiment. These may be a result of different locations, different collecting areas, different triggering conditions, different analysis techniques, different energy sensitivity or sensitivity to different components of the air shower (e.g. muons, electrons, Cerenkov light, etc.). It is even possible that data collected by the same array in different energy ranges may be incompatible (Clay 1987). This suggests that it may be unlikely that a significant anisotropy will be observed and agreed upon by a number of arrays, operating essentially under the same conditions.

The data presented in Chapter 5 will hopefully contribute to a resolution of these problems. Long-term however, both detailed compositional data, and experiments with good long-term stability and lengthy exposure times (an order of 2 or so larger than those currently available) will be necessary if a resolution to these problems is to be successfully attempted.

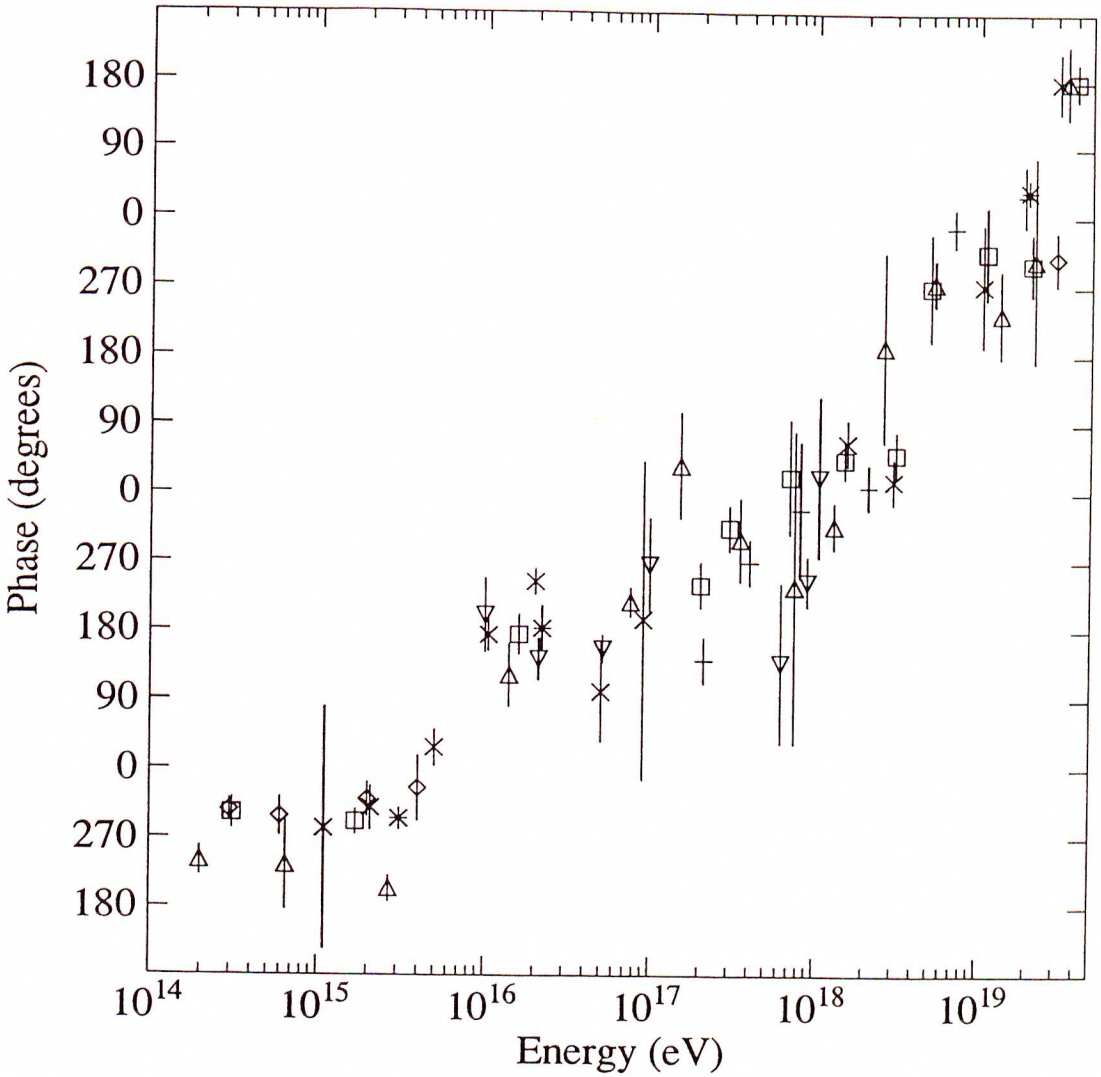

Figure 4.11: An alternative presentation of first harmonic anisotropy phase measurements above 10^{14}eV (See Figs 4.7, 4.8 for references).

Chapter 5

Anisotropy Measurements

5.1 Introduction

Measurements of the primary cosmic ray flux were carried out on the 1984–1989 data set (see 3.3 for the details of data collection and analysis). Estimates of the anisotropy in the data were calculated using an analysis technique described below. In addition, this technique was also applied to an earlier data set (1978–1981), the majority of which (1979–1981) had been previously analysed using the anti-sidereal technique of Farley and Storey (1954, 1957) by Gerhardy (1983).

The most straightforward approach to this analysis is to produce a skymap of the detected events, as a function of declination and right ascension. This is achieved by grouping the data into bins of declination and right ascension. As discussed in 3.4, the 1984–1989 data set needs to be considered in two separate periods, namely

(1) June 1984 – June 1986 (referred to as 1984–1986)

(2) July 1986 – May 1989 (referred to as 1986–1989)

However, before harmonic analysis techniques can be applied to the experimentally determined skymaps, biases introduced into the data need to be taken into account and eliminated where possible.

5.2 Corrections to Data

Effects that may introduce a bias into the skymap resulting in the introduction of coincidental or spurious variations into the data may include on-time effects, equipment failure or error, as well as atmospheric-related effects.

5.2.1 On-Time Effects

Harmonic analysis of a skymap assumes that each regime of the sky has been equally exposed in time. At a given declination, this may be achieved through a uniform and continuous exposure in sidereal time, provided by the rotation of the Earth.

Realistically, this is difficult to achieve experimentally, due to equipment down-times, resulting from tape changes, power failures, or equipment failures. On-time effects could be allowed for by weighting the skymap with respect to the sidereal exposure time. However, the width of the zenith angle distribution (see Fig 3.6) makes the array sensitive to a wide range of right ascensions at any given sidereal time, amounting to several hours (see Fig 5.1). This range is dependent upon both declination and the corresponding zenith angle. Atmospheric attenuation results in a complicated dependence of this non-uniform exposure time.

An alternative method is to consider only those data which comprise a complete and continuous sidereal day of array exposure. Once atmospheric (and other) effects have been allowed for, this guarantees equal exposure to all right ascensions within any declination band observed. The majority of the data files in this set (1984–1989) consisted of 3–4 day runs. It was found that applying this restriction resulted in a loss of approximately 20% of the acceptable events. The resulting loss of statistics was deemed acceptable in light of the effective removal of on-time effects and the associated complications.

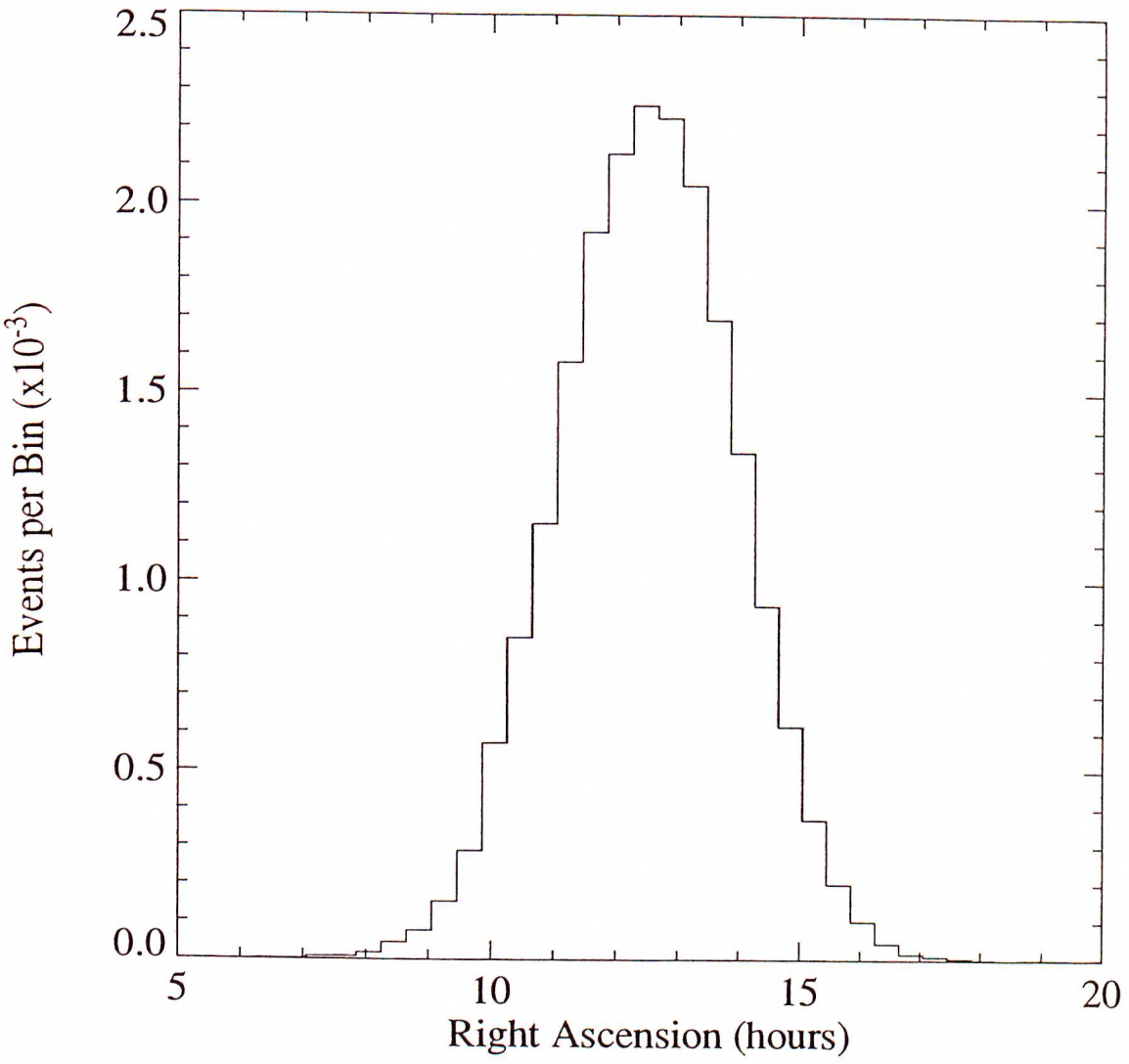

Figure 5.1: The distribution of right ascensions assigned to events recorded between 12.25 and 12.75 hours sidereal time. (Data recorded during 1987)

5.2.2 Data Rejection

In addition to on-time effects, other experimental and analytical effects may also result in an introduced bias in the resultant skymap.

The data were checked for a consistency in the detected and analysed event rate, averaged both hourly and daily. If a discrepancy was observed, usually due to one or more detectors failing, the appropriate data were deleted from the data set. A failed detector may alter the array triggering conditions, resulting in a reduced event rate, and producing an uneven exposure to the sky over that particular sidereal day. Where possible, parts of these data files which were unaffected by the failure were salvaged (usually those data previous to the detector failure). In addition, event time-spacings in excess of five minutes were also used to indicate a bad data run and resulted in the restart of the full sidereal day being analysed.

During the data analysis procedure, estimates of both shower direction, and shower size and age were calculated using minimisation techniques (see 3.3.2). Estimates of goodness-of-fit could then be used to decide if the data fit was sufficiently poor for the rejection of an event. Such limits were chosen resulting in the rejection of additional data ($\sigma < 10, \chi^2 < 6$ for direction and shower size fits respectively — see 3.3.2).

Furthermore, successfully analysed events were only considered if the fitted shower core was found to fall well within the array boundaries ($|x|, |y|, <$ 100m), as those events nearer the extremities of the array suffer from poor sampling statistics, resulting in increased uncertainty in the shower size and core position fits. The derived shower age parameter, s, was constrained to lie within the range $0.55 < s < 1.95$, as ages outside of this range were considered to be poor fits.

The discussed rejection criteria resulted in the rejection of $\sim 22\%$ of the recorded events. The remaining effects that need to be taken into account are either atmospheric or extra-galactic in origin.

5.2.3 Atmospheric Rate Coefficients

The way in which shower development takes place is affected by the medium in which it occurs (i.e. the atmosphere). Therefore, although the primary spectrum of cosmic rays is not affected by atmospheric effects, the resultant E.A.S. are. The probability of detecting such a shower is dependent upon atmospheric conditions. Due to the steepness of the shower size spectrum (see Fig. 3.12), these effects result in a noticeable modulation of the detection rate.

The two atmospheric effects that need to be investigated are those due to barometric pressure and temperature.

The mass of atmosphere vertically above the detector (the absorber contributing to the development and attenuation of E.A.S.) will vary with variations in barometric pressure. For arrays where E.A.S. are detected over a range of zenith angles (such as Buckland Park), this attenuation is complicated by a factor of $\sec\theta$ increase in the mass of the absorber for inclined showers.

This implies that sea-level shower sizes are reduced when barometric pressure increases, and as a result E.A.S. detection probabilities decrease. This results in a decrease in the rate of detection of E.A.S. which may introduce a spurious effect in the search for a sidereal anisotropy in the cosmic ray flux.

The barometric pressure coefficient, b is defined by

$$\frac{dR}{R} = b.dp \tag{5.1}$$

where R is the rate of shower detection and p is the barometric pressure.

Similarly, variations in the lower atmospheric temperature result in changes in the air density. It is this effect which is generally assumed to be the cause of the temperature coefficient, a, defined by

$$\frac{dT}{T} = a.dT \tag{5.2}$$

where T is the atmospheric temperature.

So far, only the effect of the lower atmosphere has been considered. However, atmospheric conditions at the top of the atmosphere are also significant to shower

development lower down, as this is the region where the primary cosmic ray undergoes its first few interactions. This is of most importance to the production of the muon component, and these measurements have been carried out for several decades (e.g. Duperier 1949, 1951; Dutt and Thambyapillai 1965; Lyons 1979). Such a data set was unavailable for the Buckland Park array, so these effects could not be taken into account and will not be discussed further.

For the 1984–1989 data set, atmospheric pressures were recorded every 15 minutes, along with atmospheric and sample detector temperatures, and selected individual detector rates, as well as overall trigger and event rates.

Mean coefficients were calculated from these data using a multiple linear regression fit, with the estimates being

$a = 0.05 \pm 0.1\%\ ^{\circ}C^{-1}$

$b = -0.8 \pm 0.1\%\ \text{mbar}^{-1}$

From these results, it is obvious that the barometric pressure is the dominant atmospheric effect on E.A.S. detection rates. However, it will be shown that an overall solar effect (i.e. a rate variation related to solar time) is also significant (see 5.2.4). It is assumed that this includes an atmospheric temperature effect, which is dependent more upon the occurrence of the maximum and minimum of temperatures rather than the absolute temperature (hence the essentially non-existent absolute temperature coefficient). The two coefficients determined here are in agreement with those measured previously at other arrays (e.g. Cranshaw *et al.* 1958) and at Buckland Park (Gerhardy 1983; Gerhardy and Clay 1983).

To take the pressure effect into account, each event was suitably weighted with the corresponding atmospheric pressure, with respect to the mean atmospheric pressure of 1016 mb (although this reference is somewhat arbitrary). The weighting factor, w_p, was calculated using

$$w_p = 1 + (\text{pressure} - 1016) \times 0.008 \tag{5.3}$$

and it was this weight that was added to the skymap for each event, rather than purely counting the events.

Lloyd-Evans (1982) suggested that a better estimate of the barometric pressure rate coefficient may be determined by examining only the data in which the barometric pressure varies rapidly with time. A suitable subset of data was selected, and a pressure/rate coefficient determined. This new coefficient was found to be identical to that previously determined. Lloyd-Evans (1982) also suggested the possibility of a shower size dependence on this coefficient. Such a dependence was investigated using the Buckland Park data and was found to be statistically insignificant. Consequently, the value of -0.8% mbar^{-1} was used in all subsequent analysis.

In addition to these effects, the detectors themselves may be affected by the prevailing atmospheric conditions. Fig 5.2 shows the variation of temperature and barometric pressure over a period of $\sim$ 10 days, recorded at Buckland Park. The majority of the detectors are thermally insulated, and Fig 5.2 clearly shows the reduction in the amplitude of the temperature fluctuations experienced by the sample detector (C). In addition, the time profile is altered, lagging behind the atmospheric fluctuations. However, they are not completely dampened. If these variations have Fourier components in sidereal time, then spurious variations may be introduced into the event detection rate. The temperature variations of the electronics used for analysis and recording of the data are minimised by airconditioning of the electronics hut, and will be ignored.

5.2.4 Solar-Related Effects

To examine solar-related effects, and those associated with other periods close to the sidereal period of 23 hrs 56 mins (which may have an influence on the estimated sidereal amplitude as a result of Fourier sidebands) detection rates were examined as a function of these periods, in a similar manner to the full sidereal day method discussed in 5.2.1. As an example, annual modulation of the solar period amplitude will result in sidebands at periods ± 4 mins the solar period (i.e. the sidereal and anti-sidereal periods), resulting from the beating of these two frequencies.

The periods examined ranged from 23 hrs 32 mins to 24 hrs 28 mins in 4 minute intervals. Event arrival times were binned into 96 bins representing the corresponding

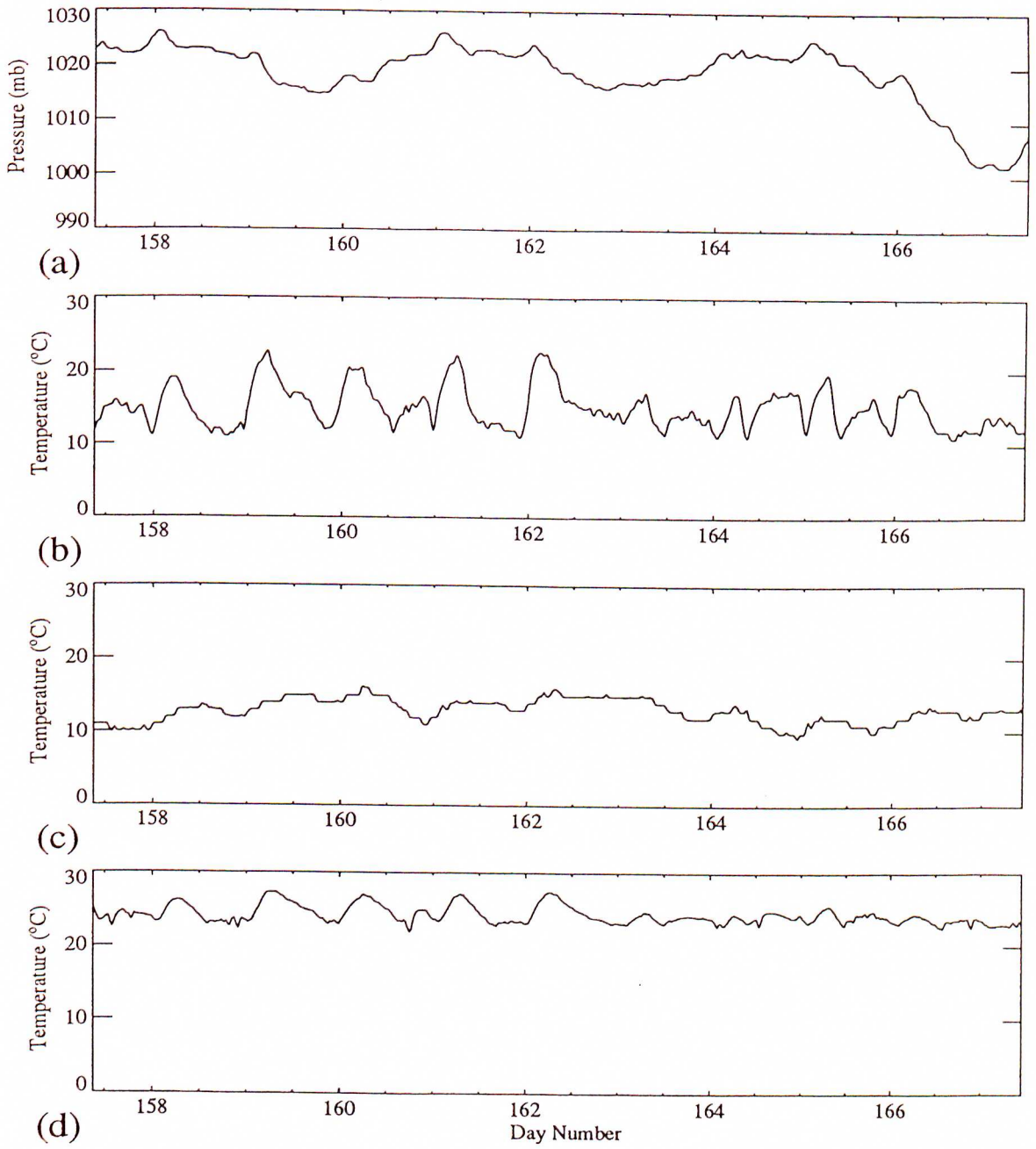

Figure 5.2: Barometric pressure and temperature variations recorded over a 10 day period at Buckland Park.

(a) Barometric Pressure (mb)

(b) Atmospheric Temperature ($°C$)

(c) Detector C Temperature ($°C$)

(d) Electronics Hut Temperature ($°C$)

phase for the period being examined. Phases were chosen to correspond at the September equinox, as each period results in an integral number of cycles per calendar year, but this is arbitrary and the phases (apart from the solar and sidereal phases) have no physical meaning.

Harmonic analysis of these periods produced a distribution of first harmonic amplitudes consistent with noise (see Fig 5.3), apart from the solar period, which produced a significant first (and in the case of the 1986–1989 data, second) harmonic amplitude. Such an effect could quite possibly result in a spurious contribution to the estimate for the sidereal amplitude.

Table 5.1 lists the annual solar period first and second harmonic amplitudes and phases of the event detection rate. The majority of the first harmonic amplitude estimates are highly significant with only one of the second harmonic amplitude estimates being significant, suggesting a dominant diurnal effect which depends upon factors other than the recorded atmospheric temperature.

There is also remarkable agreement of the first harmonic phases within the two data sets (1984–1986, 1986–1989), despite the fact that two of the three years in the 1986–1989 data set show relatively less significant amplitudes.

The shift in phase between the two data sets is puzzling, but may perhaps be reconciled by the addition of the extra timing tubes and resultant change in event analysis acceptance and subsequently in the array characteristics (see 3.4).

To remove the effect of this observed dependence of the event rate with solar time, in compiling the skymaps, each event was weighted with respect to its arrival time (as measured in solar time), using the observed dependence as an estimate for this weighting. In order to maintain the independence of the sidereal and solar frequencies, it was necessary to average this weighting over at least two years of data. The weights employed were the estimates for the 1984–1986, and 1986–1989 maps respectively (see Table 5.1). In this way, a skymap was produced for each period under consideration, which is essentially free from solar period effects.

Table 5.2 lists the total number of events detected during the periods under ques-

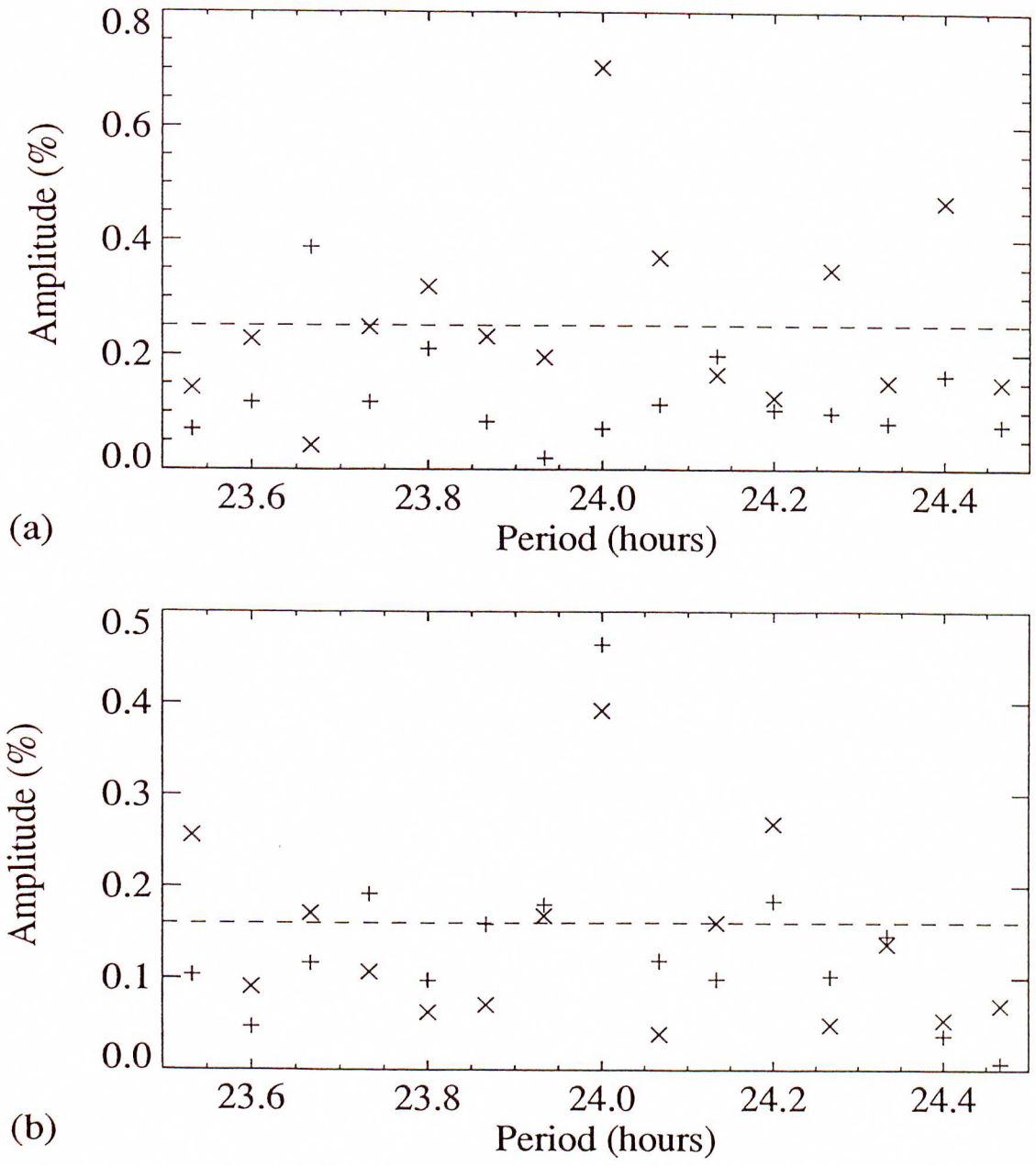

Figure 5.3: First and second harmonic amplitudes of event rate as a function of period from 23.53 to 24.47 hours. ((×) 1st harmonic, (+) 2nd harmonic). (Dashed line indicates RMS noise levels).
(a) 1984–1986 data set
(b) 1986–1989 data set

Period	Number of Events	1^{st} Harmonic			2^{nd} Harmonic		
		Amplitude (%)	Phase (hrs)	Prob[1] (%)	Amplitude (%)	Phase (hrs)	Prob (%)
1984–1985	1.09×10^6	0.75 ± 0.14	18.30 ± 0.69	2×10^{-5}	0.13 ± 0.14	1.55 ± 3.97	62.7
1985–1986	8.38×10^5	0.66 ± 0.16	17.28 ± 0.90	0.01	0.14 ± 0.16	5.77 ± 4.30	67.4
1986–1987	1.04×10^6	0.25 ± 0.14	12.92 ± 2.10	19.1	0.63 ± 0.14	0.22 ± 0.84	3×10^{-3}
1987–1988	7.72×10^5	0.33 ± 0.16	13.96 ± 1.88	12.6	0.41 ± 0.16	2.17 ± 1.49	3.8
1988–1989	6.96×10^5	0.70 ± 0.17	14.57 ± 0.93	0.02	0.34 ± 0.17	11.21 ± 1.88	12.8
1984–1986	1.93×10^6	0.70 ± 0.10	17.89 ± 0.55	5×10^{-9}	0.07 ± 0.10	10.32 ± 5.46	78.3
1986–1989	2.52×10^6	0.39 ± 0.09	13.99 ± 0.87	6×10^{-3}	0.46 ± 0.09	0.52 ± 0.73	3×10^{-4}
1984–1989	4.44×10^6	0.46 ± 0.07	16.28 ± 0.56	6×10^{-9}	0.24 ± 0.07	0.79 ± 1.08	0.19

Table 5.1 : Results of the harmonic analysis on the solar period data (Phases defined with respect to Universal Time).

[1]Here, as well as in Figs 5.5–5.8, and in Tables 5.3, 5.5, 5.7, 5.8, 5.10, 5.11 the probability referred to is that of a random distribution giving rise to a variation with less than or equal to the same amplitude as defined in Eqn 4.13.

	Total Number of Events Recorded	Total Number of Events Considered	Number Of Full Sidereal Days Contributing
1984–1986	3.6×10^6	2.0×10^6	339
1986–1989	4.0×10^6	2.5×10^6	460
Total	7.6×10^6	4.5×10^6	799

Table 5.2 : Total number of events recorded by the Buckland Park E.A.S. Array and the corresponding number of events used in the anisotropy analysis, together with the number of full sidereal days exposure used in the analysis.

tion, together with the number of events used in the final analysis, and the corresponding number of full sidereal days of data used. Fig 5.4 displays graphically the array exposure times, and the corresponding daily event rates used in the calculation of the sidereal skymaps, and in the subsequent estimation of the anisotropy of the primary cosmic ray flux.

5.3 Sidereal Skymap

To construct a sidereal skymap, the recorded events, once suitably analysed, tested and weighted, were binned in terms of both right ascension and declination, based upon the equatorial co-ordinates assigned to the event, calculated from the estimated azimuth and zenith angles, and the arrival time of the event. Bin sizes chosen for the analysis were :

$15'$ for Right Ascension; $5°$ for Declination.

With the exception of high declinations ($|\delta| > 70°$), these ranges are larger than the angular resolution of the array (typically $\sim 3°$). 'Improved' directions, based upon the fitting of a curved shower-front, had been calculated for the purposes of U.H.E. γ-ray astronomy for this data set. However, due to the requirements in calculating such 'improvements' (see 3.3.2), only $\sim 55\%$ of the events had these 'better' directions available. Since only low-order harmonics were to be searched for, the slight improvement in angular resolution (to $< 2°$) was not deemed to be necessary, in view of the significant loss of statistics resulting from such an analysis.

Knowledge of the event arrival direction, in addition to the event arrival time allows a more sophisticated analysis of the cosmic ray anisotropy to be carried out than that possible with the hour-angle approach, in which the event arrival time is converted to an hour-angle and then used in harmonic analysis. Employing hour angles leads to a 'smearing' of the data (see e.g. Fig 5.1). Event arrival directions allow a limited investigation into the declination dependence of the cosmic ray flux intensity, as well as the traditional right ascension dependence.

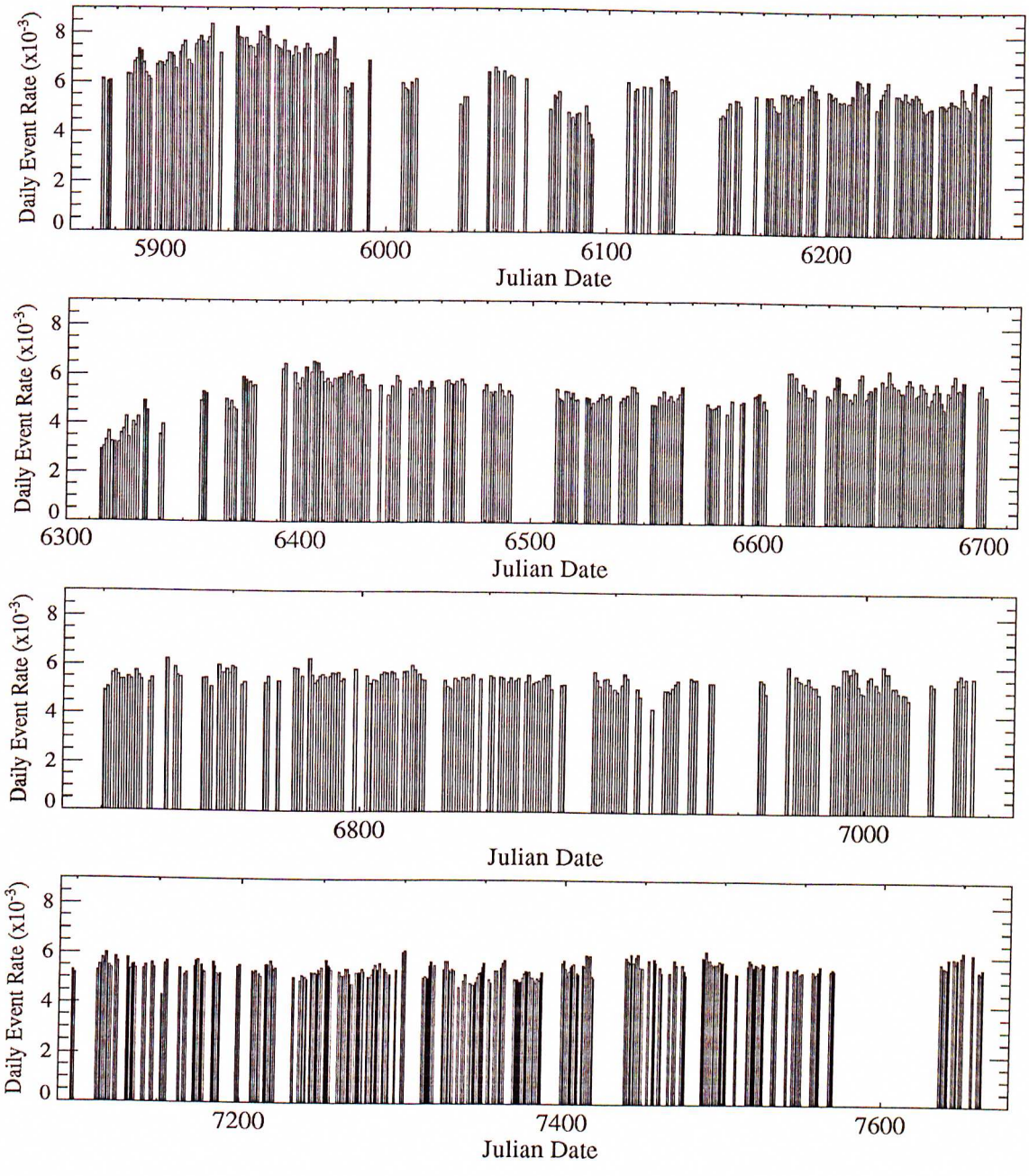

Figure 5.4: Array exposure in Full Sidereal Days for the 1984–1989 data sets, and the corresponding analysed event rate (Julian Dates quoted are 244 xxxx).

Harmonic analysis was carried out on the two skymaps produced (1984–1986, 1986–1989), initially ignoring any declination or shower size dependence. Estimates for the first and second harmonic amplitudes and phases of the overall right ascension distribution, along with the appropriate statistical errors (as defined in 4.3.1) were calculated, and appear in Table 5.3.

The relatively high significances (< 10% random probability) of the first harmonic amplitudes for the first three years under examination, and the inconsistent phases required further investigation, as it was suspected that the solar effect may not have been correctly eliminated.

Six-monthly sidereal first harmonic amplitudes and phases for the overall data were calculated and appear in Fig 5.5. The presence of a remaining solar effect would manifest itself as an approximately twelve hour difference in the phase between adjacent six-monthly periods. The 'see-sawing' effect apparent in Fig 5.5(c) is an indication of such an effect. It was then decided to examine this effect as a function of shower size. Six shower size bins had been selected, *a priori*, in order to investigate the dependence of the anisotropy on shower size (and hence primary particle energy), and these are defined in Table 5.4 (the conversion of shower size to primary energy will be discussed in 5.4.1). The results of this investigation appear in Fig 5.6 and from these diagrams it is clear that several of the size bins (and in particular, bin 4), have a significant solar component present which may be interfering with the sidereal harmonic investigation.

It was then decided to return to the solar skymap for further investigation, as the averaged overall weighting applied appeared to be inadequate in eliminating this diurnal effect from these data.

5.3.1 Solar Effect Revisited

The first harmonic of the solar skymap was examined on a calendar month basis, and the results of the overall analysis appear in Fig 5.7. Several months over the five year period being examined display highly significant amplitudes with phases around 14 hours U.T., which were found not to be the result of an isolated day's bad data but to

Period	Number of Events	1^{st} Harmonic			2^{nd} Harmonic			Statistical Errors			
		s_1 (%)	θ_1 (hrs)	P_1 (%)	s_2 (%)	θ_2 (hrs)	P_2 (%)	σ_{rms} (%)	σ_r (%)	σ_{θ_1} (hrs)	σ_{θ_2} (hrs)
1984–1985	1.10×10^6	0.27	9.23	7.9	0.085	3.82	82.0	0.19	0.14	1.70	6.08
1985–1986	8.40×10^5	0.32	12.75	6.9	0.065	4.14	91.4	0.22	0.15	1.65	9.00
1986–1987	1.05×10^6	0.28	0.51	8.0	0.24	6.48	13.5	0.20	0.14	1.70	1.91
1987–1988	7.91×10^5	0.18	1.76	53.7	0.20	6.38	45.8	0.23	0.16	3.42	3.06
1988–1989	7.00×10^5	0.22	10.54	41.7	0.38	8.45	5.2	0.24	0.17	2.89	1.57
1984–1986	1.94×10^6	0.27	10.88	1.6	0.02	3.36	98.1	0.15	0.10	1.33	19.38
1986–1989	2.54×10^6	0.10	1.90	31.1	0.14	7.88	19.1	0.13	0.089	2.50	2.10
1984–1989	4.48×10^6	0.091	8.43	39.7	0.089	8.22	41.6	0.094	0.067	2.81	2.88

Table 5.3 : Results of the harmonic analysis on the overall data sets ignoring any shower size or declination dependence.

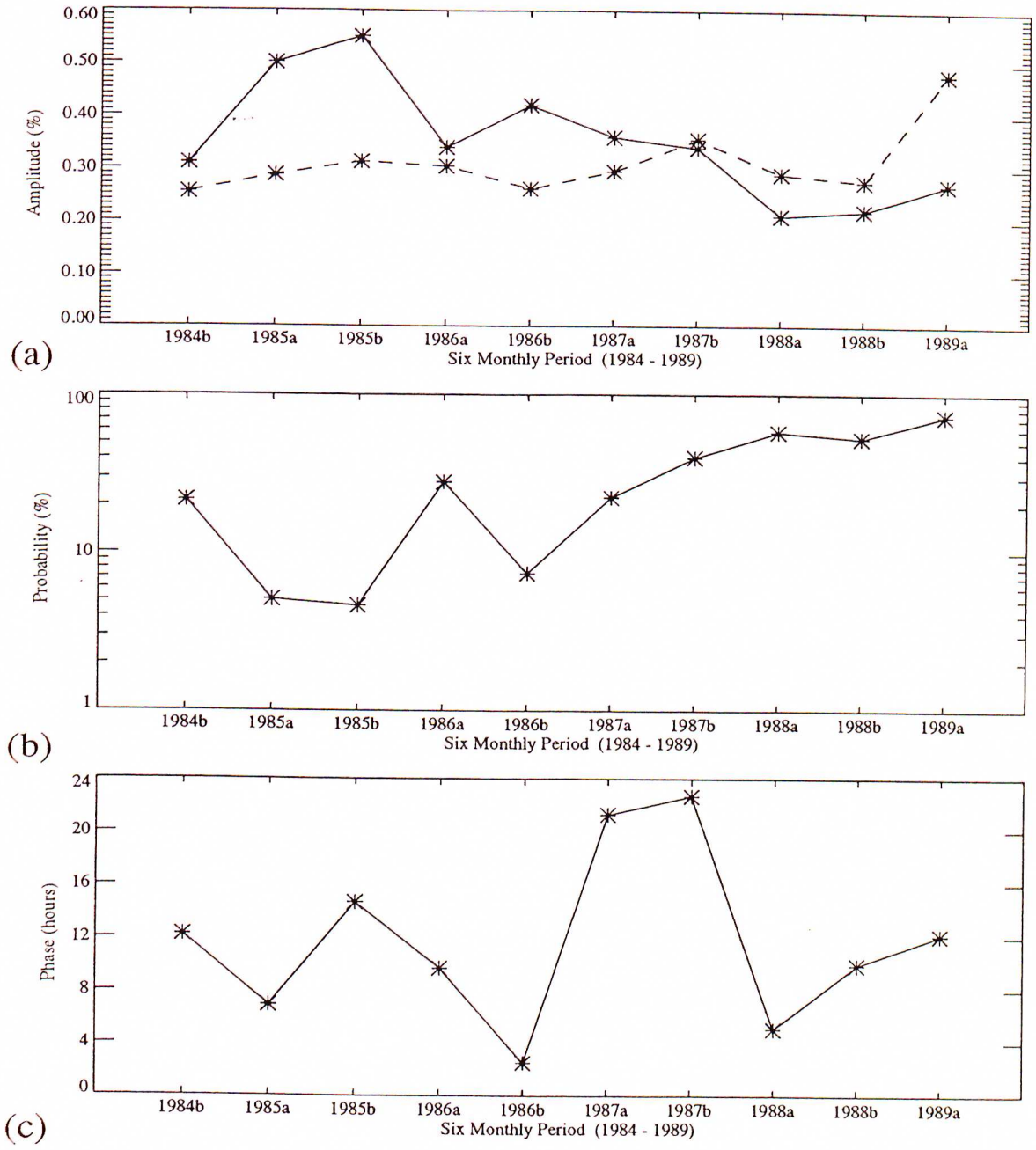

Figure 5.5: The first harmonics of the sidereal component in 6 monthly intervals for the overall data set (1984–1989).

(a) First Harmonic Amplitude (dashed line indicates the RMS noise level).

(b) First Harmonic Amplitude Probability.

(c) First Harmonic Phase.

Label	Shower Size (particles)	Mean Shower Size	Mean Energy (eV)	Number of Events	
				Total	Contributing
1	$< 10^4$	6.6×10^3	3.2×10^{14}	6.62×10^5	4.26×10^5
2	$10^4 - 3 \times 10^4$	1.97×10^4	1.0×10^{15}	2.12×10^6	1.37×10^6
3	$3 \times 10^4 - 10^5$	5.68×10^4	1.6×10^{15}	2.39×10^6	1.54×10^6
4	$10^5 - 10^6$	2.32×10^5	5.0×10^{15}	1.60×10^6	1.04×10^6
5	$10^6 - 10^7$	1.62×10^6	2.0×10^{16}	1.05×10^5	6.86×10^4
6	$> 10^7$	1.47×10^7	1.1×10^{17}	1.32×10^3	8.53×10^2
Total Number of Events				6.87×10^6	4.44×10^6

Table 5.4 : The shower size ranges considered in the analysis of the 1984–1989 data set and the corresponding mean shower sizes and primary particle energies, together with both the total number of recorded events, and the total number of events contributing to the skymaps.

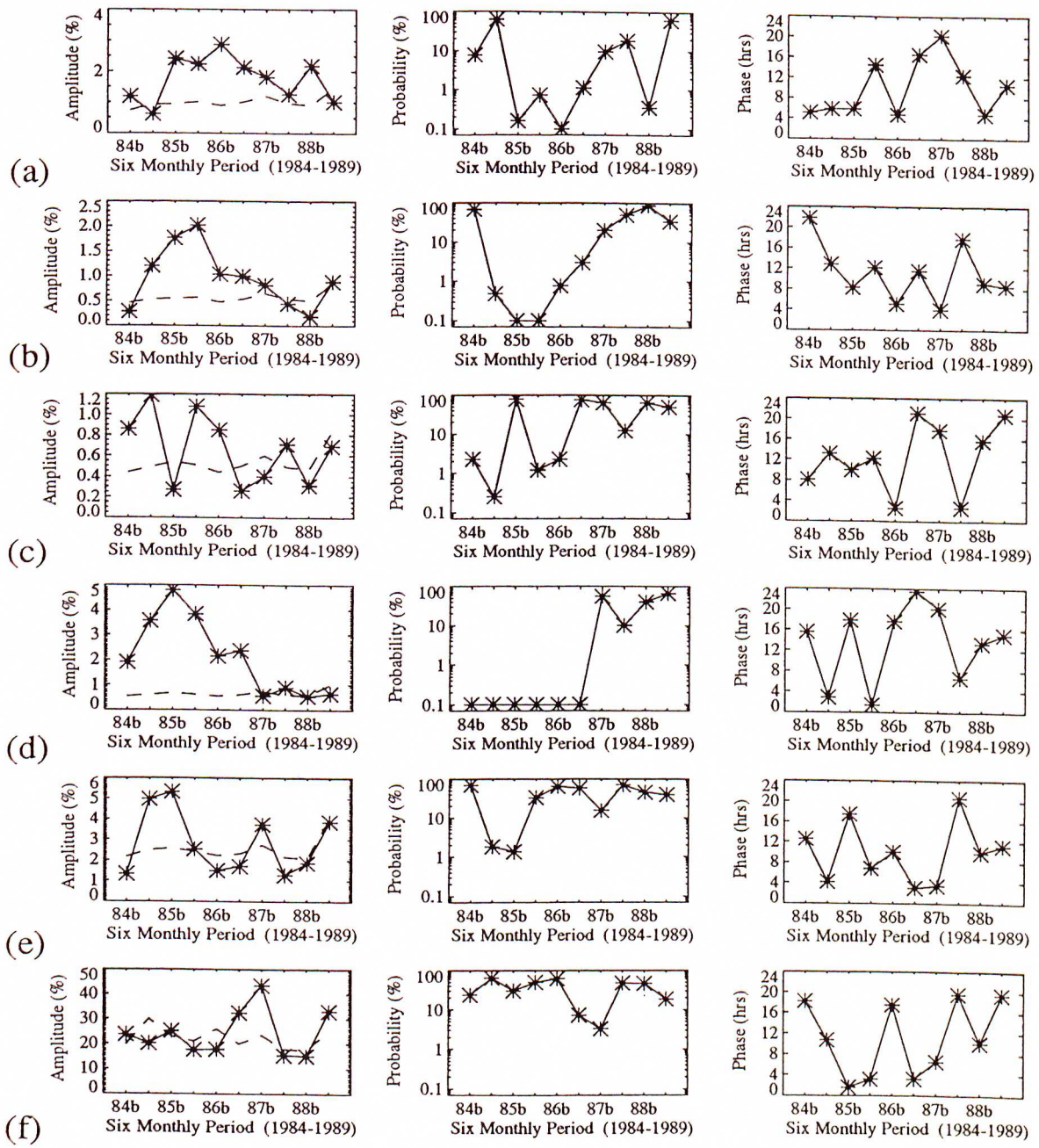

Figure 5.6: The first harmonics of the sidereal anisotropy, averaged in six monthly intervals for the entire data set (1984–1989) in terms of each of the shower size (primary energy) bins considered. The three graphs for each bin are in the same format as used in Fig 5.5.

(a) Size Bin 1 (3×10^{14}eV).
(b) Size Bin 2 (10^{15}eV).
(c) Size Bin 3 (1.5×10^{15}eV).
(d) Size Bin 4 (5×10^{15}eV).
(e) Size Bin 5 (2×10^{16}eV).
(f) Size Bin 6 (1.1×10^{17}eV).

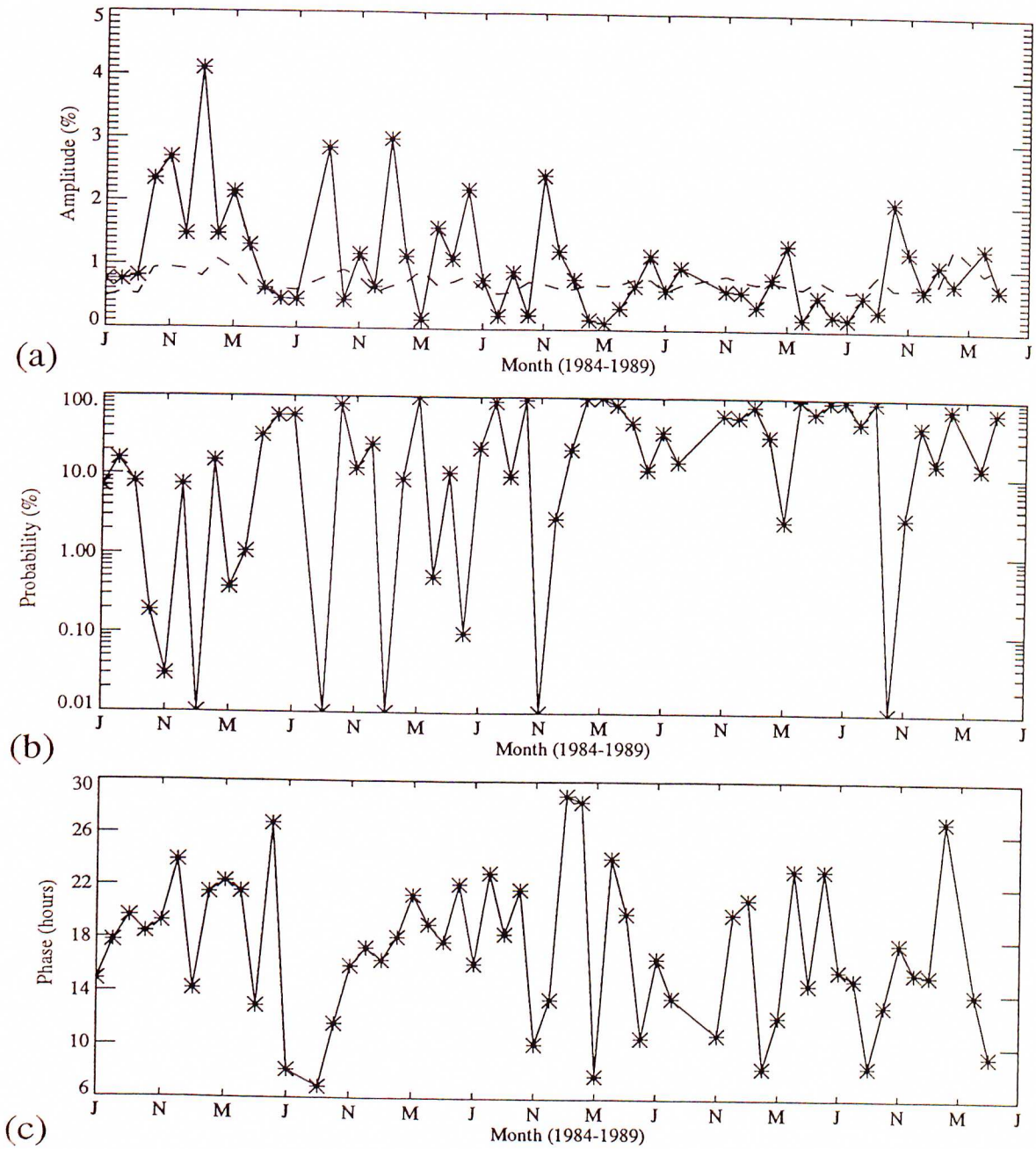

Figure 5.7: The monthly first harmonics of the solar componentof the cosmic ray flux for the overall data set (1984–1989). (The months indicated are July, November and March).

(a) First Harmonic Amplitude (dashed line indicates the RMS noise level).

(b) First Harmonic Amplitude Probability.

(c) First Harmonic Phase (in the range 6 to 30 hours).

be reasonably consistent over the entire month. Carrying out this monthly analysis on a shower size basis however, is more informative, and the results of this investigation appear in Fig 5.8.

There appears to be a significant enhancement in the solar period first harmonic amplitude in the first four size bins, during the 'summer' months (mostly between November and March), in the first three years of the data, after which the effect essentially vanishes. It is possible that this may be either a temperature-related effect, or a light-leak effect which was not apparent when the array event rates were examined. The cause of this effect and its subsequent demise were not determined despite an extensive investigation into the happenings at Buckland Park during the period in question (1984–1987)[1].

Most significantly, the first three size bins examined show a consistent phase of the peak during these months at $\sim$ 18 hours U.T. ($\sim$ 4 a.m. local time), whereas bin 4 ($10^5 < N_e < 10^6$) shows a consistent phase of peak during these months at $\sim$ 6 hours U.T. ($\sim$ 4 p.m. local time). This difference may result from the fact that the smaller showers rely mostly upon the 'inner' detectors of the 'old' array for detection, whereas bin 4 showers rely on the more distant detectors, indicating some fundamental differences in the array properties not previously determined.

These differing phases, and corresponding wildly varying amplitudes resulted in the failure of the averaged overall solar weighting in removing the observed diurnal effect from the sidereal skymap. As a result of this analysis, it was decided that only a restricted portion of these data would be acceptable for use in producing unbiased skymaps to be used for harmonic analysis, as listed in Table 5.5.

The size-independent (overall) skymap used in subsequent analyses appears in Figs 5.9–5.11. Fig 5.9 presents the raw data for the sidereal skymap with reduced resolution in right ascension in order to allow the map to fit legibly onto one page. Fig 5.10 displays the raw skymap data in three dimensional form as a function of equatorial

[1]It is this 'effect' which is believed to be largely responsible for the non-uniformity observed in the event time-spacing distribution of the 1984–1986 analysed data (see 3.4.3; Fig 3.16(a)).

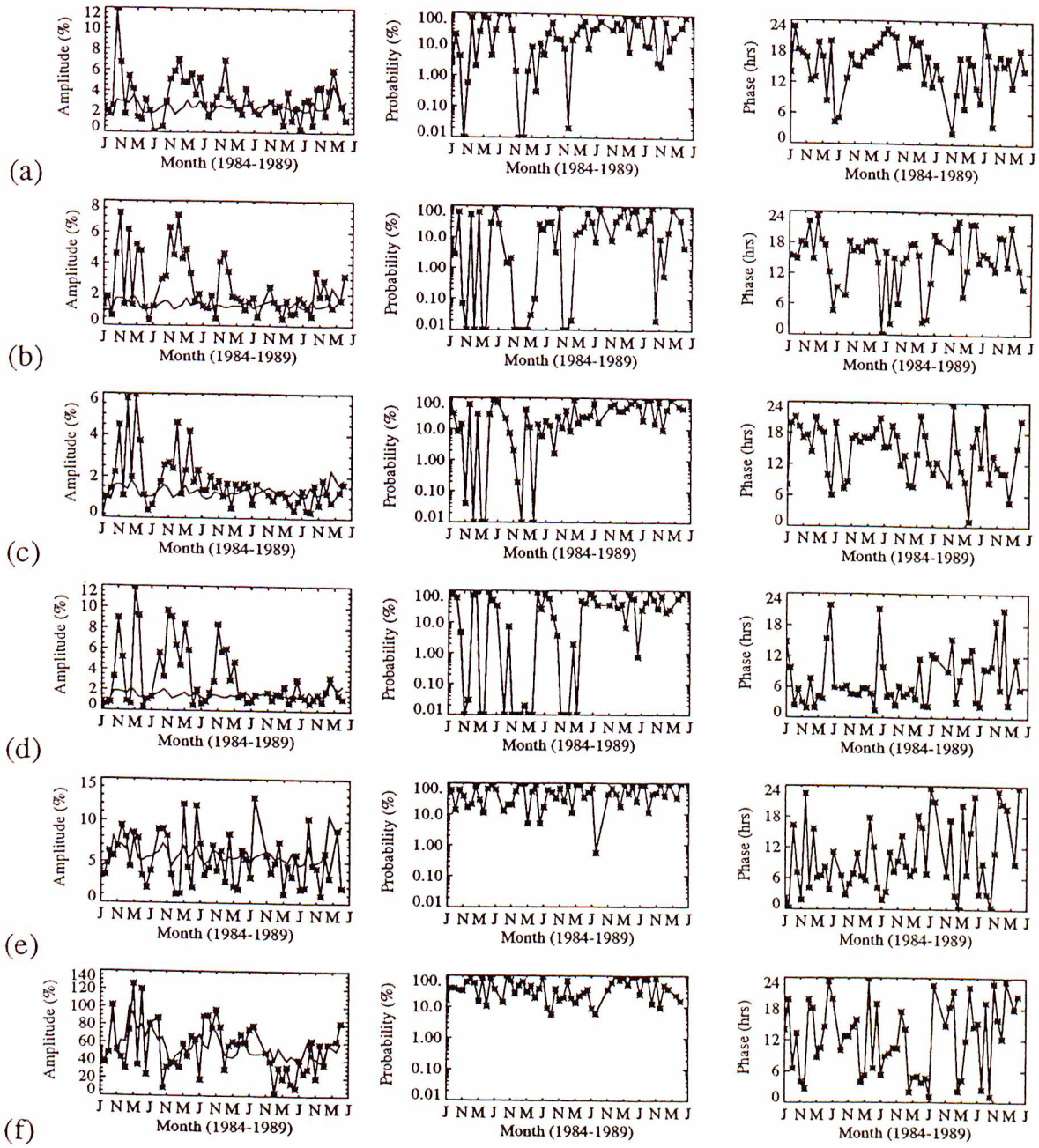

Figure 5.8: The first harmonics of the solar component month by month for the entire data set (1984–1989) in terms of each of the shower size (primary energy) bins considered. The three graphs for each bin are in the same format as used in Fig 5.7.

(a) Size Bin 1 (3×10^{14}eV).
(b) Size Bin 2 (10^{15}eV).
(c) Size Bin 3 (1.5×10^{15}eV).
(d) Size Bin 4 (5×10^{15}eV).
(e) Size Bin 5 (2×10^{16}eV).
(f) Size Bin 6 (1.1×10^{17}eV).

0	0	0	0	1	0	0	0	0	0	0	0	0	0	0	0	0	0	3	0	0	0	0
0	0	1	0	1	1	1	0	0	2	3	1	0	0	0	3	0	0	0	0	0	0	0	2
0	0	1	2	3	2	0	0	0	2	1	3	2	1	2	0	0	1	4	0	1	0	1	3
3	5	1	1	3	1	1	1	0	1	0	3	2	4	1	1	1	1	2	3	2	1	4	2
4	2	2	2	0	3	3	1	4	2	1	3	4	3	4	9	5	1	4	1	2	2	2	4
7	4	5	5	5	7	8	4	3	2	4	3	9	3	4	5	11	0	1	6	8	2	6	4
26	18	17	22	16	14	8	19	21	13	22	13	16	13	22	25	18	20	19	13	13	22	21	20
60	70	83	71	68	69	57	82	65	65	76	53	49	72	53	79	72	76	56	63	53	60	70	72
185	218	181	186	188	202	193	203	194	196	203	186	218	206	220	210	221	200	196	217	197	211	200	192
477	507	453	506	516	526	515	482	492	513	498	471	500	504	493	462	453	479	513	455	475	489	557	483
955	1023	947	973	1015	963	955	962	1030	1028	916	994	933	929	929	956	949	932	962	1029	986	975	1033	1006
1678	1677	1712	1641	1702	1684	1658	1618	1618	1683	1642	1661	1690	1655	1666	1677	1660	1688	1727	1696	1620	1599	1636	1660
2347	2532	2459	2547	2463	2351	2487	2476	2508	2449	2444	2506	2483	2448	2480	2578	2469	2516	2451	2402	2459	2505	2534	2489
3303	3291	3254	3335	3254	3346	3351	3271	3399	3323	3290	3437	3286	3335	3305	3351	3222	3191	3312	3359	3487	3339	3293	3263
3988	3949	4056	3933	4042	4079	4043	4032	4162	4063	3962	4042	4207	3972	4123	3969	4109	4107	4123	4051	4005	4036	4194	4200
4525	4582	4611	4613	4573	4771	4538	4675	4634	4616	4571	4638	4681	4600	4478	4599	4531	4503	4655	4510	4539	4598	4555	4669
4736	4660	4789	4703	4663	4668	4695	4773	4708	4621	4749	4531	4799	4656	4840	4716	4770	4809	4760	4828	4747	4748	4709	4753
4431	4564	4645	4642	4637	4468	4538	4534	4546	4513	4622	4637	4594	4430	4598	4552	4624	4553	4517	4619	4510	4519	4487	4556
3986	4071	4051	4087	3982	3998	4119	4110	4046	4130	4152	4095	4025	4154	3980	4044	3961	3995	4031	4094	4080	3975	4125	4145
3330	3318	3403	3353	3352	3361	3317	3389	3223	3384	3312	3322	3441	3336	3341	3443	3338	3333	3365	3439	3416	3275	3285	3371
2583	2585	2556	2549	2510	2573	2465	2462	2562	2532	2465	2532	2526	2600	2549	2449	2458	2453	2474	2515	2499	2464	2520	2524
1731	1684	1675	1712	1752	1780	1707	1736	1681	1644	1754	1719	1662	1698	1718	1692	1662	1750	1706	1714	1710	1717	1745	1660
1030	1035	1051	1024	1014	1046	987	1019	1055	1076	1076	1030	1028	993	1069	1047	1084	1005	1037	1036	986	1017	1025	1029
527	526	492	534	524	499	526	573	558	491	542	535	543	560	507	535	542	551	518	535	592	573	534	512
230	252	285	247	219	268	245	251	241	260	227	237	240	241	252	243	267	263	255	223	255	264	241	217
93	103	85	78	93	84	84	96	104	80	95	68	96	88	84	88	92	87	91	76	95	103	75	68
14	17	19	29	19	28	20	26	27	20	22	22	31	35	17	20	23	22	20	35	30	28	25	19
2	2	4	5	4	4	3	3	4	3	7	3	0	6	5	6	4	1	3	3	6	5	5	4

Figure 5.9: The raw data for the overall skymap in celestial coordinates. Right Ascension is in hourly bins starting at 0 hours across the page, and Declination is in 5 degree bins starting at $-90°$ going up the page.

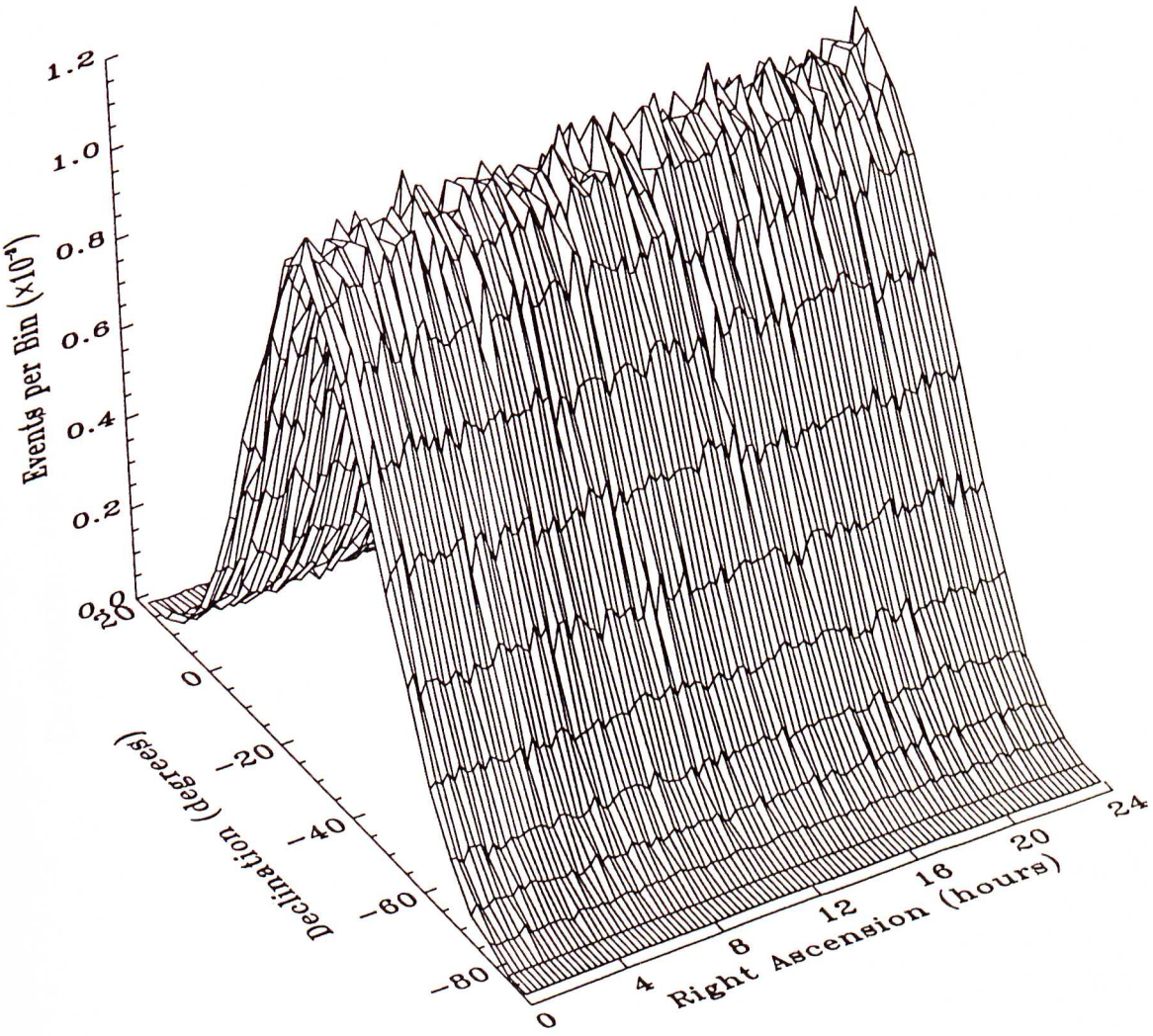

Figure 5.10: Raw Data for the Overall Skymap in 3-D.

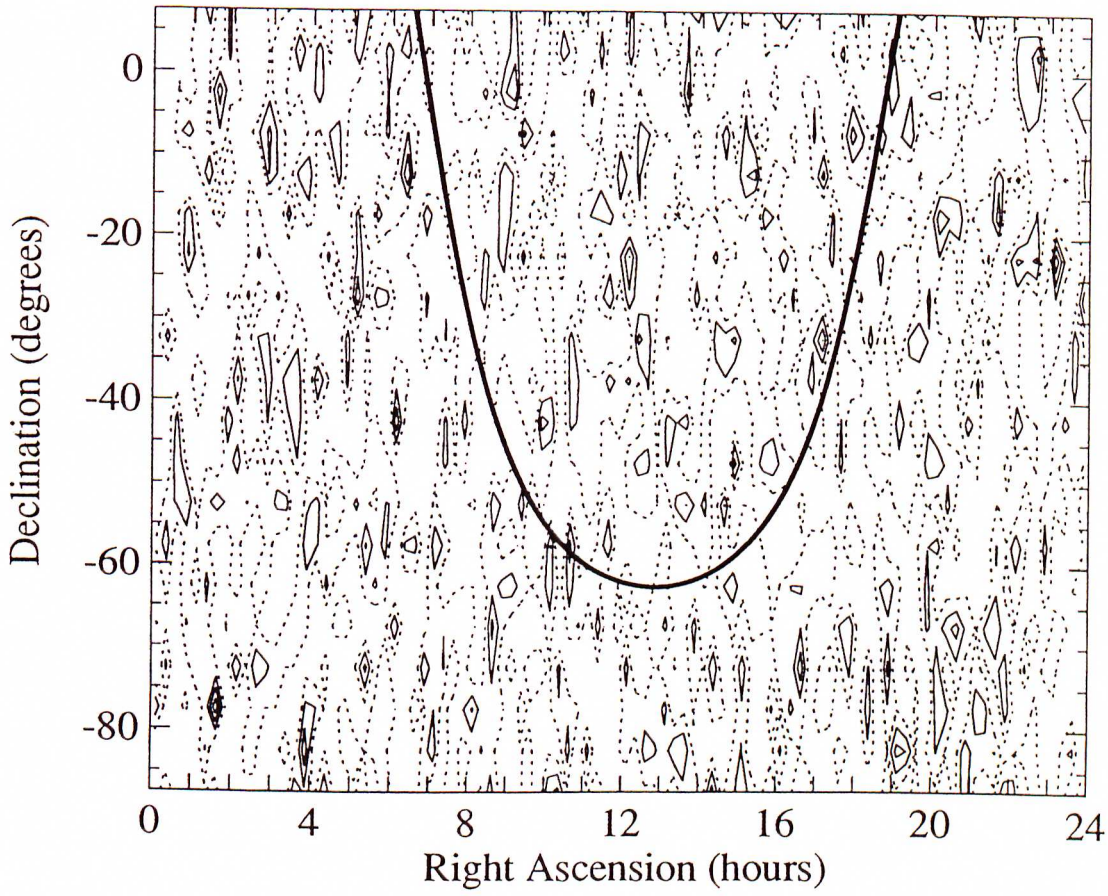

Figure 5.11: Weighted Skymap of the overall results. Contours are in 1 sigma intervals with 0 indicated by the dashed lines. The Galactic Plane has been superimposed (solid line).

co-ordinates. The major feature of this diagram is the shape of the array declination exposure distribution. Due to this uneven exposure as a function of declination, interpretation of this map is difficult. A more useful presentation of the skymap data is shown in Fig 5.11. Here, the number of events recorded in each cell of the skymap have been presented in terms of the deviation from the expected number of events. This expected number of events was calculated by averaging the number of events for each cell in the corresponding declination band. The deviation (Δ) is then expressed in terms of standard deviations (σ) from this mean, based upon Poisson statistics (see e.g. Bevington 1969), namely

$$\Delta = \frac{N_{obs} - N_{exp}}{\sqrt{N_{exp}}} \tag{5.4}$$

Such a presentation is useful in searching for regions of enhancements in the event detection rate in equatorial co-ordinates, possibly due to astrophysical sources emitting U.H.E. γ-rays or neutral particles, which would be unaffected by the galactic magnetic field and hence travel in a straight line.

No significant enhancements (e.g. $> 3\sigma$) are evident in this skymap. In addition, the galactic plane has been superimposed upon this skymap. There appears to be no overall correlation of the contours of this map with the galactic plane. Further considerations of the relationship of the primary cosmic ray flux with the galactic plane (and galactic co-ordinates in general) will be discussed in 5.5.

5.4 Harmonic Analysis

As a first step in the anisotropy analysis procedure, declination and shower size dependence were ignored, and estimates for the first and second harmonic amplitudes and phases of the overall right ascension distribution were calculated (see Table 5.5).

The 0.067% first harmonic amplitude estimate for the overall data set has a 90% random probability assigned to it (based upon Rayleigh statistics). Examining these data on a yearly basis, the distributions of the first and second harmonic amplitudes and phases are consistent with a random distribution of samples at the statistical level

Period	Primary Energy (eV)	Number of Events	1^{st} Harmonic			2^{nd} Harmonic			Statistical Errors			
			s_1 (%)	θ_1 (hrs)	P_1 (%)	s_2 (%)	θ_2 (hrs)	P_2 (%)	σ_{rms} (%)	σ_r (%)	σ_{θ_1} (hrs)	σ_{θ_2} (hrs)
1987–1989	All	9.78×10^5	0.067	10.5	90	0.096	9.4	80	0.20	0.14	8.2	2.8
1986–1989	3.2×10^{14}	1.97×10^5	0.26	7.6	72	0.77	8.7	3	0.45	0.32	4.7	0.8
1987–1989	1.0×10^{15}	2.39×10^5	0.25	3.1	69	0.35	3.4	29	0.41	0.29	4.4	1.2
1987–1989	1.6×10^{15}	5.16×10^5	0.23	23.0	52	0.15	10.9	74	0.28	0.20	3.3	2.5
1987–1989	5.0×10^{15}	3.13×10^5	0.17	17.6	80	0.28	9.6	55	0.36	0.25	5.8	1.7
1984–1989	2.0×10^{16}	6.80×10^4	0.47	8.4	69	0.44	2.7	72	0.77	0.54	4.4	2.4
1984–1989	1.1×10^{17}	8.68×10^2	4.48	1.6	65	2.06	3.5	91	6.79	4.80	4.1	4.5

Table 5.5 : Summary of the results of the harmonic analysis on the 1984–1989 data set, including primary energy dependence.

being considered ($\sim 5 \times 10^5$ events per year).

It is concluded that there is no evidence for an anisotropy in the overall right ascension distribution of events detected at Buckland Park, independent of shower size and declination, with a corresponding upper limit of 0.4% (at the 95% (2σ) confidence level).

5.4.1 Shower Size (Energy) Dependence

There is no strong basis theoretically for the independence of the primary cosmic ray flux anisotropy with energy. On the contrary, there is sufficient evidence that such an energy-dependence exists, both theoretically and experimentally (see Chapter 4 for a detailed discussion), to warrant an investigation.

To allow an investigation into the shower size (and hence primary energy) dependence of the anisotropy estimates calculated, the data were divided, *a priori*, into shower size bins as listed in Table 5.4. As a rough guide, a conversion factor of 10^{10}eV per particle has been suggested (Allan 1971) in converting sea-level shower sizes to primary particle energies. However, for the conversion of the mean shower size to a mean primary energy for each of the size intervals chosen, a more detailed approach was followed, as discussed below.

The calculation of the factor used in converting the mean sea-level shower size to a mean primary particle energy relies on the knowledge of the mean depth of shower maximum as a function of primary particle energy. Such a calculation has been carried out by Protheroe and Patterson (1984) for various compositions and their results have been applied to this analysis. Past this maximum, the shower size (electromagnetic component) is attenuated, predominantly by ionisation, with an experimentally determined, size-dependent attenuation length of ~ 200 gcm^{-2} (see e.g. Ashton *et al.* 1975; Bird and Clay 1990b).

Combining these results, and assuming a predominantly (90%) proton composition of the primary cosmic ray flux in the energy range 3×10^{14}eV – 10^{17}eV, a calibration curve was calculated (see Fig 5.12). Using this curve, it was possible to estimate the

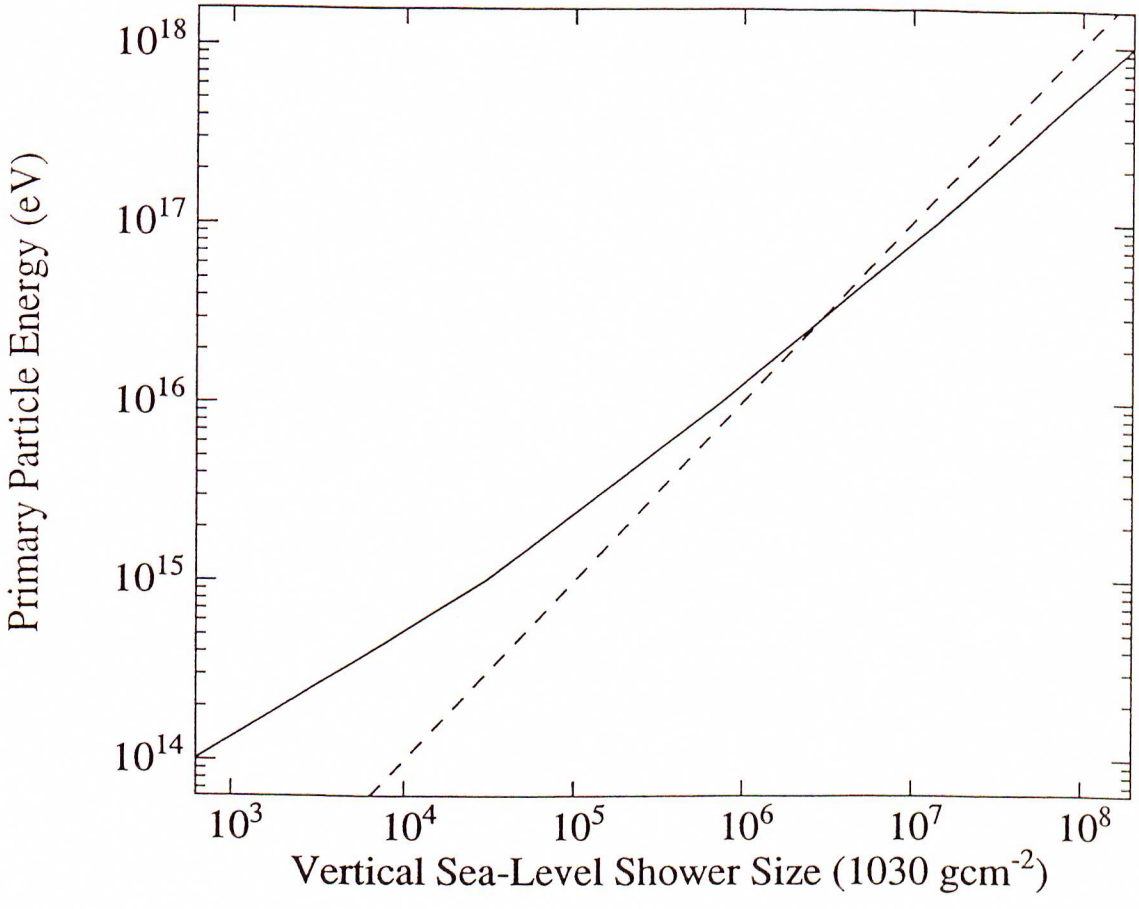

Figure 5.12: Calibration curve used to convert vertical sea-level shower size to primary particle energy. Dashed line indicates the 10^{10}eV per particle conversion factor discussed in the text.

mean primary energy corresponding to each of the chosen shower size intervals. Mean shower sizes for each of the intervals chosen were calculated from the data sets, and then converted to energies. The results of this conversion are shown in Table 5.4. Harmonic analysis was then applied to each of these intervals, and the resultant amplitudes and phases determined are presented in Table 5.5, and compared to previously determined southern hemisphere anisotropy estimates in Fig 5.13.

The periods examined vary for each of the size bins, based upon the uncertainty in estimating the solar effect, as discussed in 5.3.1. Only for the highest two shower size bins was it possible to sample essentially over the entire five year data set. In addition, no attempt was made to calculate a solar weight for bin 6 due to the relatively small number of events and associated large uncertainty in such an estimate.

All first harmonic amplitudes and phases are consistent with those expected from a random distribution at the statistical levels being considered, and the appropriate limits are displayed in Fig 5.13.

It is interesting to note that despite no statistically significant first harmonic amplitudes being recorded, the corresponding phases are, in general, consistent with those previously determined by other experiments (see Fig 5.13). In particular, the phases of Gerhardy (1983) compare favourably with corresponding phases in the present work, in spite of the differing amplitudes (see Table 5.6).

This general phase agreement may be indicative of the presence of an anisotropy below the current statistical limits, but is nevertheless somewhat puzzling.

5.4.2 Declination Dependence

Whilst the right ascension exposure can be made essentially uniform through the use of full sidereal days of data, the array exposure in declination suffers from the non-uniformity of both the azimuth and zenith angle distributions (see Figs 3.5 & 3.6). Consequently, analysis and interpretations of the declination dependence on the anisotropy are inherently more difficult.

In spite of this, two investigations were carried out into such a dependence.

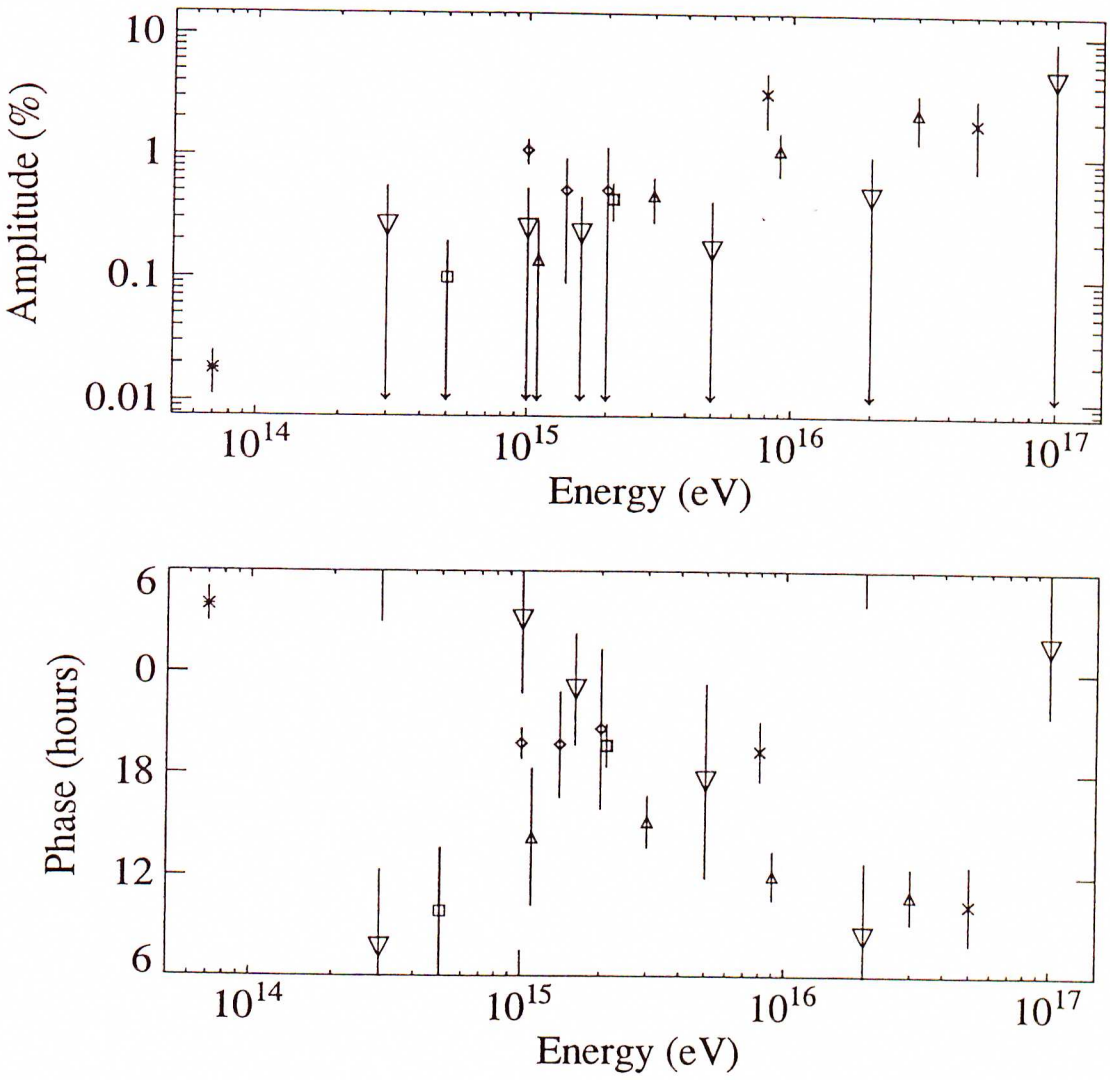

Figure 5.13: A comparison of the present results with previous southern hemisphere medium energy anisotropy measurements (first harmonic amplitude and phase). All errors and upper limits presented are at the one sigma level.

($\diamond$) Farley and Storey (1954)
($\triangle$) Farley and Storey (1957)
($\times$) Gerhardy and Clay (1983)
($\square$) Escobar *et al.* (1960)
($*$) Fenton *et al.* (1990)
($\triangledown$) this experiment

Gerhardy (1983)			Present Work		
Primary Energy (eV)	1^{st} Harmonic		Primary Energy (eV)	1^{st} Harmonic	
	Amplitude (%)	Phase (hrs)		Amplitude (%)	Phase (hrs)
8×10^{15}	3.29 ± 1.60	19.2 ± 1.9	5×10^{15}	0.17 ± 0.25	17.6 ± 5.8
1.7×10^{16}	1.86 ± 1.14	10.3 ± 2.3	2×10^{16}	0.47 ± 0.54	8.4 ± 4.4

Table 5.6 : Comparison of the present results with those obtained by a previous anisotropy experiment at Buckland Park (Gerhardy 1983). (errors quoted at the 1 σ level).

The first investigation involved dividing the sky into three regions of declination :

(1) North : $-25° < \delta < 0°$

(2) Overhead : $-45° < \delta < -25°$

(3) South : $-70° < \delta < -45°$

Harmonic analysis was then applied to the resultant right ascension distributions for each declination band in order to search for any trends in this anisotropy as a function of declination. The results of this analysis are presented in Table 5.7.

Overall, there is no statistically significant first (or second) harmonic amplitude recorded in any of the three declination bands considered. Furthermore, it is not possible to accurately compare the numbers of events recorded in each declination range, due to the non-uniformity of the array exposure as a function of declination (see Fig 3.8), and the non-uniform azimuth distribution (see Fig 3.6).

To investigate any possible size *and* declination dependence, the data were separated into the previously discussed size intervals. The results of the harmonic analysis on these data also appears in Table 5.7.

Once again, the results are generally in agreement with expectations from a random distribution, but it is interesting to note that there is phase agreement in shower size bins 3 and 4 between the Northern and Overhead regions, with a large shift in phase in the southern region (but no correlation of phases between these bins).

A much larger data set is required before any further conclusions may be reached regarding the energy/declination variations in the primary cosmic ray flux in terms of right ascension.

An alternative method attempted involved considering events from two regions of the sky in opposite directions to one another. To achieve some degree of uniformity in exposure, the zenith angle of the events under consideration were constrained to be in the range $20° < \theta < 35°$, and the azimuth angles were constrained to be North or South, $\pm 45°$ (i.e. $\phi < 45°, \phi > 315°$ and $135° < \phi < 225°$ respectively).

For this analysis, atmospheric pressure, and solar period variations were not taken into account. The regions of the sky were viewed simultaneously, and as a result, the

Primary Energy (eV)	Declination Band	Number of Events	1^{st} Harmonic			2^{nd} Harmonic			Statistical Errors			
			s_1 (%)	θ_1 (hrs)	P_1 (%)	s_2 (%)	θ_2 (hrs)	P_2 (%)	σ_{rms} (%)	σ_r (%)	σ_{θ_1} (hrs)	σ_{θ_2} (hrs)
All	$-25° < \delta < 0°$	2.02×10^5	0.03	0.1	99	0.30	9.1	63	0.44	0.31	12.0	2.0
	$-45° < \delta < -25°$	6.09×10^5	0.12	13.6	80	0.07	8.8	92	0.26	0.18	5.7	5.7
	$-70° < \delta < -45°$	1.39×10^5	0.36	5.6	64	0.34	0.5	68	0.54	0.38	4.1	2.2
3.2×10^{14}	$-25° < \delta < 0°$	4.38×10^4	0.46	15.6	79	1.40	9.8	7	0.96	0.68	5.6	0.9
	$-45° < \delta < -25°$	1.14×10^5	0.54	7.3	26	0.61	8.1	21	0.59	0.42	2.3	1.1
	$-70° < \delta < -45°$	2.97×10^4	1.00	0.2	48	0.88	9.2	34	1.16	0.82	3.1	1.3
1.0×10^{15}	$-25° < \delta < 0°$	4.99×10^4	0.37	1.9	84	0.94	3.3	20	0.90	0.63	6.5	1.1
	$-45° < \delta < -25°$	1.48×10^5	0.12	9.1	95	0.46	2.9	46	0.52	0.37	11.5	1.6
	$-70° < \delta < -45°$	3.43×10^4	0.99	0.6	26	0.60	8.5	73	1.08	0.76	2.3	2.5
1.6×10^{15}	$-25° < \delta < 0°$	1.06×10^5	0.46	0.7	57	0.12	2.2	96	0.61	0.43	3.6	6.0
	$-45° < \delta < -25°$	3.23×10^5	0.13	0.1	87	0.19	9.4	75	0.35	0.25	7.3	2.5
	$-70° < \delta < -45°$	7.21×10^4	0.38	14.7	77	0.66	12.0	45	0.75	0.53	5.3	1.5
5.0×10^{15}	$-25° < \delta < 0°$	6.35×10^4	0.40	16.9	78	0.38	8.3	80	0.79	0.56	5.4	2.8
	$-45° < \delta < -25°$	1.98×10^5	0.37	16.5	52	0.38	11.0	50	0.45	0.32	3.3	1.6
	$-70° < \delta < -45°$	4.41×10^4	1.45	2.4	10	0.41	7.0	83	0.95	0.67	1.8	3.2
2.0×10^{16}	$-25° < \delta < 0°$	1.42×10^4	1.63	6.6	39	1.33	6.9	32	1.68	1.19	2.8	1.3
	$-45° < \delta < -25°$	4.36×10^4	0.06	1.5	99	0.77	1.5	53	0.96	0.68	12.0	1.7
	$-70° < \delta < -45°$	8.70×10^3	1.50	11.3	61	0.76	2.7	88	2.15	1.52	3.9	3.8
1.1×10^{17}	$-25° < \delta < 0°$	1.48×10^2	14.9	9.6	44	12.4	2.5	57	16.5	11.7	3.0	1.8
	$-45° < \delta < -25°$	5.92×10^2	7.85	3.1	40	4.43	6.3	75	8.22	5.81	2.8	2.5
	$-70° < \delta < -45°$	1.23×10^2	23.4	20.1	11	15.7	0.6	50	18.0	12.7	1.8	1.6

Table 5.7 : Results of the harmonic analysis of the declination dependence of the primary cosmic ray flux, including the primary energy dependence.

vector difference between the amplitudes measured in these regions should be independent of these effects. The southern region viewed consisted of declinations in the range $-70° < \delta < -50°$, and due to the tightening of the right ascension lines with high declinations, this region should produce vectors predominantly due to the atmospheric and solar period effects mentioned above. This vector may then be subtracted from the Northern direction vector ($-20° < \delta < 0°$) to determine an anisotropy estimate for the difference and hence a declination dependence on the anisotropy. Because this method allows for any solar effects (or other biases introduced into the data), *in situ*, it was possible to include the entire five years of data in this investigation without fear of bias, significantly improving the statistics of this analysis.

The results of this analysis appear in Table 5.8, and are compared with those determined using the full sidereal skymaps in Fig 5.14.

The amplitudes are generally in agreement with those previously determined, but the first harmonic amplitudes determined by this method are in general higher than those previously determined, but remain consistent with the earlier results. There is also general agreement between the phases at all but the highest energy examined where the number of events sampled is extremely small.

5.4.3 Summary

The harmonic analysis technique has been applied to the right ascension distributions derived from data collected by the Buckland Park E.A.S. Array over the period 1984–1989 through the calculation of sidereal skymaps, and appropriate weighting to remove atmospheric and diurnal effects from these data. All measured amplitudes were found to be consistent with noise at the 95% (2σ) level, but in spite of this, there is remarkable agreement between the corresponding phases and those determined by comparable southern hemisphere experiments.

In addition, a limited investigation has been carried out into the anisotropy of the primary cosmic ray flux in terms of declination, but all results were found to be consistent with a random distribution. It is therefore concluded that no evidence was

Primary Energy (eV)	Declination Band	Number of Events	1^{st} Harmonic			2^{nd} Harmonic			Statistical Errors			
			s_1 (%)	θ_1 (hrs)	P_1 (%)	s_2 (%)	θ_2 (hrs)	P_2 (%)	σ_{rms} (%)	σ_r (%)	σ_{θ_1} (hrs)	σ_{θ_2} (hrs)
All	North	473913	0.44	8.5	6	0.10	4.5	89	0.29	0.21	1.6	3.9
	South	456061	0.02	8.0	99	0.27	3.2	43	0.30	0.21	12.0	1.5
	Resultant	929974	0.42	8.5		0.21	8.6			0.21	3.3	4.5
3.2×10^{14}	North	45390	0.75	8.9	32	0.60	9.1	67	0.94	0.66	2.5	2.1
	South	45063	0.91	5.0	24	0.39	7.6	84	0.94	0.67	2.3	3.2
	Resultant	90453	0.82	13.6		0.40	10.4			0.93	3.5	4.5
1.0×10^{15}	North	147446	0.55	9.5	20	0.11	9.7	96	0.52	0.37	2.1	6.0
	South	140589	0.66	10.7	13	0.71	3.9	17	0.53	0.38	1.9	1.0
	Resultant	288035	0.22	2.1		0.82	9.9			0.52	3.0	2.5
1.6×10^{15}	North	164238	0.98	6.9	1	0.38	1.1	55	0.49	0.35	1.3	1.8
	South	156997	0.33	13.1	65	0.34	10.9	64	0.51	0.36	4.1	2.0
	Resultant	321235	1.05	5.7		0.40	2.8			0.51	3.5	3.0
5.0×10^{15}	North	109235	0.80	18.4	11	0.71	5.0	25	0.61	0.43	1.8	1.2
	South	106929	1.44	22.4	0.2	0.67	3.3	30	0.61	0.43	1.1	2.5
	Resultant	216164	1.24	12.6		0.60	7.0			0.61	2.5	3.0
2.0×10^{16}	North	7539	2.46	5.4	19	3.44	5.8	11	2.30	1.63	2.1	0.9
	South	6388	2.49	10.9	37	1.59	1.0	67	2.50	1.77	2.7	2.2
	Resultant	13927	3.26	2.1		4.82	6.2			2.40	3.5	2.8
1.2×10^{17}	North	65	23.4	11.9	25	23.7	3.0	40	24.9	17.5	2.3	1.4
	South	95	21.8	22.7	20	21.2	1.1	34	20.5	14.5	2.1	1.3
	Resultant	160	44.6	11.3		21.5	4.9			21.2	3.4	2.2

Table 5.8 : Results of the harmonic analysis of the declination dependence of the primary cosmic ray flux, calculated by viewing selected northern and southern regions of the sky (see text), including primary energy dependence.

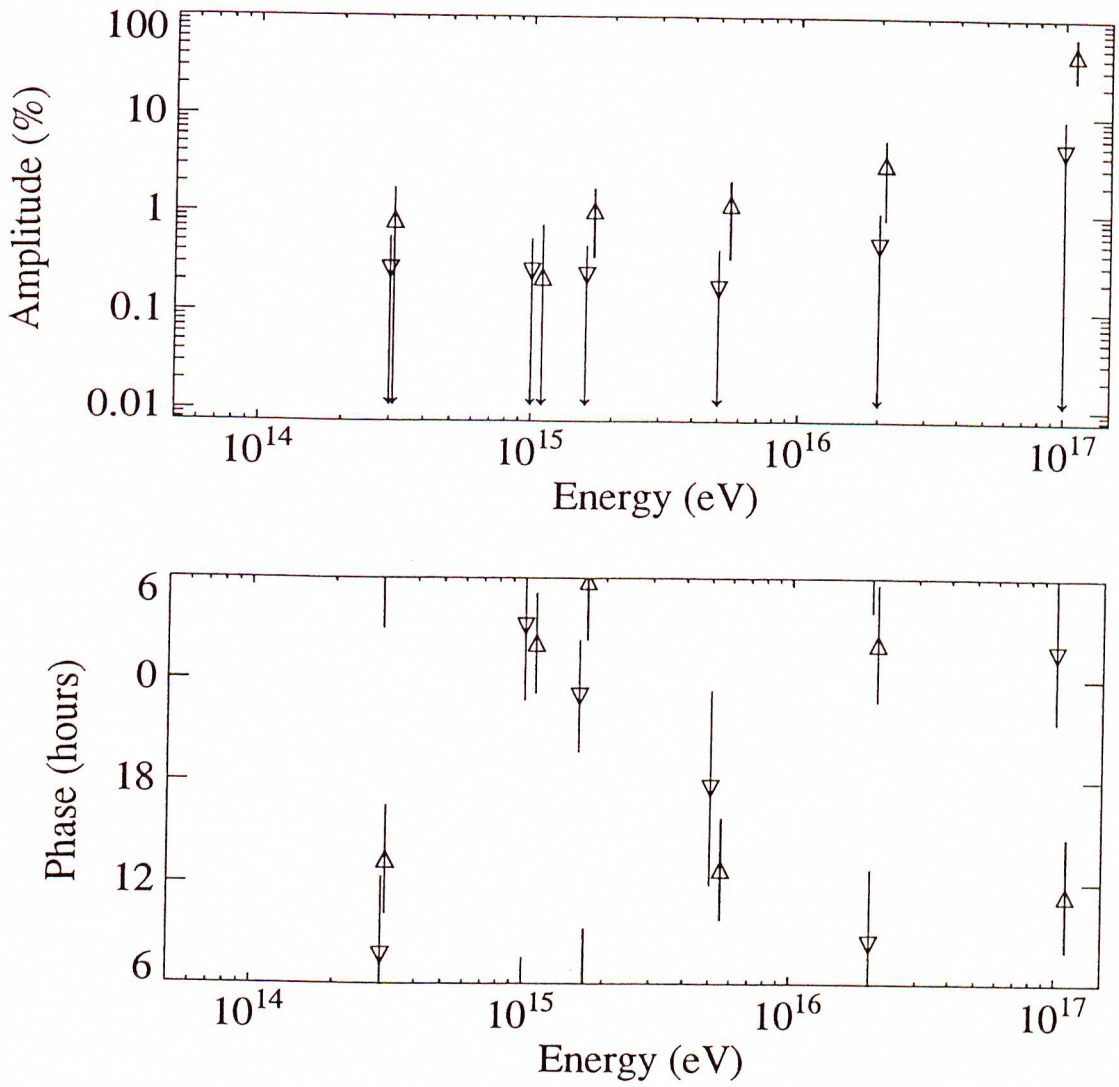

Figure 5.14: A comparison of the present results derived using the two different methods discussed in the text for allowing for experimental biases (first harmonic amplitude and phase). All errors and upper limits presented are at the one sigma level.
($\triangle$) North-South analysis (see 5.4.2)
($\triangledown$) Skymap analysis (see 5.4.1)

found for a declination dependence of the primary cosmic ray flux by this experiment.

The North-South method described above was also applied to the data as an alternative to the sidereal skymap technique of anisotropy determination. Results were found to be generally consistent with those of the latter technique but possessing higher (but clearly comparable) amplitude estimates, with phases generally in agreement. It is clear that a further investigation with improved statistics is required in order to positively confirm the existence and strength of the anisotropy in the primary cosmic ray flux at the energies under consideration (3×10^{14}eV – 10^{17}eV).

The analysis of anisotropies in the primary cosmic ray flux in terms of right ascension allows on-time and other exposure effects such as the array declination exposure to be taken into account, and is therefore analytically very useful.

However, a more natural set of co-ordinates in which to carry out an analysis of the primary cosmic ray flux is the galactic co-ordinate system, which is directly tied to the distribution of matter within the Galaxy. Attempts at such an analysis will now be briefly discussed.

5.5 Galactic Co-ordinates

Galactic co-ordinates are defined with the Earth at the origin, and the equator defined by the galactic plane. galactic latitude, b, is measured with respect to the galactic plane, and galactic longitude, l, is defined as being 0° in the direction of the galactic centre, and 180° in the direction of the anti-centre. The co-ordinate transform from equatorial co-ordinates (α, δ) which are essentially tied to the Earth, to galactic co-ordinates (b, l) which are tied to the Galaxy, is extremely non-linear and may be expressed by the following equations :

$$\cos(b)\cos(l - 33°) = \cos(\delta)\cos(\alpha - 282.25°) \tag{5.5}$$

$$\cos(b)\sin(l - 33°) = \cos(\delta)\sin(\alpha - 282.25°)\cos(62.6°) + \sin(\delta)\sin(62.6°) \tag{5.6}$$

$$\sin(b) = \sin(\delta)\cos(62.6°) - \cos(\delta)\sin(\alpha - 282.25°)\sin(62.6°) \qquad (5.7)$$

(Lang 1974)

This non-linearity presents problems and limits the types of analyses that may be applied. Harmonic analysis in its most general form is clearly inappropriate, as exposure is non-uniform in both galactic latitude and longitude.

Two alternative methods were attempted in examining the primary cosmic ray flux in terms of galactic co-ordinates, and these will now be discussed.

5.5.1 Galactic Latitude

Investigations into the galactic latitude dependence of the primary cosmic ray flux have been previously carried out (see e.g. Astley *et al.* 1981; 4.3.3) in a search for an enhancement in the flux in the direction of the galactic plane at high energies. Such an investigation was carried out for the present sidereal data as follows.

For each cell in the sidereal skymap, the corresponding galactic latitude was calculated and the number of events in the cell added to the appropriate galactic latitude bin (in divisions of 5°). To overcome the non-uniform exposure in galactic latitude (see Fig 5.15), a 'background' galactic latitude distribution was also set up with the expected number of events from each cell for weighting purposes. This expected number of events was calculated by averaging over all of the right ascension bins within the appropriate declination band, making use of the uniform exposure within each declination band. These two distributions were then compared and the excess/deficiency defined in terms of standard deviations (Δ) (see Eq 5.4).

Fig 5.16 shows the results of this analysis on the overall data set. Clearly, there are no major (i.e. $> 3\sigma$) deviations from the expected number of events, nor are there any significant enhancements in the direction of the galactic plane.

This analysis was also applied to the shower size intervals being considered, and the results are presented in Figs 5.17–5.22. Once again, there are no statistically significant excesses/deficiencies in these data.

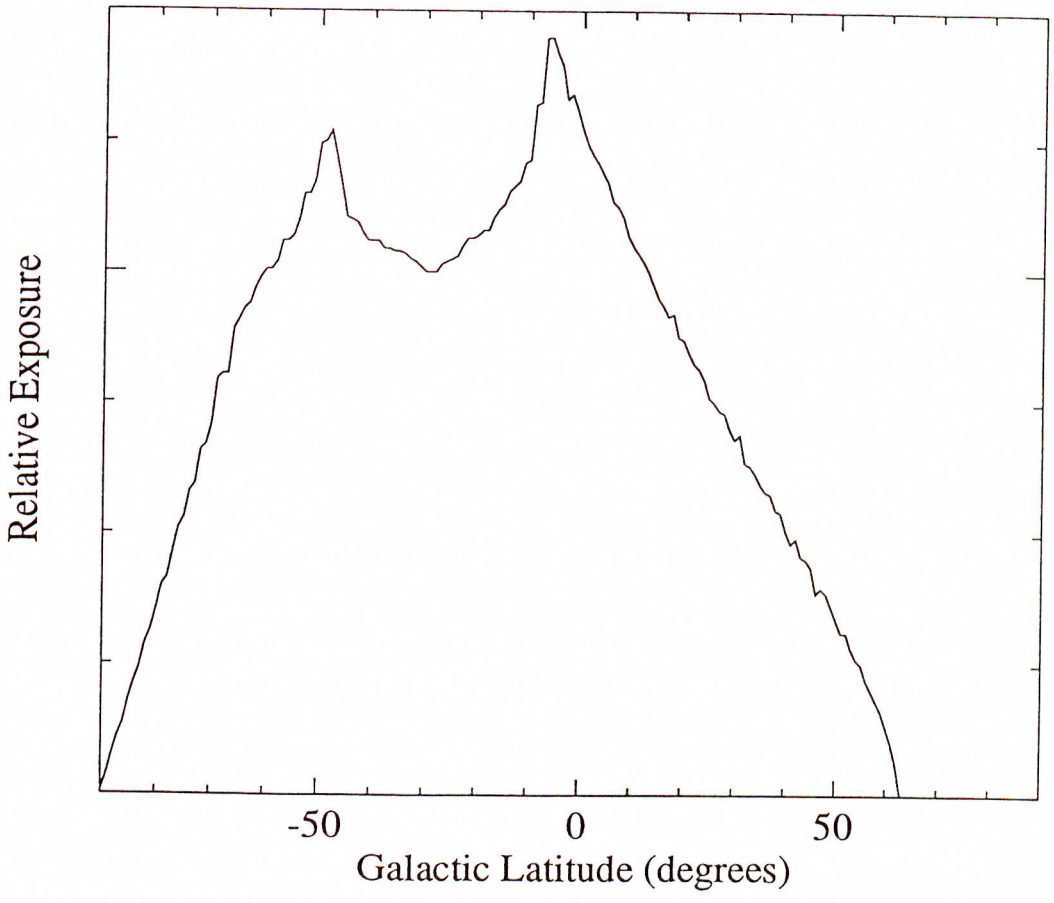

Figure 5.15: The exposure of the Buckland Park E.A.S. Array in terms of galactic latitude, corresponding to the declination range $-70° < \delta < 0°$.

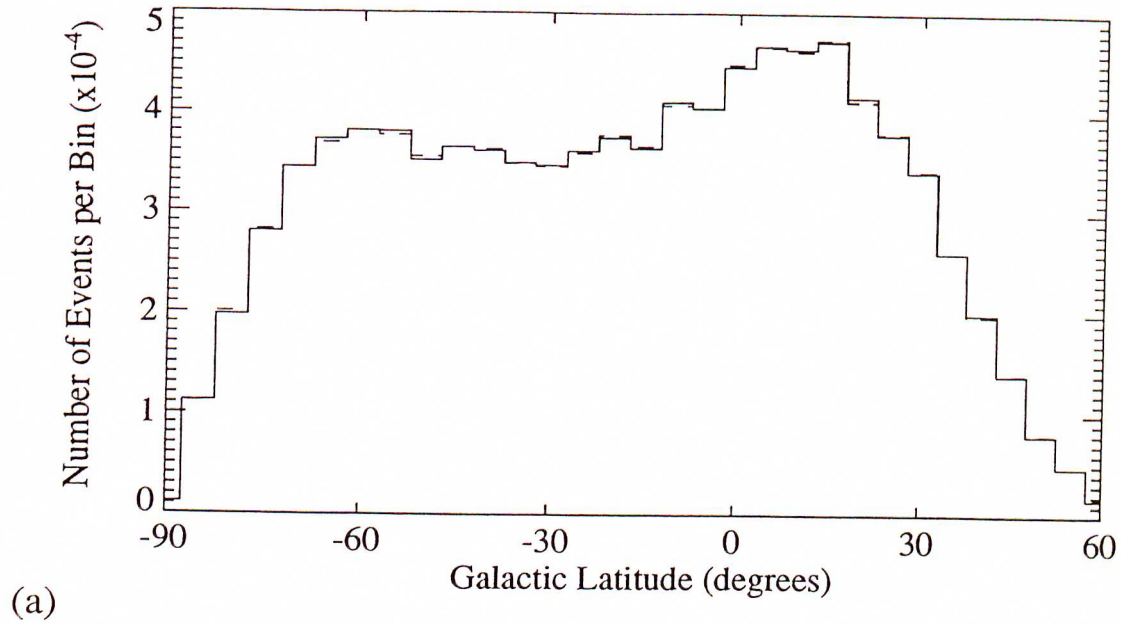

(a)

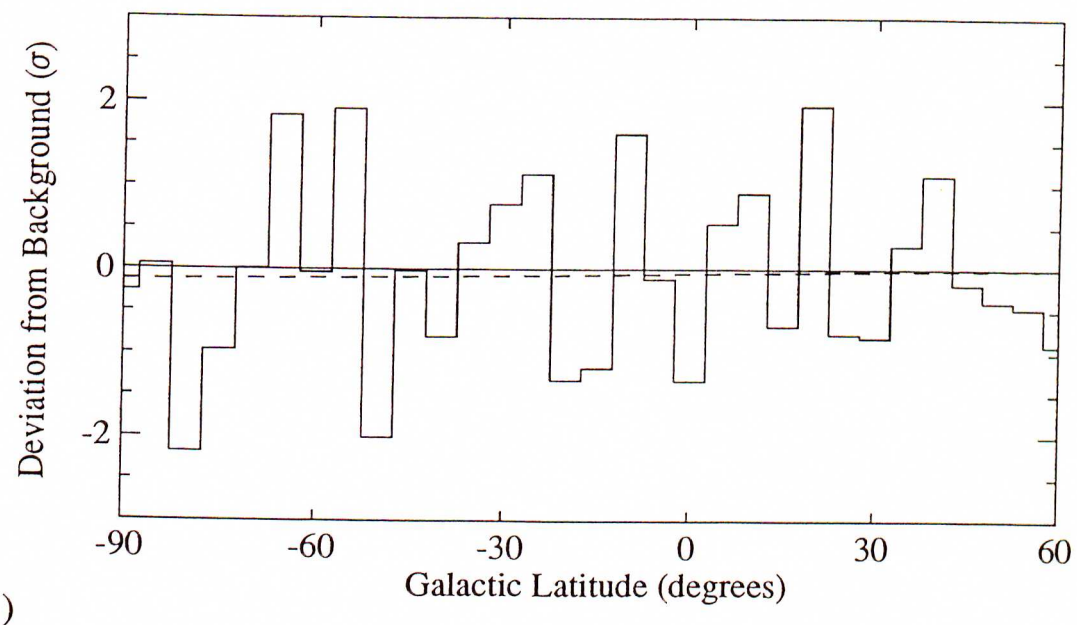

(b)

Figure 5.16: Deviations from the expected number of events as a function of galactic latitude in both raw data and sigma deviation from the background for the overall data set. (The dashed line indicates the expected background in **(a)**, and a linear fit to the data in **(b)**.)

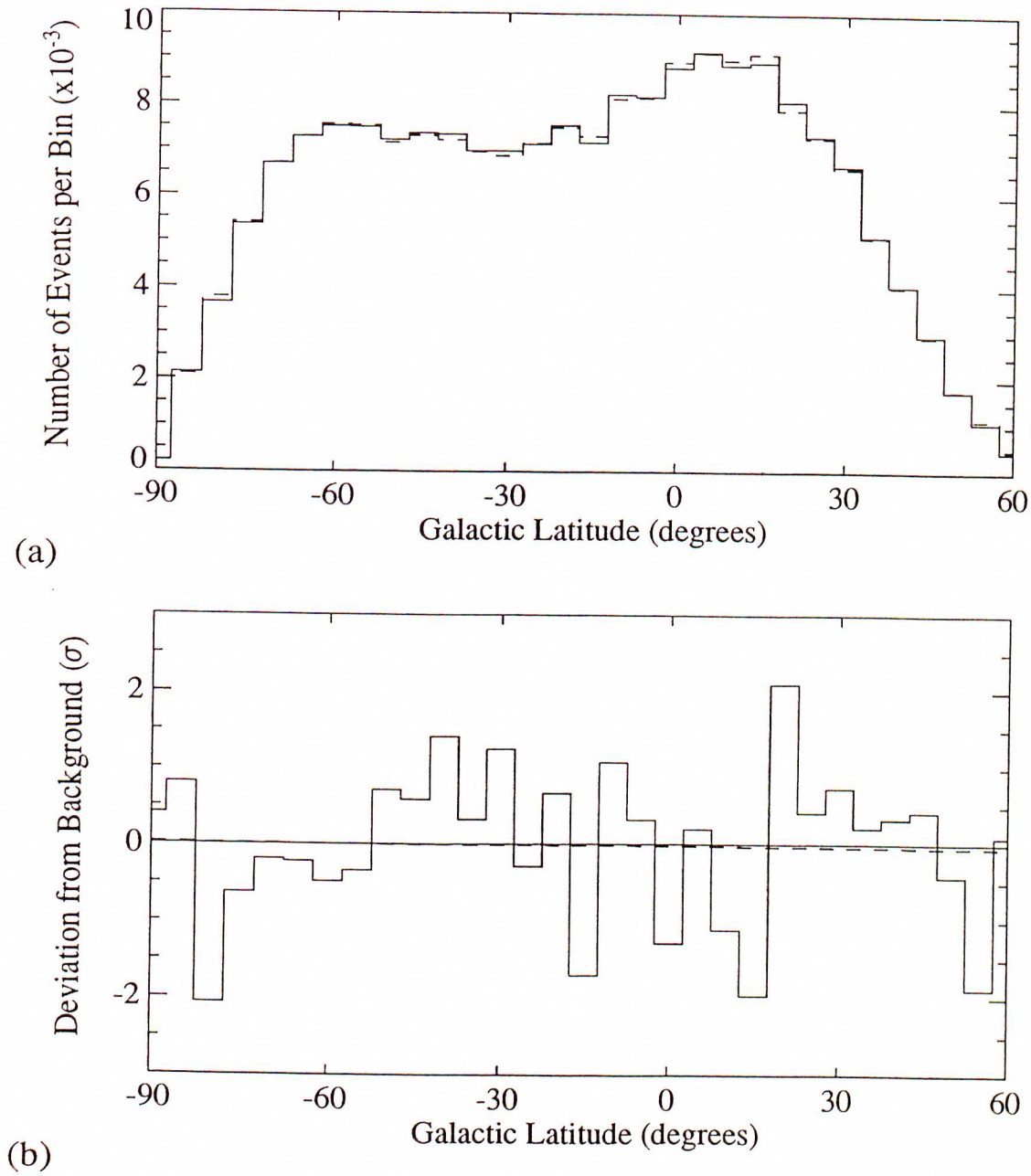

Figure 5.17: Deviations from the expected number of events as a function of galactic latitude in both raw data and sigma deviation from the background for the size bin corresponding to a mean energy of 3×10^{14}eV (1). (The dashed line indicates the expected background in **(a)**, and a linear fit to the data in **(b)**.)

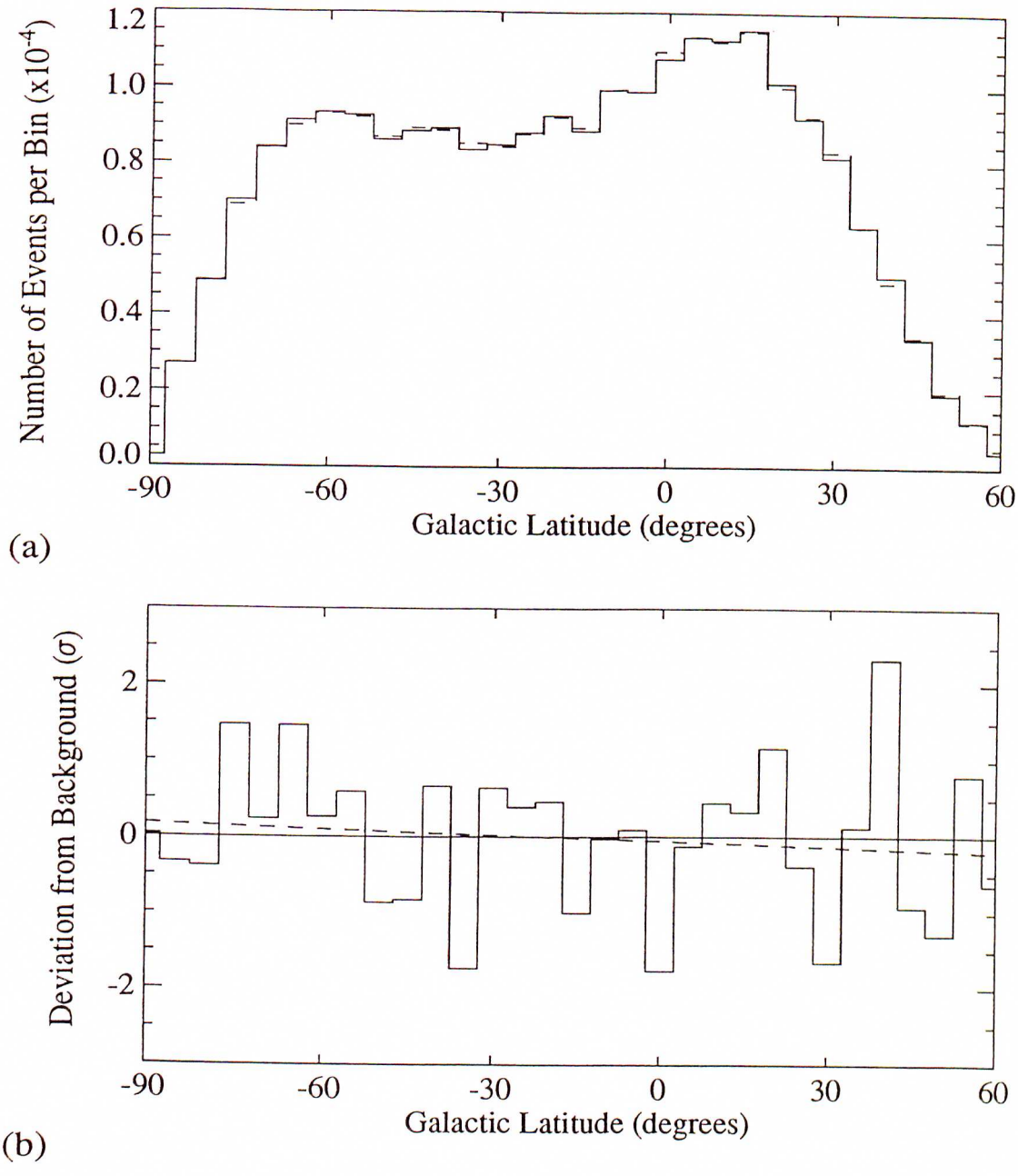

Figure 5.18: Deviations from the expected number of events as a function of galactic latitude in both raw data and sigma deviation from the background for the size bin corresponding to a mean energy of 10^{15}eV (2). (The dashed line indicates the expected background in **(a)**, and a linear fit to the data in **(b)**.)

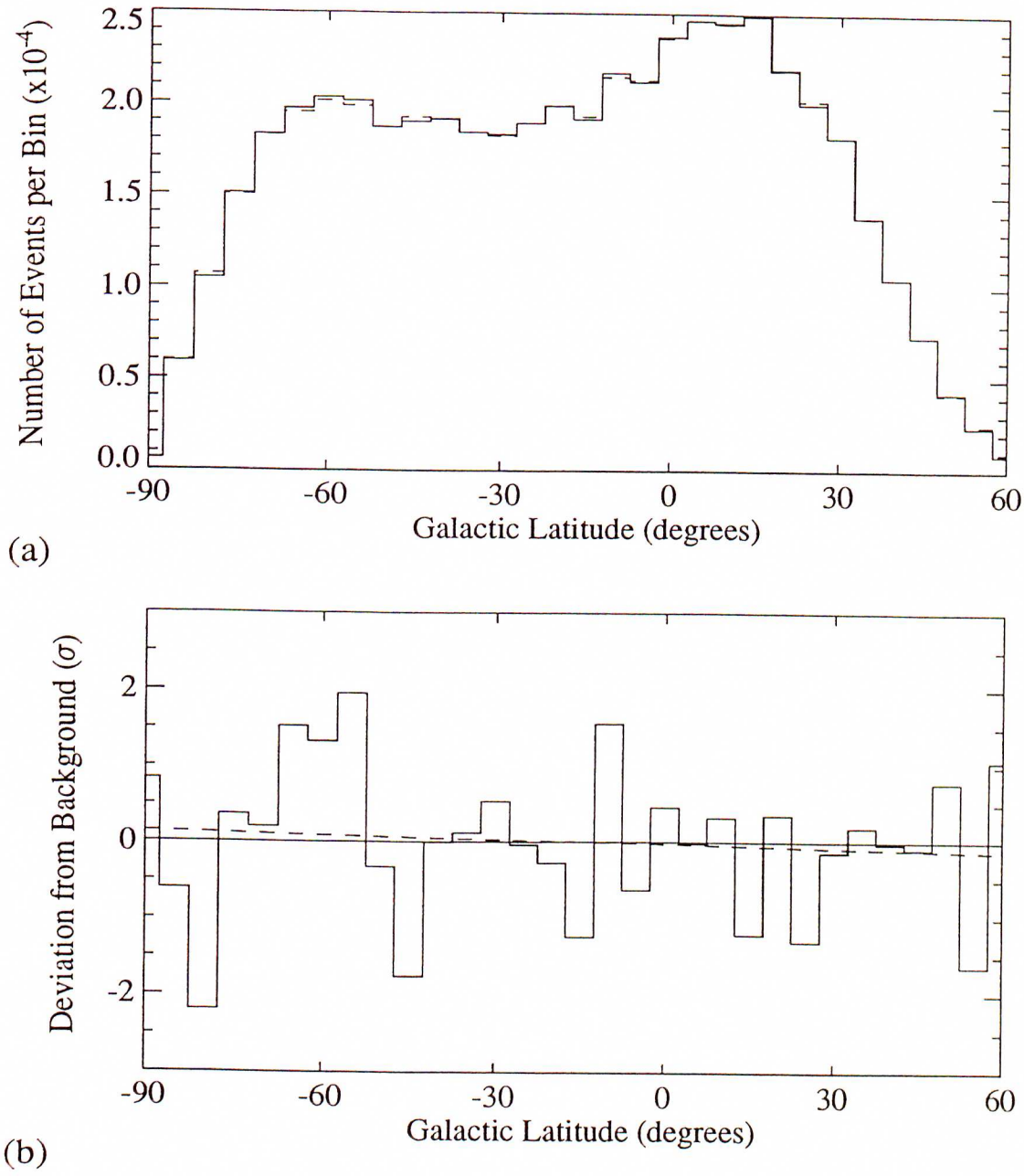

Figure 5.19: Deviations from the expected number of events as a function of galactic latitude in both raw data and sigma deviation from the background for the size bin corresponding to a mean energy of 1.6×10^{15}eV (3). (The dashed line indicates the expected background in **(a)**, and a linear fit to the data in **(b)**.)

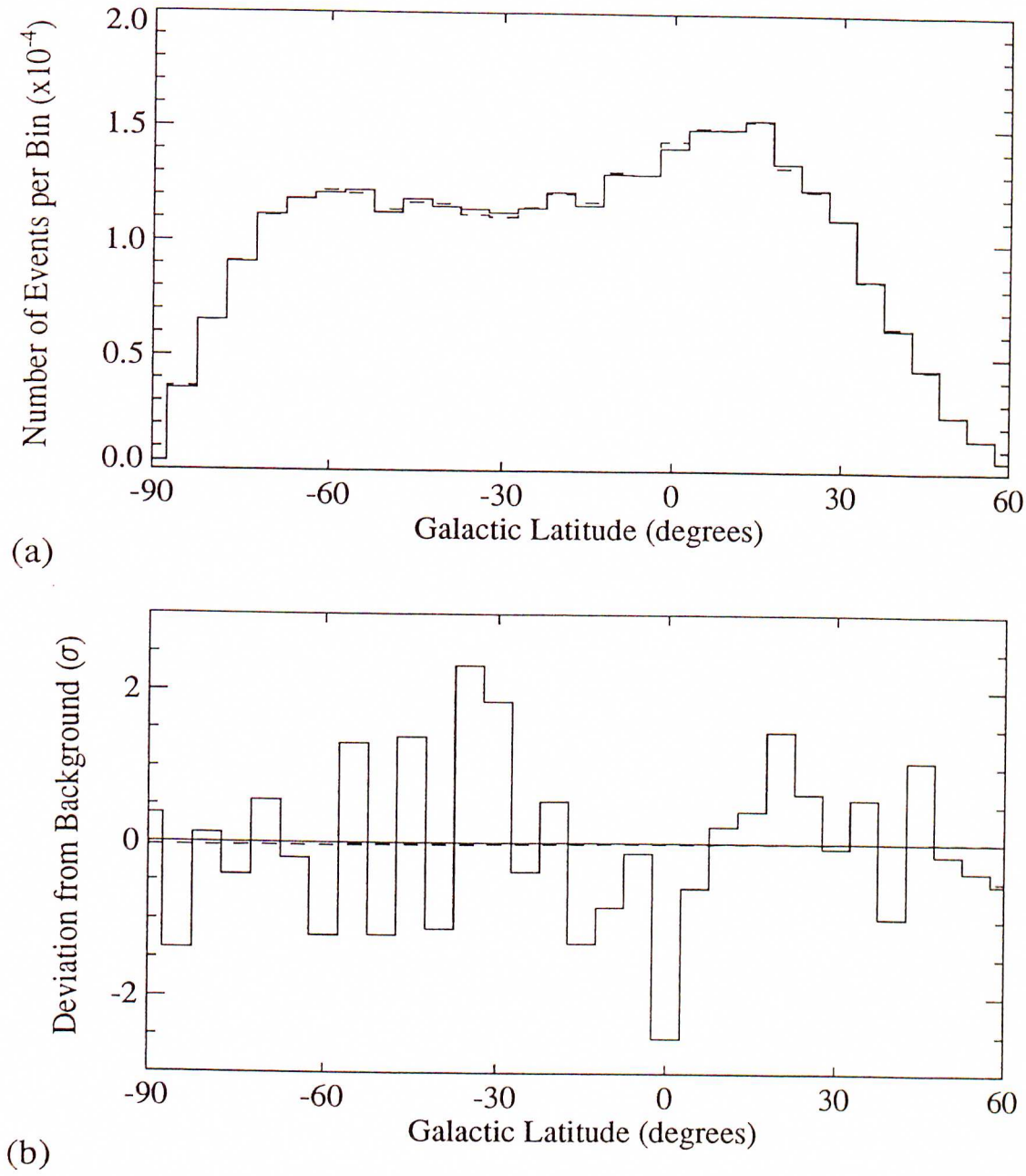

Figure 5.20: Deviations from the expected number of events as a function of galactic latitude in both raw data and sigma deviation from the background for the size bin corresponding to a mean energy of 5×10^{15}eV (4). (The dashed line indicates the expected background in **(a)**, and a linear fit to the data in **(b)**.)

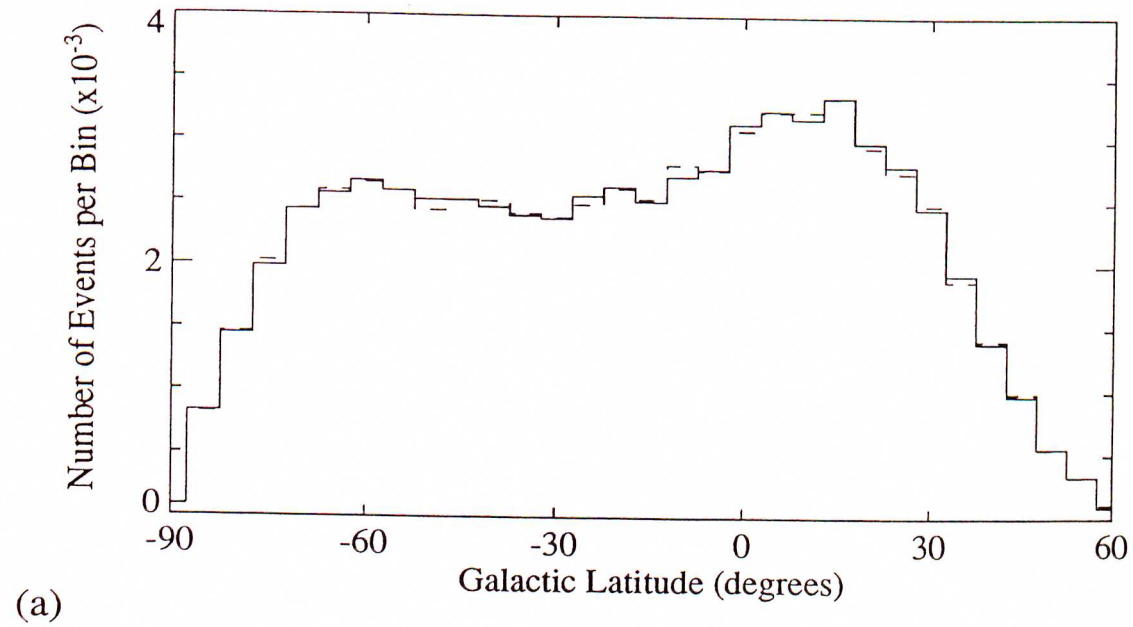

(a)

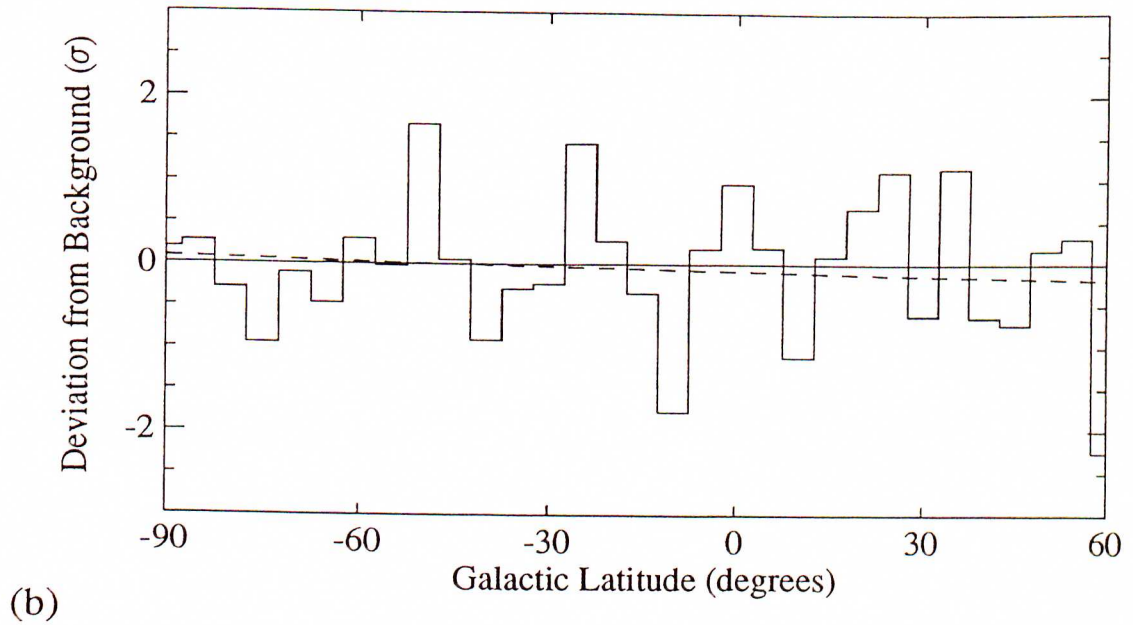

(b)

Figure 5.21: Deviations from the expected number of events as a function of galactic latitude in both raw data and sigma deviation from the background for the size bin corresponding to a mean energy of 2×10^{16}eV (5). (The dashed line indicates the expected background in **(a)**, and a linear fit to the data in **(b)**.)

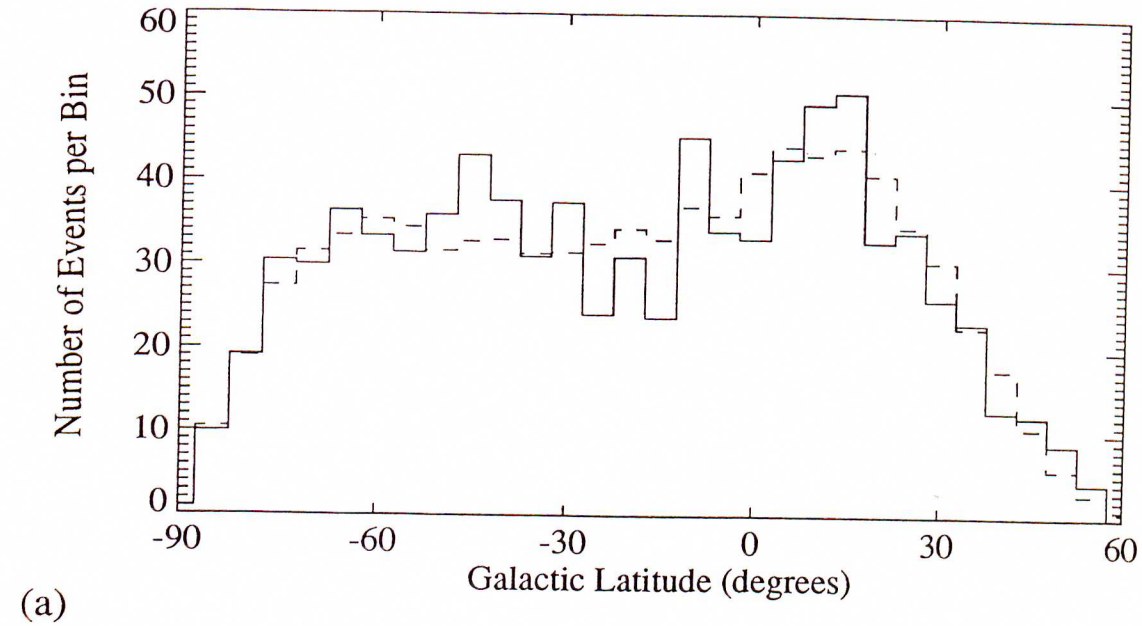

(a)

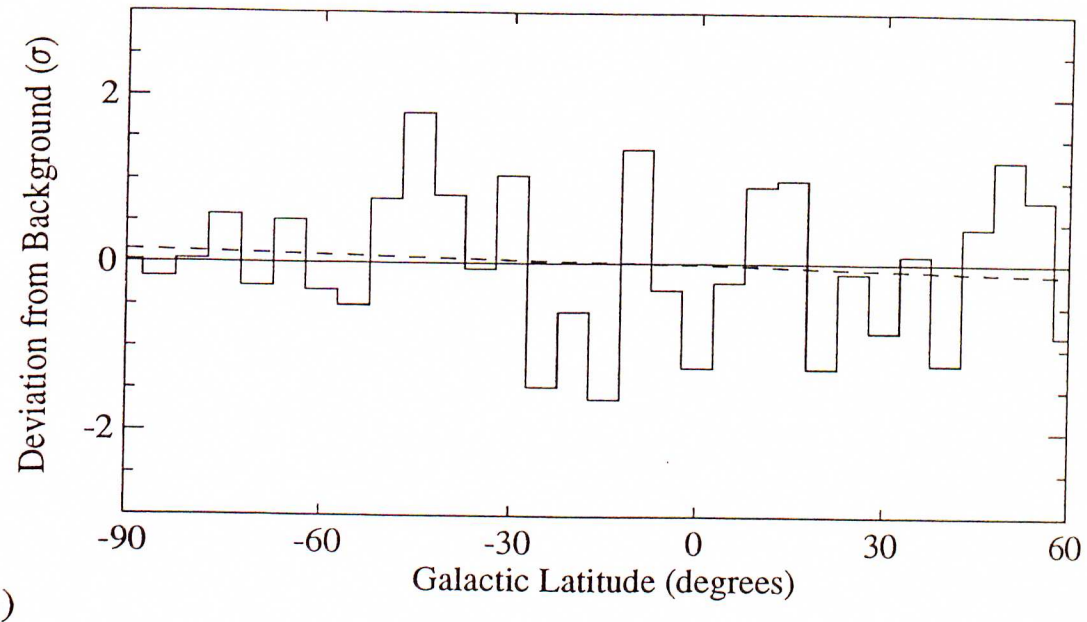

(b)

Figure 5.22: Deviations from the expected number of events as a function of galactic latitude in both raw data and sigma deviation from the background for the size bin corresponding to a mean energy of 1.1×10^{17}eV (6). (The dashed line indicates the expected background in **(a)**, and a linear fit to the data in **(b)**.)

Previous results have suggested that there exists a latitude gradient at higher energies (see 4.5.3). The dashed lines in Figs 5.16–5.22 are lines of best fit to these data and indicate that there exists no significant latitude gradient at the energies being considered in this investigation, consistent with previous results (see e.g. Linsley 1983).

In addition to a latitude gradient, it has also been suggested (Clay 1990) that the spiraling of medium cosmic ray particles may result in enhancements in the flux of charged cosmic ray particles at galactic latitudes of $b \sim \pm 30°$. Fig 5.23 displays the results of fitting high degree polynomials ($\sim$ 10th degree) to these data in order to search for such an enhancement. Only shower size bins 1 and 4 ((a) and (d) in Fig 5.23) show any indication of such behaviour at a very marginal statistical level. It is concluded that no significant evidence for such behaviour exists in these data.

5.5.2 Galactic Skymap

Using a similar technique to that just described, it was also possible to construct a map in galactic co-ordinates, (l, b), showing contours in standard deviations (σ), analogous to Fig 5.11. In constructing these maps, only events with declinations in the range $-70° < \delta < 0°$ were considered, in order to avoid problems incurred as a result of the angular resolution of the array. To minimise problems resulting from the non-linearity of the mapping, cells of size 1° by 1° were used in translating from equatorial to galactic co-ordinates. The results of this transformation are shown in Fig 5.24. The array coverage in terms of galactic co-ordinates is clearly evident, the 'hole' the result of the lower limit on declination applied for this analysis.

Such a map is useful for examining the sky for any point, or extended sources or deficiencies in terms of this co-ordinate system. No significant excesses or deficiencies are apparent in these maps.

It was concluded that there is no evidence for a preferred arrival direction for cosmic ray events in galactic co-ordinates at the energies being considered at the available statistical level.

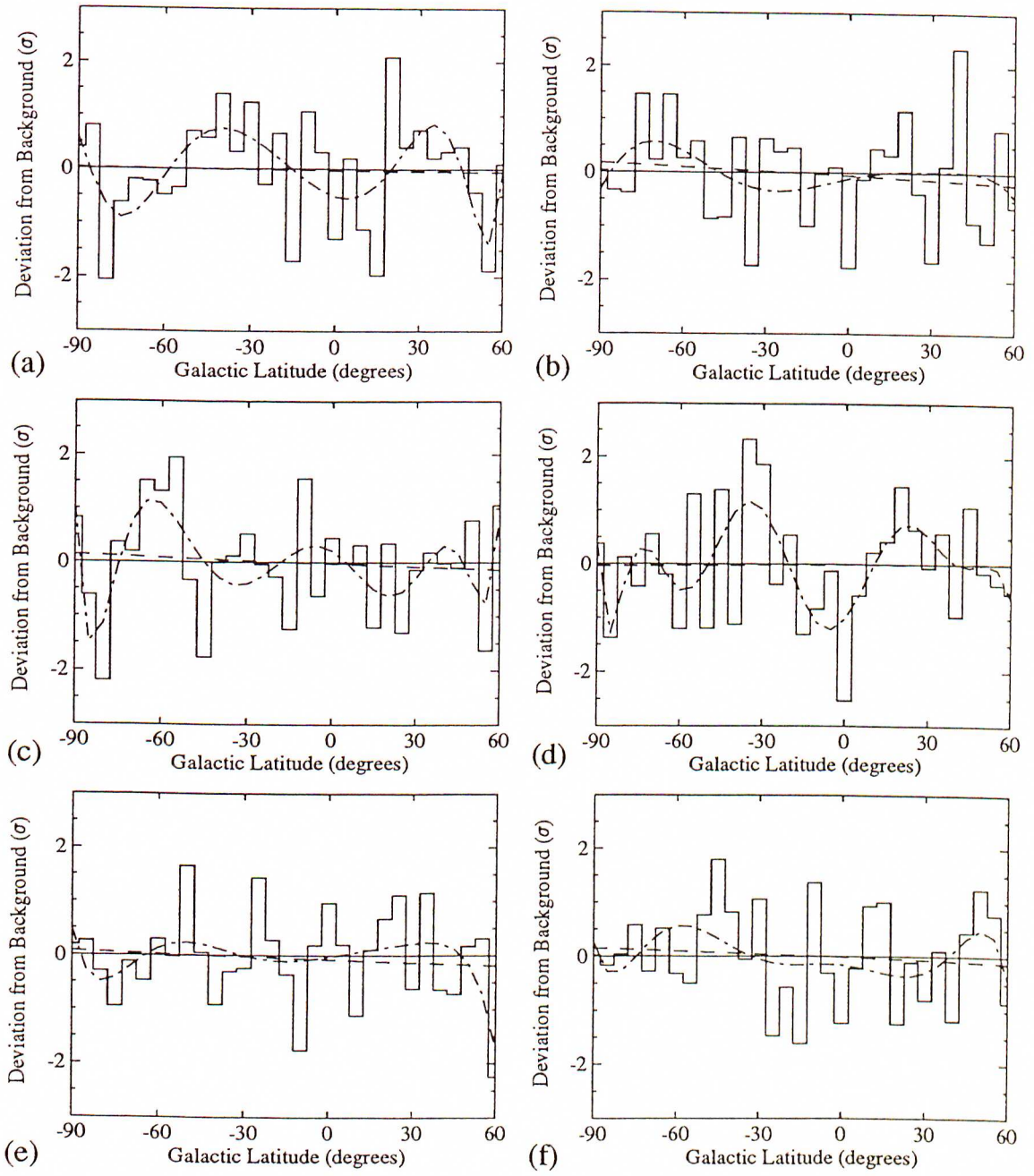

Figure 5.23: Deviations from the expected number of events as a function of galactic latitude in both raw data and sigma deviation from the background for all size bins considered. The dashed curve indicates a fit to these data in order to search for enhancements at galactic latitudes of $b \sim \pm 30°$.

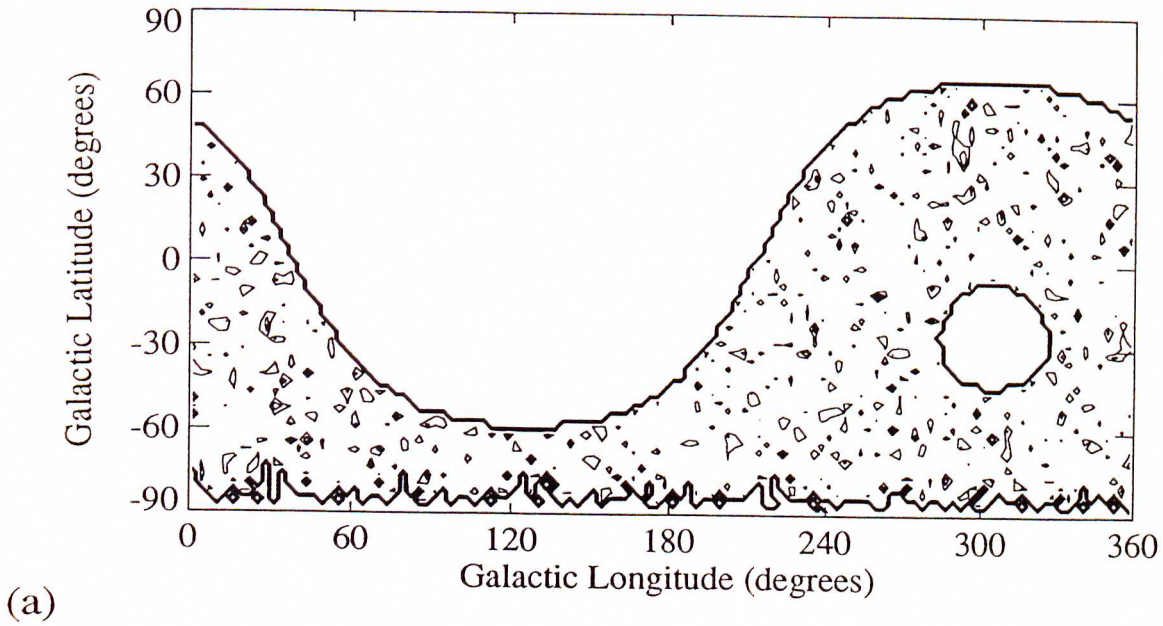

(a)

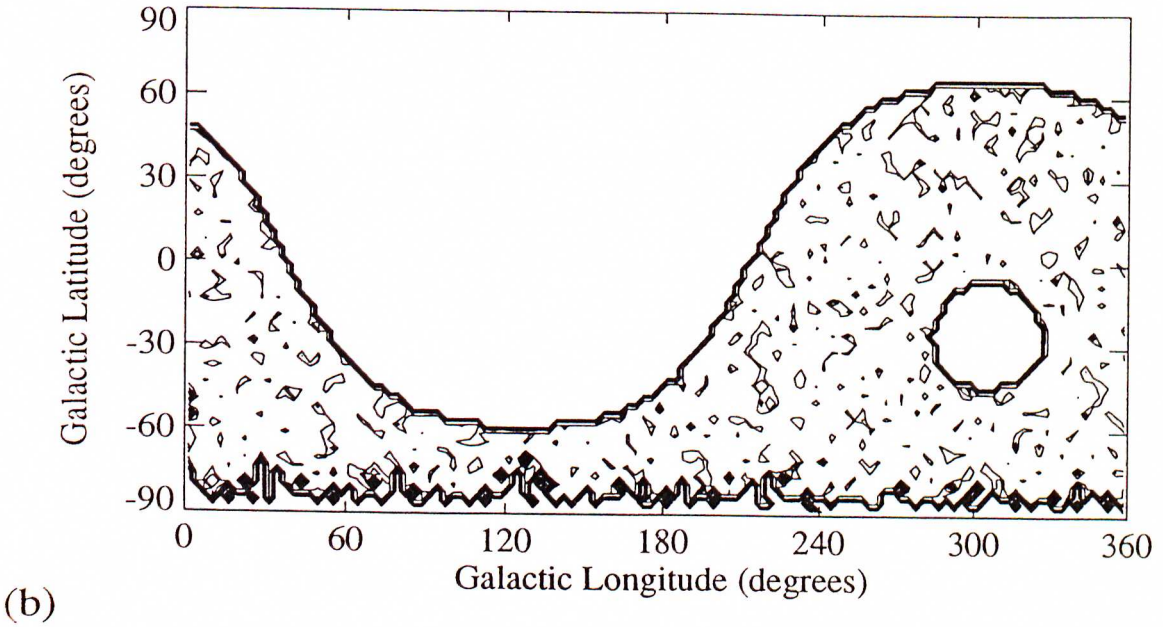

(b)

Figure 5.24: Contour maps of the detected number of events versus the expected number of events in terms of sigma, plotted in galactic coordinates, for the overall data set.
(a) Contours of positive sigma (ie. 1,2,3...)
(b) Contours of negative sigma (ie. -1,-2,-3...)

5.6 Analysis of the 1978–1981 Data Set

Using an earlier version of the Buckland Park E.A.S. Array consisting of twelve detectors (see e.g. Crouch *et al.* 1981; Gerhardy 1983), four years of data were recorded (1978–1981), three of which (1979–1981) had been previously analysed for anisotropy in the primary cosmic ray flux by Gerhardy (1983), using the anti-sidereal technique of Farley and Storey (1954, 1957) (see 4.3.2 for a brief discussion of this technique). The 1978 data were not included in this analysis due to the severe lack of continuity in data collection, a prerequisite for the application of the anti-sidereal analysis technique.

The analysis techniques discussed in 5.2 and applied to the 1984–1989 data set for anisotropy analysis were applied to the 1978–1981 data set. However, before such an analysis can be carried out, the array characteristics for this period need to be examined.

5.6.1 Array Characteristics (1978–1981)

The arrival directions and shower parameters for these data had been previously determined by Gerhardy (1983) through techniques similar to those discussed in 3.3.2 (see Gerhardy 1983 for details). The arrival direction and shower parameter distributions are shown in Figs 5.25 & 5.26, along with the event time-spacing distribution for these data. During this period, the angular resolution of the array was $\sim 3^\circ$ for shower sizes $> 10^5$ particles (Ciampa *et al.* 1986), which was deemed to be more than adequate for the relatively coarse directional investigation to be undertaken.

The azimuth angle distribution shown in Fig 5.25(c), (e) demonstrates significant first and second harmonics (amplitudes 1.3% and 4.0% respectively — Gerhardy 1983). Gerhardy (1983) attributed the presence of the second harmonic to the triggering conditions active during this period, and suggested that the first harmonic may result from timing calibration errors of the order of the timing resolution of the array (Clay and Gerhardy 1982). However, uniformity of exposure in sidereal time eliminates the majority of the problems posed by the non-uniformity of this distribution when

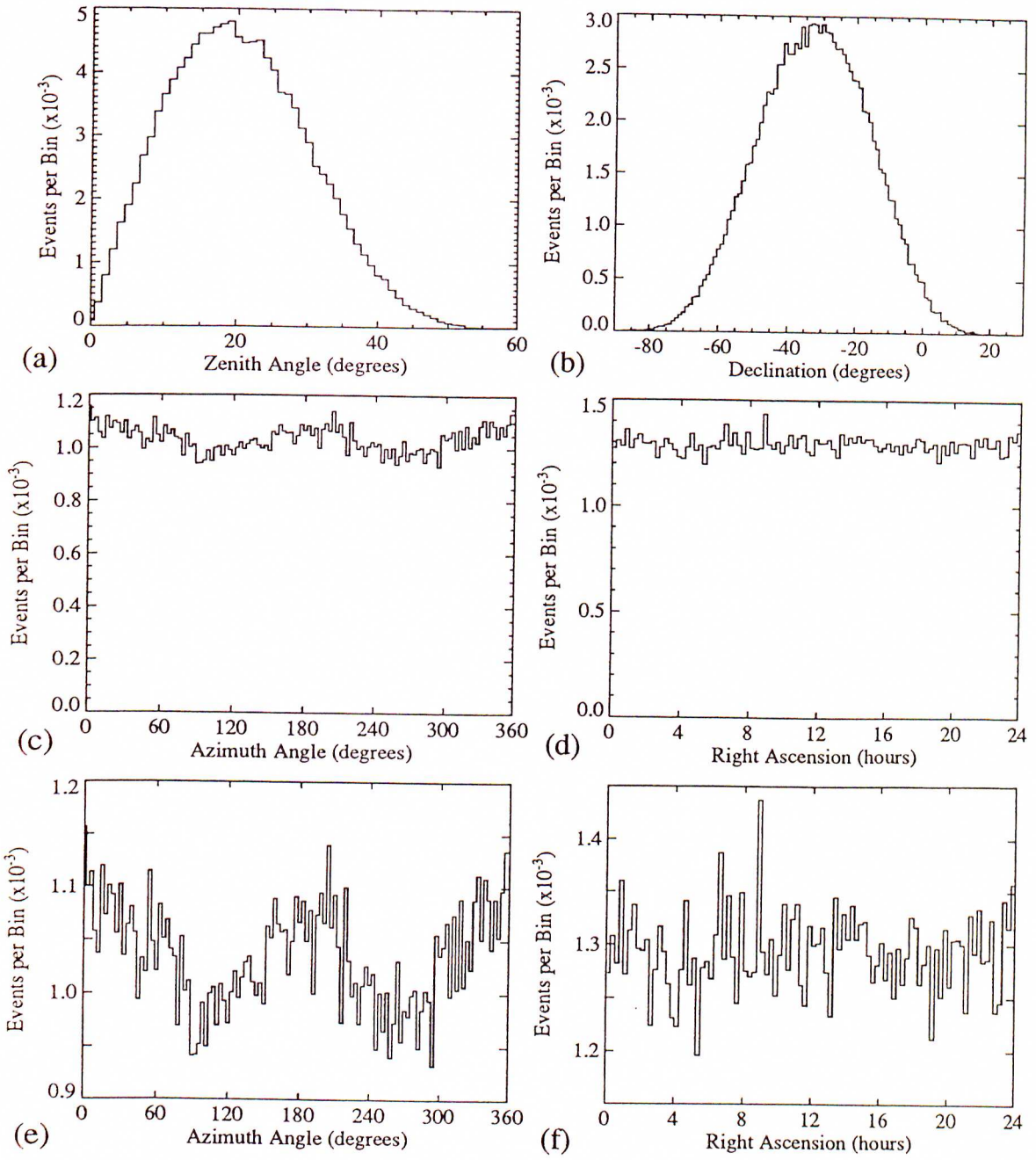

Figure 5.25: The angular distributions for the 1978–1981 data set.
(a) Zenith Angle.
(b) Declination.
(c), (e) Azimuth Angle.
(d), (f) Right Ascension.

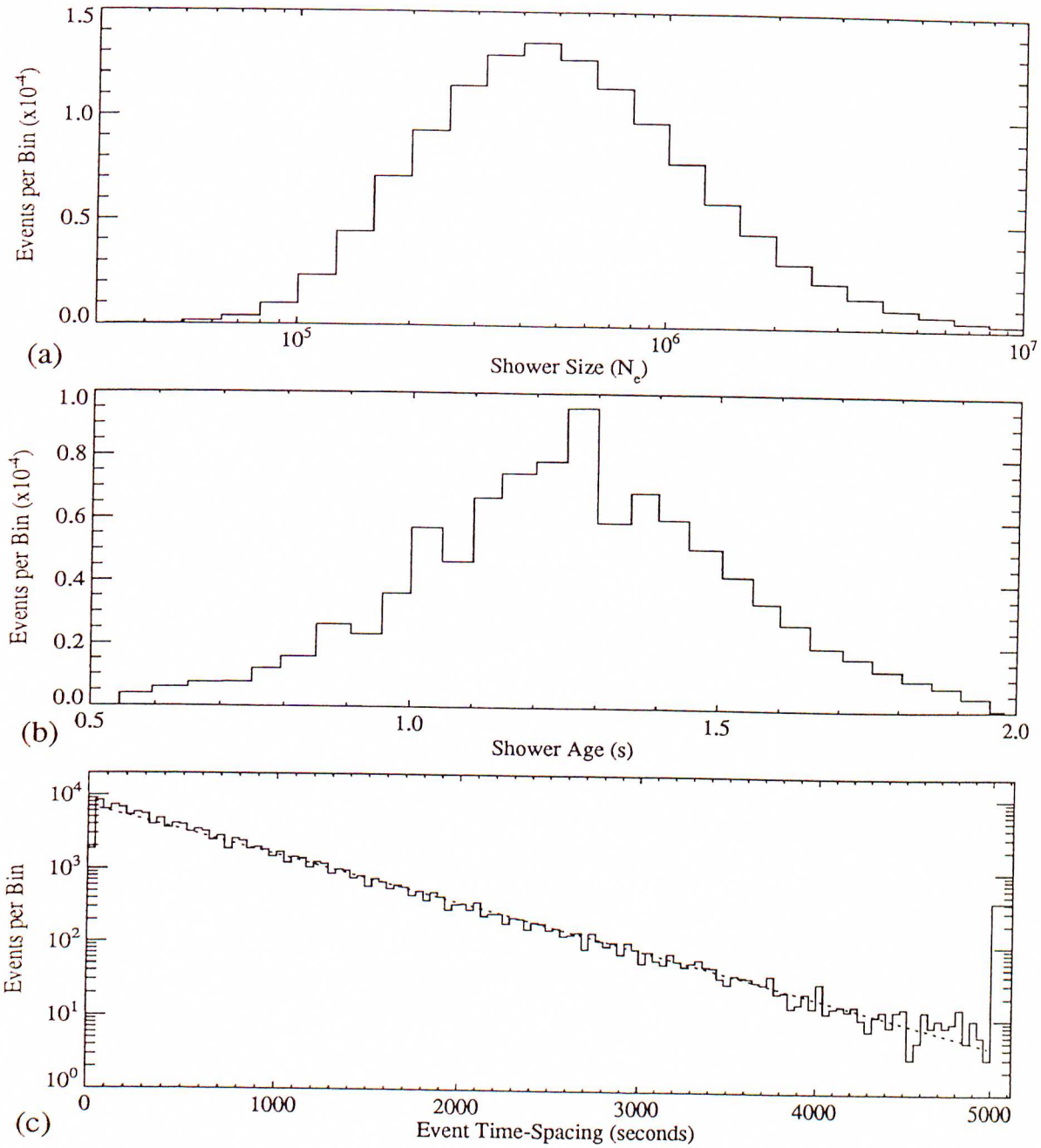

Figure 5.26: The shower parameter distributions, and event time-spacing distribution for the 1978–1981 data set.

(a) Shower Size.

(b) Shower Age.

(c) Event Time-Spacing Distribution (the last bin indicates event spacings in excess of 5000 seconds, and the dotted line is a line of best bit to the data below spacings of 5000 seconds and corresponds to a mean event spacing of 420 ± 7s, compatible with that derived by Gerhardy (1983) (418 ± 8s) for the 1979–1981 portion of the data).

considering the right ascension exposure for a given declination band (as discussed in 5.2.1).

As was the case with the 1984–1989 data set, in compiling these distributions, and in the subsequent anisotropy analysis, limits were applied to the shower parameters as follows:

$\sigma < 10$

$\chi^2 < 6$

$|x| < 60\text{m}$

$|y| < 60\text{m}$

$0.55 < s < 1.95$

where these parameters are as defined in 3.4, 5.2.2.

The application of these limits reduced the total number of events available for analysis, from the 164523 events triggered by the array over this period, to 124147 events (75% of the total).

The event time-spacing distribution of Fig 5.26(c) displays behaviour consistent with a 'random' arrival time distribution, indicating the suitability of these data for an anisotropy analysis. Based upon this distribution, a maximum event spacing of 4000 seconds was applied to these data, resulting in the resetting of the full sidereal day if violated. The application of full sidereal days resulted in the acceptance of 88790 events (54% of the total), covering 662 full sidereal days, at an average event rate of 134 events per day. The distribution of these days and the corresponding daily event rates are displayed in Fig 5.27.

Initially, the same size bins as considered in the 1984–1989 analysis (see Table 5.4) were applied to these data, with the corresponding mean primary energies being estimated using Fig 5.12, and are shown in Table 5.9.

Once these parameters had been determined, it was then possible to proceed with the anisotropy analysis.

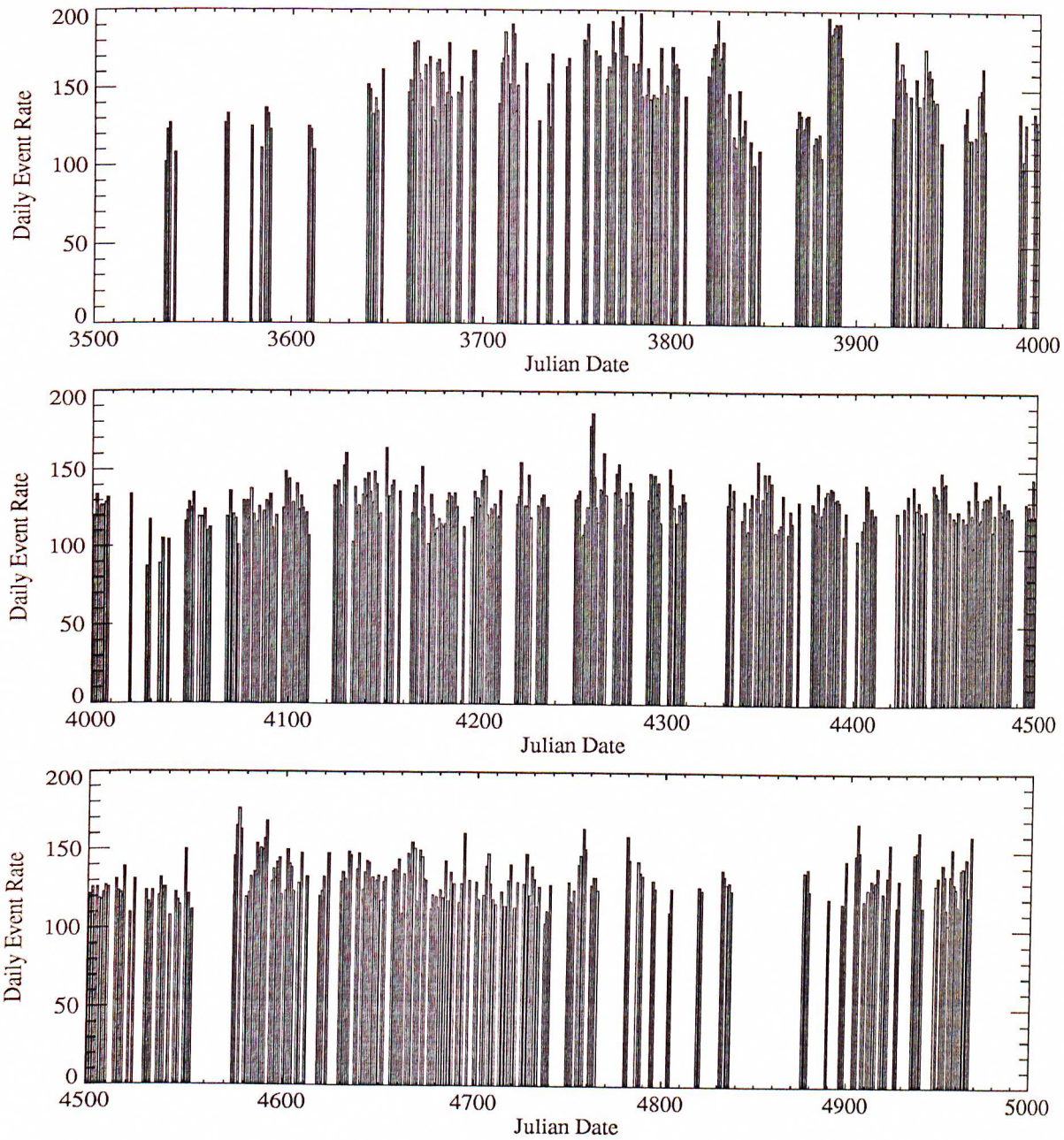

Figure 5.27: Array exposure in Full Sidereal Days for the 1978–1981 data set, and the corresponding analysed event rate (Julian dates quoted are 244 xxxx).

Label	Shower Size (particles)	Mean Shower Size	Mean Energy (eV)	Number of Events
3	$3 \times 10^4 - 10^5$	7.8×10^4	2.0×10^{15}	1848
4	$10^5 - 10^6$	3.5×10^5	6.0×10^{15}	75286
5	$10^6 - 10^7$	1.8×10^6	1.7×10^{16}	11625
6	$> 10^7$	1.2×10^7	1.0×10^{17}	31
Total Number of Events				88790

Table 5.9 : The shower size ranges considered in the analysis of the 1978–1981 data set and the corresponding mean shower sizes and primary particle energies, together with the total number of events contributing to the skymaps.

5.6.2 Anisotropy Analysis

The effect of atmospheric presure on the event rate of the 1978–1981 array had been previously investigated by Gerhardy (1983) who determined a coefficient of $-0.72 \pm 0.08\%$ mb^{-1}, and this was applied to the data. The atmospheric temperature effect determined by Gerhardy (1983) was consistent with a null effect. In both cases, the results are comparable to those coefficients determined in 5.2.3 for the 1984–1989 data set.

Solar weighting was initially calculated on a calendar yearly basis, and the first harmonic phase of this dependence was found to be consistently $\sim$ 10 hours U.T. Similarly, size bin weights were found to be consistent over the four year period in both amplitude and phase. No anomalous behaviour (as in the case of the 1984–1989 data; see 5.3.1) was found and the yearly solar maps were combined to form a four year average map from which the solar weightings to be applied were derived.

A weighted skymap for the four year period was thus produced, upon which harmonic analysis was applied. The results of this harmonic analysis appear in Table 5.10. All amplitudes determined were found to be consistent with a random distribution at the one sigma level. In spite of this, there is remarkable agreement of the first harmonic phases with those previously determined by other southern hemisphere experiments (including the 1984–1989 results) for both the overall result, and the individual size bins examined, as shown in Fig 5.28. A declination-type analysis, such as that discussed in 5.4.2 for the 1984–1989 data set was not attempted due to the relatively low number of events and the resulting poor statistics.

In addition to this analysis, the data were divided into the size bins used by Gerhardy (1983) in the anti-sidereal analysis of the 1979–1981 data, as shown in Table 5.11(a). Solar weighting was calculated for these shower size bins, and harmonic analysis applied to these data, with the results shown in Table 5.11(b). Comparing these results with those of Gerhardy (1983) (as shown in Table 5.6), there is excellent agreement in the results of the upper size bin in both first harmonic amplitude and phase. However, in the lower size bin, the previously determined value has a signifi-

Primary Energy (eV)	Number of Events	1^{st} Harmonic			2^{nd} Harmonic			Statistical Errors			
		s_1 (%)	θ_1 (hrs)	P_1 (%)	s_2 (%)	θ_2 (hrs)	P_2 (%)	σ_{rms} (%)	σ_r (%)	σ_{θ_1} (hrs)	σ_{θ_2} (hrs)
All	88790	0.59	11.3	46	0.63	3.1	25	0.67	0.48	3.1	1.2
2.0×10^{15}	1850	3.98	3.1	47	8.52	3.1	2	4.65	3.29	3.2	0.6
6.0×10^{15}	75287	0.58	11.3	53	0.56	3.4	33	0.73	0.52	3.4	1.3
1.7×10^{16}	11630	1.38	12.6	58	1.78	3.6	24	1.86	1.31	3.6	1.1

Table 5.10 : Summary of the results of the harmonic analysis on the 1978–1981 data set, including primary energy dependence.

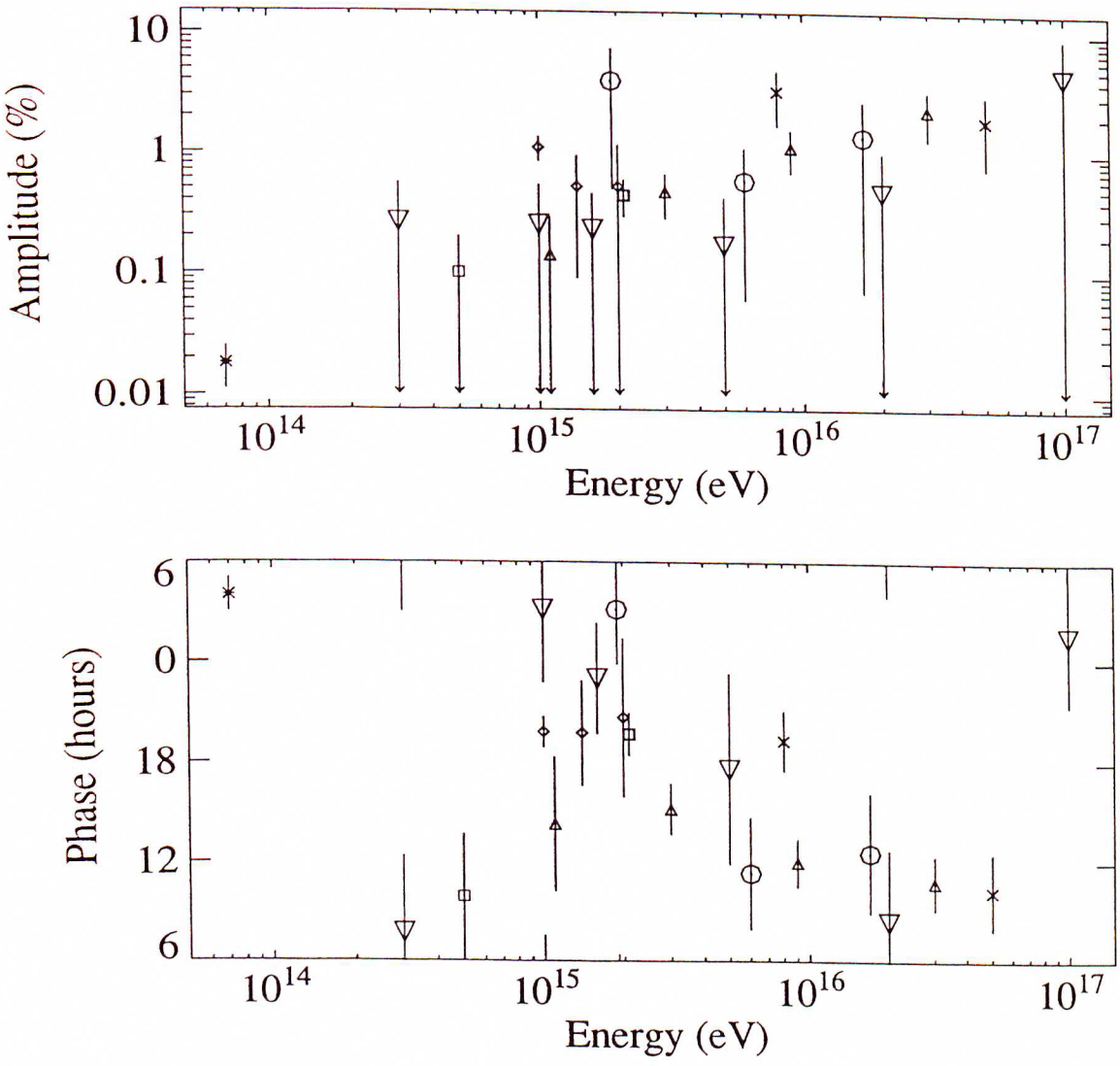

Figure 5.28: A comparison of the current results with previous southern hemisphere medium energy anisotropy measurements (first harmonic amplitude and phase). All errors and upper limits presented are at the one sigma level.

($\diamond$) Farley and Storey (1954)
($\triangle$) Farley and Storey (1957)
($\times$) Gerhardy and Clay (1983)
($\square$) Escobar *et al.* (1960)
($*$) Fenton *et al.* (1990)
($\triangledown$) 1984–1989 data
($\bigcirc$) 1978–1981 data

Shower Size (particles)	Mean Shower Size	Mean Energy (eV)	Number of Events
$5 \times 10^5 - 10^6$	6.9×10^5	6.0×10^{15}	27053
$> 10^6$	1.8×10^6	1.78×10^{16}	26188
Total Number of Events			53241

Table 5.11(a) : Shower size bins used by Gerhardy (1983) and the corresponding mean primary energy.

Primary Energy (eV)	Number of Events	1^{st} Harmonic			2^{nd} Harmonic			Statistical Errors			
		s_1 (%)	θ_1 (hrs)	P_1 (%)	s_2 (%)	θ_2 (hrs)	P_2 (%)	σ_{rms} (%)	σ_r (%)	σ_{θ_1} (hrs)	σ_{θ_2} (hrs)
6.9×10^{15}	27053	0.58	4.1	79	0.13	2.4	99	1.22	0.86	5.6	6.0
1.7×10^{16}	26188	1.36	11.2	18	1.66	11.9	10	1.23	0.87	2.1	1.0

Table 5.11(b) : Summary of the results of the harmonic analysis on the 1978–1981 data set using the shower size bins of Gerhardy (1983).

cant amplitude, whereas the new amplitude is consistent with a random distribution at the one sigma level. In spite of this, there is once again significant phase agreement at the one sigma level, which may be indicative of the presence of a real anisotropy with a first harmonic amplitude below that of the current statistical level. Once again, only improved statistics from an experiment with a much larger collecting area and/or longer time span of self-consistency[2] can resolve these uncertainties.

The 1978–1981 and 1984–1989 data sets essentially comprise the results of two different experiments, most notably in their respective shower size and azimuth angle exposures. It would therefore be inappropriate to combine these skymaps in order to examine the anisotropy of the primary cosmic ray flux in more detail, even in the case of selected shower size intervals.

In summary, it is interesting to note the consistent agreement in phase between the two experiments discussed here (and with other comparable southern hemisphere experiments), in spite of the majority of the first harmonic amplitudes being upper limits at the one or two sigma level. As has been previously stated several times, this may be indicative of the presence of a real anisotropy in the primary cosmic ray flux at these energies with an as yet undetermined amplitude, perhaps below that accessible by current experimental results. Whatever the case, these results remain somewhat puzzling.

In the following chapter, the emphasis shifts to the continuing search for southern hemisphere sources of U.H.E. γ-rays carried out at Buckland Park, based upon the 1988–1989 data set collected by the author.

[2]One of the major problems plaguing medium-high energy anisotropy work is that the E.A.S. arrays employed in these investigations are regularly upgraded as a result of the requirements of other concurrent investigations which, in general, significantly alter the characteristics of the array essentially ending that particular experiment. Ideally, arrays used for anisotropy work should be used primarily for this purpose thus ensuring self-consistency over a significant time-span. Unfortunately, this is rarely the case.

Chapter 6

A Search for Ultra-High-Energy Gamma-Ray Sources

6.1 Introduction

A discussion of and search for the sources of U.H.E. γ-rays is relevant to this thesis on a number of grounds. As has been previously discussed, γ-rays are not affected by the magnetic fields permeating the Galaxy, and their arrival directions will therefore not be randomised, but be a true indication of the direction of their source in the sky. It is for this reason that any anisotropies observed may, in part, be due to U.H.E. γ-rays, rather than an anisotropy in the cosmic ray charged particle flux. Previous investigations into the arrival directions of the 1984–1986 and 1986–1988 data sets by Edwards (1988) and Ciampa (1988) have focussed on searches for these sources, and as a matter of completeness, searches on the remainder of the 1984–1989 data set (March 1988 – May 1989) not previously attempted were considered necessary to complete the analysis of this data set (as discussed in Chapter 3). Furthermore, the recent explosion of SN1987A in the Large Magellanic Cloud has provided an unprecedented first-hand opportunity to study nature at its most energetic and, as supernovae are expected to contribute to the production of medium and high energy cosmic rays perhaps producing V.H.E. and U.H.E γ-rays as a signature of this acceleration of particles, a continual

monitoring of SN1987A and its remnant for a measurable flux of these U.H.E. γ-rays is vital.

Following is a brief discussion of these investigations and their results.

6.2 Sources

6.2.1 Introduction

The majority of sources considered possible candidates for the emission of U.H.E. γ-rays contain a compact body (usually a neutron star), which may either be isolated or, more commonly, be part of a binary system with a stellar companion, orbiting about a common centre of mass.

Such systems are known as X-ray Binary Systems, as they are identifiable sources of significant pulsed X-ray emission. In these systems, X-ray photons are emitted as the result of interactions between particles being accreted from the stellar companion by the compact body. This accretion may be driven by the stellar wind of the companion body, or may be the result of the stellar companion filling the majority of its Roche lobe, with matter passing through the inner Lagrangian point (see e.g. Nagle *et al.* 1988; Canal *et al.* 1990 for a discussion of X-ray binary systems).

Edwards (1988) examined the 1984–1986 data set for evidence for the emission of U.H.E. γ-rays from six X-ray binary systems with negative results (Edwards *et al.* 1989), and Ciampa (1988) examined the 1986–1988 data set (and partial re-analysis of the 1984–1986 data set) for evidence of U.H.E. γ-ray emission from eleven X-ray binary systems in the southern hemisphere, with evidence for the possible emission of U.H.E. γ-rays from three of these sources. In particular, one of these sources (2A 1822–37.1), which is believed to be similar in nature to the northern hemisphere source Cygnus X-3, displayed evidence of a complex behaviour (Ciampa *et al.* 1989), and the 1988–1989 data set was examined for evidence of U.H.E. γ-ray emission from this source as discussed in 6.2.5.

In addition to this system, an active galaxy, Centaurus A, has been examined for

evidence of possible U.H.E. γ-ray emission, based upon previous reports of excess events at U.H.E. energies from its direction (Clay *et al.* 1984a; Ciampa *et al.* 1988b), as well as the recent SN1987A, which is expected to be the site of high energy processes (see e.g. Gaisser *et al.* 1987, 1989a), and has been the subject of a number of previous searches in the earlier data sets of Buckland Park (Bird *et al.* 1987; Ciampa *et al.* 1988a; Bird *et al.* 1989).

Where possible, comparisons have been made with results from previous investigations, as well as the combination of previous results with those of the current investigation, in order to improve the statistical significance of the results.

Before the results of these searches are presented however, the methods of data analysis to be applied will be discussed.

6.2.2 Analysis Techniques

In searching for evidence of emission of U.H.E. γ-rays from a suspected source, two analysis techniques are commonly employed. The first of these involves searching the data for an excess of events from the source direction, compared to some average background number of events (a DC excess). The second technique relies on the detection of a periodic modulation of events, related to some characteristic of the source (e.g. the orbital period of an X-ray binary system), where this period has usually been previously determined by X-ray, optical, or radio observations. This technique is only applicable to those sources capable of such periodic emission, and will only be considered for the X-ray binary system 2A 1822–37.1 in the present investigation.

Search for a DC Excess of Events

A search for a DC excess of events is a search for a time-averaged excess of events from the direction of a candidate source, relative to an average, off-source background. It is obviously most suited to the search for a source expected to be continuously emitting U.H.E. γ-rays over a significant period of time.

Such an analysis is very dependent upon the angular resolution to be applied in the

search. The angular search region needs to be sufficiently large to contain the majority of events from the source direction, but also sufficiently small to prevent the swamping of source events by background events. For each source considered in this investigation, the appropriate angular resolution and its determination are discussed individually.

The significance of a measured DC excess may be described by either a Poisson distribution in terms of the number of standard deviations (Δ), as defined in Eq 5.4 or, more correctly, by the maximum likelihood method, which allows for the uncertainty in the background estimate (see Nagle *et al.* 1988 for a discussion). The maximum likelihood statistic, λ, is given by

$$\lambda = \left\{ \frac{\xi}{(1+\xi)} \frac{(N_{on} + N_{off})}{N_{on}} \right\}^{N_{on}} \left\{ \frac{1}{(1+\xi)} \frac{(N_{on} + N_{off})}{N_{off}} \right\}^{N_{off}} \qquad (6.1)$$

(Li and Ma 1983)

where N_{on} = number of on-source events,

N_{off} = number of off-source events

ξ = ratio of on-source to off-source exposure.

Related to this statistic, $-2 \ln \lambda$ is distributed as $\chi^2(1)$, and the significance of the excess is equivalent to $\sqrt{-2 \ln \lambda}$ standard deviations. It is this statistic which will be employed in the DC searches discussed in 6.2.3 & 6.2.4.

Periodic Searches

The X-ray binary system under investigation (2A 1822–37.1) has a characteristic periodicity associated with its emitted radiation (as measured at X-ray and radio wavelengths). This allows the application of a more powerful test for evidence of U.H.E. γ-ray emission, by searching for the periodic modulation of events from the direction of this source.

In this search, no comparisons are made with background events, implying an independence from any DC search carried out. All of the events under consideration were initially re-analysed to take into account shower-front curvature and timing uncertainties, as discussed in 3.3.2.

Given a source period P_o, at a given epoch T_o, with associated period time derivative $\dot{P}$, the phase ϕ_i corresponding to arrival time t_i (corrected to the solar system barycentre) may be calculated using

$$\phi_i = \frac{t_i - T_o}{P_o} - \frac{1}{2}\dot{P}\left(\frac{t_i - T_o}{P_o}\right)^2 - n \tag{6.2}$$

where n is an integer suitably chosen to ensure $0 \leq \phi_i < 1$.

In previous observations of U.H.E. γ-ray emission from X-ray binary systems, modulated by the orbital period of these systems, the emission has been found to occur in general over a narrow range in phase (typically ≤ 0.05) (see e.g. Lloyd-Evans *et al.* 1983; Protheroe *et al.* 1984). It is therefore appropriate to apply a circular statistic sensitive to such narrow emission phases when testing the uniformity of the phase distributions. Two commonly applied statistics are the Protheroe statistic Υ_n (Protheroe 1985), and the Z^2_{10} test of the Z^2_n family of statistics, a generalisation of the Rayleigh test (Z^2_1) to include second and higher order harmonics (Buccheri and Sacco 1985) (c.f. Eq 4.9).

The Z^2_n statistic is defined by

$$Z^2_n = \frac{2}{N}\sum_{k=1}^{n}\left\{\left(\sum_{j=1}^{N}\cos 2\pi k\phi_j\right)^2 + \left(\sum_{j=1}^{N}\sin 2\pi k\phi_j\right)^2\right\} \tag{6.3}$$

where N is the number of on-source events under consideration.

The Z^2_n statistic has the advantage over the Protheroe test in that its probability level is well-known for $N \geq 100$[1], being distributed as $\chi^2(2n)$, whereas the latter is not well-known for $N > 200$, requiring CPU-intensive Monte Carlo simulations for determination. The Protheroe test is more applicable to smaller data sets, such as the analysis of the 1979–1981 data set for U.H.E. γ-ray sources carried out by Protheroe and Clay (1985). Consequently, the Z^2_{10} test was chosen to be used in the periodic search to be carried out, as was the case with the searches of Edwards *et al.* (1989) and Ciampa (1988).

[1]For $N < 100$, the probability levels of the Z^2_n test can be calculated as determined by the work of de Jaeger (1987).

The initial application of circular statistics avoids the problems associated with the initial use of phase histograms (phaseograms) in determining significances, as problems result when binning the data, through the number of alternatives available when choosing the appropriate bin widths and origin. However, phaseograms can still be useful in determining the preferred phases of emission (as discussed in 6.2.5), once a significance has been determined.

The first two sources to be discussed (SN1987A and Centaurus A) were both examined only for a DC excess due to the lack of any significant observed periodic emission at any wavelength.

6.2.3 SN1987A

The first naked eye supernova since the invention of the telescope was discovered by Shelton (1987) on February 24th, 1987 (U.T.), in the Large Magellanic Cloud. SN1987A[2] resulted from the collapse of the blue supergiant Sanduleak -69° 202 (White and Malin 1987) to form a neutron star (Burrows 1988), and both the initial light curve and progenitor mass ($\sim$ 15–20 $M_{\odot}$) were indicative of a type II supernova. However, blue supergiants had not previously been considered candidates for type II supernovae. This required revision of the conventional models to take into account the relatively low metallicity of the stellar population of the Large Magellanic Cloud (see e.g. Schramm and Truran 1990).

Such stellar collapses are expected to release $\sim 10^{51}$ ergs of gravitational energy (Woosley and Weaver 1986), along with $\sim 10^{53}$ ergs in a burst of neutrinos at the time of stellar collapse (Shapiro and Silberberg 1979). These neutrinos are expected to arrive several hours prior to the optical outburst, as the latter is expected to be delayed until the shock breaks through the photosphere (Shapiro and Silberberg 1979).

A search for a neutrino burst amongst suitable detectors revealed two such bursts

[2]The IAU convention for supernovae naming is capital letter suffixes, whilst comets are labelled with lower case suffixes (Olsson-Steel 1987).

prior to the optical detection of SN1987A. The Kamiokande-II group (Hirata *et al.* 1987), and the IMB group (Bionta *et al.* 1987), both operating underground proton decay experiments detected a coincident burst of neutrinos, lasting for $\sim$ 10 seconds, during February 23rd, 1987 (U.T.), initiating the new field of extra-galactic neutrino astronomy. Several hours prior to this burst, a detector located beneath Mt. Blanc recorded another burst of neutrinos (Aglietta *et al.* 1987). However, the failure of the Kamiokande-II experiment, operating at a comparable energy threshold, to detect this burst, and the energy requirements implied by this burst have lead to the conclusion that this burst may be spurious (see e.g. Arnett *et al.* 1989).

Subsequent to these reports, observations by ground, balloon and space-based observatories at all wavelengths from the radio through to γ-rays have been carried out in order to study the evolution of the supernova remnant (SNR) of this explosion. These observations have been summarised in numerous reviews (e.g. Cannon 1990; Arnett *et al.* 1989; Dopita 1988).

Apart from the confirmation of the occurrence of nucleosynthesis within SN1987A through the detection of γ-rays produced by the decay of Cobalt 56 (see e.g. Kumagi *et al.* 1989 and references therein), one of the major points of interest of the SNR, is whether a pulsar will be observed within the remnant. It has long been believed that neutron stars (pulsars) are born with the occurrence of type II supernovae (Baade and Zwicky 1934a, 1934b). The infamous 'discovery' of the sub-millisecond optical pulsar within the remnant by Kristian *et al.* (1989), and the subsequent controversy generated, followed by the retraction of the claim[3], which was found to be due to electrical interference generated by a video camera, highlights the interest in this topic.

As pulsars are leading candidates for the source of high energy cosmic rays (see e.g. Chapter 1; Trimble 1983 for a review), the birth of a neutron star is viewed with considerable interest. Several theories predict the likely turn-on of U.H.E. γ-ray emission shortly after the initial collapse of a type II supernova, and the production and possible emission of this radiation will now be discussed.

[3]see *Nature*, **343**, 79, (1990)

U.H.E. γ-ray Production

It has been suggested that at energies above $\sim 10^{15}$eV, the shock acceleration of cosmic rays is no longer a valid process. One possible replacement candidate is a rapidly rotating neutron star either isolated, or as part of a binary system. Previous work on the production of high energy particles by a young supernova remnant (e.g. Sato 1977; Berezinsky and Prilutsky 1978; Shapiro and Silberberg 1979) has been supplemented by a series of more recent calculations, initiated by the occurrence of SN1987A (e.g. Gaisser *et al.* 1987; Berezinsky and Ginzburg 1987; Honda and Mori 1987; Storey *et al.* 1987; Yamada *et al.* 1988; Gaisser *et al.* 1989a).

These models propose that particle acceleration takes place via either the energy loss associated with a rapidly rotating magnetised neutron star created by the supernova event, or by first order Fermi acceleration associated with the shock wave resulting from the stellar core collapse. In general, it is assumed that cosmic ray particles accelerated to energies $\geq 10^{17}$eV subsequently interact with some target material to produce U.H.E. γ-rays with energies $\geq 10^{15}$eV. This target material is most likely to be the shell of matter surrounding the SNR, which consists of the ejecta of the supernova shock wave.

In a recent review, Kifune (1990) outlined two different views in estimating the emission of these γ-rays as a function of time after the explosion. To produce these γ-rays (through the creation and subsequent demise of π° mesons) it is necessary for the accelerated protons to interact with the dense material of the ejecta, as discussed above. If it is assumed that the accelerated protons travel directly to this matter, then the predicted U.H.E. γ-ray flux would be expected to peak approximately six months to one year after the explosion (e.g. Yamada *et al.* 1988). This occurs when the column density of the target matter is still dense enough to allow a sufficient number of proton-proton interactions to occur, but is thin enough to allow the γ-rays thus produced to escape from their production region without suffering significant absorption. Alternatively, if there is a delay in this mixing, resulting perhaps from the confinement of these particles in a cavity formed by the pulsar wind within the inner radius of the expanding ejecta, the emission of γ-rays may be significantly delayed,

depending upon the degree of mixing, peaking between 2 and 6–8 years after the initial explosion (e.g. Gaisser *et al.* 1989a).

Photon-photon interactions are also believed to play an important role in the absorption of γ-rays in their production region, but this effect is believed to be most important at V.H.E. energies (Protheroe 1987c). At U.H.E. energies, a delay in emission is more likely to result from a delay in the onset of particle production. Estimates for the time-scale over which the emission of these energetic γ-rays will begin range from $\sim$ 1 month after the explosion (e.g. Sato 1977; Shapiro and Silberberg 1979), through to several years (e.g. Gaisser *et al.* 1987, 1989a).

In general, the predicted γ-ray spectra are quite similar for the different models being considered, and typically consist of a power law spectrum with a differential index of $\gamma \sim -2$. Observations made at the earth need to be corrected for the absorption feature expected due to the interactions of γ-rays with the universal microwave background radiation. The depth of this absorption at $\sim 10^{15}$eV is determined by both the distance to the supernova ($\sim$ 50 kpc), and the type of interaction processes involved (most notably if cascading occurs in the microwave background — see Protheroe 1986).

Previous U.H.E. γ-ray Observations

At the time of explosion, Buckland Park was the only E.A.S. array suitably situated for the detection of U.H.E. γ-ray emission from SN1987A. A search was carried out for a burst of events perhaps associated with the emission of U.H.E. γ-rays at the same time as the reported neutrino bursts (Bird *et al.* 1987). At these times, the array had corresponding energy thresholds for SN1987A of $\sim 5\times10^{16}$eV and $\sim 2\times10^{15}$eV, and no evidence was found for a burst of E.A.S. events coincident with (or around the time of) either of the neutrino bursts (Bird *et al.* 1987). Corresponding upper limits to the amount of energy radiated in prompt U.H.E. γ-rays of 2×10^{45} and 4×10^{43} ergs respectively were calculated, assuming a distance of $\sim$ 50 kpc.

In addition to this investigation, searches were also carried out on the first six months (Ciampa *et al.* 1988a) and the first twelve months (Bird *et al.* 1989) following

the supernova explosion for evidence of both the continuous and/or sporadic emission of U.H.E. γ-rays. No such evidence was found for the emission of U.H.E. γ-rays over this period (Ciampa *et al.* 1988a; Bird *et al.* 1989).

The occurrence of SN1987A initiated the construction of a purpose-built E.A.S. array at Black Birch in New Zealand, known as the JANZOS (Japan Australia New Zealand Observations of Supernova 1987A) array (Bond *et al.* 1988a). This location is more suited to carry out V.H.E./U.H.E. observations of SN1987A due to its more southerly position (41.8°S, c.f. 34.6°S for Buckland Park) and higher altitude (1640m c.f. $\sim$ sea-level). This array began observations in October 1987. More recently, the SPASE (South Pole Air Shower Experiment) array (Hillas 1989), located in an even more favourable position at the south pole has come on-line, and has also contributed to V.H.E./U.H.E. investigations of SN1987A (e.g. Gaisser *et al.* 1990).

Numerous upper limits from V.H.E. (e.g. Chadwick *et al.* 1988; Raubenheimer *et al.* 1988; Elton 1989; Gaisser *et al.* 1989b; Bond *et al.* 1989, 1990a), and U.H.E. (e.g. Bond *et al.* 1988a; Ciampa *et al.* 1988; Bird *et al.* 1989; Bond *et al.* 1990b) γ-ray observations have been reported, and the more recent upper limits have been summarised by Kifune (1990). The only possible positive detection to date at these energies is a burst of TeV γ-ray emission reported by the JANZOS collaboration (Bond *et al.* 1988b) on the nights of January 14 and 15, 1988. Assuming this burst was genuine, the combined integral flux of this burst corresponded to $(1.9 \pm 0.5) \times 10^{-11} \gamma$ cm^{-1}s^{-1} above an energy threshold of $\sim$ 3 TeV (Bond *et al.* 1988b), implying a particle luminosity during the burst of $L_p \geq 2 \times 10^{39}$ ergs s^{-1} (Berezinsky and Stanev 1989).

A search of the Buckland Park data during this time revealed evidence to suggest that a burst-like effect may have been detected from the direction of SN1987A at U.H.E. energies at the time of this reported V.H.E. γ-ray burst, with the majority of these events possessing unusually high zenith angles, in comparison to the overall zenith angle distribution of events from the direction of SN1987A (Ciampa and Clay 1989). This burst was also found to coincide with an X-ray flare detected by the Ginga X-ray satellite (Tanaka 1989), supporting the overall claim.

Several explanations have been proposed for this burst, relating it to either the collision of accelerated protons with a denser cloud in the surrounding circumstellar matter, resulting in the eventual emission of V.H.E. γ-rays (Honda *et al.* 1989, 1990), or to the continuous acceleration of cosmic ray particles resulting from pulsar activity. In this scenario, Berezinsky and Stanev (1989, 1990) proposed that the energetic protons accelerated by the supernova shock are somehow stored before they diffuse outward into a particularly dense region in the surrounding ejecta material.

Interest in SN1987A remains high in view of the report by Bouchet *et al.* (1989) that the bolometric light curve of SN1987A displays a flattening at $\sim 10^{38}$ ergs s^{-1}, which may be most easily explained by the emergence of pulsar activity within the SNR (Kifune 1990).

Kifune (1990) has derived an upper limit of V.H.E. and U.H.E. γ-ray emission from SN1987A of $L_\gamma < 2 \times 10^{37}$ ergs s^{-1} for energies $10^{11}eV < E < 10^{17}eV$, based upon the observations reported to January 1990. Kifune (1990) also noted that the inferred possible pulsar activity is larger than this upper limit, but smaller than the resulting cosmic ray luminosity ($L_p \sim 10^{39}$ ergs s^{-1}), and emphasises the necessity of continued monitoring of SN1987A.

Following is a discussion of the search for U.H.E. γ-ray emission from the direction of SN1987A, carried out at Buckland Park during months 13–27 after the initial explosion.

Present U.H.E. γ-ray Observations

The observing period under consideration in this investigation encompasses the second year of the SNR, and a portion of the third (March 1988 – May 1989). These data were examined for evidence of both a continuous U.H.E. γ-ray flux, and sporadic bursts of U.H.E. γ-ray emission. No attempt was made to search for evidence of periodic emission due to the lack of a known (or suspected) period (and period derivative), which would be essential for such a search, in light of the relatively small on-source event rate of 1.15 events per day (see below).

As discussed in some detail by Ciampa (1988), the appropriate angular resolution for

this search consists of a cone with a half-angle of 2°, making suitable allowance for the zenith angle of observation. This leads to an elliptical search region with semi-major and semi-minor axes $2° \sec\theta$ and 2° respectively (Ciampa 1988). The shower-front curvature correction of Ciampa (1988) was not applied to these data, as such a fit is more uncertain than the planar shower-front fit (see 3.3.2), due to the large zenith angles involved in observing SN1987A ($\theta > 30°$) (Ciampa 1988) which result in the fore-shortening of the array in the north-south direction, increasing the uncertainty in E.A.S. direction estimates.

The results of this search for excess events from the direction of SN1987A (R.A.: 5^{hr} 35' 49.4"±0.039"; δ: -69° 17' 57.9"±0.27" (B1950.0) — White and Malin 1987) over months 13–27 of the SNR are summarised in Table 6.1(a) for both the individual calendar months and the entire period in question. The background number of events used for comparison were estimated by considering 23 identical off-source regions at the same declination as SN1987A, but spaced at intervals of one hour in right ascension. In order to maintain a uniform exposure in sidereal time, therefore eliminating the introduction of any on-time biases into these data, only full sidereal days of data were considered (as discussed in 5.2.1). This resulted in a useful exposure of 191 sidereal days during this period. No significant excess was observed during any particular calendar month, or over the entire period under investigation. The 95% upper limits to the number of γ-rays have also been calculated, using the method of Protheroe (1984b), and appear in Table 6.1(a).

In addition to these results, the daily on-source event rates were examined for a deviation from that distribution expected randomly (described by a Poisson distribution — see e.g. Bevington 1969), with a mean of 1.15 events per day (the on-source event rate). These data appear in Fig 6.1, with the appropriate on-source (and off-source) Poisson distributions superimposed. Five and six events per day were each recorded once over the period in question, with corresponding chance probabilities of $\sim 4 \times 10^{-3}$ and $\sim 8 \times 10^{-4}$ respectively of occurring on any given day. Considering that 191 days of data were examined, the probabilities of these daily event rates being recorded over

Julian Date (−244 0000)[a]	Full Sidereal Days	Observed Events	Expected Background[b]	95% Upper Limit[c]
7232–7254	14	18	13.1	14.1
7254–7283	20	21	20.7	12.1
7284–7315	11	15	11.4	12.5
7316–7345	17	19	18.0	11.9
7345–7376	19	17	20.6	9.1
7376–7407	19	23	20.3	14.2
7408–7419	9	8	10.3	6.7
7439–7467	16	17	20.1	9.0
7469–7497	16	25	20.1	15.7
7498–7529	17	19	19.9	10.5
7529–7559	15	16	14.2	11.7
7560–7570	4	5	4.7	6.3
7636–7647	8	10	9.2	8.6
7649–7663	6	7	7.3	7.4
7232–7663	191	220	210.0	39.1

Table 6.1 (a) : The number of observed and expected events from the direction of SN1987A in monthly intervals over the period March 1988 to May 1989. Events are from an elliptical search region with semi-major and semi-minor axes $2° \sec\theta$ and $2°$ respectively.

Julian Date (−244 0000)[a]	Full Sidereal Days	Observed Events	Expected Background[b]	95% Upper Limit[c]
6850–7221[d]	351.8[e]	387	416.1	30.6
7232–7663	191	220	210.1	39.1
6850–7663	542.8[e]	607	626.1	42.5

Table 6.1 (b): Summary of the SN1987A analysis at Buckland Park over the first 27 months of SN1987A (1987–1988 data from Bird *et al.* 1989).

a – The break between days 7570 and 7636 was due to a computer malfunction.

b – The background events were calculated from 23 off-source regions spaced at 1 hour intervals of right ascension at an identical declination to that of SN1987A.

c – The 95% upper limits for the number of γ-rays were calculated using the method of Protheroe (1984).

d – Data from Bird *et al.* (1989).

e – The results of Bird *et al.* (1989) were time-averaged rather than sampled from full sidereal days.

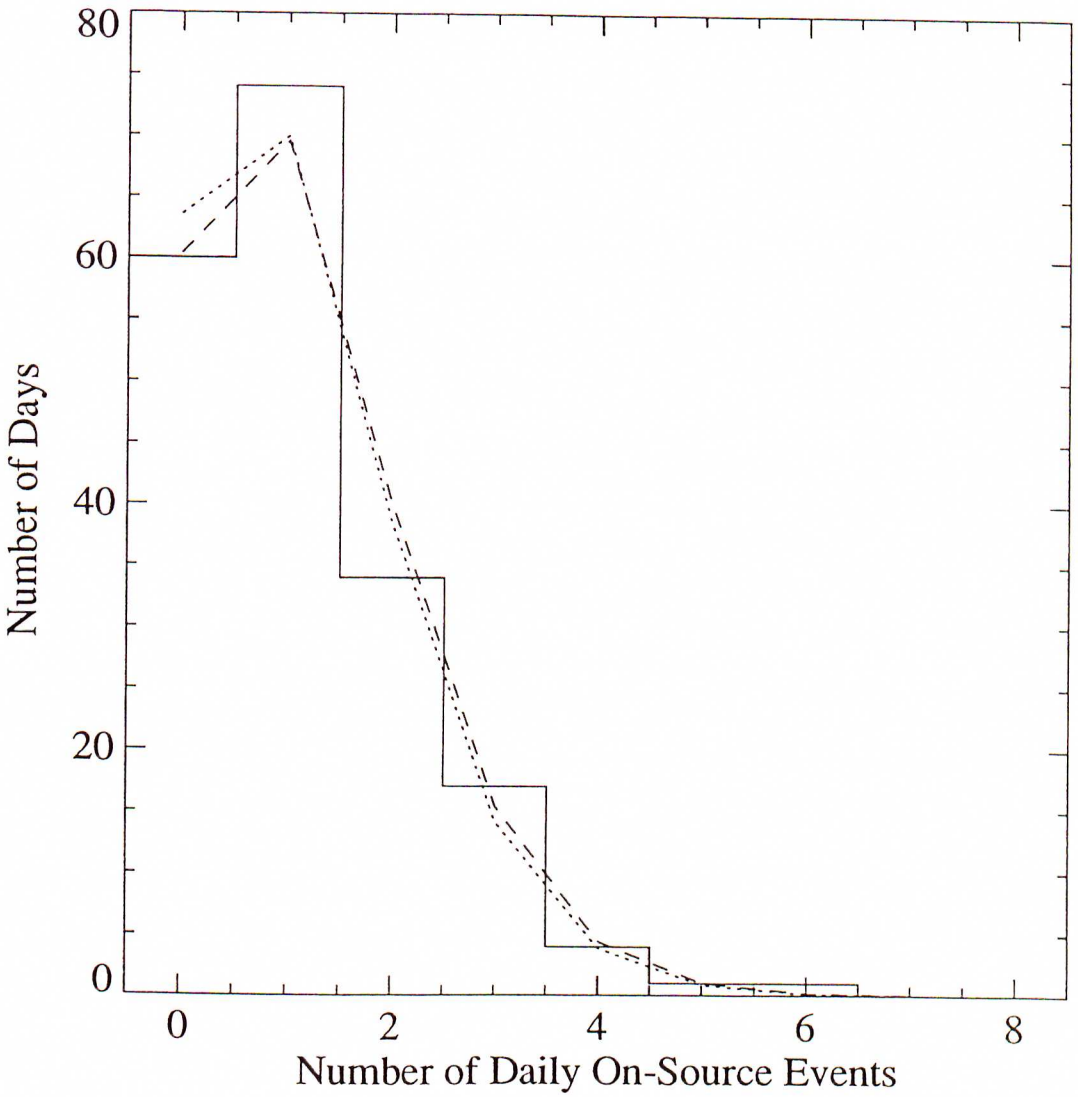

Figure 6.1: The distribution of daily on-source events for SN1987A during the period March 1988 to May 1989. The dashed and dotted lines indicate the predicted distribution from Poisson statistics for the on-source and background event rates of 1.15 and 1.10 events per day respectively.

this period are 85% and 15% respectively. These results are therefore not considered significant, and it is concluded that there is no evidence for the sporadic emission of U.H.E. γ-rays from the direction of SN1987A.

The results of the present investigation are combined with those of Ciampa (1988) in Table 6.1(b). Overall, there is no evidence for the emission of U.H.E. γ-rays during the first twenty-seven months of the SNR of SN1987A. In addition, the corresponding 95% upper limit to the number of U.H.E. γ-rays has not increased in proportion to the increase in exposure, further confirming the lack of any evidence for U.H.E. γ-ray emission within these data.

Expected Number of U.H.E. γ-ray Events

In order to estimate the number of U.H.E. γ-rays expected from SN1987A, based upon the models of Gaisser *et al.* (1987) and Storey *et al.* (1987), it was first necessary to estimate the effective 'exposure time' of the array to SN1987A, and the predicted form of the γ-ray spectrum. These calculations were carried out by Ciampa *et al.* (1988a) for a period of $\sim$ 200 days, and these results will be applied to the results of the 1988–1989 data set, which contains a comparable period of observation (see Fig 6.2; Ciampa *et al.* 1988a).

The expected number of U.H.E. γ-ray events based upon these models for both the 1988–1989 data set, and for the overall period of observation from the time of the explosion to May 1989, based upon these models are presented in Table 6.2, for both cascading and no cascading in the microwave background (see Protheroe 1986 for a discussion of these processes).

In the calculations of Gaisser *et al.* (1987), and Yamada *et al.* (1988), it was assumed that the maximum energy to which the protons in the vicinity of the supernova are accelerated is $\sim 10^{17}$eV. This implies an upper limit of $\sim 5\times10^{15}$eV in the production of U.H.E. γ-rays (see Fig 6.2), which is crucial for the comparison of observations, in light of the significant sensitivity of the Buckland Park E.A.S. Array to U.H.E. γ-rays above this energy (most notably above the absorption peak). The model of Storey *et al.*

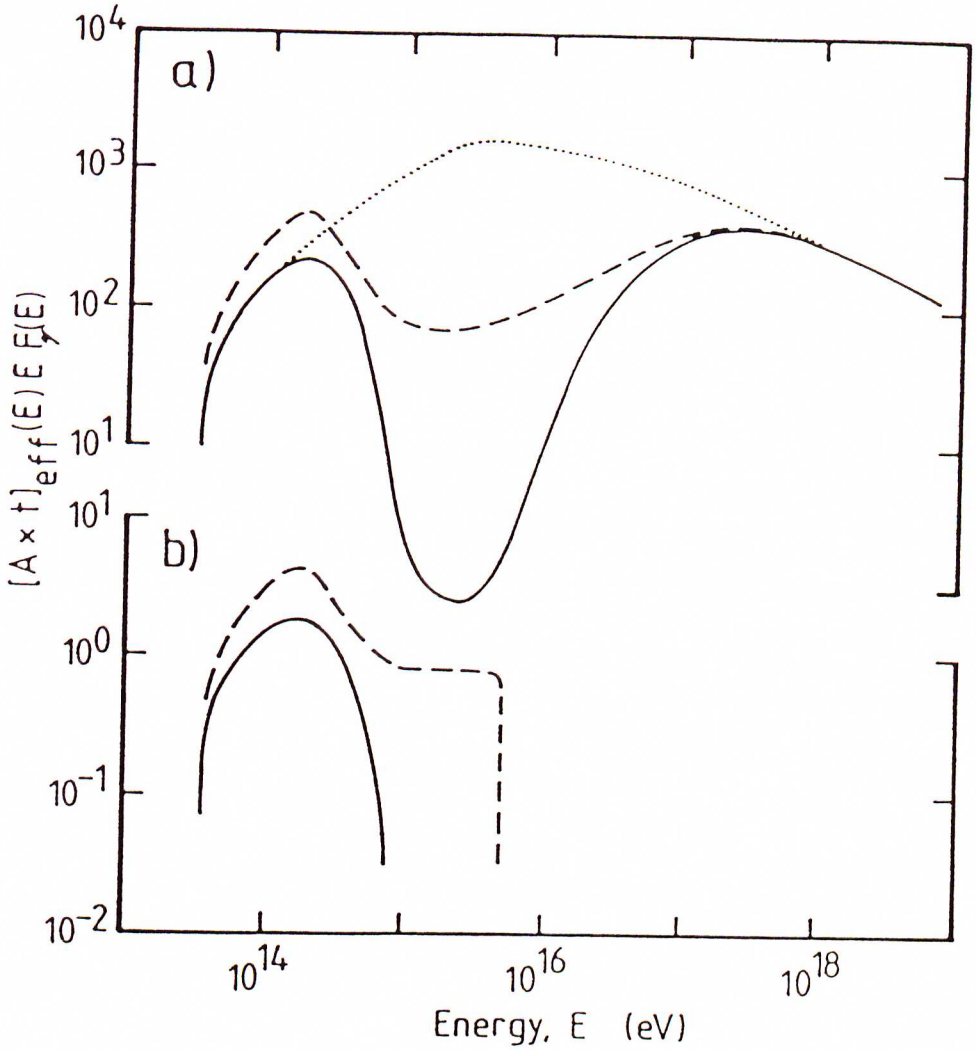

Figure 6.2: The spectrum of γ-ray events from SN1987A expected to have been observed over the period in question as predicted by the models of **(a)** Storey *et al.* (1987), and **(b)** Gaisser *et al.* (1987). The solid lines correspond to no cascading in the microwave background, and the dashed lines to cascading (see Protheroe (1986) for details of these processes). In (a), the dotted line indicates the spectrum which would have been observed had there been no attenuation in the microwave background (from Ciampa *et al.* 1988a).

	Model			
	Gaisser *et al.* (1987)		Storey *et al.* (1987)	
Case	Predicted Events[a]	95% Upper Limit L_p (ergs s^{-1})	Predicted Events[b]	95% Upper Limit F_γ/Cyg X-3
No Cascading	2.3	9.6×10^{40}	1.5×10^3	14.5
Cascading	7.0	3.3×10^{40}	2.1×10^3	10.5

Table 6.2 (a) : The predicted number of γ-ray events and the corresponding upper limits to the proton luminosity calculated for the observations of SN1987A, derived from the 1988–1989 data set.

	Model			
	Gaisser *et al.* (1987)		Storey *et al.* (1987)	
Case	Predicted Events[a]	95% Upper Limit L_p (ergs s^{-1})	Predicted Events[b]	95% Upper Limit F_γ/Cyg X-3
No Cascading	6.3	6.4×10^{40}	4.2×10^3	9.4
Cascading	18.8	2.2×10^{40}	5.8×10^3	6.9

Table 6.2 (b): The predicted number of γ-ray events and the corresponding upper limits to the proton luminosity calculated for the observations of SN1987A, calculated for the overall observations by the 'old' Buckland Park E.A.S. array (1987–1989). (1987–1988 data from Bird *et al.* 1989).

---

a – For an assumed proton luminosity of $L_p \sim 10^{40}$ ergs s^{-1}.

b – For an unattenuated flux of 10^3 times that from Cygnus X-3, with a spectrum extending to the highest energies.

(1987) highlights this fact, with only 25% of the expected events being due to γ-rays below the absorption feature, whereas in the former model, the majority (if not all) of these γ-rays will be below the absorption feature (see Fig 6.2).

In agreement with those results previously determined by Ciampa *et al.* (1988a) and Bird *et al.* (1989), the upper limits derived from the current observations continue to rule out fluxes as high as those suggested by Storey *et al.* (1987), regardless of whether or not cascading occurs in the microwave background. The source flux assumed in this model is 10^3 times that of Cygnus X-3, based upon the suspected pulsar period of the SNR. Corresponding upper limits to this flux have been calculated and appear in Table 6.2.

In the model of Gaisser *et al.* (1987), it is assumed that 10^{40} ergs s^{-1} is injected into protons with energies in the range 10^9eV - 10^{17}eV. The predicted number of U.H.E. γ-rays based upon this model remains consistent with the upper limits derived from the Buckland Park observations (Ciampa *et al.* 1988a; Bird *et al.* 1989), regardless of whether or not cascading occurs in the microwave background. In general, the predictions of the model of Yamada *et al.* (1988) are similar to those of Gaisser *et al.* (1987), with the exception of a higher assumed proton luminosity of 10^{41} erg s^{-1} in the former model. It is also important to note that, due to the sensitivity of the Buckland Park E.A.S. Array to U.H.E. γ-ray events above the absorption feature, if the supernova accelerates cosmic rays to energies well above 10^{17}eV, the upper limits quoted for the model of Gaisser *et al.* (1987) become more stringent.

From the derived proton luminosity upper limits of the Gaisser *et al.* (1987) model, the corresponding 95% upper limits to the γ-ray flux from SN1987A above 10^{14}eV were calculated to be $\sim 1.4 \times 10^{-11}$ $cm^{-2}s^{-1}$ and $\sim 9.5 \times 10^{-12}$ $cm^{-2}s^{-1}$ for the cases of no cascading and cascading respectively, for the 1987–1989 data. These results are consistent with those upper limits previously determined by other experiments, as summarised in the compilation of Kifune (1990), and are $\sim$ 25% lower than those obtained by Ciampa *et al.* (1988a) and Bird *et al.* (1989).

Summary

A search for U.H.E. γ-ray emission over the first 27 months of SN1987A has failed to find evidence for either bursts or a continuous flux of U.H.E. γ-rays. The 95% upper limits obtained are consistent with other observations (see Kifune 1990 and references therein). The suggestion of Ciampa *et al.* (1988a), that either the assumed proton luminosities are too high, or that U.H.E. γ-rays are not yet emerging from the shell of matter surrounding the supernova remains valid in light of these more recent results. Continued monitoring of SN1987A and its remnant remains a necessity in order to further test the various models proposed.

6.2.4 Centaurus A

Centaurus A (NGC 5128) is the closest active galaxy to our own, at a distance of $\sim$ 5 Mpc (estimates range from 3 to 8.5 Mpc — see the review by Ebneter and Balick 1983). It is the closest and brightest elliptical galaxy, and possesses extended radio lobes, which imply the ejection of energetic material from the nucleus. Centaurus A was the first extra-galactic X-ray source detected (Bowyer *et al.* 1970), and was also amongst the first V.H.E. γ-ray sources to be identified (Grindlay *et al.* 1975). For these reasons, Centaurus A is considered a prime candidate source for the emission of V.H.E. and U.H.E. γ-rays. The detection of any such emission has important astrophysical implications, as it is expected that these extra-galactic U.H.E. γ-rays should be severely attenuated through interactions with the 3K microwave background (interaction length $\leq$ 10 kpc at $\sim 10^{15}$eV — see e.g. Rana and Wolfendale 1984; Protheroe 1986).

The most recent V.H.E. observations of Centaurus A are those of the JANZOS (Bond *et al.* 1990c), Narrabri (Brazier *et al.* 1990), and Woomera (Gregory *et al.* 1990) groups, who all failed to find any significant excess of events from the direction of Centaurus A at energies E > 300 GeV (> 1 TeV for the JANZOS result), using the atmospheric Cerenkov technique. Brazier *et al.* (1990) suggest that the lack of a signal may be the result of a quiescence of the high energy source in Centaurus A during the

period of observation, noted also in the X-ray (see Brazier *et al.* 1990 and references therein), and that the observation of Grindlay *et al.* (1975) may have coincided with an active period of the X-ray source within Centaurus A, which is believed to also be the source region of V.H.E. γ-ray emission (Grindlay 1975).

U.H.E. γ-ray Observations

Previous searches carried out for the detection of U.H.E. γ-rays by the Buckland Park E.A.S. Array (Clay *et al.* 1984a; Ciampa *et al.* 1988b) consistently show some evidence for U.H.E. γ-ray emission in the direction of Centaurus A.

The earlier of these searches (Clay *et al.* 1984a) was based upon the 1979–1981 data set of Gerhardy (1983). Examination of this data set for small-scale effects revealed a 2.7σ DC excess in the general direction of Centaurus A, and these excess events were found to be prominent in the size range $2 \times 10^5 < N_e < 5 \times 10^5$ particles (Ciampa *et al.* 1987). The corresponding primary energy range is that in which attenuation resulting from photon-photon interactions with the 3K background is expected to be most severe. In addition to this result, a slight excess of events was detected for showers with sizes $N_e > 10^6$ particles.

In a more recent search (Ciampa 1988; Ciampa *et al.* 1988b), the 1984–1986 and 1986–1988 data sets were examined for evidence of U.H.E. γ-ray emission from the direction of Centaurus A. In this analysis, events within 5° of Centaurus A were re-analysed to allow for shower-front curvature and timing uncertainties (see 3.3.2), as well as four comparable background regions at the same declination. This analysis yielded a total of 2112 on-source events, compared to an average off-source background of 2023 events, corresponding to a DC excess of $\sim 1.75\sigma$ (compared to a 2.3σ DC excess for the 'uncorrected' data, when compared to a background averaged over 39 off-source regions — Ciampa *et al.* 1988b).

These data were then divided into three size ranges and three search regions centred on Centaurus A to examine the data for any excess peaked towards the direction of Centaurus A, as shown in Table 6.3(a). A 2.5σ excess was found in the middle size bin

Angle from Source (degrees)	Shower Size Range (N_e)					
	$N_e < 2 \times 10^5$		$2 \times 10^5 < N_e < 5 \times 10^5$		$N_e > 5 \times 10^5$	
	Source	Background	Source	Background	Source	Background
< 1.65	715	697	128	98	45	35
1.65–2.15	473	469	76	69	21	28
2.15–2.65	524	555	96	88	27	29

Table 6.3 (a) : Number of Events in the 1986–1988 experiment of Ciampa (1988) within three angular ranges centred on Centaurus A, and in three shower size intervals. The background is derived from the analysis of events in four similar off-source regions (after Ciampa *et al.* 1988).

Angle from Source (degrees)	Shower Size Range (N_e)					
	$N_e < 2 \times 10^5$		$2 \times 10^5 < N_e < 5 \times 10^5$		$N_e > 5 \times 10^5$	
	Source	Background	Source	Background	Source	Background
< 1.65	477	429	85	64	27	29
1.65–2.15	288	300	32	45	23	20
2.15–2.65	342	379	49	57	24	25

Table 6.3 (b) : Number of Events in the 1984–1986 data of Edwards (1988) within three angular ranges centred on Centaurus A, and in three shower size intervals. The background is derived from the number of events expected in the solid angle of each range, knowing the total number of events within 5° of the source (after Ciampa *et al.* 1988).

for the central region, with slight excesses (0.61σ, 1.43σ respectively) for the other size bins within this central region.

In addition to these results, the 1984–1986 data were examined with a planar shower-front fit resulting in 3061 on-source events, compared to an off-source background average of 3089.3 events. Re-analysis of event directions within 5° was carried out by Ciampa (1988) for on-source events only, using the previously determined background rate for comparison. Shower size and angular ranges were used as in the above analysis, and the results displayed in Table 6.3(b). Whilst caution must be used in interpreting these results, there is once again clear evidence for emission in the size range $2 \times 10^5 < N_e < 5 \times 10^5$ particles (Ciampa *et al.* 1988b).

In light of these results, a search was carried out for evidence of U.H.E. γ-ray emission from the direction of Centaurus A on the remainder of the 1986–1989 data set (March 1988 – May 1989) for which the author was primarily responsible for both the collection and analysis (see Chapter 3). The results of this search have been previously published (Bird and Clay 1990a).

For this analysis, in order to obtain an unbiased background and source exposure, only data from full sidereal days were considered, as discussed in 5.2.1. This resulted in a useful exposure of 191 days.

The initial planar shower-front analysis as discussed above was applied to regions roughly square, 5° on a side. 1467 events were observed on-source, compared to an average off-source background of 1411 events. This background was averaged over 23 similar, but independent off-source regions centred on the same declination as Centaurus A, but separated by one hour in right ascension. This result corresponds to a statistically insignificant DC excess of 1.4σ.

To these data, the shower-front curvature corrections of Ciampa (1988) were applied to both the on-source, and 23 off-source regions[4] and the angular restrictions and shower size ranges of the previous investigations applied (see Table 6.4(a)). These

[4]this had not been attempted in the previous work of Ciampa *et al.* (1988b) due to CPU time and disk space restrictions.

Angle from Source (degrees)	Shower Size Range (N_e)					
	$N_e < 2 \times 10^5$		$2 \times 10^5 < N_e < 5 \times 10^5$		$N_e > 5 \times 10^5$	
	Source	Background	Source	Background	Source	Background
< 1.65	260	267	51	48	11	21
1.65–2.15	190	183	46	34	8	15
2.15–2.65	223	233	37	43	18	18

Table 6.4 (a) : Number of Events in the 1988–1989 experiment as discussed in the text, within three angular ranges centred on Centaurus A, and in three shower size intervals. The background is derived from the analysis of events in four similar off-source regions (after Bird and Clay 1990a).

Angle from Source (degrees)	Shower Size Range (N_e)	
	$2 \times 10^5 < N_e < 5 \times 10^5$	
	Source	Background
< 1.65	264	210
1.65–2.15	154	148
2.15–2.65	182	188

Table 6.4 (b) : Number of Events in the overall 1984–1989 data within three angular ranges centred on Centaurus A, for events in the size range $2 \times 10^5 < N_e < 5 \times 10^5$. (after Bird and Clay 1990a).

angular regions had been chosen by Ciampa (1988) to be consistent with an expected region, a marginal region, and a background region respectively. The results shown in Table 6.4(a) show no evidence for any significant excess of events from the direction of Centaurus A. In spite of this, it is noteworthy that there exists a numerical excess in the size range $2 \times 10^5 < N_e < 5 \times 10^5$ particles, the range in which both of the previous experiments reported a significant excess.

Combining the 1984–1989 data yields the results shown in Table 6.4(b) for the size range $2 \times 10^5 < N_e < 5 \times 10^5$ particles. This table suggests evidence at the 3.7σ level for an excess of events from the direction of Centaurus A, comparable to the result of the initial search carried out using the 1979–1981 data set (Clay *et al.* 1984a; Ciampa *et al.* 1987).

If this excess of events is due to the detection of primary γ-rays from Centaurus A, then this result places constraints on the magnitude of γ-ray absorption resulting from photon-photon interactions with the 3K microwave background and the strength of the inter-galactic magnetic field (in order to prevent significant non-cascading energy loss by electrons — see Protheroe 1986), as well as requiring the original source γ-rays to possess energies well above 10^{16}eV (see Ciampa *et al.* 1988b for a detailed discussion of these factors which remain valid in light of these additional results).

Both Centaurus A and SN1987A were examined only for evidence of a DC excess of events. Neither source has been observed to exhibit high energy behaviour at an established period to date[5].

In their previous searches for evidence of U.H.E. γ-ray emission from astrophysical sources carried out at Buckland Park, Edwards *et al.* (1989) and Ciampa (1988) examined the 1984–1986 and 1986–1988 data sets for evidence of periodic emission from a number of sources observed to exhibit such periodic behaviour at relatively high

[5]It is quite feasible that the suspected pulsar within SN1987A will eventually be observed directly, providing a suitable period (and period derivative) for such a search to be undertaken.

energies (e.g. X-ray energies). In particular, the X-ray binary system 2A 1822–37.1 was found to exhibit a periodic nature at U.H.E. energies at a significant confidence level (98.7% — Ciampa *et al.* 1989), and the remainder of the 1986–1989 data set were examined for similar behaviour (Clay *et al.* 1990). This search and its results will now be discussed.

6.2.5 2A 1822–37.1

The southern hemisphere low-mass X-ray binary system 2A 1822–37.1 was probably first detected during a rocket flight (Friedman *et al.* 1967), and its existence had been firmly established by the time of the publication of the second UHURU catalogue (Giacconi *et al.* 1972). Its optical counterpart was identified by Griffiths *et al.* (1978), at a distance of $\sim$ 2.5 kpc. The orbital period of $\sim$ 5.6 hours was initially detected optically (Mason *et al.* 1980; see also Charles *et al.* 1980) and subsequently confirmed by X-ray observations made with the HEAO-1 and Einstein X-ray satellites (see White *et al.* 1981)[6].

White and Holt (1982) empirically modelled the X-ray light curve, based upon an accretion disk corona model. This model was later extended by Mason and Cordova (1982) in order to explain the observed infra-red, optical, and ultra-violet emission of 2A 1822–37.1. The model consists of an accretion disk with a large bulge at an orbital phase of $\sim$ 0.9, assumed to result from the confluence of inflowing gas with the accretion disk, and a second, smaller bulge at an orbital phase of $\sim$ 0.25. Three-dimensional calculations of stream-disk interactions by Livio *et al.* (1986) support the existence of such bulges, and it is these bulges which could possibly serve as the target material for the production of U.H.E. γ-rays.

This accretion disk corona model has also been successfully applied in explaining observations of Cygnus X-3 (Protheroe and Stanev 1987), and 2A 1822–37.1 has been found to exhibit a number of properties similar to Cygnus X-3 (White *et al.* 1981),

[6]The most recent X-ray ephemeris is $P_o = (0^d.232108)$, T_o = 244 4105.674 JD (Mason *et al.* 1982)

making it a strong candidate for the emission of U.H.E. γ-rays.

Since its initial observation at U.H.E. energies (Samorski and Stamm 1983a; Lloyd-Evans *et al.* 1983; Protheroe 1987a), Cygnus X-3 has apparently diminished greatly in U.H.E. intensity over a period of years, and it has been suggested that 2A 1822–37.1 also exhibits a complex variability (Clay *et al.* 1990).

U.H.E. γ-ray Observations

Several previous investigations have been carried out at Buckland Park for evidence of periodic U.H.E. γ-ray emission from 2A 1822–37.1 (Edwards *et al.* 1989; Ciampa *et al.* 1989; Clay *et al.* 1990). These investigations have been summarised and discussed in some detail by Clay *et al.* (1990), including the present search.

Ciampa *et al.* (1989), using the events corrected for shower-front curvature and timing uncertainties (as discussed in 3.3.2) from the 1986–1988 data set (see 3.4), carried out a period search about the previously determined orbital periods for 2A 1822–37.1 (e.g. White *et al.* 1981; Mason *et al.* 1982; Cowley *et al.* 1982), with the most recent X-ray period of Mason *et al.* (1982) ($0^d.232108$) having a Z^2_{10} value of 37.8, corresponding to a significance at about the 1.3% probability level (see e.g. Bevington 1969 for a discussion of the calculation of this probability from the χ^2_{20} distribution). In addition, the Z^2_{10} test was also applied to the 1979–1981 and 1984–1986 data sets but, in spite of exhibiting interesting features in the respective phaseograms (see Fig 6.3(a), (b)), neither were found to be significant, with Z^2_{10} probability levels of 31% and 24% respectively, for this period. The phaseograms of the epochs of observation in question, shown in Fig 6.3, exhibit inconsistent phases of emission (i.e. ~ 0.2 for 1979–1981; 0.4–0.5 for 1984–1986; 0.9–1.0 for 1986–1988). An attempt by Ciampa *et al.* (1989) to unify these results through the introduction of a simple period derivative was unsuccessful.

In re-examining the 1979–1981 data set, an error in the Julian date (by 1 day) was identified by Clay *et al.* (1990), effectively shifting the phase of the peaks of emission in the corresponding phaseogram (see Fig 6.4(b); c.f. Fig 6.3(a)) to 0.35–0.6 and ~ 0.9, to

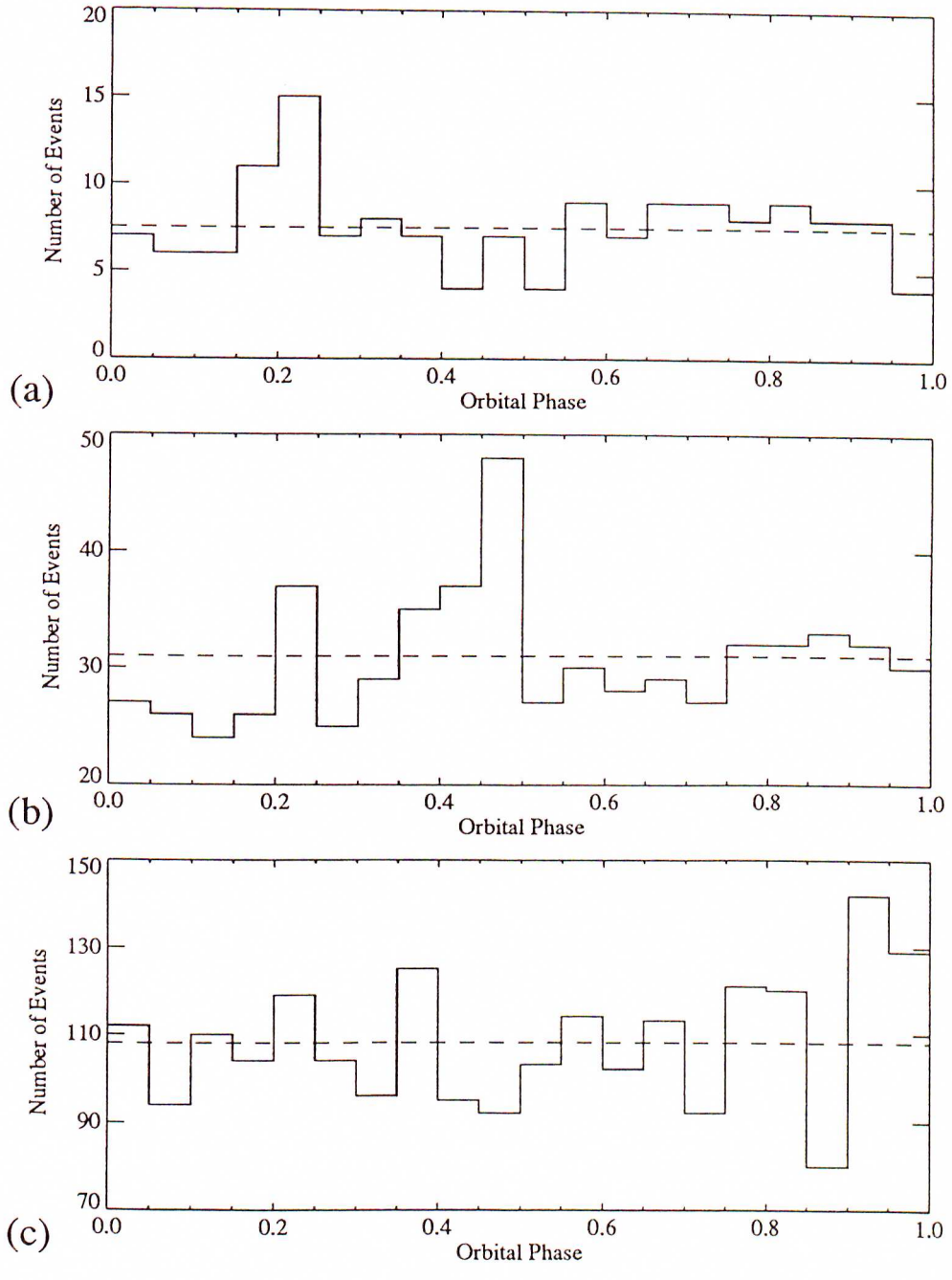

Figure 6.3: Phaseograms for events detected from the direction of the X-ray Binary system 2A 1822–37.1 as reported by Ciampa *et al.* (1989), using the ephemeris of Mason *et al.* (1982) (dashed line indicates the mean number of on-source events per phase bin).

(a) 1979–1981 data set

(b) 1984–1986 data set

(c) 1986–1988 data set

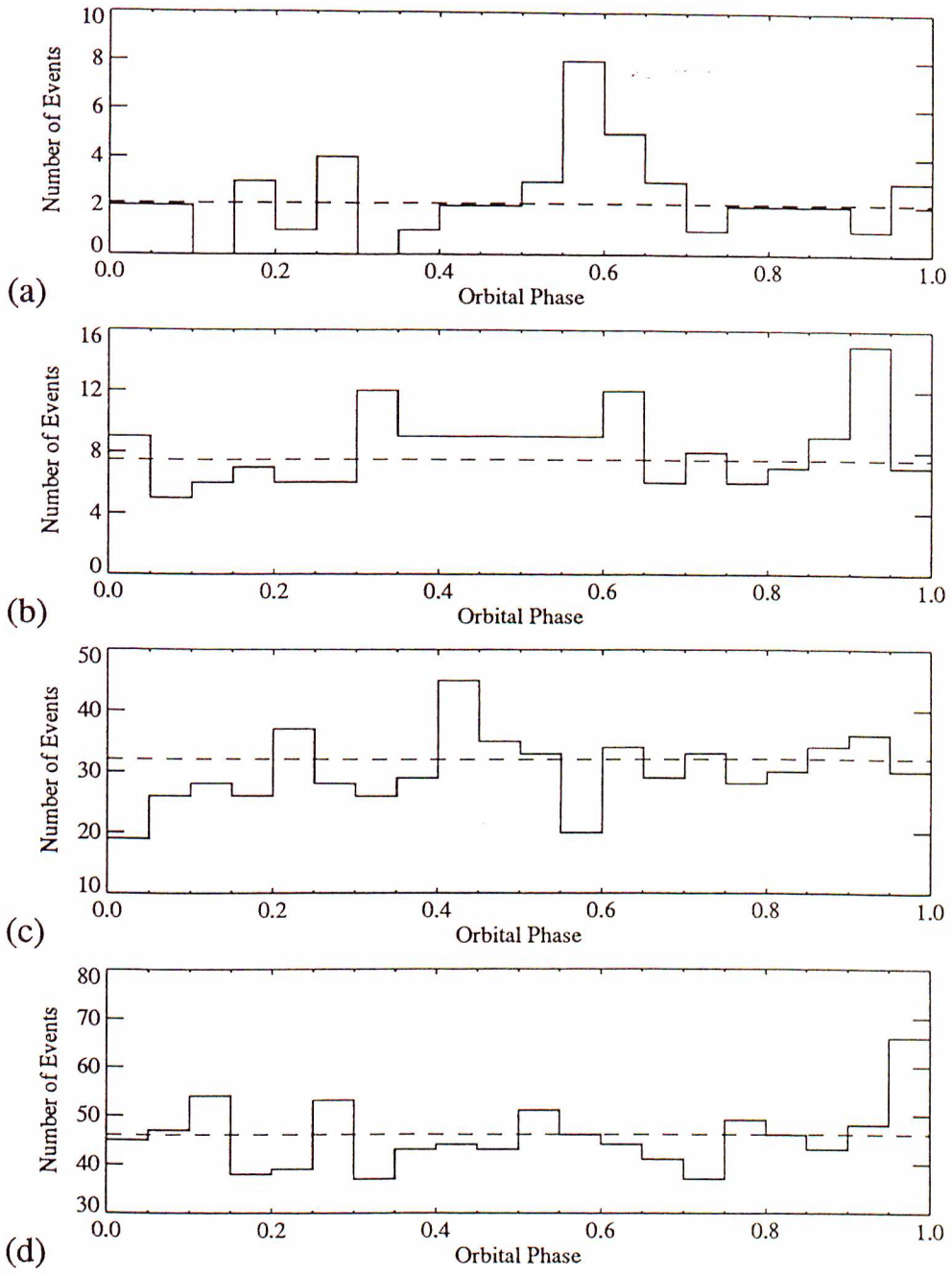

Figure 6.4: Phaseograms for events detected from the direction of the X-ray Binary system 2A 1822–37.1 as reported by Clay *et al.* (1990), including the revised 1979–1981 data ((**b**) — see text for discussion), using the ephemeris of Mason *et al.* (1982) (dashed line indicates the background level derived from 35 equivalent off-source regions).

(**a**) 1978 data set
(**b**) 1979–1981 data set
(**c**) 1984–1986 data set
(**d**) 1986–1989 data set

be in excellent agreement with the previously incompatible features in the other data sets examined by Ciampa *et al.* (1989), giving more confidence to the original claim of Ciampa *et al.* (1989) that evidence for the periodic emission of U.H.E. γ-rays from the direction of 2A 1822–37.1 had been found.

In light of these results, the remainder of the 1986–1989 data set (see 3.4) was examined for additional evidence of emission. The results of this analysis appear in Clay *et al.* (1990). An angular uncertainty of 2.5° was applied to these data, corrected as discussed in 3.3.2 (a slightly different uncertainty to that used by Ciampa *et al.* 1989, but more compatible with those of the previous data sets), as well as a shower size threshold of 10^5 particles. The overall 1986–1989 data set was found to exhibit a significant excess of events ($\sim 3\sigma$) in the last phase bin (0.95–1.0) (see Fig 6.4(a)) (Clay *et al.* 1990).

Fig 6.4 displays the phaseograms for the relevant data over the period 1978–1989, suggesting evidence for U.H.E. γ-ray emission from 2A 1822–37.1 produced preferentially in limited phase ranges, centred roughly on 0.5 and 1.0, with the preferred phase of emission at a given time being in a small range within the overall allowed ranges of phase. Increasingly stringent angular cuts were also found to emphasise the periodic component in the phaseograms (see Fig 6.5), further enhancing the evidence for periodic emission (see Clay *et al.* 1990 for details).

Overall, these data suggest that 2A 1822–37.1 is variable both in U.H.E. γ-ray luminosity and phase of emission, and that the observed phases of emission have preferred regions, namely 0.35–0.65 (possibly consisting of two regions near 0.4 and 0.6), and 0.9–0.1 (Clay *et al.* 1990). In this binary system these regions are diametrically opposed (orbital inclination between 76° and 84°).

If the emission of U.H.E. γ-rays from this system is the result of π° production and subsequent decay, resulting from the interaction of U.H.E. protons from a neutron star source with a local target material, then the emission phase 0.9–0.1 would most naturally be identified as having the outer regions of the stellar companion as the target material. Examination of the optical light curve of 2A 1822–37.1 by Mason *et al.* (1980)

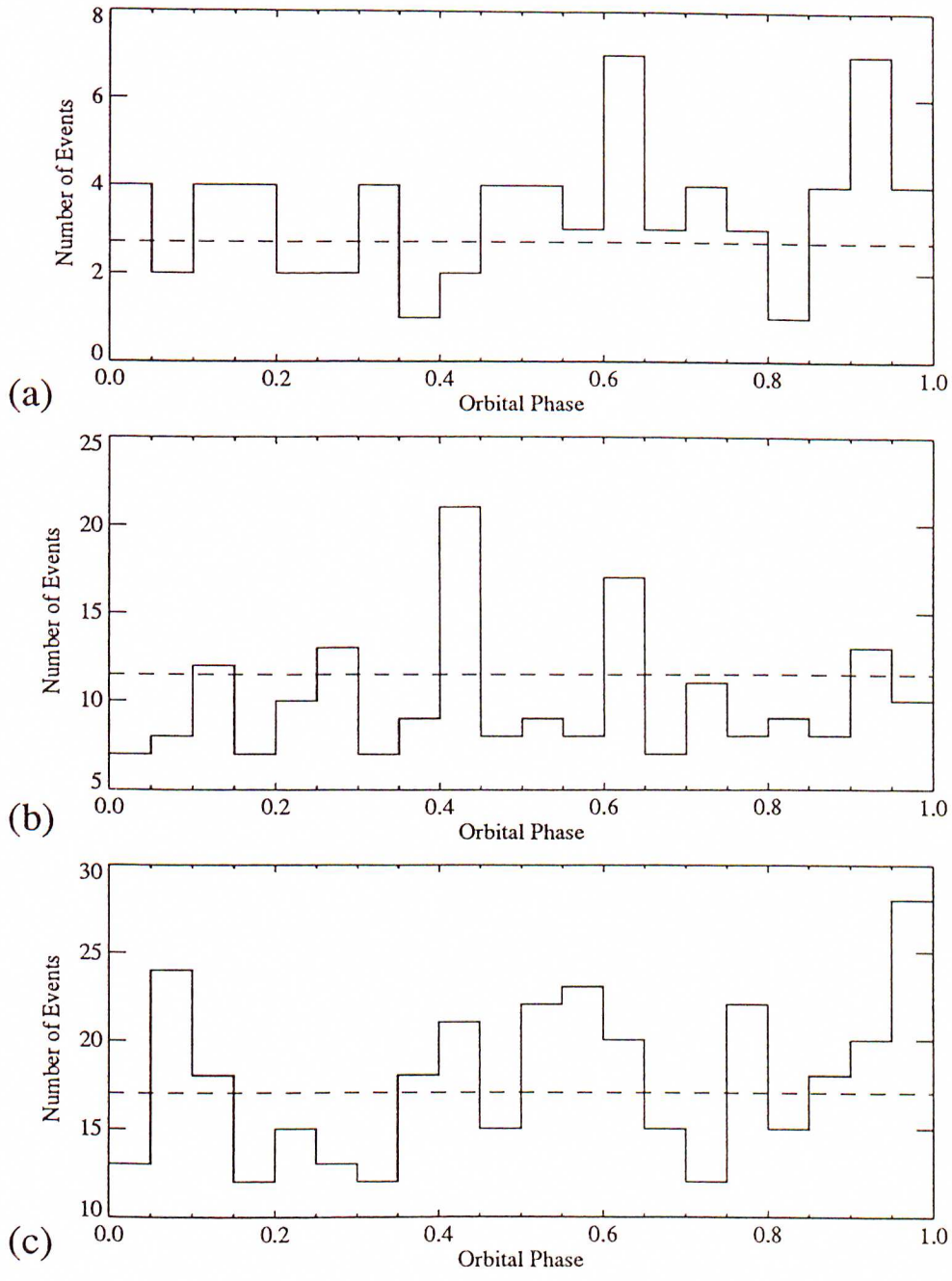

Figure 6.5: Phaseograms for events detected from the direction of the X-ray Binary system 2A 1822–37.1 with the angular range reduced to 1.5°, apparently enhancing the periodic nature of the phaseograms of Fig 6.4, as reported by Clay *et al.* (1990), using the ephemeris of Mason *et al.* (1982) (dashed line indicates the background level derived from 35 equivalent off-source regions).

(a) 1979–1981 data set

(b) 1984–1986 data set

(c) 1986–1989 data set

lead to the identification of two minima in the light curve, the one at phase 0.0 most likely resulting from occultation. The second minimum was found to be broad and relatively shallow, lasting $\sim$ 20% of the cycle (i.e. from phase 0.4 to 0.6), with optical peaks occurring at phases 0.4 and 0.6, believed to represent the edges of the absorbing material. Clay *et al.* (1990) suggest that the outer regions of this material may possess suitable conditions for the significant production of π°, combined with a very limited absorption of the produced γ-rays. Such a scenario could explain the observed preferred phases of U.H.E. emission evident in Figs 6.4 & 6.5.

In addition to this periodic investigation, a search for a DC excess of events from the direction of 2A 1822–37.1 was also carried out on the 1988–1989 data set, uncorrected for shower-front curvature and timing uncertainties. This search failed to identify an excess of events, based upon an angular uncertainty of 2.5° (1370 on-source events, compared to 1390 background events, averaged over 39 background regions over a period of 191 full sidereal days — see 5.2.1), consistent with the null result of Ciampa (1988) (2456 on-source events, compared to 2518 background events, averaged over 39 background regions, and applying an angular uncertainty of $\sim$ 2.0°). Clay *et al.* (1990) applied a number of angular uncertainties with a shower size threshold of 10^5 particles to these data , ranging from 2.5° to 1.1°, and found that 2.5° was the best estimate for maximising the signal to statistical noise ratio for a DC search for this source. No evidence was found to suggest any significant DC excess of events from the direction of 2A 1822–37.1 over this eleven year period by Clay *et al.* (1990).

6.3 Summary

Three southern hemisphere sources have been examined for evidence of U.H.E γ-ray emission over the period March 1988 – May 1989. All three of these sources were examined for a DC excess of events, with no significant excess of events being identified for any of the sources examined over this period.

Lower upper limits have been presented for the emission of U.H.E. γ-rays from the

direction of SN1987A, after combining these results with the previous, compatible results of Bird *et al.* (1989), based upon the 1987–1988 data set of Ciampa (1988). An overall excess of events from the direction of Centaurus A remains generally consistent over the period 1979–1989 (Bird and Clay 1990a). No evidence was found for a DC excess of events from the direction of 2A 1822–37.1, consistent with previous observations (Ciampa *et al.* 1989; Clay *et al.* 1990).

In addition, a search for evidence of the periodic emission of U.H.E. γ-rays from the X-ray binary system 2A 1822–37.1 was also carried out, and combined with the 1988–1989 data set of Ciampa (1988). These data show significant evidence for the periodic emission of U.H.E. γ-rays at an orbital phase 0.9–0.1. When compared with the analysis of earlier data sets (Ciampa *et al.* 1989; Clay *et al.* 1990), it appears that 2A 1822–37.1 exhibits a variability in both U.H.E. γ-ray luminosity and phase of emission, in some ways similar to that of the northern hemisphere X-ray binary system Cygnus X-3.

Chapter 7

Conclusion

7.1 Summary

The anisotropy of the primary cosmic ray flux has been the subject of investigation for more than forty years. The measurement of a significant, real anisotropy (or lack thereof), especially in the medium and high energy ranges above $\sim 10^{16}$eV (where only upper limits to the magnitude of the anisotropy have been established to date), would have important implications for our ideas on the source of origin, acceleration mechanisms, and propagation characteristics of the cosmic ray flux, as well as the properties of the galactic magnetic field and inter-stellar medium through which these particles propagate.

In this thesis, a data set encompassing eight years of observations by the Buckland Park E.A.S. Array (1979–1981, 1984–1989) have been analysed and examined for evidence of an anisotropy in the medium energy cosmic ray flux in the primary particle energy range 3×10^{14}eV – 10^{17}eV. In this analysis, the removal of a number of artificial and natural spurious effects from the data through the use of suitable weighting was attempted and, after the location and removal of a period of bad data, the results of the anisotropy analysis were found to be generally consistent with a random distribution and appropriate upper limits were calculated which were found to be in general agreement with previously determined results. In spite of this lack of a significant measured

amplitude, the phases associated with these upper limits were found to be generally in agreement with those of comparable experiments, indicating the possibility of an underlying anisotropy below the statistical level of the present data set. This result will only be clarified by experiments possessing superior statistics.

In contrast to the study of the cosmic ray anisotropy, the field of U.H.E. γ-ray astronomy is just entering its second decade of investigation. In this thesis, the author has contributed evidence, through the analysis of data for which the author was primarily responsible (March 1988 – May 1989), of U.H.E. γ-ray emission from a number of potential U.H.E. γ-ray sources, to complement the previous searches of Edwards *et al.* (1989), and Ciampa (1988). No DC excess of events was found from the direction of any of the three sources examined, although the cumulative data for Centaurus A over the period 1979–1989 displays a significant and generally consistent excess of events. For the case of SN1987A, new upper limits to the number of U.H.E. γ-rays and source luminosity were calculated for the first twenty-seven months of observation, improving the upper limits of Bird *et al.* (1989), based upon the first twelve months of observation. When combined with the 1986–1988 data and analysis of Ciampa *et al.* (1989), the overall 1986–1989 data suggest that the X-ray binary system 2A 1822–37.1 exhibits significant periodic emission of U.H.E. γ-rays and, when considering the entire 1979–1989 data set, Clay *et al.* (1990) concluded that there is reasonable evidence for a complex behaviour of emission, somewhat similar to the that of the northern hemisphere U.H.E γ-ray source Cygnus X-3.

In order to improve the suitability of the Buckland Park E.A.S. Array, which had been previously employed for studies below the knee of the energy spectrum and U.H.E. γ-ray astronomy, to medium and high energy anisotropy measurements, without significantly compromising the U.H.E. γ-ray sensitivity of the array, suitable modifications and additions to the array were designed, tested with computer simulations and installed by the author during the period of candidature. Six months of data were collected and analysed by the author and the array was found to exhibit behaviour consistent with the design criteria and computer simulations.

7.2 Future Work

The studies of both cosmic ray anisotropy and U.H.E. γ-ray astronomy at sea-level E.A.S. energies suffer from poor statistics resulting in marginal results or upper limits. To improve this situation, an increase in both the array exposure time and physical area are necessary as well as improved theoretical models and analysis techniques.

The Buckland Park E.A.S. Array now possesses an increased exposure area, as well as improved facilities for monitoring the array behaviour and for the quick identification and rectification of associated array problems, minimising the array down-time. It is feasible that several years of essentially continuous operation of the 'new' Buckland Park E.A.S. Array will provide improved sampling statistics for both fields of cosmic ray study, the 'new' (U.H.E. γ-ray astronomy), and the 'old' (anisotropy of the primary cosmic ray flux). This may resolve some of the problems which currently exist, such as the determination of the existence of a significant anisotropy in the medium energy primary cosmic ray flux, and may also confirm the existence of currently suspected U.H.E. γ-ray sources in the southern hemisphere at a significant statistical level.

References

The abbreviation *Xth I.C.R.C.* represents the *Xth International Cosmic Ray Conference.* Papers with more than 10 authors have been abbreviated to *et al.*

Acharya B.S., Rao M.U.S., Sivaprasad K., Sreekantan B.V., and Viswanath P.R. (1990) *Nature*, **347**, 364.

Aglietta M., *et al.* (1987) *Europhys. Lett.*, **3**, 1315.

Aguirre C. (1974) *J. Phys. A: Math. Nucl. Gen.*, **7**, 1474.

Alexeenko V.V. and Navarra G. (1985) *Lett. Nuovo Cim.*, **42**, 321.

Alexeenko V.V., Chudakov A.E., Gulieva E.N., and Sborshikov V.G. (1981) *Proc. 17th I.C.R.C. (Paris)*, **2**, 146.

Allan H.R. (1971) *Prog. Elem. Part. and Cos. Ray Phys.*, **10**, 170.

Allkofer O.C., Carstensen K., Dav W.D., and Jokisch H. (1975) *J. Phys. G: Nucl. Phys.*, **1**, L151.

Alvarez L.W. and Compton A.H. (1933) *Phys. Rev.*, **43**, 835.

Amos N.A., *et al.* (1989) *Phys. Rev. Lett.*, **63**, 2784.

Anderson C.D. (1933) *Phys. Rev.*, **43**, 368.

Andreyev Y.M., Chudakov A.E., Kozyarivsky V.A., Sidorenko A.M., Tulupova T.I., and Voevodsky A.V. (1987) *Proc. 20th I.C.R.C. (Moscow)*, **2**, 22.

Armaldi U., *et al.* (1977) *Phys. Lett.*, **B66**, 390.

Armitage M.L., Blake P.R., and Nash W.F. (1973) *Proc. 13th I.C.R.C. (Denver)*, **4**, 2551.

Armitage M.L., Blake P.R., Nash W.F., Saltmarsh C.G., Sephton A.J., Shelley C.C., and Strutt R.B. (1987) *J. Phys. G: Nucl. Phys.*, **13**, 707.

Arnett W.D., Bahcall J., Kirshner R.P., and Woosley S.E. (1989) *Ann. Rev. Astron. Astrophys.*, **27**, 629.

Asakimori K., Maeda T., Misaki Y., Nishijima K., Toyoda Y., Yamamoto K., Yoshida M., and Kameda T. (1983) *Proc. 18th I.C.R.C. (Bangalore)*, **11**, 189.

Ashton F., Parvaresh A., and Saleh A.J. (1975) *Proc. 14th I.C.R.C. (Munich)*, **8**, 2831.

Astley S.J., Cunningham G., Lloyd-Evans J., Reid R.J.O., and Watson A.A. (1981) *Proc. 17th I.C.R.C. (Paris)*, **2**, 156.

Auger P., Maze R., and Grivet-Mayer T. (1938) *C.R. Acad. Sci. (Paris)*, **206**, 151.

Axford W.I. (1981) *Proc. 17th I.C.R.C. (Paris)*, **12**, 155.

Axford W.I. (1987) *Proc. 20th I.C.R.C. (Moscow)*, **8**, 120.

Baade W. and Zwicky F. (1934a) *Proc. Nat. Acad. Sci.*, **20**, 254.

Baade W. and Zwicky F. (1934b) *Proc. Nat. Acad. Sci.*, **20**, 259.

Badino G., Periale L., Galeotti P., and Saavedra O. (1980) *Lett. Nuovo Cim.*, **28**, 93.

Baldwin J.E. (1959) in *"Radio Astronomy"*, ed. Bracewell R.N. (Stanford University Press), p460.

Baltrusaitis R.M., *et al.* (1985a) *Astrophys. J. Lett.*, **293**, L69.

Baltrusaitis R.M., Cady R., Cassiday G.L., Cooper R., Elbert J.W., Gerhardy P.R., Ko S., Loh E.C., Mizumoto Y., Salamon M., Sokolsky P., and Steck D. (1985b) *Proc. 19th I.C.R.C. (La Jolla)*, **2**, 146.

Baltrusaitis R.M., *et al.* (1988) *Nucl. Instr. Meth.*, **A264**, 87.

Barish-Schmidt N., *et al.* (1976) *Rev. Mod. Phys.*, **48**, S21.

Bassi P., Clark G., and Rossi B. (1953) *Phys. Rev.*, **92**, 441.

Bell M.C., Kota J., and Wolfendale A.W. (1974) *J. Phys. A: Math. Nucl. Gen.*, **7**, 420.

Benecke J., Chou T.T., Yang C.M., and Yen E. (1969) *Phys. Rev. Lett.*, **188**, 2159.

Bercovitch M. and Agrawal S.P. (1981) *Proc. 17th I.C.R.C. (Paris)*, **10**, 246.

Berezinsky V.S. and Ginzburg V.I. (1987) *Nature*, **329**, 807.

Berezinsky V.S. and Mikhailov A.A. (1985) *Proc. 18th I.C.R.C. (Bangalore)*, **2**, 174.

Berezinsky V.S. and Prilutsky O.F. (1978) *Astron. Astrophys.*, **66**, 325.

Berezinsky V.S. and Stanev T. (1989) *Phys. Rev. Lett.*, **63**, 1035.

Berezinsky V.S. and Stanev T. (1990) *Proc. 21st I.C.R.C. (Adelaide)*, **2**, 218.

Berezinsky V.S., Mikhailov A.A., and Syrovatski S.I. (1979) *Proc. 16th I.C.R.C. (Kyoto)*, **2**, 86.

Bergeson H.E., Cutler D.J., Davis J.F., and Groom D.E. (1979)
Proc. 16th I.C.R.C. (Kyoto), **4**, 188.

Bevington P.R. (1969) *"Data Reduction and Error Analysis for the Physical Sciences."* (McGraw-Hill Book Company — New York).

Bhat C.L., Sarma P.R., Sapru M.L., and Kaul C.L. (1979)
Proc. 16th I.C.R.C. (Kyoto), **8**, 57.

Bhat C.L., Sapru M.L., and Kaul C.L. (1980) *Nature*, **288**, 146.

Binns W.R., Fixsen D.J., Garrad T.L., Israel M.H., Klarmann J., Stone E.C., and Waddington C.J. (1984) *Adv. Sp. Res.*, **4**, 25.

Bionta R.M., *et al.* (1987) *Phys. Rev. Lett.*, **58**, 1494.

Bird D.J. and Clay R.W. (1989) *Proc. Astron. Soc. Aust.*, **8**, 46.

Bird D.J. and Clay R.W. (1990a) *Proc. Astron. Soc. Aust.*, **8**, 266.

Bird D.J. and Clay R.W. (1990b) *Proc. 21st I.C.R.C. (Adelaide)*, **3**, 139.

Bird D.J., Bruce T.E.G., Ciampa D., Clay R.W., Corani C.L., Edwards P.G., Gregory A.G., Patterson J.R., and Protheroe R.J. (1987)
Proc. Astron. Soc. Aust., **7**, 73.

Bird D.J., Ciampa D., and Clay R.W. (1989) *Proc. Astron. Soc. Aust.*, **8**, 52.

Bøggild H., Hansen K.H., and Suk M. (1971) *Nucl. Phys.*, **27**, 1.

Bond I.A., *et al.* (JANZOS Collaboration) (1988a) *Phys. Rev. Lett.*, **60**, 1110.

Bond I.A., *et al.* (JANZOS Collaboration) (1988b) *Phys. Rev. Lett.*, **61**, 2292.

Bond I.A., *et al.* (JANZOS Collaboration) (1989) *Astrophys. J. Lett.*, **344**, L17.

Bond I.A., *et al.* (JANZOS Collaboration) (1990a)
Proc. 21st I.C.R.C. (Adelaide), **2**, 198.

Bond I.A., *et al.* (JANZOS Collaboration) (1990b)
Proc. 21st I.C.R.C. (Adelaide), **2**, 210.

Bond I.A., *et al.* (JANZOS Collaboration) (1990c)
Proc. 21st I.C.R.C. (Adelaide), **2**, 271.

Bonnet-Bidaud J.M. and Chardin G. (1988) *Phys. Rep.*, **170**, (6), 325.

Bouchet P., Danziger I.J., and Lucy L.B. (1989) *I.A.U. Circular #4933.*

Bowyer C.S., Lampton M., Mack J., and de Mondonca F. (1970)
Astrophys. J. Lett., **161**, L1.

Braun O. and Sitte K. (1965) *Proc. 9th I.C.R.C. (London)*, **9**, 712.

Brazier K.T.S., *et al.* (1990) *Proc. 21st I.C.R.C. (Adelaide)*, **2**, 288.

Broten N.W., Macleod J.M., and Vallée J.P. (1985) *Astrophys. Lett.*, **24**, 165.

Bruce T.E.G., Clay R.W., Dawson B.R., Protheroe R.J., Blair D.G., and Cinquini P. (1985) *Proc. 19th I.C.R.C. (La Jolla)*, **2**, 266.

Buccheri R. and Sacco B. (1985) in *"Data Analysis in Astronomy"*,
ed. Scarsi L., *et al.* (Plenum Press), p15.

Burrows A. (1988) *Astrophys. J.*, **334**, 891.

Canal R., Isern J., and Labay J. (1990) *Ann. Rev. Astron. Astrophys.*, **28**, 183.

Cannon R.D. (1990) *Proc. 21st I.C.R.C. (Adelaide)*, **12**, 1.

Capdevielle J.N. and Gawin J. (1982) *J. Phys. G: Nucl. Phys.*, **8**, 1317.

Cassé M. and Paul J.A. (1980) *Astrophys. J.*, **237**, 236.

Cassiday G.L. (1985) *Ann. Rev. Nucl. Part. Sci.*, **35**, 321.

Cassiday G.L., *et al.* (1990a) *Proc. 21st I.C.R.C. (Adelaide)*, **3**, 196.

Cassiday G.L., *et al.* (1990b) *Astrophys. J.*, **351**, 454.

Cassiday G.L., *et al.* (1990c) *Proc. 21st I.C.R.C. (Adelaide)*, **3**, 163.

Cebula D., Corbato S.C., Daily T., Kieda D.B., Land K., Lee C.R., and Cherry M.L. (1990) *Astrophys. J.*, **358**, 637.

Chadwick P.M., Dipper N.A., Lincoln E.W., Mannings V.G., McComb T.J.L.,
Rayner S.M., Orford K.J., Turver K.E., and Williams D.G. (1988)
Astrophys. J. Lett., **333**, L19.

Chantler M.P., Craig M.A.B., McComb T.J.L., Orford K.J., Turver K.E., and
Walley G.M. (1982) *J. Phys. G: Nucl. Phys.*, **8**, L51.

Chapman S. and Bartels J. (1940) *"Geomagnetism Vol. 2"* (Oxford University Press).

Chardin G. and Gerbier G. (1989) *Astron. Astrophys.*, **210**, 52.

Charles P., Thorstensen J.R., and Barr P. (1980) *Astrophys. J.*, **241**, 1148.

Cheung T. and MacKeown P.K. (1988) *Nuovo. Cim.*, **11C**, 193.

Chitnis E.V., Sarabhai V.A., and Clark G.W. (1960) *Phys. Rev.*, **119**, 1085.

Ciampa D. (1988) Ph.D. Thesis, University of Adelaide.

Ciampa D. and Clay R.W. (1988) *J. Phys G: Nucl. Phys.*, **14**, 787.

Ciampa D. and Clay R.W. (1989) *Proc. Astron. Soc. Aust.*, **8**, 49.

Ciampa D., Clay R.W., Corani C.L., Edwards P.G., Patterson J.R., and Protheroe R.J. (1986) *Proc. Astron. Soc. Aust.*, **6**, 335.

Ciampa D., Clay R.W., Corani C.L., Edwards P.G., Patterson J.R., and Protheroe R.J. (1987) in *"Very-High-Energy Gamma-Ray Astronomy"*, ed. Turver K.E. (D. Reidel — Dordrecht), p275.

Ciampa D., Bird D.J., Clay R.W., Edwards P.G., and Protheroe R.J. (1988a) *Astrophys. J. Lett.*, **326**, L9.

Ciampa D., Clay R.W., and Edwards P.G. (1988b) University of Adelaide preprint ADP-88-92/E47.

Ciampa D., Clay R.W., and Edwards P.G. (1989) *Astrophys. J.*, **346**, 151.

Ciampa D., *et al.* (1990) *Phys. Rev. D*, **42**, 281.

Citron A. and Stiller G. (1958) *Nuovo Cim. Supp.*, **8**, 675.

Clark G.W. (1957) *Phys. Rev.*, **108**, 450.

Clark G.W., Earl J., Kraushaar W.L., Linsley J., Rossi B., Scherb F., and Scott D.W. (1961) *Phys. Rev.*, **122**, 637.

Clay J. (1927) *Proc. Roy. Acad. Amsterdam*, **36**, 1115.

Clay R.W. (1984) *Aust. J. Phys.*, **37**, 97.

Clay R.W. (1985) *Proc. 19th I.C.R.C. (La Jolla)*, **9**, 357.

Clay R.W. (1987) *Aust. J. Phys.*, **40**, 423.

Clay R.W. (1988) *Aust. J. Phys.*, **41**, 749.

Clay R.W. (1990) private communication.

Clay R.W. and Ciampa D. (1986) *Aust. J. Phys.*, **39**, 93.

Clay R.W. and Dawson B.R. (1981) *Aust. J. Phys.*, **34**, 591.

Clay R.W. and Gerhardy P.R. (1980) *Aust. J. Phys.*, **33**, 753.

Clay R.W. and Gerhardy P.R. (1982) *Aust. J. Phys.*, **35**, 441.

Clay R.W. and Gerhardy P.R. (1983) *Aust. J. Phys.*, **36**, 357.

Clay R.W. and Gregory A.G. (1978) *Nucl. Instr. Meth.*, **153**, 471.

Clay R.W., Gerhardy P.R., Liebing D.F., Thornton G.J., and Patterson J.R. (1981) *Nuovo Cim.*, **4C**, 668.

Clay R.W., Gerhardy P.R., and Liebing D.F. (1984a) *Aust. J. Phys.*, **37**, 91.

Clay R.W., Protheroe R.J., and Gerhardy P.R. (1984b) *Nature*, **309**, 687.

Clay R.W., Corani C.L., Patterson J.R., Dawson B.R., Edwards P.G., Gregory A.G., Prescott J.R., Elton S.D., and Ciampa D. (1985)
Proc. 19th I.C.R.C. (La Jolla), **3**, 414.

Clay R.W., Meyhandan R., and Bird D.J. (1990) (submitted to *Astron. Astrophys.*).

Cocconi G. (1961) *Handbuch der Physic*, **46**, 215.

Cocconi G., Koester L.G., and Perkins D.H. (1961) UCRL–10022.

Colgate S.A. and Johnson M.H. (1960) *Phys. Rev. Lett.*, **5**, 235.

Compton A.H. (1932) *Phys. Rev.*, **41**, 111, 681.

Compton A.H. and Getting I.A. (1935) *Phys. Rev.*, **47**, 817.

Corani C.L. (1986) Masters Thesis, University of Adelaide.

Cowley A.P., Crampton D., and Hutchings J.B. (1982) *Astrophys. J.*, **255**, 296.

Cranshaw T.E. and Elliot H. (1956) *Proc. Phys. Soc.*, **A69**, 102.

Cranshaw T.E. and Galbraith W. (1954) *Phil. Mag.*, **44**, 1109.

Cranshaw T.E. and Galbraith W. (1957) *Phil. Mag.*, **52**, 804.

Cranshaw T.E., De Beer J.F., Galbraith W., Hillas A.M., Norris S., and Porter N.A. (1958) *Phil. Mag.*, **3**, 811.

Crookes I.N. and Rastin B.C. (1971) *Proc. 12th I.C.R.C. (Hobart)*, **10**, 171.

Crouch P.C. (1979) Ph.D. Thesis, University of Adelaide.

Crouch P.C., Gerhardy P.R., Patterson J.R., Clay R.W., and Gregory A.G. (1981) *Nucl. Instr. Meth.*,, **179**, 467.

Cunningham G., Pollock A.M.T., Reid R.J.O., and Watson A.A. (1977)
Proc. 15th I.C.R.C. (Plovdiv), **2**, 303.

Daudin J., Auger P., Cachon A., and Daudin A. (1956) *Nuovo Cim.*, **3**, 1017.

Davies S.T., Elliot H., and Thambyapillai T. (1979)
Proc. 16th I.C.R.C. (Kyoto), **4**, 210.

Davis L. Jr. (1954) *Phys. Rev.*, **96**, 743.

Davis L. Jr., and Greenstein J.L. (1951) *Astrophys. J.*, **114**, 206.

Dawson B.R. (1985) Ph.D. Thesis, University of Adelaide.

Dawson B.R. (1990) private communication.

Dawson B.R., Prescott J.R., and Clay R.W. (1985)
Proc. 19th I.C.R.C. (La Jolla), **2**, 230.

Dawson B.R., Clay R.W., Edwards P.G., and Prescott J.R. (1986)
Nuovo Cim., **9C**, 1125.

de Beer J.F., Holyoak B., Wdowczyk J., and Wolfendale A.W. (1966)
Proc. Phys. Soc. Lond., **89**, 567.

de Jaeger O.C. (1987) Ph.D. Thesis, University of Potchefstroom.

Delvaille J., Kandziorski F., and Greisen K. (1962)
Phys. Soc. Japan, **17**, (Sup A3), 76.

Dingus B.L., *et al.* (1988a) *Phys. Rev. Lett.*, **60**, 1785.

Dingus B.L., *et al.* (1988b) *Phys. Rev. Lett.*, **61**, 1906.

Dixon H.E., Turver K.E., and Waddington C.J. (1974)
Proc. Phys. Soc. Lond., **A339**, 157.

Dopita M.A. (1988) *Sp. Sci. Rev.*, **46**, 225.

Doronina I.V., Dyakonov M.N., Knurenko S.P., Kolosov V.A., Pavlov V.N., and Sleptsov I. Ye. (1990) *Proc. 21st I.C.R.C. (Adelaide)*, **3**, 150.

Dorman L.I., Ghosh A., and Ptsukin V.S. (1985) *Astrophys. Sp. Sci.*, **109**, 87.

Drees M. and Halzen F. (1988) *Phys. Rev. Lett.*, **61**, 275.

Duperier A. (1949) *Proc. Phys. Soc.*, **A62**, 684.

Duperier A. (1951) *J. Atmos. Terr. Phys.*, **1**, 296.

Duric N. and Bloemen H. (1990) *Proc. 21st I.C.R.C. (Adelaide)*, **3**, 217.

Duric N. and Slane F.A. (1990) *Proc. 21st I.C.R.C. (Adelaide)*, **4**, 76.

Dutt J. and Thambyapillai T. (1965) *J. Atmos. Terr. Phys.*, **27**, 349.

Dzikowski T., Gawin T., Grochalska B., and Wdowczyk J. (1983)
J. Phys G: Nucl. Phys., **9**, 459.

Eames P.V.J., Lloyd-Evans J., Morello C., Reid R.J.O., and Watson A.A. (1985)
Proc. 19th I.C.R.C. (La Jolla), **2**, 254.

Ebneter K. and Balick B. (1983) *Pub. Astron. Soc. Pacific*, **95**, 675.

Edge D.M., Pollock A.M.T., Reid R.J.O., Watson A.A., and Wilson J.G. (1978)
J. Phys. G: Nucl. Phys., **4**, 133.

Edwards P.G. (1988) Ph.D. Thesis, University of Adelaide.

Edwards P.G., Protheroe R.J., and Rawinski E. (1985)
J. Phys. G: Nucl. Phys., **11**, L101.

Edwards P.G., Ciampa D., Clay R.W., and Patterson J.R. (1989)
Aust. J. Phys., **42**, 581.

Efimov N.N., Egorov T.A., Krasilnikov A.D., and Mikhailov A.A. (1987)
Proc. 20th I.C.R.C. (Moscow), **2**, 41.

Efimov N.N., Krasilnikov A.D., and Mikhailov A.A. (1990)
Proc. 21st I.C.R.C. (Adelaide), **3**, 205.

Eisberg R. and Resnick R. (1985) *"Quantum Physics of Atoms, Molecules, Solids, Nuclei, and Particles"* (Second Edition) (Wiley — New York), p659.

Elbert J.W. and Gaisser T.K. (1979) *Proc. 16th I.C.R.C. (Kyoto)*, **8**, 42.

Elbert J.W. and Sommers P. (1987) *Proc. 20th I.C.R.C. (Moscow)*, **2**, 458.

Elliot H. (1979) *Proc. 16th I.C.R.C. (Kyoto)*, **14**, 200.

Ellison D.C. (1990) *Proc 21st I.C.R.C. (Adelaide)*, **11**, 133.

Ellison D.C. and Möbius E. (1987) *Astrophys. J.*, **318**, 474.

Elton S.D. (1989) Ph.D. Thesis, University of Adelaide.

Engelman J.J., Goret P., Juliusson E., Koch-Miramond L., Lund N., Masse P., Rasmussen I.L., and Soutoul A. (1985) *Astron. Astrophys.*, **148**, 12.

Erlykin A.D. (1990) *Proc. 21st I.C.R.C. (Adelaide)*, **11**, 300.

Escobar I., Nerurkar N., and Weil R. (1960) *Planet. Sp. Sci.*, **2**, 187.

Farley F.J.M. and Storey J.R. (1954) *Proc. Phys. Soc.*, **A67**, 996.

Farley F.J.M. and Storey J.R. (1957) *Proc. Phys. Soc.*, **B70**, 840.

Fegan D.J. (1990) *Proc. 21st I.C.R.C. (Adelaide)*, **11**, 23.

Feinberg E.L. (1981) *Proc. 17th I.C.R.C. (Paris)*, **12**, 273.

Fenton A.G. (1976) in *"Proc. International Cosmic Ray Symposium on High Energy Cosmic Ray Modulation"*, ed. Nagashima K., *et al.* (Tokyo), p308.

Fenton A.G. and Fenton K.B. (1976) in *"Proc. International Cosmic Ray Symposium on High Energy Cosmic Ray Modulation"*, ed. Nagashima K., *et al.* (Tokyo), p313.

Fenton A.G., *et al.* (1990) *Proc. 21st I.C.R.C. (Adelaide)*, **3**, 177.

Fenyves E.J. (1985) in *"Proc. Workshop on Techniques in Ultra-High-Energy Gamma-Ray Astronomy (La Jolla)"*, ed. Protheroe R.J. and Stephens S.A. (University of Adelaide), p124.

Fenyves E.J., Balog S.N., Davis N.R., Suson D.J., and Stanev T. (1988) *Phys. Rev. D*, **37**, 649.

Fermi E. (1949) *Phys. Rev.*, **75**, 1169.

Fermi E. (1951) *Phys. Rev.*, **81**, 683.

Feynman R. (1969) *Phys. Rev. Lett.*, **23**, 1415.

Fichtel C.E. and Linsley J. (1986) *Astrophys. J.*, **300**, 474.

Firkowski R., Gawin J., Zawadski A., and Maze R. (1961) *J. Phys. Soc.*, **17A**, 123.

Fowler P.H., Adams R.A., Cowen V.G., and Kidd J.M. (1967) *Proc. Roy. Soc.*, **301**, 39.

Fowler P.H., Walker R.N.F., Masheder M.R.W., Moses R.T., Worley A., and Gay A.M. (1987) *Astrophys. J.*, **314**, 739.

Friedman H., Byram E.T., and Chubb T.A. (1967) *Science*, **156**, 374.

Gaisser T.K., Protheroe R.J., and Stanev T. (1983) *Proc. 18th I.C.R.C. (Bangalore)*, **5**, 174.

Gaisser T.K., Harding A.K., and Stanev T. (1987) *Nature*, **329**, 314.

Gaisser T.K., Harding A.K., and Stanev T. (1989a) *Astrophys. J.*, **345**, 423.

Gaisser T.K., Hillas A.M., Perrett J.C., Pomerantz M.A., Reid R.J.O., Smith N.J.T., Stanev T., and Watson A.A. (1989b) *Phys. Rev. Lett.*, **62**, 1425.

Gaisser T.K., Hillas A.M., Perrett J.C., Pomerantz M.A., Reid R.J.O., Smith N.J.T., Stanev T., and Watson A.A. (1990) *Proc. 21st I.C.R.C. (Adelaide)*, **2**, 209.

Gawin J., Maze R., Wdowczyk J., and Zawadski A. (1968) *Can. J. Phys.*, **46**, S72.

Gerhardy P.R. (1983) Ph.D. Thesis, University of Adelaide.

Gerhardy P.R. and Clay R.W. (1983) *J. Phys. G: Nucl. Phys.*, **9**, 1279.

Giacconi R., Gursky H., Paoline F.R., and Rossi B. (1962) *Phys. Rev. Lett.*, **9**, 439.

Giacconi R., Murray S., Gursky H., Kellogg E., Schreier E., and Tananbaum H. (1972) *Astrophys. J.*, **178**, 281.

Gibbs K.G., *et al.* (1990) *Proc. 21st I.C.R.C. (Adelaide)*, **4**, 306.

Gombosi T., Kota J., Somogyi A.J., Varga A., Betev B., Katsarski L., Kavloakov S., and Khirov I. (1975) *Proc. 14th I.C.R.C. (Munich)*, **2**, 586.

Gregory A.G., Patterson J.R., Smith N.I., and Thornton G.J. (1990) *Proc. 21st I.C.R.C. (Adelaide)* **2**, 282.

Greisen K. (1956) *Prog. Cos. Ray Phys.*, **3**, 1.

Greisen K. (1960) *Ann. Rev. Nucl. Sci.*, **10**, 63.

Greisen K. (1966) *Phys. Rev. Lett.*, **16**, 748.

Griffiths R.E., *et al.* (1978) *Nature*, **276**, 247.

Grindlay J.E. (1975) *Astrophys. J.*, **199**, 49.

Grindlay J.E., Helmken H.F., Hanbury Brown R., Davis J., and Allen L.R. (1975) *Astrophys. J. Lett.*, **197**, L9.

Grunsfield J.M., L'Heureux J., Meyer P., Müller D., and Swordy P. (1988) *Astrophys. J. Lett.*, **327**, L31.

Grunsfield J.M., L'Heureux J., Meyer P., Müller D., and Swordy P. (1990) *Proc. 21st I.C.R.C. (Adelaide)*, **3**, 69.

Gunn J.E. and Ostriker J.P. (1969) *Phys. Rev. Lett.*, **22**, 728.

Gupta S.K., Rajeev B.V., Sreekantan B.V., Srivatsan R., and Tonwar S.C. (1990) *Proc. 21st I.C.R.C. (Adelaide)*, **2**, 162.

Guseinov O.Kh., Kasumov F.K., and Yusifov I.M. (1981) *Sov. Astron.*, **25**, 567.

Halzen F. (1990) *Proc. 21st I.C.R.C. (Adelaide)*, **12**, 101.

Hara T., Hatano Y., Hayashida N., Kamata K., Kifune T., Mizumoto Y., Nagano N., Tanahashi G., and Teshima M. (1983) *Proc. 18th I.C.R.C. (Bangalore)*, **11**, 281.

Harding D.S. and Harding A.K. (1982) *Astrophys. J.*, **257**, 603.

Hartman R.C., Kniffen D.A., Thompson D.J., Fichtel C.E., Ogelman H.B., Turner T., and Ozel M.E. (1979) *Astrophys. J.*, **230**, 597.

Hayakawa S. (1969) *"Cosmic Ray Physics"* (Wiley — New York).

Heiles C. (1976) *Ann. Rev. Astron. Astrophys.*, **14**, 1.

Heiles C. (1987) in *"Interstellar Processes"*, ed. Hollenbach D.J. and Thronson H.A. (D. Reidel — Dordrecht), p171.

Hess V.F. (1912) *Physik Zeitschr.*, **13**, 1804.

Hill C.T. and Schramm D.N. (1985) *Phys. Rev. D*, **31**, 564.

Hill C.T., Schramm D.N., and Walker T.P. (1986) *Phys. Rev. D*, **34**, 1622.

Hillas A.M. (1975a) *Phys. Lett.*, **20C**, 59.

Hillas A.M. (1975b) *Phys. Rep.: "Some Recent Developments in Cosmic Rays."*, *Phys. Lett.*, **20C**, 59.

Hillas A.M. (1979) *Proc. 16th I.C.R.C. (Kyoto)*, **9**, 13.

Hillas A.M. (1980) *Aust. J. Phys.*, **33**, 911.

Hillas A.M. (1981) *Proc. 17th I.C.R.C. (Paris)*, **13**, 69.

Hillas A.M. (1982) *"School of Cosmic Ray Astrophysics, Enrice."*

Hillas A.M. (1984) *Nature*, **312**, 50.

Hillas A.M. (1985) *Proc. 19th I.C.R.C. (La Jolla)*, **3**, 445.

Hillas A.M. (1987) *Proc. 20th I.C.R.C. (Moscow)*, **6**, 432.

Hillas A.M. (1989) in *"Astrophysics in Antarctica"*, ed. Mullan D.J., *et al.* (American Institute of Physics — New York), p12.

Hillas A.M. and Lapikens J. (1977) *Proc. 15th I.C.R.C. (Plovdiv)*, **8**, 460.

Hillas A.M. and Ouldridge M. (1975) *Nature*, **253**, 609.

Hirata K., *et al.* (1987) *Phys. Rev. Lett.*, **58**, 1490.

Holynski R. (1990) *Proc. 21st I.C.R.C. (Adelaide)*, **11**, 280.

Honda M. and Mori M. (1987) *Prog. Theor. Phys.*, **78**, 963.

Honda M., Terasawa T., and Sato H. (1989) *Prog. Theor. Phys.*, **82**, 315.

Honda M., Terasawa T., and Sato H. (1990) *Proc. 21st I.C.R.C. (Adelaide)*, **2**, 230.

Horton L., McCusker C.B.A., Peak L.S., Ulrichs J., and Winn M.M. (1983) *Proc. 18th I.C.R.C. (Bangalore)*, **2**, 303.

Hoyle F. (1958) in *"La Structure et L'evolution de L'univers : XI Conseil de Physique Solvay, Bruxelles, 9–13 Juin 1958"*, ed. Stoops R., p53.

Humble J.E. and Fenton A.G. (1977) *Proc. 15th I.C.R.C. (Plovdiv)*, **11**, 245.

Jacklyn R.M. (1986) *Proc. Astron. Soc. Aust.*, **6**, (4), 425.

James F.E., and Roos M. (1975) *Comp. Phys. Comm.*, **10**, 343.

Jelley J.V., Fruin J.H., Porter N.A., Weekes T.C., Smith F.G., and Porter R.A. (1965) *Nature*, **205**, 327.

Johnson T.H. (1933) *Phys. Rev.*, **43**, 834.

Jones L.W. (1985) *Proc. 19th I.C.R.C. (La Jolla)*, **9**, 323.

Kalmykov N.N., Fomin Yu.I., and Khristiansen G.B. (1973) *Proc. 13th I.C.R.C. (Denver)*, **4**, 2633.

Kamata K., *et al.* (1968) *Can. J. Phys.*, **46**, S72.

Karakula S. and Wdowczyk J. (1963) *Acta. Phys. Pol.*, **24**, 231.

Karakula S., Osborne J.L., Roberts E., and Tkaczyk W. (1971) *Proc 12th I.C.R.C. (Hobart)*, **1**, 310.

Karakula S., Osborne J.L., and Wdowczyk J. (1974) *J. Phys. A: Math. Nucl. Gen.*, **7**, 437.

Khristiansen G.B., Kalmykov N.N., Kulikov G.V., Silaev A.A., Solovieva V.I., Sulakov V.P., Trubitsyn A.V., and Vedeneev O.V. (1990) *Proc. 21st I.C.R.C. (Adelaide)*, **2**, 362.

Kifune T. (1990) *Proc. 21st I.C.R.C. (Adelaide)*, **11**, 75.

Kifune T., Wdowczyk J., and Wolfendale A.W. (1986a) *J. Phys. G: Nucl. Phys.*, **12**, 143.

Kifune T., Hara T., Hatano Y., Hayashida N., Kamata K., Nagano M., Nishijima K., Tanahashi G., and Teshima M. (1986b) *J. Phys. G: Nucl. Phys.*, **12**, 129.

Kifune T., *et al.* (1986c) *Astrophys. J.*, **301**, 230.

Kiraly P.J. and White M. (1975) *J. Phys. A: Math. Nucl. Gen.*, **8**, 1336.

Kiraly P.J., Osborne J.L., White M., and Wolfendale A.W. (1975)
Proc. 14th I.C.R.C. (Munich), **2**, 612.

Kiraly P., Kota J., Osborne J.L., Stapely N.R., and Wolfendale A.W. (1979)
Riv. Nuovo Cim., **2**, (7), 1.

Krasilnikov D.D., *et al.* (1983) *Proc. 18th I.C.R.C. (Bangalore)*, **9**, 223.

Kraushaar W.L., Clark G.W., Gamire G.P., Helmken H., Higbie P., and Agogino M. (1965) *Astrophys. J.*, **141**, 845.

Kraushaar W.L., Clark G.W., and Gamire G.R. (1968)
Astrophys. J. Lett., **153**, L203.

Kristian J.A., *et al.* (1989) *Nature*, **338**, 234.

Kuhlmann J.D. and Clay R.W. (1981) *Proc. 17th I.C.R.C. (Paris)* , **6**, 96.

Kumagi S., *et al.* (1989) *Astrophys. J.*, **345**, 412.

Lagage P.O. and Cesarsky C.J. (1983) *Astron. Astrophys.*, **125**, 249.

Lagutin A.A., Pljasheshnikov A.V., and Uchaikin V.V. (1979)
Proc. 16th I.C.R.C. (Kyoto), **7**, 18.

Lambert A., Lloyd-Evans J., Perrett J.C., Reid R.J.O., Watson A.A., and West A.A. (1985) *Proc. 19th I.C.R.C. (La Jolla)*, **1**, 71.

Lang K.R. (1974) *"Astrophysical Formulae"* (Springer-Verlag — Berlin)

Lawrence M.A., Reid R.J.O., and Watson A.A. (1990a)
Proc. 21st I.C.R.C. (Adelaide), **3**, 200.

Lawrence M.A., Reid R.J.O., and Watson A.A. (1990b)
Proc. 21st I.C.R.C. (Adelaide), **3**, 159.

Liebing D.F., Clay R.W., Gregory A.G., Patterson J.R., Prescott J.R., and Thornton G.J. (1981) *Proc. 17th I.C.R.C. (Paris)*, **6**, 90.

Li T.P. and Ma Y.Q. (1983) *Astrophys. J.*, **272**, 317.

Linsley J. (1963) *Phys. Rev. Lett.*, **10**, 146.

Linsley J. (1975a) *Proc. 14th I.C.R.C. (Munich)*, **2**, 592.

Linsley J. (1975b) *Phys. Rev. Lett.*, **34**, 1530.

Linsley J. (1975c) *Proc. 14th I.C.R.C. (Munich)*, **2**, 598.

Linsley J. (1983) *Proc. 18th I.C.R.C. (Bangalore)*, **12**, 135.

Linsley J. (1985a) in *"Proc. Workshop on Techniques in Ultra-High-Energy Gamma-Ray Astronomy (La Jolla)"*, ed. Protheroe R.J. and Stephens S.A. (University of Adelaide), p138.

Linsley J. (1985b) *Proc. 19th I.C.R.C. (La Jolla)*, **7**, 163.

Linsley J. and Watson A.A. (1977) *Proc. 15th I.C.R.C. (Plovdiv)*, **12**, 203.

Linsley J. and Watson A.A. (1981) *Phys. Rev. Lett.*, **46**, 459.

Livio M., Soker N., and Dgani R. (1986) *Astrophys. J.*, **305**, 267.

Lloyd-Evans J. (1982) Ph.D. Thesis, University of Leeds.

Lloyd-Evans J., Pollock A.M.T., and Watson A.A. (1979) *Proc. 16th I.C.R.C. (Kyoto)*, **13**, 130.

Lloyd-Evans J., Coy R.N., Lambert A., Lapikens J., Patel M., Reid R.J.O., and Watson A.A. (1983) *Nature*, **305**, 784.

Lord Rayleigh (1880) *Phil. Mag.*, **10**, 73.

Lovelace R.V.E. (1976) *Nature*, **262**, 649.

Lyne A.G. and Smith F.G. (1989) *Mon. Not. Roy. Astron. Soc.*, **237**, 533.

Lyons P.R.A. (1979) Ph.D. Thesis, University of Tasmania.

Manchester R.N. (1974) *Astrophys. J.*, **188**, 637.

Manchester R.N. and Taylor J.H. (1981) *Astron. J.*, **86**, 1953.

Mason K.O., Middleditch J., Nelson J.E., White N.E., Seitzer P., Tuohy I.R., and Hunt L.K. (1980) *Astrophys. J. Lett.*, L109.

Mason K.O. and Cordova F.A. (1982) *Astrophys. J.*, **262**, 253.

Mason K.O., Murdin P.G., Tuohy I.R., Seitzer P., and Brandvardi-Raymont G. (1982) *Mon. Not. Roy. Astron. Soc.*, **200**, 793.

Matsubara Y., Hara T., Hayashida N., Honda M., Ishikawa F., Kamata K., Nagano M., Ohoka H., Ohnu Y., and Teshima M. (1990) *Proc. 21st I.C.R.C. (Adelaide)*, **3**, 201.

Matthewson D.S. and Ford V.L. (1970) *Mem. Astron. Soc.*, **74**, 139.

Maze R. and Zawadski A. (1960) *Nuovo Cim.*, **17**, 625.

Maze R., Wdowczyk J., Wolfendale A.W., and Zawadski A. (1969) *Phys. Rev. Lett.*, **22**, 899.

McClintock W., Henry R.C.., Linsky J.L., and Moos H.W. (1978)
Astrophys. J., **225**, 465.

McComb T.J.L., Protheroe R.J., and Turver K.E. (1979)
J. Phys. G: Nucl. Phys., **5**, 1613.

Meyhandan R. and Clay R.W. (1991) *Proc. Astron. Soc. Aust.* (in the press).

Meyer J.P. (1985) *Astrophys. J. Supp.*, **57**, 151.

Michel F.C. and Yahil A. (1973) *Astrophys. J.*, **179**, 771.

Morrison P. (1958) *Nuovo Cim.*, **7**, 858.

Murakami K., Shibata S., Fujii Z., Yamada T., Kojima H., Hayashida H., and Kifune T. (1990) *Proc. 21st I.C.R.C. (Adelaide)*, **3**, 192.

Nagano M., Hara T., Matano Y., Hayashida N., Kawaguchi S., Kamata K., Kifune T., and Mizumoto Y. (1984) *J. Phys. G: Nucl. Phys.*, **10**, 1295.

Nagashima K., Fujimoto K., Sakakibara S., Fujii Z., Ueno H., Murakami K., and Morishita I. (1989) *Nuovo Cim.*, **12**, 695.

Nagashima K., Fujimoto K., Sakakibara S., Fujii Z., Ueno H., Murakami K., and Morishita I. (1990) *Proc 21st I.C.R.C. (Adelaide)*, **3**, 180.

Nagle D.E., Gaisser T.K., and Protheroe R.J. (1988)
Ann. Rev. Nucl. Part. Sci., **38**, 609.

Nikolsky S.I., Stamenov J.N., and Ushev S.Z. (1987)
J. Phys. G: Nucl. Phys., **13**, 883.

Nishimura J. and Kamata K. (1951) *Prog. Theor. Phys.*, **6**, 628.

Olejniczah J., Wdowczyk J., and Wolfendale A.W. (1977)
J. Phys. G: Nucl. Phys., **3**, 846.

Olsson-Steel D. (1987) private communication.

Penzias A.A. and Wilson R.W. (1965) *Astrophys. J.*, **142**, 419.

Peters B. (1961) *Nuovo Cim.*, **22**, 800.

Peters P. and Westergaad N.J. (1977) *Astrophys. Sp. Sci.*, **48**, 21.

Piddington J.H. (1964) *Mon. Not. Roy. Astron. Soc.*, **128**, 345.

Poirier J., Funk E., Mikocki S., and Rohrer N. (1987) *Nucl. Instr. Meth.*, **A260**, 280.

Pollock A.M.T. (1978) Ph.D. Thesis, University of Leeds.

Powell C.F., Fowler P.H., and Perkin D.H. (1959) *"The Study of Elementary Particles by the Photographic Method"* (Pergamon Press — London).

Prescott J.R., Clay R.W., Corani C.L., Dawson B.R., Gregory A.G., and Patterson J.R. (1983) *Proc. 18th I.C.R.C. (Bangalore)*, **6**, 257.

Protheroe R.J. (1984a) *Nature*, **310**, 296.

Protheroe R.J. (1984b) *Astron. Expr.*, **1**, 33.

Protheroe R.J. (1985) *Astron. Expr.*, **1**, 137.

Protheroe R.J. (1986) *Mon. Not. Roy. Astron. Soc.*, **221**, 769.

Protheroe R.J. (1987a) *Proc. 20th I.C.R.C. (Moscow)*, **8**, 21.

Protheroe R.J. (1987b) in *"Very-High-Energy Gamma-Ray Astronomy"*, ed. Turver K.E. (D. Reidel — Dordrecht), p91.

Protheroe R.J. (1987c) *Nature*, **329**, 135.

Protheroe R.J. and Clay R.W. (1985) *Nature*, **315**, 205.

Protheroe R.J. and Patterson J.R. (1984) *J. Phys. G: Nucl. Phys.*, **10**, 841.

Protheroe R.J. and Stanev T. (1987) *Proc. 20th I.C.R.C. (Moscow)*, **1**, 254.

Protheroe R.J., Clay R.W., and Gerhardy P.R. (1984) *Astrophys. J. Lett.*, **280**, L47.

Rana N.C. and Wolfendale A.W. (1984) *Vistas in Astron.*, **27**, 199.

Rand R.J. and Kulkarni S.R. (1989) *Astrophys. J.*, **343**, 760.

Raubenheimer B.C., de Jaeger O.C., Nel H.I., North A.R., and van Urk G. (1988) *Astron. Astrophys.*, **193**, L11.

Ren J.R., *et al.* (1988) *Phys. Rev. D*, **38**, 1404.

Rossi B. (1933) *Z. Phys.*, **82**, 151.

Rossi B. (1952) *"High Energy Particles"* (Prentice-Hall, Inc.).

Rossi B. and Greisen K. (1941) *Rev. Mod. Phys.*, **13**, 240.

Ruzmaikin A.A., Shukurov A.M., and Sokoloff D.D. (1988a) *"Magnetic Fields in Galaxies"* (Kluwer Academic Publishers).

Ruzmaikin A.A., Sokoloff D.D., and Shukurov A.M. (1988b) *Nature*, **336**, 341.

Sakakibara S.J. (1965) *J. Geomag. Geoelect.* (Japan), **17**, 99.

Sakakibara S.J. (1976) in *"Proc. International Cosmic Ray Symposium on High Energy Cosmic Ray Modulation"*, ed. Nagashima K., *et al.* (Tokyo), p316.

Sakakibara S.J. (1979) *Proc. 16th I.C.R.C. (Kyoto)*, **4**, 216.

Samorski M. and Stamm W. (1983a) *Astrophys. J. Lett.*, **268**, L17.

Samorski M. and Stamm W. (1983b) *Proc. 18th I.C.R.C. (Bangalore)*, **11**, 244.

Sato H. (1977) *Prog. Theor. Phys.*, **58**, 549.

Schramm D.N. and Truran J.W. (1990) *Phys. Rep.*, **182**, 89.

Schönfelder V. (1990) *Proc. 21st I.C.R.C. (Adelaide)*, **12**, 177.

Sekido Y., Nagashima K, Kondo I., and Sakakibara S. (1976) in *"Proc. International Cosmic Ray Symposium on High Energy Cosmic Ray Modulation"*, ed. Nagashima K., *et al.* (Tokyo), p302.

Shapiro M.M. and Silberberg R. (1979) in *"Relativity, Quanta and Cosmology"*, ed. F. De Finis (New York — Johnston Reprint) **2**, p745.

Shapiro M.M. and Silberberg R. (1983) *Astrophys. J.*, **265**, 590.

Shelton I. (1987) *I.A.U. Circular # 4316.*

Simpson J.A. (1983) *Ann. Rev. Nucl. Part. Sci.*, **33**, 323.

Skobelzyn D. (1929) *Z. Phys.*, **54**, 686.

Smith A.G.K. and Clay R.W. (1990) *Aust. J. Phys.*, **43**, 373.

Sofue Y. and Fujimoto M. (1983) *Astrophys. J.*, **265**, 722.

Sofue Y. and Fujimoto M. (1985) in *"The Milky Way"*, ed. van Woerden H., *et al.* (D. Reidel — Dordrecht), p251.

Sofue Y., Fujimoto M., and Wielebinski R. (1986) *Ann. Rev. Astron. Astrophys.*, **24**, 459.

Sokolsky P. (1987) *Proc. 20th I.C.R.C. (Moscow)*, **8**, 318.

Stamenov J.N. (1987) *Proc. 20th I.C.R.C. (Moscow)*, **8**, 258.

Stanev T. (1986) in *"New Particles 1985"*, ed. Barger V., *et al.* (World Scientific — Singapore), p316.

Stanev T., Gaisser T.K., and Halzen F. (1985) *Phys. Rev. D*, **32**, 1244.

Stanev T. Halzen F., Vankov H.P., and Gaisser T.K. (1990)
Proc. 21st I.C.R.C., **9**, 146.

Storey J.R., *et al.* (1987) *JANZOS Proposal*, April 1987, (University of Tokyo).

Streitmatter R.E., Balasubratimanyan V.K., Ormes J.F., and Protheroe R.J. (1983)
Proc. 18th I.C.R.C. (Bangalore), **2**, 183.

Streitmatter R.E., *et al.* (1985) *Astron. Astrophys.*, **143**, 249.

Strong A.W., Wdowczyk J., and Wolfendale A.W (1974)
J. Phys. A: Math. Nucl. Gen., **7**, 120.

Suga K., *et al.* (1985) in *"Proc. Workshop on Techniques in Ultra-High-Energy Gamma-Ray Astronomy (La Jolla)"*, ed. Protheroe R.J. and Stephens S.A. (University of Adelaide), p48.

Swanenburg B.N., *et al.* (1981) *Astrophys. J. Lett.*, **243** , L69.

Tanaka Y. (1989) in *"Physics of Neutron Stars and Black Holes"*, ed. Tanaka Y. (Tokyo — Universal Academy Press), p431.

Teshima M., *et al.* (1990) *Proc. 21st I.C.R.C. (Adelaide)*, **3**, 158.

Thambyapillai T. (1974) *Proc. NATO Adv. Study Inst.*, **14**, 37.

Thielheim K.O. and Langhoff W. (1968) *J. Phys. A: Math. Nucl. Gen.*, **1**, 694.

Thielheim K.O, Kuckoff H.J., Steeb W.H., and Wenner G. (1971)
Proc. 12th I.C.R.C. (Hobart), **7**, 2612.

Thornton G.J. and Clay R.W. (1979) *Phys. Rev. Lett.*, **43**, 1622.
(and *Errata Phys. Rev. Lett.* **45**, 1463.)

Thornton G.J. and Clay R.W. (1981) *Phys. Rev. D.*, **23**, (9)., 2090.

Tomaszewski A. and Wdowczyk J. (1975) *Proc. 14th I.C.R.C. (Munich)*, **8**, 2899.

Tonwar S.C., Gopalakrishnan N.V., Rajeev M.R., and Sreekantan B.V. (1988)
Astrophys. J. Lett., **330**, L107.

Trimble V. (1983) *Rev. Mod. Phys.*, **55**, 511.

van der Walt D.J. (1987) *J. Phys. G: Nucl. Phys.*, **13**, 247.

van der Walt D.J. (1988) *J. Phys. G: Nucl. Phys.*, **14**, 105.

Vallée J.P. (1984) *Astron. Astrophys.*, **136**, 373.

Verschuur G.L. (1979) *Fund. Cos. Phys.*, **5**, 113.

Völk H.J. (1990) *Proc. 21st I.C.R.C. (Adelaide)*, **4**, 80.

Völk H.J., Klein U., and Wielebinski R. (1990) *Proc. 21st I.C.R.C. (Adelaide)*, **4**, 84.

Watson A.A. (1984) *Adv. Sp. Res.*, **4**, (2-3), 35.

Watson A.A. (1985) *Proc. 19th I.C.R.C. (La Jolla)*, **9**, 111.

Wdowczyk J. (1965) *Proc. 9th I.C.R.C. (London)*, **2**, 691.

Wdowczyk J. and Wolfendale A.W. (1983a) *Nature*, **305**, 609.

Wdowczyk J. and Wolfendale A.W. (1983b) *Nature*, **306**, 347.

Wdowczyk J. and Wolfendale A.W. (1984) *J. Phys. G: Nucl. Phys.*, **10**, 1453.

Wdowczyk J. and Wolfendale A.W. (1987) *J. Phys. G: Nucl. Phys.*, **13**, 411.

Wdowczyk J. and Wolfendale A.W. (1989) *Ann. Rev. Nucl. Part. Sci.*, **39**, 43.

Weekes T.C. (1988) *Phys. Rep.*, **160**, (1 & 2), 1.

Westfall G.D., Wilson L.W., Lindstrom P.J., Crawford H.J., Greiner D.E., and Heckman H.H. (1979) *Phys. Rev. C*, **19**, 1309.

White G.L. and Malin D.F. (1987) *Nature*, **327**, 36.

White G.M. and Prescott J.R. (1968) *Can. J. Phys.*, **46**, S287.

White N.E., Becker R.J., Boldt E.A., Holt S.S., Serlemitsos P.J., and Swank J.H. (1981) *Astrophys. J.*, **247**, 994.

White N.E. and Holt S.S. (1982) *Astrophys. J.*, **257**, 318.

Wilson C.T.R. (1901) *Proc. Roy. Soc.*, **68**, 151.

Wolfendale A.W. (1977) *Proc. 15th I.C.R.C. (Plovdiv)*, **10**, 235.

Woosley S.E. and Weaver T.A. (1986) *Ann. Rev. Astron. Astrophys.*, **24**, 205.

Yamada Y., Nakamura T., Kasahara K., and Sato H. (1988) *Prog. Theor. Phys.*, **79**, 416.

Yen E. (1974) *Phys. Rev. D*, **10**, 836.

Yodh G.B. (1988) Invited Talk presented at the *"Int. Conf. on Quark-Gluon Plasmas"* (Bombay, India).

Yodh G.B., Pal Y., and Trefil J.S. (1972) *Phys. Rev. Lett.*, **28**, 1005.

Yodh G.B., Goodman J.A., Tonwar S.C., and Ellsworth R.W. (1984) *Phys. Rev. D*, **29**, 892.

York D.G. (1982) *Ann. Rev. Astron. Astrophys.*, **20**, 221.

Zatsepin G.T. and Kuz'min V.A. (1966) *Sov. Phys. JETP Lett.*, **4**, 78.